

ORIGIN, DISTRIBUTION AND PARAGENETIC
SEQUENCE OF CARBONATE CEMENTS IN THE
BEN NEVIS FORMATION, WHITE ROSE FIELD,
JEANNE D'ARC BASIN, OFFSHORE NEWFOUNDLAND ,
CANADA

LEON S. NORMORE

***Origin, distribution and paragenetic sequence of
carbonate cements in the Ben Nevis Formation, White
Rose Field, Jeanne d'Arc Basin, offshore Newfoundland,
Canada***

© Leon S. Normore, B.Sc. (Hons)

A thesis submitted to the School of Graduate
Studies in partial fulfillment of the
Requirements for the degree of
Master of Science

Department of Earth Sciences
Memorial University of Newfoundland
October 2006

St. John's



Newfoundland

ABSTRACT

The Aptian-Albian quartz arenite sandstones of the Ben Nevis Formation were deposited in a storm dominated shoreface setting during a marine transgression. Sediment grain size, and poikilotopic calcite cement are largely accountable for the reduction in porosity and permeability, resulting in mean permeabilities on the order of < 1 to 300 mD. The objective of this study is to develop a knowledge of the paragenetic sequence during early and late diagenesis, relating timing and source of cements to attempt to predict cement distribution, its effect on reservoir-scale fluid connectivity and its use as a development and exploration tool at White Rose Field and potential extensions nearby. The union of several analytical methods are required to decipher 120 million years of diagenesis. Diagenetic evolution of the authigenic cements is investigated using core description, and optical petrography, with corroboration from carbon and oxygen isotopic analyses.

The paragenetic sequence identified in this study consisted of four phases of authigenic cement precipitation and four dissolution events, three of which acted on detrital components and the final dissolution phase acting on ferroan calcite cement. To understand the diagenetic sequence of any sedimentary rock unit, it is important to determine physical, geochemical and biological variations in depositional environment, as the compounded effect of all these will define the course of diagenesis. Transgressing a deep shelf environment over a shallow shoreface environment will decrease the rate of deposition, bioclastic content and sand/shale ratio, while increasing mud content, distance from shoreline and bioturbation. The transgressive nature of the Ben Nevis Formation compacts Ben Nevis sandstones beneath the Nautilus shales, building pore fluid pressure, transporting fluids vertically and obliquely towards the shoreline.

While there is a significant volume of serpulid worm tubes, bivalves and gastropods, it may be thin, compacted and often discontinuous residues of micro-crystalline textured curved shell fragments that are the primary source for calcite cement. Petrographic analyses demonstrate various stages of shell dissolution, as well as multi-layered shells typically composed of aragonite. Carbon isotopes ($\delta^{13}\text{C}$ values ranges from -13.9 to +8.8 ‰) are consistent with an aragonite source for calcite cement with a +1.20 ‰ average enrichment between shells and authigenic cement, corresponding to the aragonite-calcite conversion. Unstable aragonite is dissolved in the burial process providing an excellent source of enriched $\delta^{13}\text{C}$, to then precipitate as calcite cement.

The early stages of diagenesis enriched pore fluids with calcium carbonate providing the groundwork for the entire diagenetic history. Petrography and isotope geochemistry work collectively to confirm early precipitation of calcite cement. Petrographic analyses reveal minus cement packing up to 40%, nearly equivalent to original unconsolidated grain packing for fine grained sediments. Delicate ornaments on shells were also preserved within cements, indicating negligible compaction prior to cementation. Preservation of partially dissolved feldspar grains also indicates early cementation. Oxygen isotope analyses ($\delta^{18}\text{O}$ values range from -9.2 to -1.5 ‰) establish an approximately 13°C increase in temperature between shell formation and cement precipitation. This equates to a burial depth of only 390 m for precipitation of calcite cement.

Distributions of cements support vertical pore fluid flow within the Ben Nevis Formation. The storm dominated shoreface provides a much larger volume of bioclastic debris than the lower energy transition to the offshore environment immediately above but cementation intensity increases up-section. This indicates dissolution of shells in the lower Ben Nevis and transportation of fluid into the overlying offshore transition where sedimentation rates slow down, allowing precipitation of cement.

Calcite concretions are not laterally or vertically continuous as demonstrated by the rounded boundary types and compaction of uncemented sandstones between concretions, but the enormous volume of calcite cement is occupying pore space that could otherwise be filled with oil or gas. Concentrating on identifying the east-west constraints on the distal shoreface through seismic interpretation, additional wells and basin modelling may prove beneficial for future extensions of the White Rose Field, as well as the entire Jeanne d'Arc Basin.

ACKNOWLEDGEMENTS

The author wishes to express his deep appreciation to Dr. Rudi O. Meyer for his continuous support, and invaluable advice throughout the entire M.Sc. program. I am also thankful to my industry committee member, Neil Watson (Husky Energy) for his assistance and productive discussions.

I am grateful for the financial support provided to this project by the Pan Atlantic Petroleum Systems Consortium (PPSC) and Husky Energy - East Coast. Further support is provided by the Department of Earth Sciences of Memorial University of Newfoundland and through NSERC Discovery Grant 238252 awarded to R.Meyer. I would like to thank David Mills and the Canada-Newfoundland and Labrador Offshore Petroleum Board (CNOPB) for their assistance in facilitating the use of the Core Research Centre. I would also like to thank Alison Pye for technical assistance to carry-out isotope analyses, and Helen Gillespie for overall technical support. I would like to thank Steve Kearsey for a seismic line through the study area and James Carter for maps of the field area. Special thanks to Angie Dearin, Erin Gillis, Steve Schwartz and Nicola Tonkin for the thought provoking discussions and constant help along the way. Finally, I would like to thank my parents who have been sources of encouragement throughout my education.

TABLE OF CONTENTS

Abstract	II
Acknowledgements	IV
Table of Contents	V
List of Tables	IX
List of Figures	X
List of Appendices	XVIII

CHAPTER 1 THESIS INTRODUCTION AND BACKGROUND

1.1	Introduction	1
1.2	Geological Setting	4
1.2.1	Evolution of the Grand Banks	4
1.2.2	Jeanne d'Arc Basin	5
1.2.3	White Rose Field	9
1.2.4	Depositional Setting of the Ben Nevis Sandstone	10
1.2.5	Diagenesis of the Ben Nevis Sandstone	11
1.3	Thesis Objectives	14
1.4	Thesis Outline	15

CHAPTER 2 DATABASE AND METHODS

2.1	Introduction	17
2.2	Core Logging	17
2.3	Petrography	18
2.3.1	Optical Microscopy	19
2.3.2	Cathodoluminescence Microscopy	19
2.4	Geochemistry (Carbon and Oxygen Isotopes)	20

CHAPTER 3 DESCRIPTION OF THE BEN NEVIS FORMATION

3.1	Introduction	22
3.1.1	White Rose F-04	22
3.1.2	White Rose B-07_4	24
3.2	Well Selection	24
3.3	General Core Description	26
3.3.1	Upper Ben Nevis (Bioturbated Mudstones)	28
3.3.2	Upper Ben Nevis (Silty mudstones interbedded with siltstones and very fine grained sandstones)	28
3.3.3	Ben Nevis Sandstone (Parallel laminated to low-angle cross laminated sandstone)	32
3.3.4	Bioclastic Sandstone	34
3.3.5	Basal Unconformity and underlying marlstone	37
3.3.6	Calcite Concretions General description	39
3.3.6.1	Size and Distribution of Calcite Concretions	39

3.3.6.2	Cementation Intensity	40
3.3.6.3	Concretion Boundaries	44
3.3.6.4	Concretion Nucleation Sites	47
3.3.7	Calcite Veins	49
3.3.8	Siderite Concretions	49
3.4	Discussion	49
CHAPTER 4	PETROGRAPHY	
4.1	Introduction (With basis for sampling) and Outline	58
4.2	Rock Classification	58
4.3	Sandstone Mineralogy	59
4.3.1	Framework \ Detrital Minerals	60
4.3.1.1	Quartz	60
4.3.1.2	Feldspar	63
4.3.1.3	Rock Fragments	63
4.3.1.4	Accessory Minerals	69
4.3.1.4.1	Glauconite	69
4.3.1.4.2	Carbonaceous Material	71
4.3.1.4.3	Opaques	71
4.3.1.5	Bioclastic Fragments	71
4.3.1.5.1	Pelecypods (bivalves)	73
4.3.1.5.2	Serpulid Worm Tubes	73
4.3.1.5.3	Gastropods	77
4.3.1.5.4	Brachiopods	77
4.3.1.5.5	Corals	79
4.3.1.5.6	Bryozoans	79
4.3.1.5.7	Unidentified Shell Species	79
4.3.2	Matrix	82
4.3.3	Authigenic / Diagenetic Components	82
4.3.3.1	Calcite Cement	84
4.3.3.1.1	Non-Ferroan Calcite Cement	84
4.3.3.1.2	Ferroan Calcite Cement	87
4.3.3.2	Siderite Cement	89
4.3.3.3	Quartz Overgrowths	92
4.4	Diagenetic Sequence Based on Petrographic Observations	93
4.4.1	Introduction	93
4.4.2	Recycled Quartz Overgrowths	96
4.4.3	Early Shell Dissolution	98
4.4.4	Early Non-Ferroan Calcite Cement	100
4.4.5	Early Pyrite and Siderite Cement	103
4.4.6	Dissolution of Quartz Grains	105
4.4.7	Ferroan Calcite Cement	106
4.4.8	Early Feldspar Dissolution	110
4.4.9	Calcite Veins	111
4.4.10	Siderite Dissolution	111

4.4.11	Compaction of Uncemented Sediments	114
4.4.12	Dissolution of Ferroan Calcite Cement	114

CHAPTER 5 GEOCHEMISTRY

5.1	Introduction to Isotopes and Stable Isotope Geochemistry	116
5.2	Limitations of Carbon and Oxygen Isotopes	116
5.3	Carbon Isotopes	117
5.3.1	Carbonate Source	119
5.3.2	Results	122
5.3.2.1	Muddy Siltstones above the Ben Nevis Formation	124
5.3.2.2	White Rose Shale below the Ben Nevis Formation	125
5.3.2.3	Rankin Formation	126
5.3.2.4	Skeletal shell debris and detrital carbonate grains of the Ben Nevis Formation	129
5.3.2.5	Isotopic Pattern Across Concretion	133
5.4	Oxygen Isotopes	133
5.4.1	Paleo-thermal Reconstructions and Precipitation Temperatures	140
5.4.2	Results	145
5.4.2.1	Skeletal shell debris and detrital carbonate grains of the Ben Nevis Formation	145
5.4.2.2	Muddy Siltstones above the Ben Nevis Formation	148
5.4.2.3	White Rose Shale below the Ben Nevis Formation	149
5.4.2.4	Rankin Formation	150
5.4.2.5	Isotopic Pattern Across Concretion	151

CHAPTER 6 INTEGRATION OF RESULTS

6.1	Introduction	154
6.2	Stratigraphy and Depositional Environment	154
6.3	Distribution and Abundance of Shells	156
6.4	Sedimentation Rate	160
6.5	Early Burial Diagenesis	161
6.5.1	Role of Burial Rate	161
6.5.2	Pore Fluid Composition	162
6.5.3	Dissolution of Aragonite Shells	164
6.6	Fluid Transport	165
6.7	Formation of Concretions	168
6.8	Paragenetic Sequence	171
6.8.1	Quartz Overgrowths	171
6.8.2	Dissolution of Aragonite Shells	171
6.8.3	Dissolution of Detrital Feldspar Grains	172
6.8.4	Precipitation of Siderite Cement	172
6.8.5	Precipitation of Non-Ferroan Calcite Cement	173
6.8.6	Dissolution of Detrital Quartz Grains	173

6.8.7	Precipitation of Ferroan Calcite Cement	174
6.8.8	Calcite Veins	174
6.8.9	Dissolution of Ferroan Calcite Cement	175
6.9	Impact on Reservoir Quality	175
6.10	Future Research	176
CHAPTER 7	CONCLUSIONS	
7.1	Conclusions	179
REFERENCES		182
APPENDICES		
Appendix A:	Calcite Cemented Concretions	201
Appendix B:	Modal Analyses for Thin Sections	209
Appendix C:	Carbon and Oxygen Isotope Results	214

LIST OF TABLES

Table 3.1:	Formation depths (TVD), gas/oil contacts and corresponding gas and oil zone thickness for WR F-04 and WR B-07_4 (<i>Husky Picks</i>).-----	27
Table 3.2	Lithology Types found in WR F-04 and WR B-07_4 with corresponding core interval, thickness and percentage of core.-----	27
Table 3.3	Concretion Boundary Divisions-----	45
Table 3.4	Various types of nucleation sites-----	48
Table 5.1	$\delta^{13}\text{C}$ values for wells B-07_4 and F-04-----	129
Table 5.2	Sample types, average $\delta^{18}\text{O}$ shifts and corresponding paleo temperatures. The addition of cement and shells is a bulk sample analysis which has difficulties in applying $\delta^{18}\text{O}$ shifts but clearly indicates that values for the mixture is found between the two individual populations. The detrital carbonate grains may be harder to interpret, as the provenance of such is unknown.-----	146

LIST OF FIGURES

Figure 1.1:	Mesozoic sedimentary basins and structural framework of the Grand Banks rift margin. Modified after Tankard and Welsink, 1987; Enachescu, 1990; and McAlpine, 1990.-----	2
Figure 1.2:	White Rose Field, Top of Ben Nevis Depth Structure with well locations. From Husky, 2005.-----	3
Figure 1.3:	Stratigraphic Sequence and Petroleum Systems Event Chart for the Jeanne d'Arc Basin (modified from Parnell, 2001).-----	7
Figure 3.1:	Interpretive litholog of the White Rose F-04 well.-----	23
Figure 3.2:	Interpretative litholog of White Rose B-07_4.-----	25
Figure 3.3:	General lithologies found in the WR F-04 and WR B-07_4 cores. A: Bioturbated mudstone (WRF-04, Core 1, Box 6) 4.5 % of core; B: Interbedded silty mudstone and sandstone (F-04, Core 1, Box 17) 1.3 % of core; C: Parallel laminated to low angle cross bedded sandstone (F-04, Core 1, Box 55) 78.8 % of core; D: Bioclastic sandstone (B-07_4, Core 2, Box 22) 2.5 % of core and E: Marlstone (B-07_4, Core 3, Box 13) 13.0 % of core. (5.25" Core).-----	29
Figure 3.4	Characteristics of the Upper Ben Nevis–Bioturbated mudstones:A. Intense Bioturbation, F-04, Core 1, Box 1; B. Rare bivalve shells and serpulid worm tubes, F-04, Core 1, Box 3; C. Rare bivalves and serpulid worm tubes, F-04, Core 3, Box 5; and D. Conichnus, F-04, Core 1, Box 2.-----	30
Figure 3.5	Characteristics of the Upper Ben Nevis – Silty mudstones inter-bedded with siltstones and very fine grained sandstones: A. Massive sandstone beds with rare fractures, F-04, Core 1, Box 12; B. Sharp and irregular contacts, F-04, Core 1, Box 12; C. Bioclastic debris possibly acting as a nucleation site for siderite cement, F-04, Core 1, Box 13.-----	31
Figure 3.6	Characteristics of the main Ben Nevis sandstone: A. Low-angle cross-bedding, B-07_4, Core 1, Box 3; B. Longitudinal section of a serpulid worm tube; B-07_4, Core 2, Box 6; C. Large bivalve, B-07_4, Core 2, Box 22; and D. Thin, black, partially dissolved shells, B-07_4, Core 1, Box 62.-----	33

Figure 3.7	Characteristics of the bioclastic sandstone interval. A. Serpulid worm tubes, B-07_4, Core 2, Box 22; B. In-situ bivalve (Hinge down), B-07_4, Core 2, Box 22; C. Cephalopoda and gastropoda, B-07_4, Core 2, Box 22; and D. Coral, B-07_4, Core 2, Box 25.-----	35
Figure 3.8	Mass movement features and soft sediment deformation from bioclastic sandstone interval: A. Fracture zone, B-07_4, core 2, Box 21; and B. Slump movement, B-07_4, Core 2, Box 22.-----	36
Figure 3.9	Depositional environment of the Ben Nevis Formation at the White Rose Field, modified from Husky, White Rose Development Plan, 2001 and Aigner, 1985.-----	38
Figure 3.10	Relative frequency distribution of concretion sample size.-----	41
Figure 3.11	Concretion sample size, depth decreasing from left to right. Note decreasing concretion size trends moving up-section.-----	41
Figure 3.12	Varying cementation intensities found in the Ben Nevis Formation. A. Very well cemented concretion, B-07_4, Core 2, Box 61; B. Well cemented, F-04, Core 3, Box 31; C. Moderately cemented, F-04, Core 1, Box 38 and D. Partial cementation, F-04, Core 2, Box 22.-----	42
Figure 3.13	Cementation intensity vs. concretion thickness demonstrating decreasing cementation intensity with depth, possibly related to degree of cementation or cement preservation.-----	43
Figure 3.14	Cementation intensity vs. concretion boundary divisions demonstrating sharp boundaries for well cemented concretions and gradational boundaries for moderate to partially cemented concretions.-----	46
Figure 3.15	Types of nucleation sites for varying degrees of cementation. UNS (Upper Nucleation Site), CNS (Central Nucleation Site), LNS (Lower Nucleation Site), U&LNS (Upper and Lower Nucleation Sites), HNS (Homogeneous Nucleation site), NONE (No Nucleation Site), CV (Calcite Veins) and SS (Single Shell).-----	48
Figure 3.16	Calcite Veining. A. F-04, Core 1, Box 35, B. B-07_4, Core 2, Box 10, C. Stratigraphically confined calcite cement, B-07_4, Core 3, Box 5; and D. Zoned calcite cement, B-07_4, Core 3, Box 3.-----	50
Figure 3.17	Siderite cementation in various forms. A. Siderite concretion at bioclastic horizon, F-04, Core 1, Box 5; B. Siderite cement replacing lining of	

Ophiomorpha trace, F-04, Core 1, Box 20; C. Siderite cement following bioturbation, F-04, Core 1, Box 25; and D. Siderite concretions, F-04, Core 1, Box 56.-----51

- Figure 4.1 Quartz grains are the dominant framework grains A. Quartz grains surrounded by poikilotopic calcite cement, Cross Polars (B-07_4 Core 2, Box 10, TS 124; B. Sutured grain boundaries (B-07_4, Core 1, Box 73, TS 13); C. Fracture of quartz grains due to compaction (B-07_4, Core 1, Box 35, TS 149) D. Sub-angular to sub-rounded, good porosity and permeability (B-07_4 Core 1, Box 65, TS 207).-----61
- Figure 4.2 Quartz Overgrowths. A. Cathodoluminescence demonstrating two separate episodes of quartz precipitation (B-07_4 Core 1, Box 39, TS 144), B. Same as A in PPL, C. Same as A using ICP digital analysis to highlight quartz overgrowths; and D. Well developed quartz overgrowth prior to early calcite cementation, (F-04, Core 1, Box 73, TS 173).-----62
- Figure 4.3 Quartz Dissolution A. Quartz islets (F-04 Core 1, Box 37, TS 171), B. Embayments in quartz grains (F-04 Core 1, Box 47, TS 176), C. Quartz dissolution with embayments and quartz islets (F-04 Core 1, Box 48, TS 177) and D. Quartz dissolution and replacement by calcite cement? (F-04 Core 1, Box 48, TS 178).-----64
- Figure 4.4 Feldspar Grains . A. F-04 Core 1, Box 28, TS 151 B. F-04 Core 1, Box 35, TS 148 C. F-04 Core 1, Box 4, TS 158 ; and D. F-04 Core 1, Box 4, TS 158.-----65
- Figure 4.5 Feldspar Dissolution and replacement. A. Feldspar dissolution, (F-04, Core 1, Box 13, TS 162), B. Feldspar replacement with ferroan calcite cement, (F-04, Core 2, Box 65, TS 205), C. Feldspar dissolution (B-07_4, Core 1, Box 25, TS 152), and D. Feldspar replacement (B-07_4, Core 2, Box 10, TS 123).-----66
- Figure 4.6 Lithic Rock Fragments A. Silty carbonate grain, well rounded and eroded, possibly from the underlying Rankin Formation (B-07_4 Core 2, Box 24, TS 209) B. Opaque grain (F-04 Core 1, Box 37, TS 170), C. Chert grain (F-04 Core 1, Box 35, TS 149); and D. Chert grain (F-04 Core 1, Box 59, TS 140).-----67
- Figure 4.7 Detrital Carbonate grains A. F-04, Core 1, Box 28, TS 165 B. F-04, Core 2, Box 44, TS 199 C. F-04, Core 1, Box 47, TS 175 ; and D. B-07_4, Core 1, Box 65, TS 207.-----68
- Figure 4.8 Accessories A. Glauconite Grain (F-04 Core 1, Box 13, TS 162) B. Glauconite with cement rim (F-04 Core 1, Box 5, TS 160) C. Wood

fragment (F-04 Core 1, Box 9, TS 161); and D. Close-up of wood fragment. (F-04 Core 1, Box 9, TS 161).-----70

Figure 4.9 Shell Dissolution, source of carbonate. A. Dissolution and stylolization features; (F-04, Core 1, Box 44, TS 172), B. Opaques are commonly found within shells producing thin discontinuous intervals when shell is completely dissolved; (F-04, Core 1, Box 49, TS 179), C. Preferential dissolution in the direction of compaction; (F-04, Core 1, Box 60, TS 186), and D. Nearly complete dissolution of shells leaving behind opaques (F-04, Core 2, Box 29, TS 194).-----72

Figure 4.10 Bivalve Shells A. Foliated microstructure composed of random oriented bundles of thin calcite lamellae (F-04 Core 1, Box 28, TS 164) B. Complex crossed lamellar microstructure (F-04 Core 1, Box 37, TS 170) C. Multi-layer, foliated microstructure bivalve shell (F-04 Core 1, Box 37, TS 178) ; and D. Three layered foliated ridged bivalve shell (B-07_4 Core 1, Box 28, TS 151).-----74

Figure 4.11 Serpulid Worm Tubes . A. Transverse cut through colony of worm tubes (F-04 Core 1, Box 28, TS 165), B. Dissolution on the outer edge of worm tube (F-04 Core 2, Box 10, TS 190), C. Oblique cut through worm tube possibly identifying cone in cone structure of outer layer (F-04 Core 2, Box 45, TS 200; and D. Same as C with increased magnification (F-04 Core 2, Box 45, TS 200).-----76

Figure 4.12 Gastropods. A. Gastropod shell replaced with ferroan calcite cement (F-04 Core 2, Box 10, TS 188), B. Gastropod shell (F-04 Core 2, Box 30, TS 195), C. Gastropod shell partially replaced but retaining the original structure (B-07_4 Core 1, Box 3, TS 159); and D. Gastropod shell under compaction (B-07_4 Core 1, Box 8, TS 157).-----78

Figure 4.13 Brachiopods and Corals A. Transverse section through a pentamerid Brachiopod (F-04 Core 2, Box 10, TS 188), B. Pentamerid Brachiopod (B-07_4 Core 1, Box 8, TS 165), C. Transverse section through a solitary rugose coral (F-04 Core 1, Box 35, TS 167); and D. Coral? (B-07_4 Core 1, Box 17, TS 208).-----80

Figure 4.14 Unidentified shell species. A. Gastropod? (F-04 Core 1, Box 35, TS 167) B. Cricoconarid or Scaphopod (F-04 Core 1, Box 37, TS 171), C. Bivalve? (F-04 Core 2, Box 10, TS 189); and D. Echinoid Fragment? (B-07_4 Core 1, Box 59, TS 140).-----81

Figure 4.15 Clay Minerals A. F-04 Core 1, Box 44, TS 172 B. F-04 Core 1, Box 49, TS 180 C. F-04 Core 1, Box 57, TS 181 ; and D. F-04 Core 1, Box 57, TS 182.-----83

- Figure 4.16 Non Ferroan Calcite Cement. A. F-04 Core 2, Box 59, TS 204 B. F-04 Core 2, Box 65, TS 205 C. F-04 Core 2, Box 65, TS 205 ; and D. F-04 Core 1, Box 35, TS 168.-----85
- Figure 4.17 Distinct zonation between non-ferroan bioclasts, slightly ferroan cement and strongly ferroan calcite cements. A. Predominantly ferroan calcite cement, (B-07_4, Core 2, Box 11, TS 122), B. Non ferroan bioclast surrounded by slightly ferroan calcite cement (mauve) gradually converting to strongly ferroan calcite cement, (B-07_4, Core 2, Box 10, TS 123), C. Strongly ferroan calcite cement precipitaing on slightly ferroan calcite cement (B-07_4, Core 2, Box 5, TS 126); and D. Calcite veins under catholuminescence showing four stages of cementation, (B-07_4, Core 2, Box 10, TS 124).-----86
- Figure 4.18 Ferroan calcite cement. A. F-04 Core 1, Box 58, TS 183 B. F-04 Core 2, Box 44, TS 199 C. F-04 Core 2, Box 45, TS 200 ; and D. F-04 Core 2, Box 65, TS 205.-----88
- Figure 4.19 Late ferroan calcite cement. A. (B-07_4, Core 2, Box 11, TS 122), B. (B-07_4, Core 2, Box 11, TS 122), C. (B-07_4, Core 2, Box 5, TS 126) and D. (B-07_4, Core 1, Box 82, TS 130).-----90
- Figure 4.20 Siderite cementation in various forms. A. Siderite infilling gastropod shell, possibly developing on an organic substrate; (B-07_4, Core 1, Box 37, TS 146), B. Siderite infilling shell opening; (F-04, Core 1, Box 22, TS 163) C. Siderite crystals growing individually within open pore space; (F-04, Core 1, Box 60, TS 186) and D. Siderite cement completely replacing bioclastic material; (F-04, Core 1, Box 60, TS 186).-----91
- Figure 4.21 Seismic line North – South through White Rose Field, demonstrating the erosion of sediments allowing the Ben Nevis Formation to lie unconformably above the Rankin Formation.-----95
- Figure 4.22 Plan map of seismic line through White Rose Field.-----95
- Figure 4.23 Paragenetic Sequence for the Ben Nevis Formation at the White Rose Field.-----97
- Figure 4.24 Moldic Porosity A. F-04, Core 1, Box 5, TS 160, B. F-04, Core 1, Box 5, TS 160, C. F-04, Core 1, Box 5, TS 160 and D. F-04, Core 2, Box 28, TS 193.-----99
- Figure 4.25 Recrystallized Shells. A. Partially recrystallized serpulid worm tube (F-04 Core 1, Box 35, TS 168), B. Recrystallization of large shell demonstrating

an increase in crystal size towards the center (F-04 Core 1, Box 47, TS 176), C. Close-up of sparry calcite (F-04 Core 1, Box 47, TS 176); and D. Selective recrystallization of one shell layer (F-04 Core 2, Box 32, TS 196).-----101

Figure 4.26 Dissolution Boundaries. A. Sharp irregular dissolution boundary (F-04, Core 1, Box 31, TS 166, B. Gradual dissolution boundary (F-04, Core 2, Box 28, TS 193, C. Breached dissolution boundary (F-04, Core 2, Box 29, TS 194) and D. Remnants of a shell acting as a dissolution boundary (F-04, Core 2, Box 59, TS 204).-----107

Figure 4.27 Siderite dissolution and possible source for late stage ferroan calcite cement. A. Dissolution of siderite and precipitation of late ferroan calcite cement, (F-04, Core 1, Box 13, TS 162), B. Dissolution of euhedral siderite crystal, (B-07_4, Core 2, Box 6, TS 125), C. Siderite dissolution and precipitation of ferroan ferroan calcite cement (B-07_4, Core 1, Box 37, TS 146) and D. Dissolution of siderite and precipitation of ferroan calcite cement (B-07_4, Core 2, Box 6, TS 125).-----109

Figure 4.28 Micro-Fractures. A. F-04, Core 1, Box 35, TS 167, B. F-04, Core 1, Box 35, TS 168 C. F-04 Core 1, Box 47, TS 176 and D. F-04, Core 2, Box 44, TS 199.-----112

Figure 4.29 Compaction. A. Early compaction preserving the delicate shell structure, (F-04, Core 1, Box 58, TS 188). B. Planar grain boundaries, (F-04, Core 1, Box 58, TS 184), C. Difference in compaction between the cemented and uncemented sandstone, (F-04, Core 2, Box 7, TS 187) and D. Slight compaction of shell structures demonstrating the variable nature of compaction, (F-04, Core 2, Box 16, TS 192).-----113

Figure 4.30 Calcite Dissolution A. Dissolution of Non-Ferroan calcite cement (F-04, Core 1, Box 5, TS 160), B. Dissolution of Ferroan calcite cement (F-04, Core 1, Box 5, TS 160), C. Dissolution of Ferroan calcite cement (F-04, Core 1, Box 5, TS 160) and D. Dissolution of Ferroan calcite cement (F-04 Core 1, Box 49, TS 179).-----115

Figure 5.1 Geochemical Zones from Marine Sediments during progressive burial. Diagenetic carbonates can become imprinted during precipitation allowing recognition of the particular geochemical zone within which they formed. As burial begins, sediments move from the oxic zone to the sub-oxic zone which includes manganese, iron and bacterial sulphate reduction, followed by microbial methanogenesis and finally at temperatures greater than 75°C into the thermal decarboxylation zone, (Modified from Morad, 1998).-----118

Figure 5.2	Location of carbon isotopes relative to lithologic core of WR F-04.-----	120
Figure 5.3	Location of carbon isotopes relative to lithologic core of WR B-07_4.-	121
Figure 5.4	Variation of $\delta^{13}\text{C}$ (VPDB) values throughout the Phanerozoic, demonstrating a range of +1.5 to +3.3 during the Albian when the Ben Nevis Formation was deposited. Modified from Veizer et al. (1999).---	123
Figure 5.5	Plot of $\delta^{18}\text{O}$ versus $\delta^{13}\text{C}$ above the Ben Nevis Reservoir in muddy siltstones, dashed red lines represents marine biogenic calcium carbonate of Albian age.-----	125
Figure 5.6	Plot of $\delta^{18}\text{O}$ versus $\delta^{13}\text{C}$ for samples below the Ben Nevis Formation, White Rose B-07_4, dashed red lines represents marine biogenic calcium carbonate of Albian age.-----	126
Figure 5.7	Plot of $\delta^{18}\text{O}$ versus $\delta^{13}\text{C}$ for samples from Rankin M-16 and Archer K-19 within the Rankin Formation, dashed red lines represents marine biogenic calcium carbonate of Kimmeridgian age.-----	128
Figure 5.8	Plot of $\delta^{18}\text{O}$ versus $\delta^{13}\text{C}$ for samples containing <i>both calcite cement and shell debris</i> from wells F-04 and B-07_4, red dashed lines represent marine biogenic calcium carbonate of Albian age. -----	130
Figure 5.9:	Plot of $\delta^{18}\text{O}$ versus $\delta^{13}\text{C}$ for samples containing <i>calcite cement</i> from wells F-04 and B-07_4, red dashed lines represent marine biogenic calcium carbonate of Albian age.-----	130
Figure 5.10	Plot of $\delta^{18}\text{O}$ versus $\delta^{13}\text{C}$ for samples containing <i>shells</i> from wells F-04 and B-07_4, red dashed lines represent marine biogenic calcium carbonate of Albian age.-----	130
Figure 5.11	Plot of $\delta^{18}\text{O}$ versus $\delta^{13}\text{C}$ for samples <i>not containing shells or calcite cement</i> from wells F-04 and B-07_4, red dashed lines represent marine biogenic calcium carbonate of Albian age.-----	130
Figure 5.12	Distribution of carbon isotopic results across a concretion demonstrating the relatively depleted central nucleation site, subsequent enrichment outside the center and minor relative depletion towards the edge of the concretion. Graph to the right demonstrates the symmetric pattern of carbon isotopes within the concretion.-----	134

Figure 5.13	Central nucleation site of the above concretion. The relative depletion of carbon isotopes may represent the preservation of Albian shells and their marine biogenic calcium carbonate signature.-----	135
Figure 5.14	Variation of $\delta^{18}\text{O}$ (VPDB) values throughout the Phanerozoic, demonstrating a range of -1.25 to -0.75 during the Albian when the Ben Nevis Formation was deposited. Modified from Veizer et al. (1999).---	138
Figure 5.15	Location of oxygen isotopes relative to lithologic core of WR F-04.----	141
Figure 5.16	Location of oxygen isotopes relative to lithologic core of WR B-07_4.-	142
Figure 5.17	Plot of $\delta^{13}\text{C}$ versus $\delta^{18}\text{O}$ for samples containing <i>both calcite cement and shell debris</i> from wells F-04 and B-07_4.-----	147
Figure 5.18	Plot of $\delta^{13}\text{C}$ versus $\delta^{18}\text{O}$ for samples containing <i>calcite cement</i> from wells F-04 and B-07_4.-----	147
Figure 5.19	Plot of $\delta^{13}\text{C}$ versus $\delta^{18}\text{O}$ for samples <i>not containing unaltered shells or calcite cement</i> from wells F-04 and B-07_4.-----	147
Figure 5.20	Plot of $\delta^{13}\text{C}$ versus $\delta^{18}\text{O}$ above the Ben Nevis Reservoir in muddy siltstones.-----	148
Figure 5.21	Plot of $\delta^{18}\text{O}$ versus $\delta^{13}\text{C}$ for samples below the Ben Nevis Formation, White Rose B-07_4.-----	149
Figure 5.22	Plot of $\delta^{18}\text{O}$ versus $\delta^{13}\text{C}$ for samples from Rankin M-16 and Archer K-19 within the Rankin Formation.-----	151
Figure 5.23	Distribution of carbon isotopic results across a concretion demonstrating an initial increase of paleo-temperature from the center to the middle of the concretion followed by a decrease in paleo-temperature towards the outer edges of the concretion.-----	153
Figure 6.1	Schematic demonstrating two possible fluid flow mechanisms responsible for transfer of calcium carbonate enriched pore fluids. A) Vertical flow occurs after sufficient burial cause dissolution of shell debris in the lower Ben Nevis Fm. B) Oblique flow from site of strong aragonite dissolution within distal shoreface in the direction of the shoreline as a result of compaction of the Nautilus Shale.-----	159

LIST OF APPENDICES

Appendix A: Analysis of Calcite Cemented Concretions-----	201
Appendix B: Thin Section Modal Analysis -----	209
Appendix C: Carbon and Oxygen Isotope Results-----	214

CHAPTER 1

THESIS INTRODUCTION AND GEOLOGIC BACKGROUND

1.1 Introduction

The focus of this investigation is the paragenetic sequence of permeability inhibiting or preserving authigenic cements found in the Ben Nevis Formation sandstone of the White Rose Field, Jeanne d'Arc Basin, offshore Newfoundland. Knowledge of the diagenetic history is of great importance to understand what conditions are required to develop economic permeability, ultimately assisting in future exploration. The main factors controlling porosity and permeability are the original fabric and composition of the sediments, and diagenetic processes they encounter but easy solutions to porosity and permeability prediction are very much limited by current understanding of diagenetic processes (Horbury and Robinson, 1993).

This thesis uses core description, together with optical petrography and stable isotope geochemical analyses to derive the diagenetic evolution of this irregularly cemented reservoir sandstone in order to gain insight into the distribution and extent of cementation. This chapter provides a reconstruction of the formation of the sedimentary basins skirting the shelf and slope of the Grand Banks (Figure 1.1), concentrating on the Jeanne d'Arc Basin with special consideration for the stratigraphy and structure of the White Rose Field (Figure 1.2). Previous work on the depositional setting and diagenesis of the Ben Nevis sandstone will also be introduced followed by a summary of thesis objectives and a thesis outline.

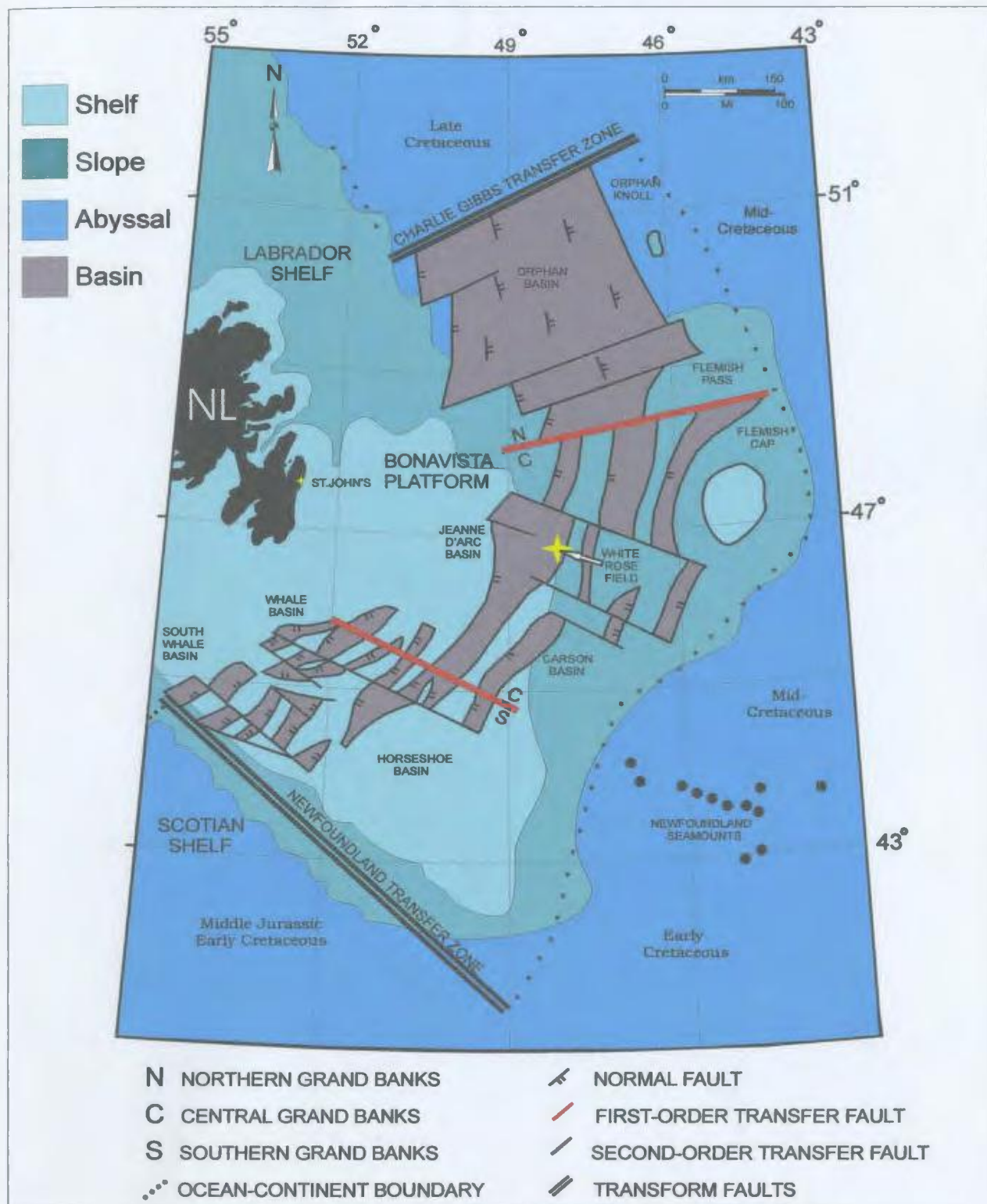


Figure 1.1 Mesozoic sedimentary basins and structural framework of the Grand Banks rift margin. (Modified after Tankard and Welsink, 1987; and McAlpine, 1990.)

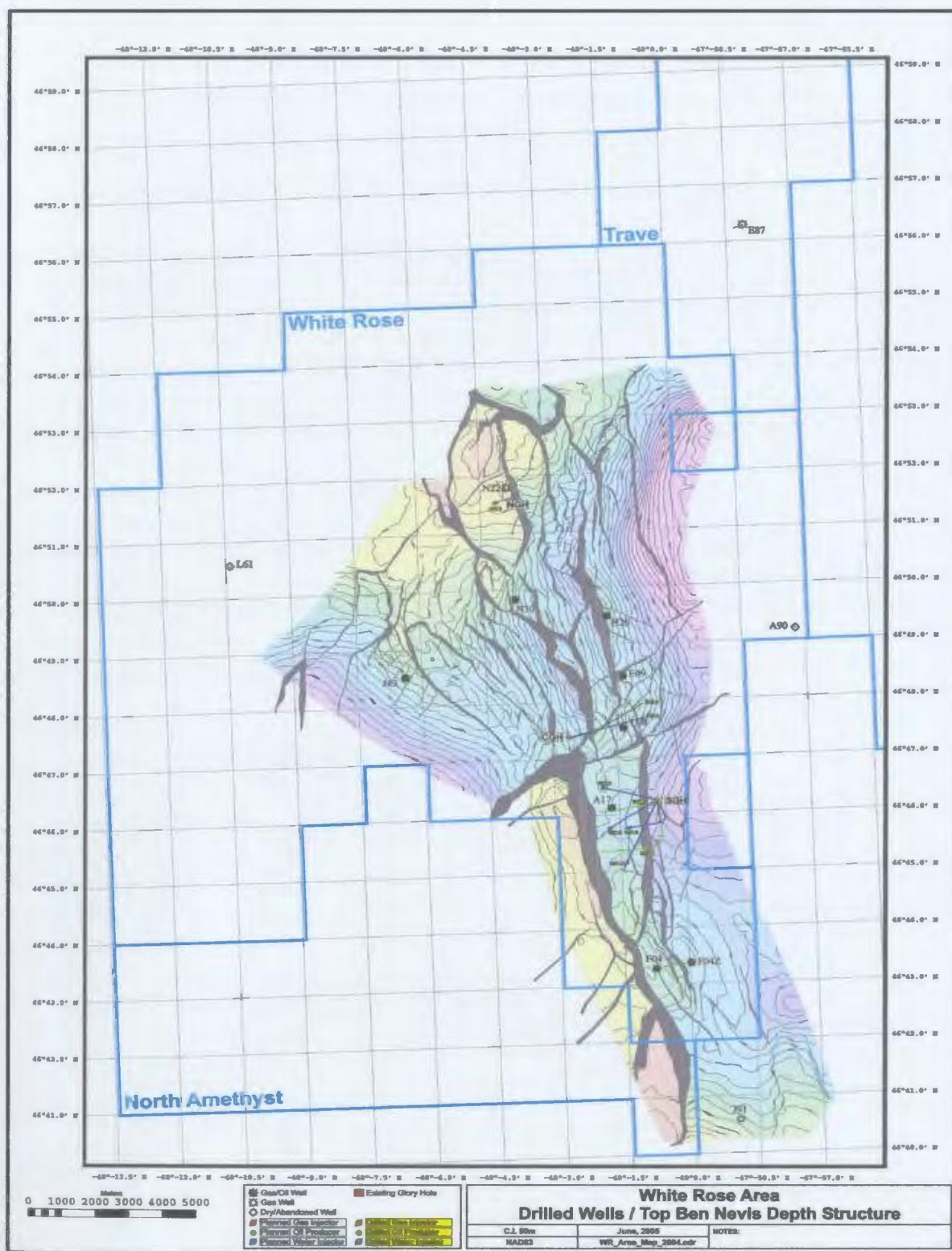


Figure 1.2 White Rose Field, Top of the Ben Nevis Depth Structure with well locations, (Husky, 2005.)

1.2 Geologic Setting

The Mesozoic sedimentary basins offshore Newfoundland's East Coast developed as a northeast-advancing rift system and sequential continental margin advancement divided Pangea to form the North Atlantic Ocean. This intracontinental failed double rift arm produced a sequence of interconnected basins with a maximum thickness of nearly 20 km of sedimentary rocks corresponding to extensional and thermal subsidence phases (Enachescu, 1987). The tectonic history of the Grand Banks margin is amagmatic (Louden and Chian, 1999) and the distribution of its basins has been well documented (Haworth and Keen, 1979; McMillan, 1982; Hubbard *et al.*, 1985; Tankard and Welsink, 1987; Enachescu, 1987; Sinclair, 1988). The interpretation has evolved into a three-stage rift sequence which, combined with salt tectonics, has complicated the differential deposition, erosion and subsidence, of the sedimentary strata.

The broad continental shelf of the Grand Banks with a maximum width of 500 km is separated from the narrow continental shelf of Labrador to the north (170 km maximum) by the Charlie Gibbs Fracture Zone, and from the Scotian Shelf to the south by the Newfoundland Transfer Zone (Figure 1.1). The major east-west confines of the Grand Banks basins include the Bonavista Platform to the west and the abyssal plain of the North Atlantic to the east.

1.2.1 Evolution of the Grand Banks

Three episodes of rifting and their associated continental break-ups have been identified in the stratigraphic record of the Grand Banks (Haworth and Keen, 1979;

Enachescu, 1987; Sinclair, 1988). The initial phase records the break-up of North America and Africa, initiated by northwest-southeast trending Triassic to Early Jurassic rifting. The second occurrence of rifting followed an east-west trend as the Grand Banks separated from Iberia during the Late Jurassic to the Early Cretaceous. The final rifting stage caused the division of the Orphan Knoll and Europe throughout the late Early Cretaceous with north-east southwest extension (Keen *et al.*, 1987; Tankard and Welsink, 1988). Overall the three phases together record a counter-clockwise rotation in rift direction. Intertwined with the rifting events are four periods of subsidence and two episodes of regional uplift which help define the evolution of the Grand Banks (Enachescu, 1987; Tankard and Welsink, 1989; Grant and McAlpine, 1990; Sinclair, 1995).

1.2.2 Jeanne d'Arc Basin

Although the Jeanne d'Arc Basin has a complicated history of nomenclature, being first described as the Jeanne d'Arc (Jansa and Wade, 1975 a;), followed by the Avalon (Powell, 1984) and finally the East Newfoundland Basin (Ervine, 1984), there is no disputing the world class oil fields that have been discovered there since the late 1970's. The Jeanne d'Arc Basin has petroleum reserves and resources of over 2 billion barrels of oil and over 5 trillion cubic feet of gas with the bulk in four major fields (Hibernia, Terra Nova, Hebron, and White Rose containing 89% of the oil and 76% of the gas) and the remainder in fourteen smaller satellite fields (C-NLOPB, 2004).

East Coast production from the Jeanne d'Arc Basin totaled 35 % of Canadian light/medium conventional oil in 2004. With declining reserves in western Canada and the beginning of production in the White Rose Field in late 2005, East Coast production is forecast to jump to 43 % during the first quarter of 2006 (www.cnlopb.nl.ca, 2004 and www.capp.ca, 2004, 2005 Canadian Crude Oil Production and Supply Forecast).

The Jeanne d'Arc Basin is a northeast plunging, trough shaped, half graben located on the edge of the Grand Banks, approximately 300 km east-south-east of St. John's in an average water depth of 110 m. The basin dimensions range from 25 to 80 km wide to 130 km long with a maximum sediment thickness of about 20 km (Enachescu, 1987). The main structural components defining the Jeanne d'Arc Basin are the Bonavista platform to the west, the Cumberland Volcanic Belt to the north, the Central Ridge Complex to the east and the Avalon uplift to the south. The western boundary of the basin is formed by the listric Murre fault (Tankard and Welsink, 1987) whereas the eastern boundary is defined by the antithetic Voyager fault (Deptuck *et al.*, 2003).

Tectonic movements and eustatic sea-level changes are responsible for the thick stratigraphic sequences developed in the Jeanne d'Arc Basin (Figure 1.3), controlling the variations in sediment supply, subsidence, and depositional environment (Sinclair, 1993). Interpretations of the Mesozoic-Cenozoic tectonostratigraphic evolution of the Jeanne d'Arc Basin have been published by Amoco Canada Petroleum and Imperial Oil (1973), Jansa and Wade (1975a, b), Enachescu (1987), Keen *et al.*, (1987, 1990), Tankard and Welsink (1987), Sinclair (1988, 1993), Tankard *et al.*, (1989), Edwards (1990), Grant and

McAlpine (1990), and Driscoll *et al.*, (1995). Although there is broad agreement as to the role that multiple rift events had on the formation of the Jeanne d'Arc Basin, Sinclair (1993) provides a summary on the variability of timing and tectonic interpretations in the published literature. The timing of the various aspects of the Jeanne d'Arc Petroleum System is also shown in Figure 1.3.

During the initial Late Triassic rifting, alluvial fan conglomerates and red beds of the Eurydice Formation were deposited, followed by a period of hyper-saline conditions resulting in the deposition of the Argo Formation, a halite-rich evaporite sequence and finally marine limestones of the Iroquois Formation. The next sequence of sediments developed as a result of thermal contraction during a pause in continental crust extension, depositing shales and carbonates of the Downing, Voyager and Rankin Formations in a continental sea. The Egret Member of the Rankin Formation is interpreted to be the organic-rich source rock for the Jeanne d'Arc petroleum system (Swift and Williams, 1980). A series of transgressive/regressive sequences followed during the Late Jurassic and Early Cretaceous causing the development of the fluvial- dominated Jeanne d'Arc Formation, the deltaic Hibernia Formation, the shallow marine Ben Nevis/Avalon Formations and their distal equivalent shales.

With structural development essentially complete by the Late Cretaceous, continued subsidence and intermittent sediment supply produced predominantly deep water shales with occasional distal turbidites and deep-water chinks throughout the Cenozoic.

1.2.3 White Rose Field

The White Rose Field is the latest field under development in the Jeanne d'Arc Basin, estimated to contain 250 Million barrels of 30 API oil, and 4 Trillion cubic feet of natural gas in the North, West and South pools. It is located approximately 40 km west of Hibernia and 40 km north-east of Terra Nova, on the east side of the Jeanne d'Arc Basin. The White Rose field is structurally complex, forming on a westerly dipping fault fan on the hanging-wall of the Voyager Fault, overlying the Amethyst salt ridge and White Rose diapir (Husky Website, 2004). The main boundaries of the field include the Amethyst Ridge and Grand Bruit Low to the West, the flanks of the White Rose salt dome to the North, and the Voyager Fault Zone to the East. The southern limit of the field is as of yet not completely determined as a result of poor quality seismic data in this area, but has been substantially extended by delineation drilling of the White Rose F-04 and F-04Z sidetrack wells.

With 350 m of sandstone and 100 m of net oil pay, the south Avalon pool is the foundation of the White Rose Field development. The principal reservoir is the Albian age Ben Nevis Formation, which consists of fine to very fine-grained quartzose sandstones deposited in a shallow marine to shoreface setting. The Ben Nevis and Avalon Formations with significant accumulations in nine discovery wells, provide the most consistent hydrocarbon-bearing reservoir in the Jeanne d'Arc Basin (Sinclair, 1993).

1.2.4 Depositional Setting of the Ben Nevis Sandstone

The Ben Nevis Formation is a fining upward transgressive succession that overlies, and has hydraulic continuity with the upward coarsening progradational Avalon Formation. In contrast to the relative inactive faulting during Avalon Formation deposition, the fault growth during Ben Nevis and Nautilus deposition resulted in rapid thickness changes across northwest – southeast faults (DeSilva, 1987 and Sinclair, 1988). Competing rift induced subsidence and high sediment input caused by basin margin uplift preserved a thick package of back barrier/shoreface sandstones (Sinclair, 1993). This regressive/transgressive set, separated by a mid-Aptian unconformity, contains reserves in all discoveries made to date (Pemberton *et al.*, 2001), making it the most prolific reservoir in eastern Canada. On the eastern side of the Jeanne d'Arc Basin, at the White Rose Field, the mid-Aptian Unconformity has eroded the majority of the Avalon Formation resulting in the Ben Nevis Formation containing the bulk of the oil and gas.

The main reservoir facies of the Ben Nevis Formation is a light grey, very fine to fine grained, well sorted, quartz-rich, compositionally and texturally mature sandstone. Plint (1999) divides the Ben Nevis Formation into reservoir and non-reservoir facies. The first non-reservoir facies (Facies 1) consists of interbedded fine grained sandstone, siltstone and bioturbated mudstone, interpreted to be storm deposits on a low-energy muddy shelf in water depths of 20 to 50 m. The second non-reservoir facies (Facies 2) are shelly accumulations, which are typically cemented with calcite cement. This facies is interpreted as the basal lag of major storm events, (White Rose DA Volume 2

{Development Plan}, 2001). Harms *et al.*, 1982, suggest that the average steady state is much less important in determining sediment distribution than are unusual storm events.

The main reservoir facies are Facies 3: Bioturbated fine to very fine silty sandstone, Facies 4: Laminated very fine sandstone, and Facies 5: Bioclastic Sandstone. Facies 3 was deposited in a shallow shelf environment during fair-weather conditions with relatively low sediment supply. Facies 4 is interpreted to be a shoreface setting during intense storms. Plint (1999) interprets Facies 5 as a transgressive deposit that accumulated on the Eastern Shoals Formation by marine erosion associated with the basal Avalon transgression.

1.2.5 Diagenesis of the Ben Nevis Sandstone

The Ben Nevis Formation is the most widely preserved and cored formation deposited in the Jeanne d'Arc Basin during the Cretaceous. Industry and academia have accumulated a small volume of work on the many geological issues concerning the Jeanne d'Arc Basin. One of the omissions in this assemblage is that of sandstone diagenesis which has an enormous impact on reservoir quality. With little information in the literature regarding the diagenetic evolution of the Ben Nevis Formation, the primary objective of this study is to fill the gap of this crucial component for one of the primary reservoirs of the Jeanne d'Arc Basin petroleum system.

While the majority of research is located in oil company archives, there are a few published works (Hutcheon *et al.*, 1985; Lee, 1987; Soliman, 1995; Abid, 1988, 1996; Hesse and Abid, 1998 and Abid *et al.*, 2004). Hutcheon *et al.*, (1985) measured $\delta^{18}\text{O}$ and

$\delta^{13}\text{C}$ of carbonate cement to conclude that cementation of the Avalon Formation sandstone resulted from input of meteoric waters during the formation of the mid-Aptian unconformity. While this is a realistic interpretation for the Avalon Formation, it is not applicable to the Ben Nevis Formation, which is deposited above the mid-Aptian unconformity. Hutcheon *et al.*, (1985) also note that interpretation of paragenesis is difficult due to extensive recrystallization of much of the carbonate.

Lee (1987) determined the source of calcite cements to be the dissolution of fossil fragments and possibly the “A” marker limestone below the Avalon Formation. She also predicted a late diagenetic cementation between 40 to 60 °C and 2.2 km burial depth even though loose compaction of the calcite cemented sandstone was acknowledged. Abid (1988) agreed with Lee (1987) with regards to the source of the calcite cement but disagreed regarding the timing of cementation. He suggested early cement because of loose packing of detrital grains, high minus-cement porosity and the lack of other cements. Abid (1988), had a different interpretation regarding the source of carbonate cementation compared with Hutcheon *et al.*, (1985), suggesting early cementation was the result of hot fluids expelled from shales deep in the basin rather than meteoric input.

Soliman (1995) investigated the sedimentation and fluid flow patterns in the Hibernia rollover-anticline while addressing the origin and paleo-flow of the calcite cementing fluids in the Avalon Formation. The validity of these results may be in question if one follows the purely internal precipitation of calcite hypothesis put forward by Walderhaug and Bjorkum (1998). It would be difficult to address paleo-flow of the precipitating fluids if they are sourced internally from a close distance. Soliman (1995)

also suggested a high chance of concretion interconnection creating laterally continuous boundaries. "Distribution of calcite cement is controlled by facies and stratigraphic position. On the other hand, lateral extension of the calcite cemented beds is the function of continuity and depositional geometry of the host sandstone bodies" (Soliman, 1995, p.212). Facies containing abundant skeletal debris were thought to be the most favourable for calcite precipitation, with the carbonate debris acting as nucleation sites (Soliman, 1995).

Hesse and Abid (1998) assessed the relative timing of calcite cementation through four reservoir sandstones of the Hibernia Field on the basis of petrography and oxygen carbon isotopes. The main conclusion from this study is the increase of secondary porosity with depth from 20 % in the Ben Nevis/Avalon Formation to 80 % in the Hibernia Formation. Hesse and Abid's (1988) interpretation of a meteoric source for the calcite precipitating fluids of the Ben Nevis/Avalon Formation may require additional work owing to insufficient data (only one of the 24 isotope samples was taken from the Ben Nevis Avalon Formation). They also observed an increase in secondary porosity next to shale contacts which may imply fluid transfer from compacting shales rather than meteoric input.

Abid *et al.*, (2004) studied variations in Illite/Smectite diagenesis as a function of burial depth, geothermal gradient, proximity to fault zones and salt diapirs, lithology, uplift, stratigraphy and denudation. This has indirect implications on episodes of fluid flow related to periods of cementation.

The Ben Nevis Formation dominates the eastern side of the Jeanne d'Arc Basin in the White Rose Field, with a major reduction in the thickness of the Avalon Formation, possibly due to erosion by the Avalon Unconformity. Since most previous work concentrates on the Ben Nevis/Avalon Formations in the Hibernia Region, results are not always directly applicable to the Ben Nevis Formation in the east.

1.5 Thesis Objectives

The primary objective of this investigation is to improve knowledge of the paragenetic sequence, relating timing and extent of cementation during eogenesis, telogenesis and/or mesogenesis in the Ben Nevis reservoir sandstone. The concept of diagenesis has been considered by some to originate from Johannes Walther (1860-1937). For a historical discussion and review of this subject, see Larson and Chilingar 1967.

The Glossary of Geology (Jackson, J., ed., 1997) defines diagenesis as:

“all of the chemical, physical and biological changes, modifications or transformations undergone by a sediment after its initial deposition, and during and after its lithification, exclusive of surficial alteration (weathering) and metamorphism. Diagenesis involves addition and removal of material, transformation by dissolution and recrystallization or replacement, or both, and by phase changes (Twenhofel, 1939).”

Each stage of diagenesis may be further complicated by the possible hydrologic regimes in action, defined by Galloway (1984), as meteoric, compactional and

thermobaric. In addition to porosity (ϕ) and permeability (k), diagenetic reactions influence pore size distribution, pore geometry, specific surface area and ion-exchange capacity (Bjørlykke, 1988). To resolve the controlling mechanisms on pore system configuration, distribution of cements must be mapped both vertically and laterally. This will provide insight to vertical and horizontal permeability trends in various diagenetic facies and possibly lead to the development of a more refined reservoir model, which may be applied to the development of the North and West Pools.

Primary authigenic minerals include iron-poor calcite, ferroan calcite, dolomite, siderite, and silica in the form of overgrowths on quartz grains. Hesse and Abid, (1998) estimated that 20% of the Ben Nevis/Avalon sandstone in their five-well study of the Hibernia area were tightly cemented as a result of early ferroan calcite completely occluding porosity. Whereas calcareous cements appear distributed in discrete bodies, quartz overgrowth is dispersed throughout the interval.

This study utilizes core description, petrography and isotopic analysis to examine the diagenetic evolution of authigenic cements found in the Ben Nevis Formation at the White Rose Field

1.6 Thesis Outline

All methods used to create the database for this project are provided in Chapter Two. These include geological core description, petrography and geochemical analyses. This is followed by an overview of core description of the Ben Nevis Formation in Chapter Three. The primary composition and texture of detrital framework grains, matrix

and authigenic cements as described from petrographic observation are discussed in Chapter Four. Carbon and oxygen isotope results are covered in Chapter Five. All results are covered in Chapter Six with a thorough discussion and interpretation and the final chapter reviews all major conclusions and suggests the direction of future research.

CHAPTER 2

DATABASE AND METHODS

2.1 Introduction

This study uses a multidisciplinary approach to produce a model of the diagenetic evolution of the Ben Nevis sandstone in the White Rose field. Data collection commenced with the logging of two wells; development well WR B-07_4 and exploration well WR F-04 (Figures 1.2), totalling 244.60 m of core. This was followed up by a series of petrographic and geochemical analyses designed to develop a paragenetic sequence for the reservoir to document the origin, preservation or dissolution of authigenic cements. During core logging a total of 105 thin-sections, and 118 carbon and oxygen isotope samples were taken throughout the entire reservoir section.

2.2 Core Logging

Megascopic description of core was undertaken at the Core research Center of the Canada-Newfoundland Offshore Petroleum Board and focused primarily of stratigraphic architecture, cement identification and definition of depositional facies, using a 1:50 scale. On the log the following parameters are recorded: depth-core-box, environment classification, facies interpretation, graphic drawing of log, inorganic and biogenic sedimentary structures, major constituents, grain size, sorting, and cement type and abundance.

Well selection was designed to incorporate a representative sampling of the complete Ben Nevis reservoir from its basal contact with the Hibernia Formation shale to the upper

contact with the Nautilus Formation shale. White Rose F-04 is an exploration well which established the presence of additional reserves in a fault block to the south of the main south pool. This well was chosen for logging because the core begins in the muddy siltstones of the Lower Nautilus and continues through the transgressive fining upwards sequence of upper Ben Nevis sandstones. White Rose B-07_4 is a deviated development well, designed for water injection into the south pool and is located 3.5 km north and 100 m west of the F-04 spud position. It was chosen because it cored the corresponding lower half of the Ben Nevis Formation including the basal contact with the underlying White Rose shale. A rough estimate of 10 m overlap occurs between these two wells.

2.3 Petrography

Thin section sampling is concentrated on, but not restricted to, calcite-cemented horizons or “concretions”, with particular emphasis on concretion boundaries but also maintained a larger scale selection from the base of the Ben Nevis Formation to the top. Omni Laboratories Inc. processed 59 thin sections from WR B-07_4 and 46 from WR F-04, impregnating with blue dyed epoxy to identify porosity and applying alizarin red and potassium ferricyanide stains to distinguish ferroan content of calcite cement (Dickson, 1965). Milliken (2006 pers. comm.) stressed the unreliability of stain in determining ferroan content, so the validity of ferroan vs non-ferroan cement must be treated with a healthy suspicion.

2.3.1 Optical Microscopy

Petrographic techniques are used to provide detailed mineralogical composition, textural characteristics and information on post depositional history of sedimentary rocks. Scholle (1979) recognized that the most valuable data collected from petrography, as well as the most complex, is information about the precipitation and dissolution of authigenic cements. For this project a Nikon Eclipse E600 POL polarizing microscope was used with a Nikon DXM 1200F digital camera utilizing Nikon ACT-1 Version 2.62 and Compix Inc. Imaging Systems, SIMPLE PCI version 5.2.1.1609 software.

2.3.2 Cathodoluminescence Microscopy

Cathodoluminescence is used to provide specific information that is not available using other petrographic techniques (e.g., Barker and Kopp, 1991). It is a practical method of distinguishing between detrital and authigenic quartz (Sippel, 1968) or interpreting carbonate cement sequences, "cement stratigraphy" (Evamy, 1969; Meyers, 1974, 1978; Koepnick, 1976; and Machel and Burton, 1991). Cathodoluminescence was used in this study to attempt to distinguish different types of quartz overgrowths as well as distinguishing recycled quartz from previous sedimentary rock and authigenic quartz that formed in-situ. A Nikon petrographic microscope with transmitted and reflected light was used in conjunction with a Nuclide luminoscope, vacuum chamber and a 12 mega pixel Leica DC500 digital camera for cathodoluminescence microscopy.

2.4 Geochemistry (Carbon and Oxygen Isotopes)

A variety of geochemical analytical techniques have are employed in the oil industry to differentiate diagenetic components and interpret the diagenetic sequence to help predict reservoir performance and continuity. In this study carbon and oxygen isotopes are used to establish a source for the dominant pore occluding authigenic cements as well as the timing of cementation.

Stable isotope fractionation is partitioning of an element's isotopes during chemical, physical or biological processes, which can lead to understanding the isotopes behaviour during natural processes (Anderson and Arthur, 1983). Particular fractionations identifiable in authigenic cements can reveal specific environmental or diagenetic processes, which lead to precipitation, determine sources of cements or identify isotopic composition of formation waters. Diagenesis of sedimentary rocks is characterized by widely varying and constantly changing conditions, which can be traced by the sensitivity of carbon and oxygen isotopes. Carbon and oxygen are significant stable isotopes to focus on due to their low atomic weight (isotopic variations are proportional to the relative mass difference of isotopes). They are also two of the most important elements in biological systems, participating in most important geochemical reactions and are components of calcite cement, the main cement in the Ben Nevis sandstone. The procedure for preparation of isotopes follows Al-Aasm *et al.*, (1990).

Sampling focused on cemented horizons, selecting samples throughout the interval with additional samples above and below. Where possible, samples were used from the leftover portions of thin sections if they were in the proper location. Samples were taken

from the core using a hammer and small rock chisel, generally from the outer edge of the core and were approximately 1-2 cm³ in volume (5 to 10 grams weight). Most of the samples are either calcite cement or a mixture of calcite cement and bioclastic shell debris. In addition, there were uncemented samples selected as well as individual shells. Aside from the latter, specific mineral phases were not sampled (e.g. micro-drill or in-situ analyse). Samples were placed in small sample bags, labelled and recorded with depth-core-box. Samples were then crushed in an agate pestle and mortar, requiring only 500 mg for extraction of CO₂ from double-arm reaction vessels under vacuum for subsequent determination of $\delta^{13}\text{C}$ and $\delta^{18}\text{O}$ using the Matt 252 mass spectrometry. The analytical procedure sampled a known standard (NBS-19) after each ten samples. Repeat runs were required when standard deviation of samples was greater than 0.1 ‰.

CHAPTER 3

DESCRIPTION OF BEN NEVIS FORMATION SANDSTONES

3.1 Introduction

Core description provided a lithofacies framework documenting the stratigraphic distribution of calcareous cemented layers and concretions of the Ben Nevis Formation. Logging forms for the complete core of both White Rose F-04 and White Rose B-07_4 were completed at the Canadian-Newfoundland and Labrador Offshore Petroleum Board Core Storage and Research Center at 30-32 Duffy Place, St. John's, Newfoundland and were subsequently digitized using Adobe Illustrator version 10.0 to produce interpretative lithologs of the core (Figures 3.1 and 3.2).

Location and details of the selected wells, along with rationale for well selection will be followed up by a generalized review of lithology and depositional environments. Details of the sedimentology and stratigraphy are bypassed to focus on the various modifiers of the calcite cemented horizons. Diagenetic elements such as concretion size, degree of cementation, contacts and nucleation sites were clearly recognizable in core allowing easy measurement and sampling.

3.1.1 White Rose F-04

White Rose F-04 was a delineation well spud on July 21st, 2003 in 119.4 m water depth by the semi-submersible Glomar Grand Banks, drilling to 2993.6 m measured

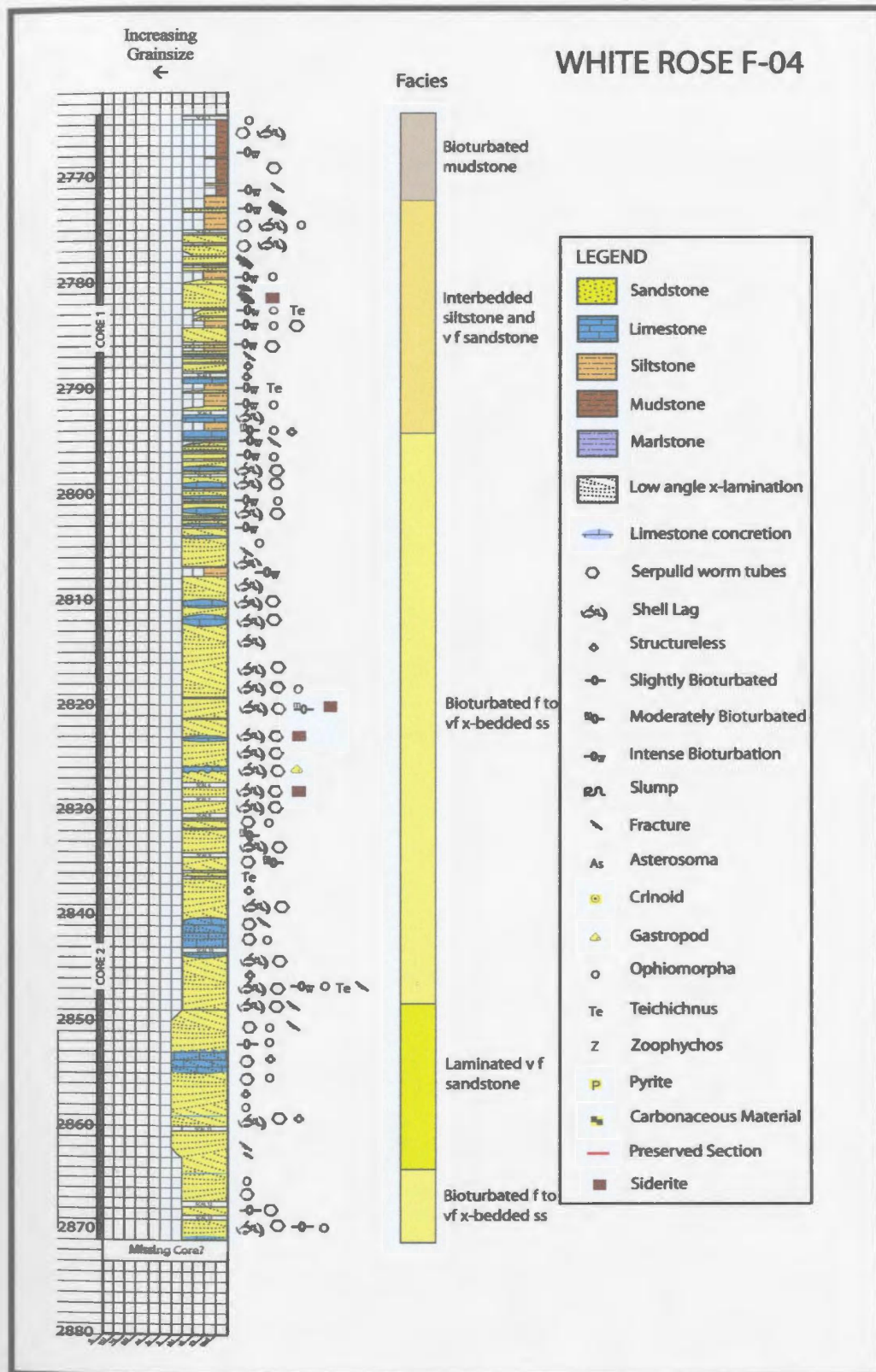


Figure 3.1: Interpretive litholog of the White rose F-04 well.

depth (2988.5 m TVD) by August 29th, 2003 (CNLOPB, Schedule of wells, 2005). White Rose F- 04 is located at the southern limits of the South Pool in a separate fault block, potentially increasing the current estimated recoverable light oil reserves for the White Rose project by approximately 20-30 million barrels (Husky website, 2005). Two cores were taken; Core 1 measured from 2764 m MD to 2818 m MD with 98.7 % recovery and Core 2 measured from 2818 m MD to 2873 m MD with 95.27 % recovery.

3.1.2 White Rose B-07_4

White Rose B-07_4 is a deviated well spud on October 14th, 2003 in 130.7 m water depth, drilling to 3998.0 m MD (3002.4 m TVD) by January 9th, 2004. White Rose B-07_4 is a water injector in the South pool of the White Rose Field. Three cores were taken; Core 1 measured from 3844 m MD to 3914 m MD, Core 2 from 3914 m MD to 3935.7 m MD and Core 3 from 3935.7 m MD to 3982.9 m MD with 96.4 %, 100 % and 100 % recovery, respectively.

3.2 Well Selection

Both wells have over 90 meters of core in the Ben Nevis Formation. The White Rose F-04 well, delineated a separate fault block, drilling through a thicker reservoir section (Table 3.1), with a much larger gas cap, resulting in over 50% reduction in net oil pay when compared to the B-07_4 well. Table 3.1 lists formation depths and gas / oil contact depths for both wells, along with reservoir thicknesses and net pay.

WHITE ROSE B-07_4

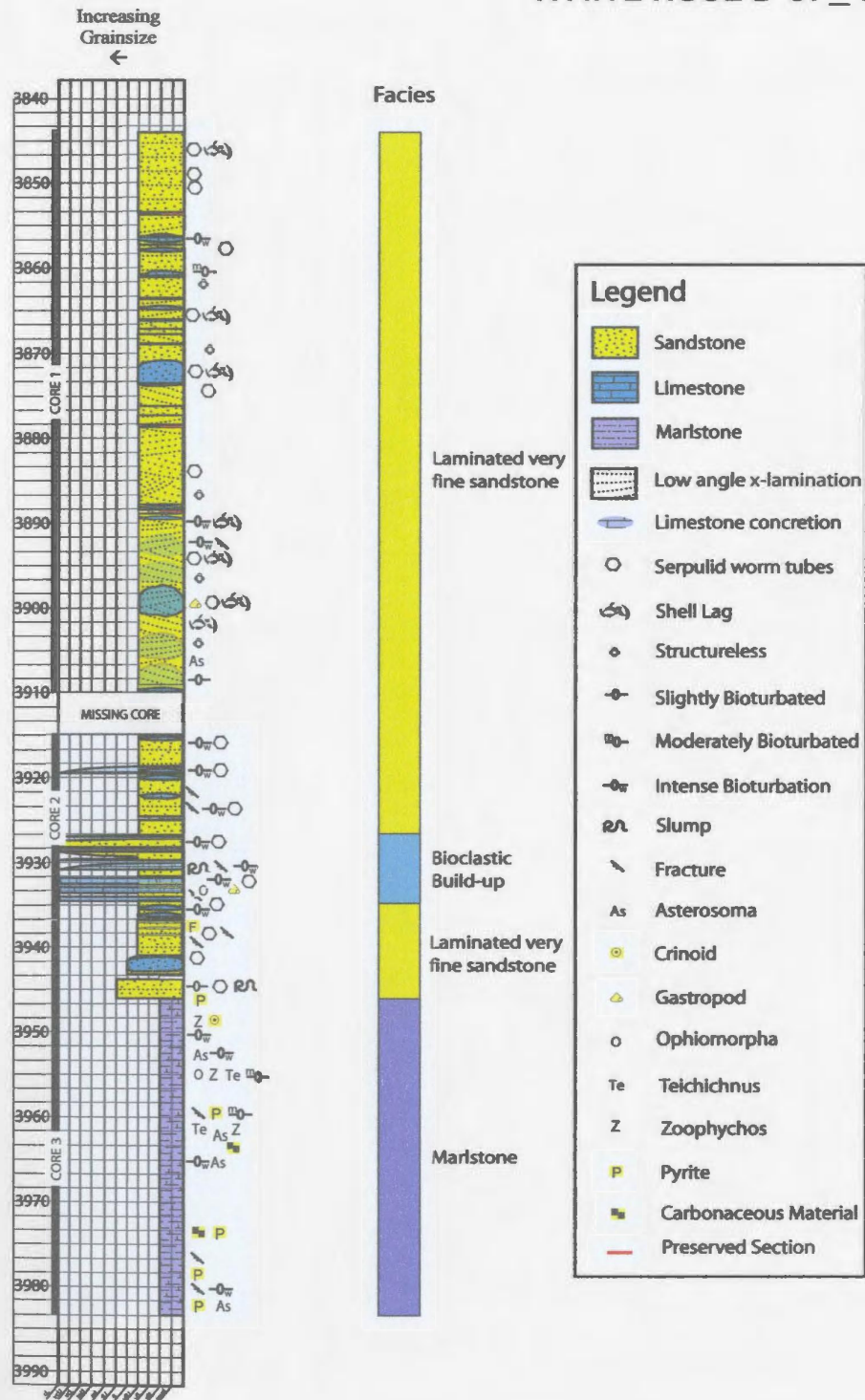


Figure 3.2: Interpretive litholog of the White Rose B-07_4 well.

The main reason for choosing these two wells is the stratigraphic location of core within the Ben Nevis Formation, as well as their location in the south pool of the White Rose Field which is currently under development. White Rose F-04 captures the upper limits of the Ben Nevis Formation within the gas leg of the reservoir and White Rose B-07_4 cores the lower section of the Ben Nevis Formation, capturing the oil leg, as well as the contact with the underlying marlstone. Comparing formation tops from B-07_4 and F-04 was difficult as Husky, Petro-Canada and C-NOPB all had a considerable difference in formation selection and their corresponding depth.

3.3 General Core Descriptions

The Ben Nevis Formation represents an overall transgressive depositional system separated from the underlying progradational Avalon Formation by the mid-Aptian Unconformity (McAlpine, 1990). Although it has an unconformable to disconformable transition with the deep water shales of the overlying Nautilus Formation near the edge of the basin (McAlpine, 1990), the transition appears conformable away from the basin edges. The Nautilus Formation coarsens downwards into silty mudstones interbedded with sandstones and finally into parallel to low angle cross laminated, very fine grained reservoir sandstones. At this locality the Avalon Formation is completely eroded, with a marlstone unit, thought to be the distal equivalent to the Hibernia Formation, lying directly below the mid-Aptian unconformity (Hodder, 2005, pers.comm.). A heretofore undescribed bioclastic build-up is identified towards the base of the Ben Nevis Formation in White Rose B-07_4. Examples of the five major lithotypes and their percentage of core described in this study are listed in Table 3.2 and shown in Figure 3.3.

Table 3.1: Formation depths (TVD), gas/oil contacts and corresponding gas and oil zone thickness for WR F-04 and WR B-07_4 (*Husky Picks*).

CONTACT	F-04 (TVD m)	B-07_4 (TVD m)
Top of Ben Nevis Fm	2749	2798
Top of Ben Nevis SS	2775.50	2809.75
Gas/Oil Contact	2910.50	2875.50
Thickness of Gas Zone	135	65.75
Bottom of Ben Nevis Fm	2952.75	2964.25
Thickness of Oil Zone	42.25	88.75
Thickness of Reservoir	177.25	154.5
Cored Interval	109	96.6
Core 1 Interval	2764-2818	2888.50-2937
Core 2 Interval	2818-2873	2937-2952
Core 3 Interval	NA	2952-2985

Table 3.2: Lithology Types found in WR F-04 and WR B-07_4 with corresponding core interval, thickness and percentage of core.

Lithology Type	Well	Core Interval TVD	Thickness TVD	Percentage of core TVD
Bioturbated Mudstone	F-04	2764.00 – 2773.10	9.10	4.5 %
Silty Mudstones interbedded with siltstones and very fine grain sandstones	F-04	2773.10 – 2775.70	2.6	1.3 %
Parallel to low angle laminated very fine grain sandstones	F-04	2775.70 – 2873.00	97.30	48.0 %
	B-07_4	2889.15 – 2935.63	46.48	30.8 %
		2938.74 – 2947.28	8.54	
		2952.34 – 2953.78	1.44	
Bioclastic Conglomerate	B-07_4	2954.08 – 2960.01	5.93	
Hibernia? Marlstone	B-07_4	2947.28 – 2952.34	5.06	2.5 %
	B-07_4	2960.01 - 2986.39	26.38	13.0 %

3.3.1 Upper Ben Nevis (Bioturbated Mudstones)

White Rose F-04 core encapsulates over nine meters of the upper portion of the Ben Nevis Formation (Figure 3.3 A) as demonstrated by the increasing ratio of fines to sand, as well as the general fining upwards trend (Core #1: 2764.00 m TVD – 2773.10 m TVD). The uppermost mudstones are dark grey to tan grey, occasionally brown/orange grey, and were intensely bioturbated (Figure 3.4 A) with sporadic to locally abundant bivalve shells and serpulid worm tubes (Figures 3.4 B and C).

An excellent specimen of *Conichnus* (Figure 3.4 D) is also found in this rock type implying a higher energy, arenaceous middle shoreface environment, Pemberton *et al.*, (2001). This clay rich facies clearly demonstrates a low energy offshore environment with low sediment supply allowing various fauna to colonize and rework the sediments. The variations of energy levels along with thin layers of sandstone within the storm wave base may indicate a transition to an offshore environment.

3.3.2 Upper Ben Nevis (Silty mudstones interbedded with siltstones and very fine grained sandstones)

The very thickly bedded mudstone facies gradually decreases in thickness downward to medium bedded silty mudstone and also becomes interbedded with thin very fine grained sandstone beds (Figure 3.3 B), (WR F-04; Core #1: 2773.10 m TVD – 2775.70 m TVD). Mudstones are bioturbated with rare traces extending into the underlying sandstones. Sandstone beds are parallel laminated to massive with rare fractures (Figure 3.5 A). Both mudstone and sandstone beds host thin, cm-scale intervals

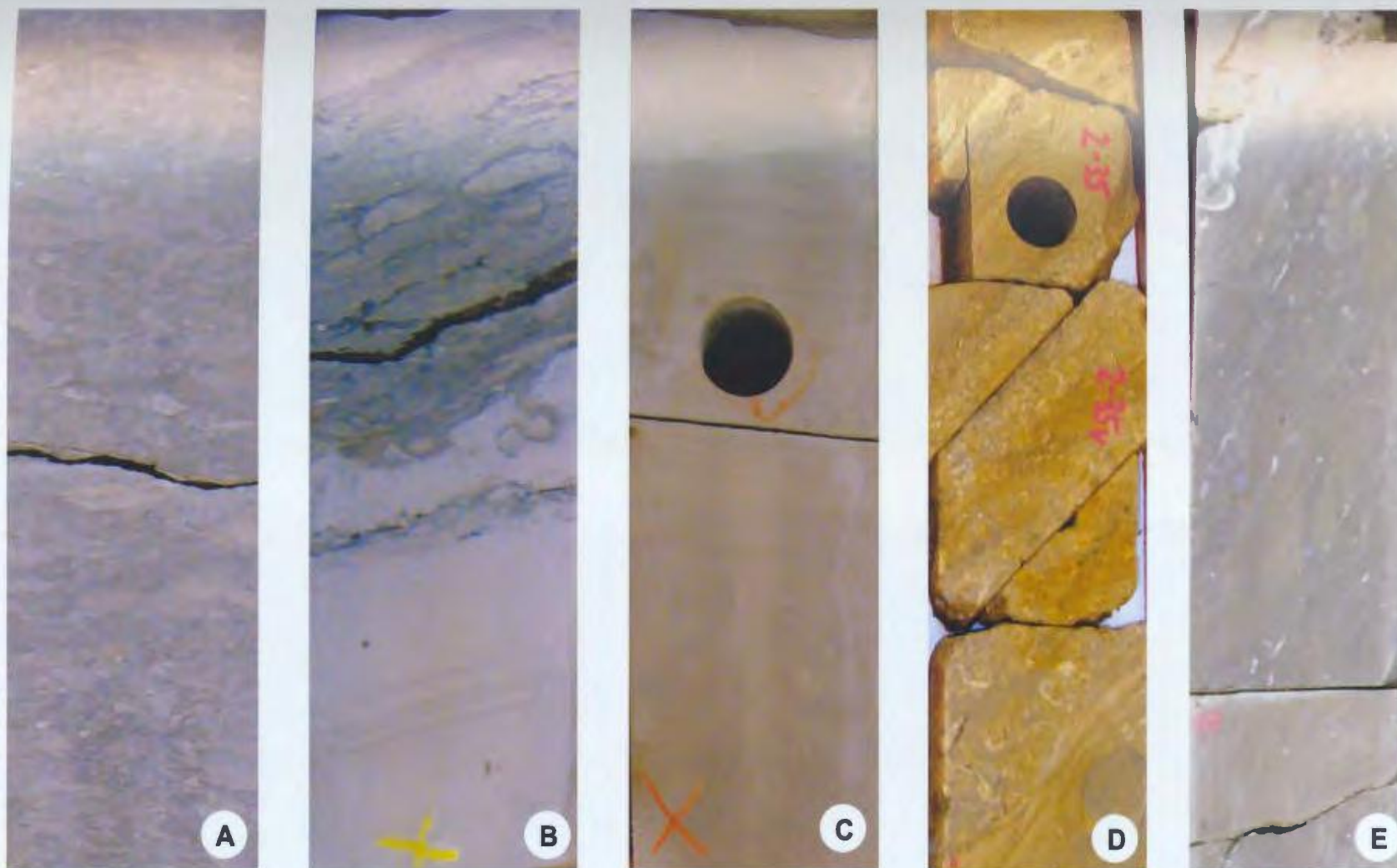


Figure 3.3: General lithologies found in the WR F-04 and WR B-07_4 cores. **A:** Bioturbated mudstone (WRF-04, Core 1, Box 6) 4.5 % of core; **B:** Interbedded silty mudstone and sandstone (F-04, Core 1, Box 17) 1.3 % of core; **C:** Parallel laminated to low angle cross bedded sandstone (F-04, Core 1, Box 55) 78.8 % of core; **D:** Bioclastic sandstone (B-07_4, Core 2, Box 22) 2.5 % of core and **E:** Marlstone (B-07_4, Core 3, Box 13) 13.0 % of core. (5.25" Core)

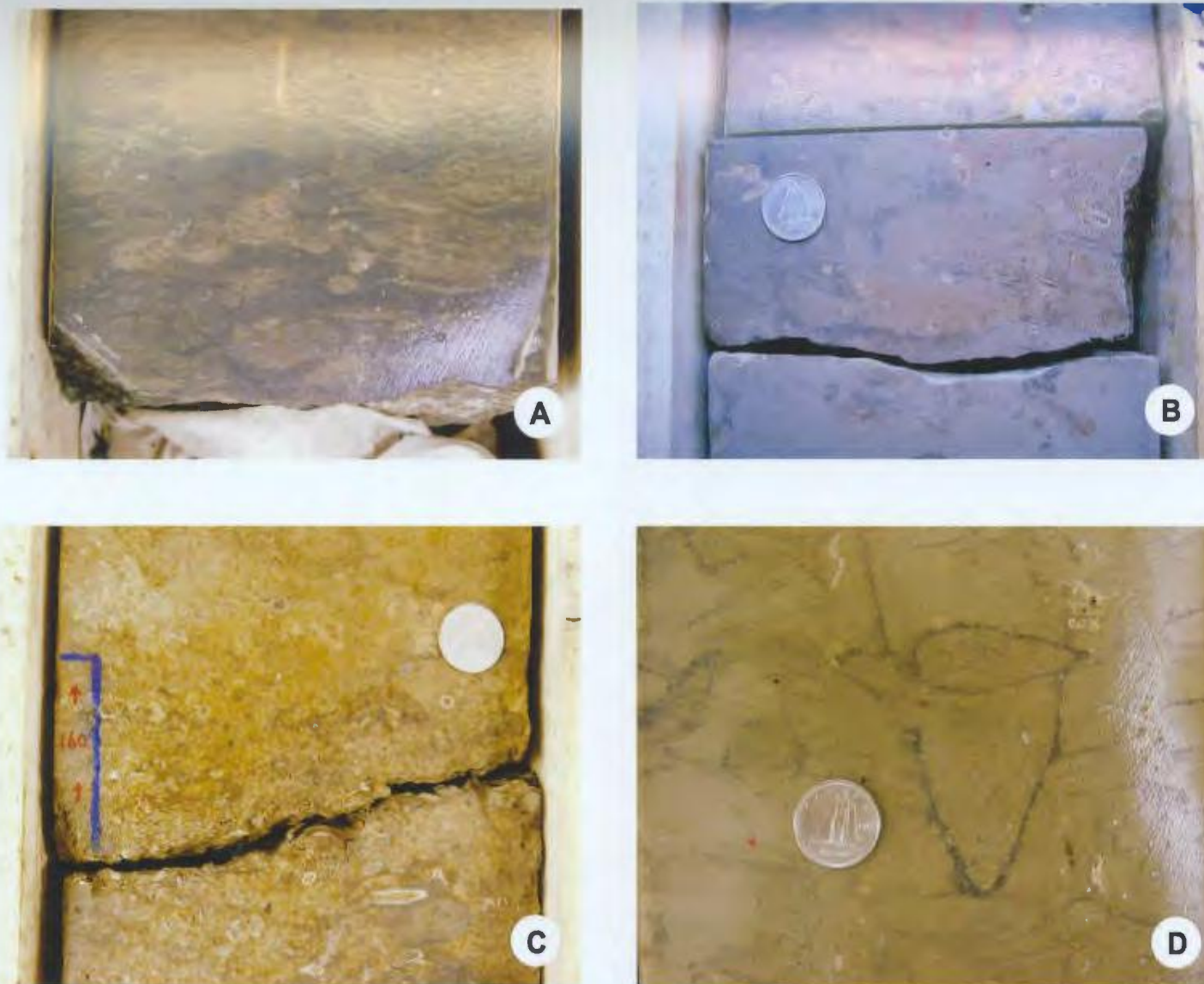


Figure 3.4: Characteristics of the Upper ben Nevis - Bioturbated Mudstones: A. Intense Bioturbation, F-04, Core #1 Box 1, B. Rare Bivalve Shells and Serpulid Worm Tubes, F-04, Core #1, Box 3; C. Rare Bivalve Shells and Serpulid Worm Tubes, F-04, Core 31, Box 5; and D. Conichnus, F-04, Core #1, Box 2.

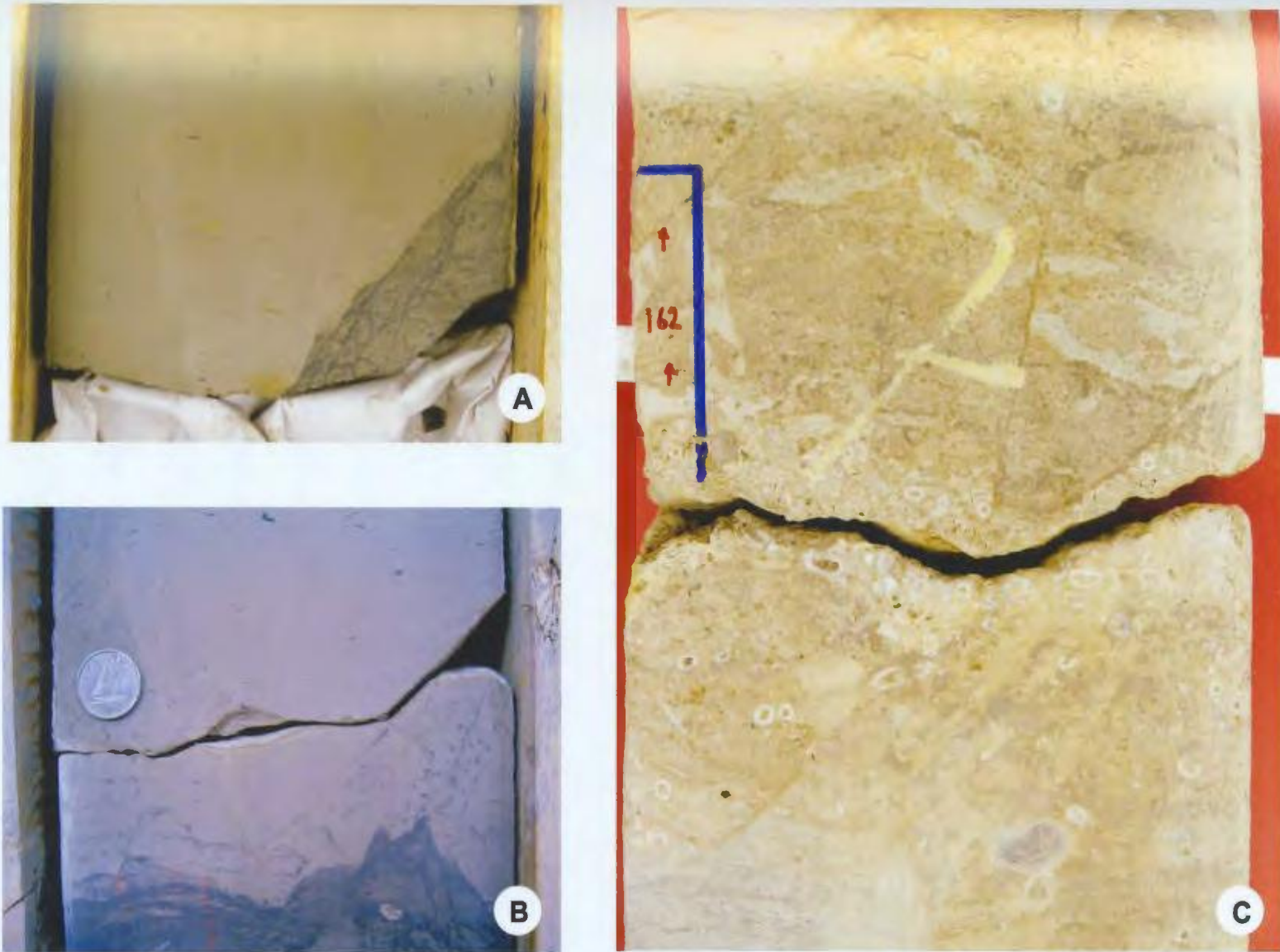


Figure 3.5: Characteristics of the Upper Ben Nevis - Silty mudstones interbedded with siltstones and very fine grained sandstones: A. Massive sandstone beds with rare fractures, F-04, Core # 1, Box 12; B. Sharp and irregular contacts, F-04, Core #1, Box 12; C. Bioclastic debris possibly acting as nucleation site for siderite cement, F-04, Core #1, Box 13.

of bioclastic debris (Figure 3.5 C) which appear to act as nucleation sites for siderite cement (Figure 3.5 C). Siderite cement was originally identified as mud but petrographic analysis clearly made this distinction. Contacts between beds are generally sharp and irregular (Figure 3.5 B), representing erosional events or bioturbation fronts.

This fairly thin section (< 3 m) represents the transition from offshore shales to shelf sands. Based on trace fossil assemblages and the lack of evidence of fair-weather reworking, Plint (1999) interpreted this facies as storm deposits on a low energy muddy shelf, within water depths ranging from 20 to 50 meters.

3.3.3 Ben Nevis Sandstone (Parallel laminated to low-angle cross laminated sandstone)

The top of the Ben Nevis sandstone is taken at 2775.70 m MD of the WR F-04 well and appears to be the first occurrence of a > 50 cm thick sandstone bed (F-04: Core # 1; 2775.70 m TVD – 2818.00 m TVD, Core # 2; 2818.00 m TVD – 2873.00 m TVD; B-07_4: Core # 1; 2889.15 m TVD – 2935.63 m TVD, Core 2; 2938.74 m TVD – 2953.78 m TVD, Core # 3; 2954.08 m TVD – 2960.01 m TVD). This reservoir sandstone is light tan grey, very fine grained, sub-angular to sub-rounded, well sorted, mm to cm scale parallel to low angle cross laminations (Figure 3.6 A), with layers of serpulid worm tube (Figure 3.6 B) and shell debris (Figure 3.6 C) deposited sporadically throughout. Thin (less than one mm), black-colored shells originally thought to be disrupted clay laminations, appear to be a primary source of calcite cement. (Figure 3.6 D); (See Chapter 4: Petrography).

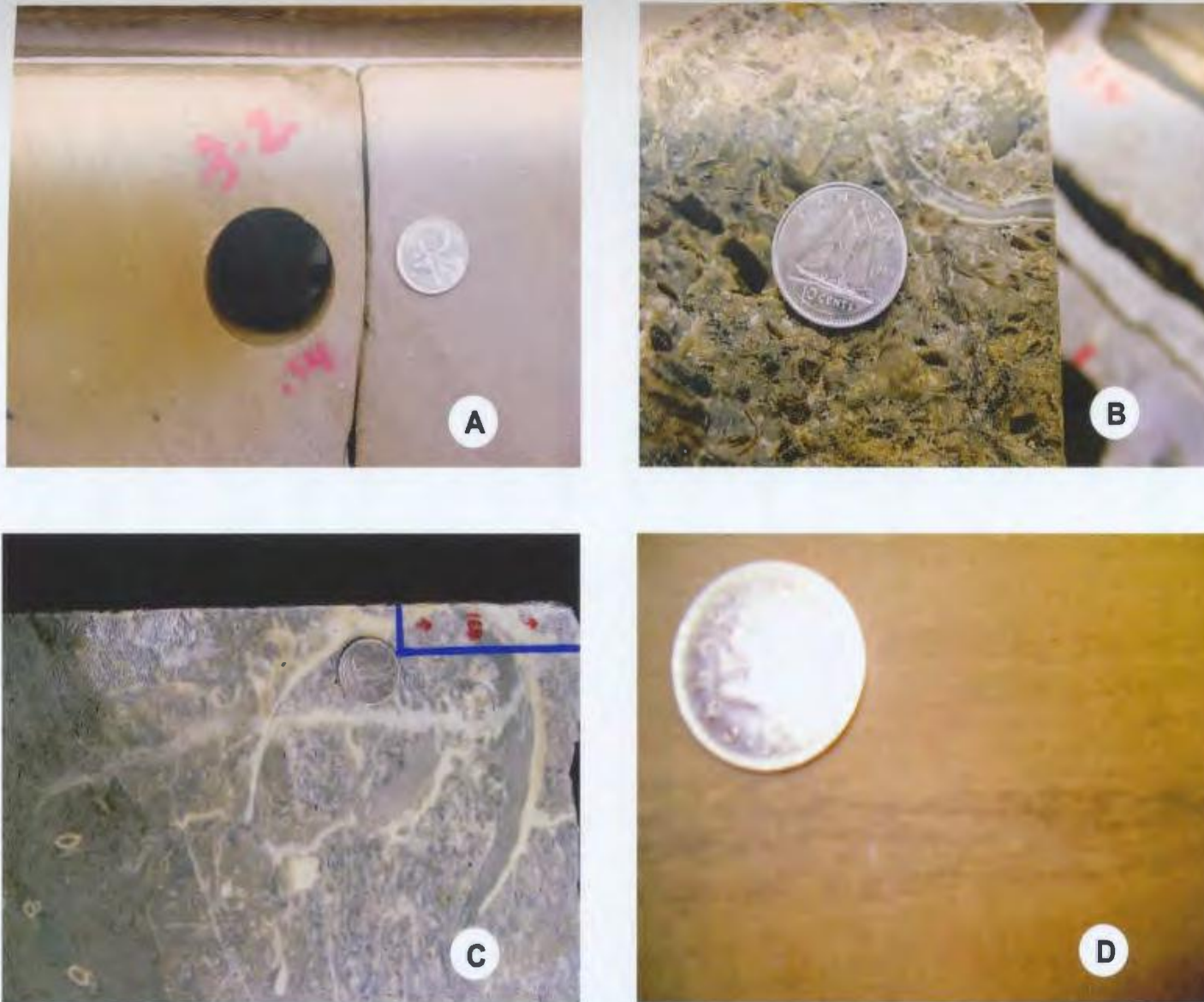


Figure 3.6: Characteristics of the main Ben Nevis sandstone **A.** Low Angle Cross Bedding, B-07_4, Core 1, Box 3; **B.** Longitudinal section of Serpulid Worm Tube B-07_4, Core 2, Box 6; **C.** Large Bivalve, B-07_4, Core 2, Box 22; **D.** Thin Black Partially Dissolved Shells, B-07_4, Core 1, Box 62.

Bed thickness ranges from thin to very thick and occasionally becomes massive with cryptobioturbation (Pemberton *et al.*, 2001). Plint (1999) interprets this facies as an inner shelf to lower shoreface environment with deposition controlled by major storm events.

3.3.4. Bioclastic Sandstone

An approximately 5 m thick bioclastic sandstone unit found towards the base of the Ben Nevis Formation in the B-07_4 core is characterized by a high abundance of skeletal debris. This bioclastic sandstone generally is matrix supported with very fine grained sand but is occasionally conglomeratic or can be classified as a grainstone. Serpulid worm tubes (Figure 3.7 A) and various bivalves (Figure 3.7 B) make up the bulk of the shell debris but cephalopods, gastropods (Figure 3.7 C), and corals (Figure 3.7 D) are also present. Husky (Development Plan, website 2001) interprets this bioclastic sandstone deposit as a transgressive accumulation, representing the shoreline position during marine erosion associated with the basal Avalon transgression. Indicators of structural displacement occurring in this facies include fracture zones (Figure 3.8 A) as well as occasional slump zones (Figure 3.8 B), probably resulting from rapid deposition of sediments.

Aigner (1985), demonstrated the various bank morphologies produced when exceptionally large storms passed the coast of Florida. Dominant depositional environments associated with storms in the Floridian skeletal bank complex are off-bank spill over lobes (Wanless, 1969), which are prominent lobes of skeletal material up to

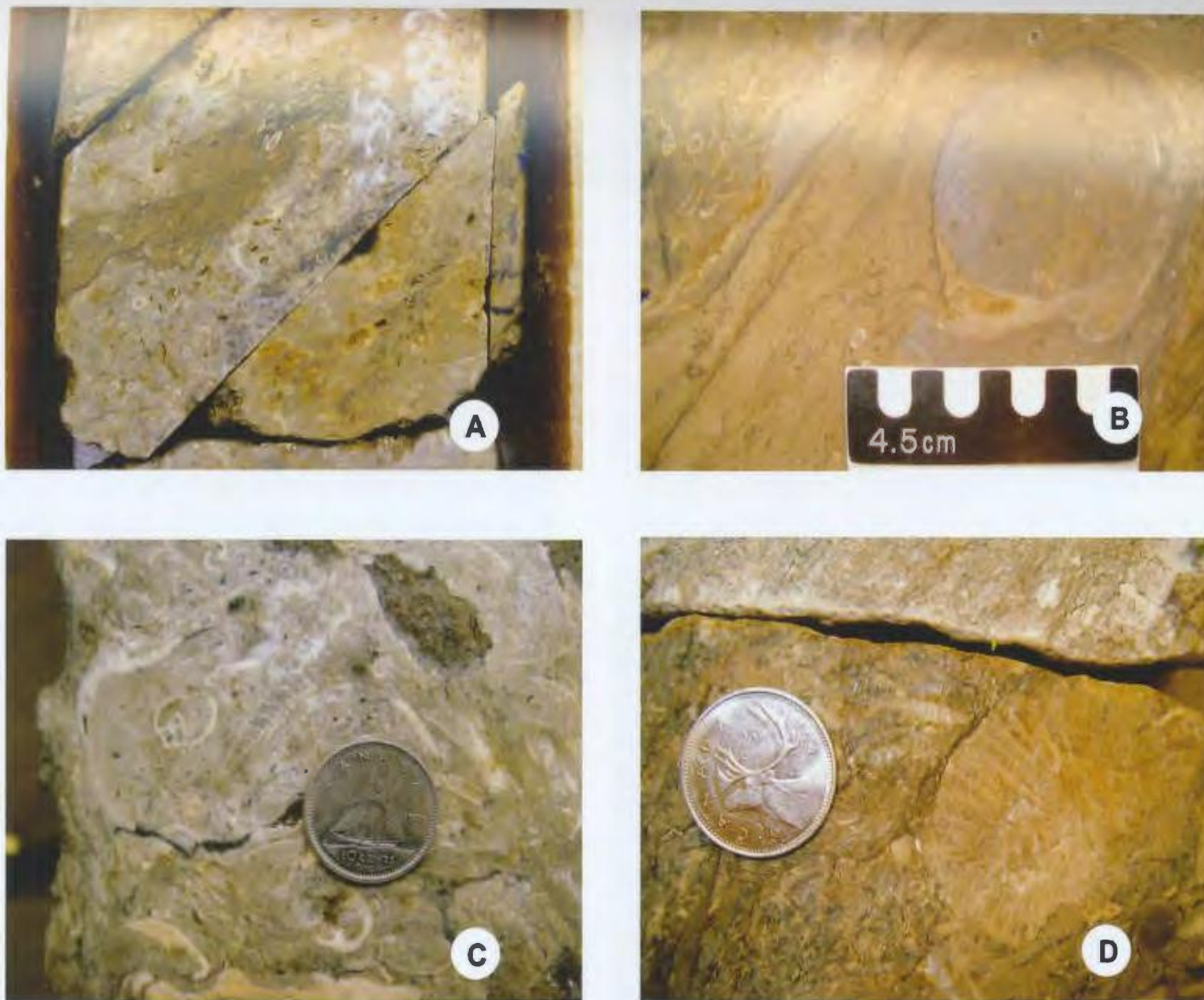


Figure 3.7: Characteristics of the Bioclastic Sandstone Interval - **A.** Serpulid Worm Tubes, B-07_4, Core 2, Box 22; **B.** In-Situ Bivalve (Hinge down), B-07_4, Core 2, Box 22; **C.** Cephalopoda and Gastropoda, B-07_4, Core 2, Box 22; **D.** Coral, B-07_4, Core 2 Box 25.

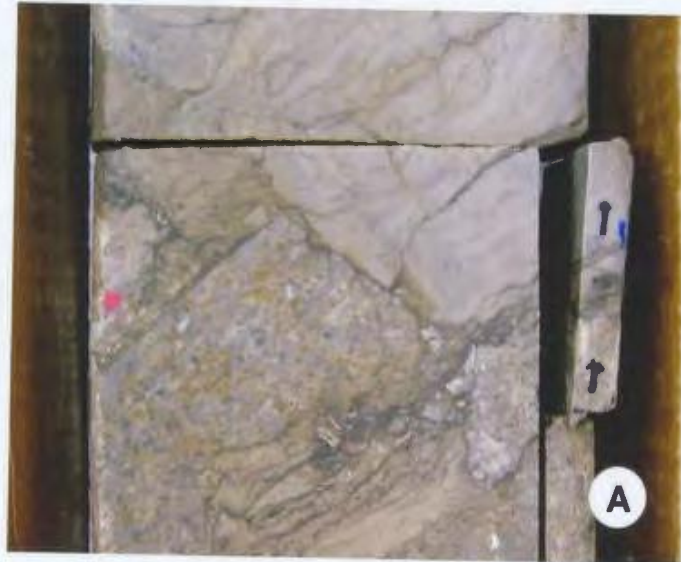


Figure 3.8: Mass movement features and soft sediment deformation from Bioclastic Sandstone Interval: **A.** Fracture Zone, B-07_4, Core 2, Box 21; and **B.** Slump movement, B-07_4, Core 2, Box 22.

1000 m in length and 500 m wide and located off the seaward end of tide channels (Aigner, 1985). The bioclastic sandstone found at the base of the B-07_4 well occurs above the mid-Aptian unconformity within the Ben Nevis Formation and possibly results from multiple episodes of wash-over lobes off a localized carbonate bank (Figure 3.9). The only other wells to core this section in the White Rose Field are the N-30 and the E-18 wells (Husky Development Plan).

A brief examination of the E-18 well located the bioclastic build-up as approximately 10.1 m thick with fining upward carbonate beds. Carbonate beds consist of cm scale angular clasts and shell fragments infilled with a muddy matrix at the base, gradually decreasing in clast size up-section and terminated by a sharp erosional boundary with the overlying bed. Aigner, 1985 included stratigraphic elements as evidence for storm deposition such as erosive boundaries followed by fining upward sequences as well as biostratigraphic evidence of fauna preservation.

3.3.5. Basal Unconformity and underlying marlstone

White Rose B-07_4 intercepts the base of the Ben Nevis Formation where some discrepancies arise regarding which formations are completely eroded as well as the designation of the underlying marlstone. This unit consists of light grey, calcareous mudstones with abundant pyrite along fractures and occasional black mud clasts with reduction rims. Bioturbation is sporadic in nature with moderate to well developed horizons. The fine grained nature of this unit suggests a deep water depositional environment.

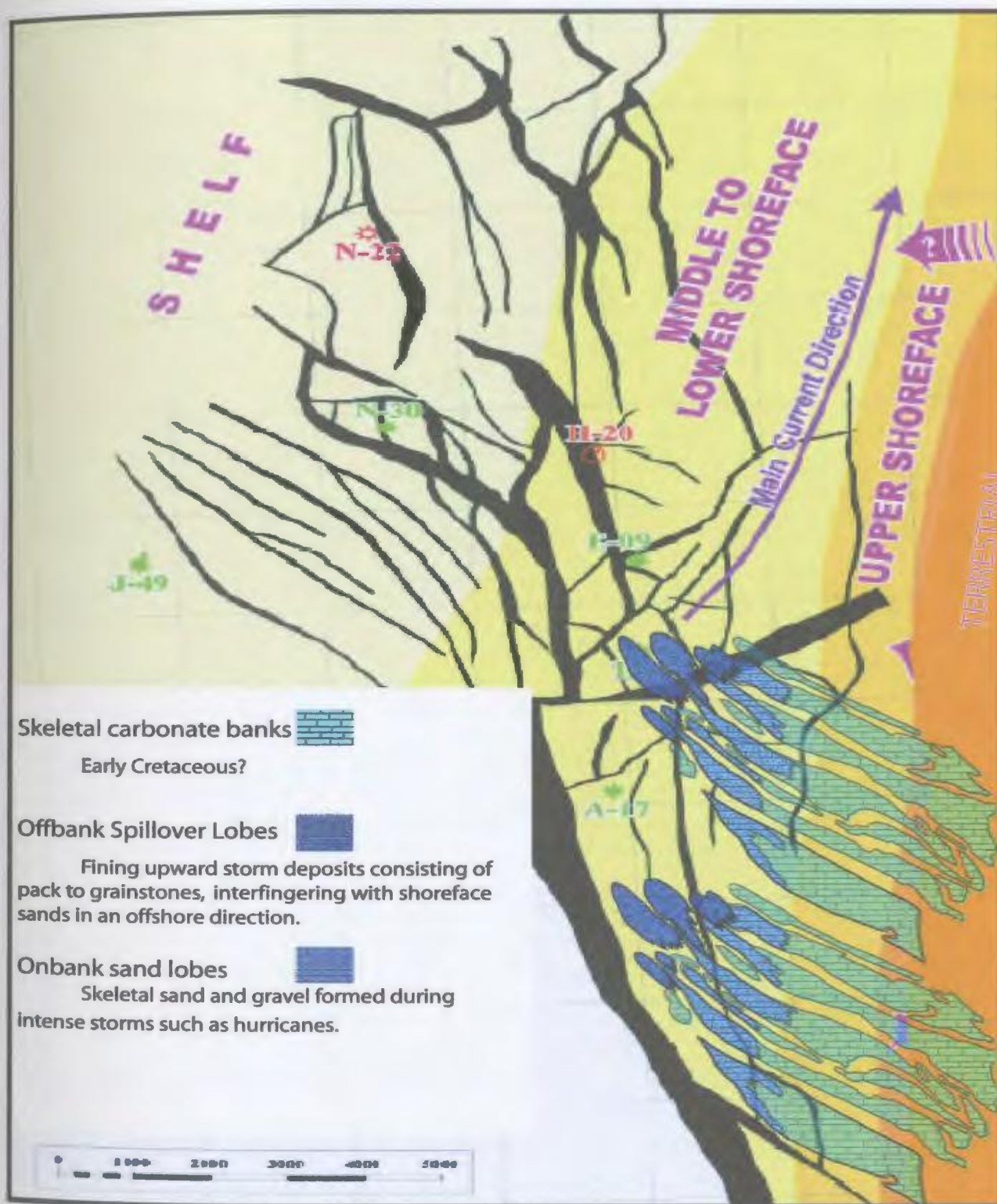


Figure 3.9 Depositional Environment of the Ben Nevis Formation at the White Rose Field, after Husky, White Rose Development Plan, 2001 and Aigner, 1985.

3.3.6. Calcite Concretions: General description

The most dominant textural features within the Ben Nevis Formation are the calcite cemented intervals, known as concretions, which range from partial cementation to completely occluding all porosity. The Ben Nevis concretions are irregularly spaced throughout both F-04 and B-07_4 (Figures 3.1 and 3.2), range from cm to m scale and are generally associated with worm tube/shell accumulations.

Calcite concretions demonstrate a wide variability of development throughout the Ben Nevis Formation in the White Rose F-04 and B-07_4 cores. A total of 61 separate concretions were identified as beds or layers and grouped based on size, degree of cementation, nature of upper and lower contacts, and apparent nucleation sites (Appendix A provides the complete list of calcite cemented concretions).

3.3.6.1. Size and Distribution of Calcite Concretions

Excluding the large bioclastic build-up which occupies over 6 m of core in B-07_4, calcite cemented concretions range from 2 cm to 316 cm thick with an average thickness of approximately 56 cm. It must be noted that B-07_4 is deviated to approximately 45 degrees resulting in a recalculation of apparent concretion thickness to true thickness. The relative frequency distribution of concretions is shown in Figure 3.10, clearly showing a positively skewed distribution with nearly two thirds of the population under 61 cm thick and the 31 to 40 thickness range making up the mode of the population.

Figure 3.11 illustrates thickness of concretion versus stratigraphic position in both cores from the shallowest on the right to the deepest on the left. This demonstrates the irregularity of concretion size throughout the Ben Nevis Formation with no distinct large scale correlation of concretion size with stratigraphic position. Some small scale trends seem to decrease concretion thickness with decreasing depth, creating discrete concretion forming cycles. These cycles may be related to pulses of fluids supersaturated with calcium carbonate that gradually become depleted up-section as precipitation of cement occurs. This may suggest a source below the forming concretion or a compaction driven upward flowing fluid force pushing calcium and carbonate ions into nucleation sites.

3.3.6.2 Cementation Intensity

Initial classification of concretions was based on cementation intensity (Figure 3.12), with over 31 % of concretions being well cemented (Type A, zero \emptyset), 24.6 % were well cemented (Type B), 18 % were moderately cemented (Type C) and 23 % consisted of poor to partial cementation (Type D) with significant porosity and permeability. Siderite concretions and bioclastic build-ups are anomalous occurrences and account for the remaining 3 %. Figure 3.13 illustrates the concentration of very well and well cemented concretions in the upper portion of the Ben Nevis Sandstone (F-04) and the moderate to partially cemented zones in the lower section of the Ben Nevis Sandstone (B-07_4). This may reflect the degree of cementation or the preservation of cements at different stratigraphic intervals. The rate of sedimentation as well as the volume of

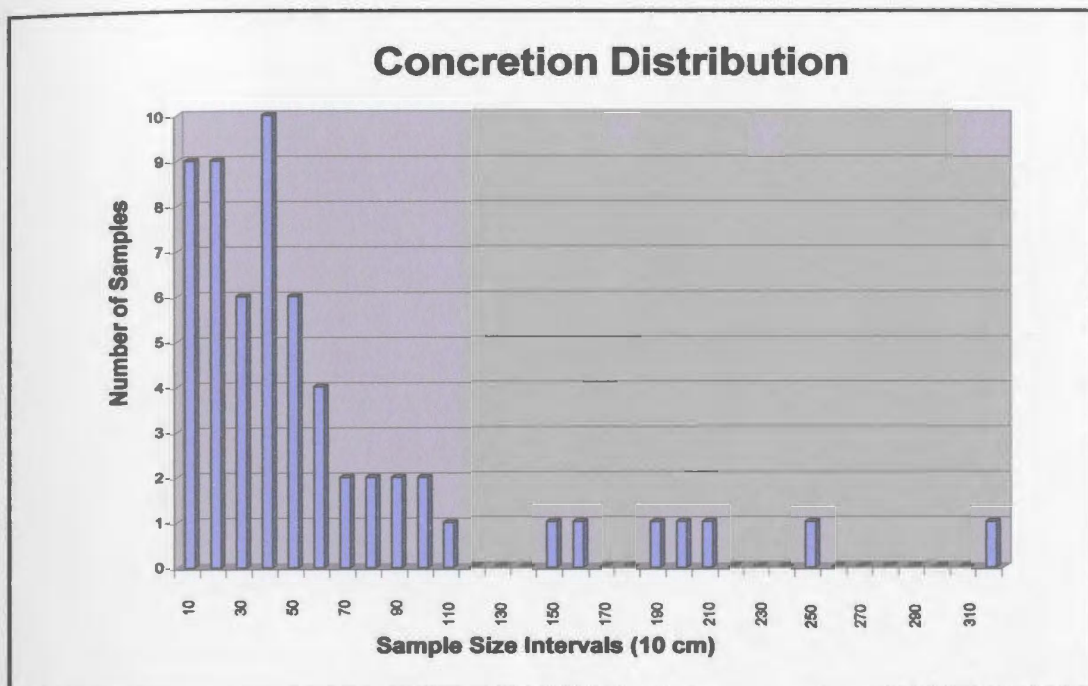


Figure 3.10: Relative frequency distribution of concretion sample size.

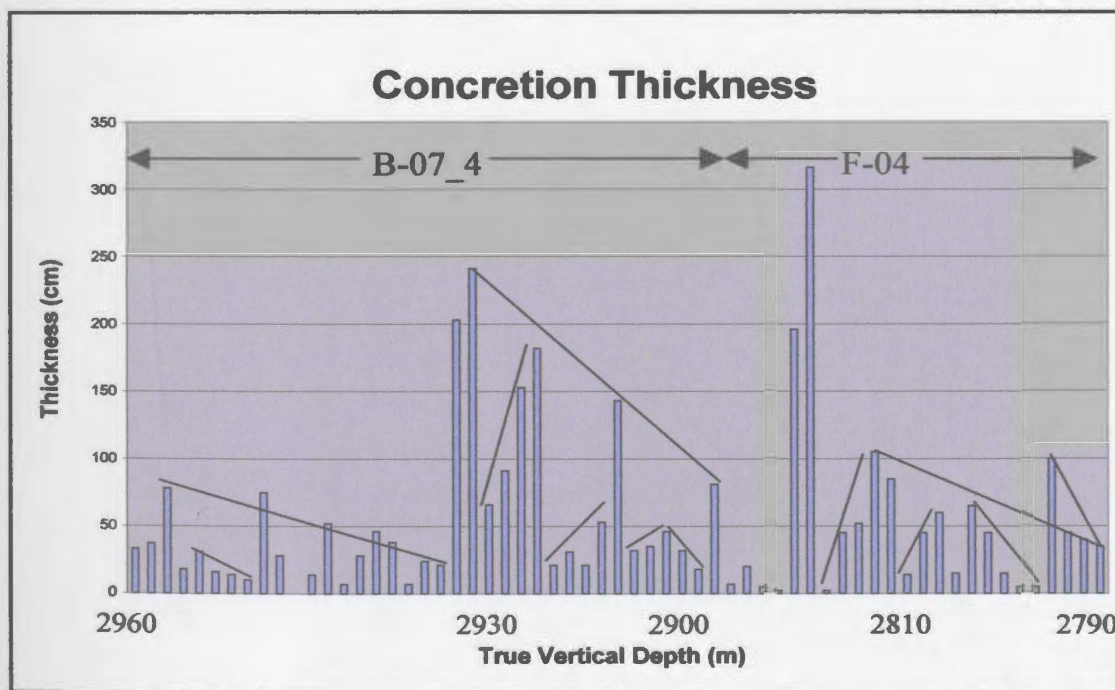


Figure 3.11: Concretion sample size, depth decreasing from left to right. Note decreasing concretion size trends moving up-section.



Figure 3.12: Varying cementation intensities found in the Ben Nevis Formation. **A.** Very well cemented concretion B-07_4, Core 2, Box61, **B.** Well cemented, F-04, Core 3, Box 31, **C:** Moderately cemented, F-04, Core 1, Box 38 and **D.** Partial cementation, F-04, Core 2, Box 52.

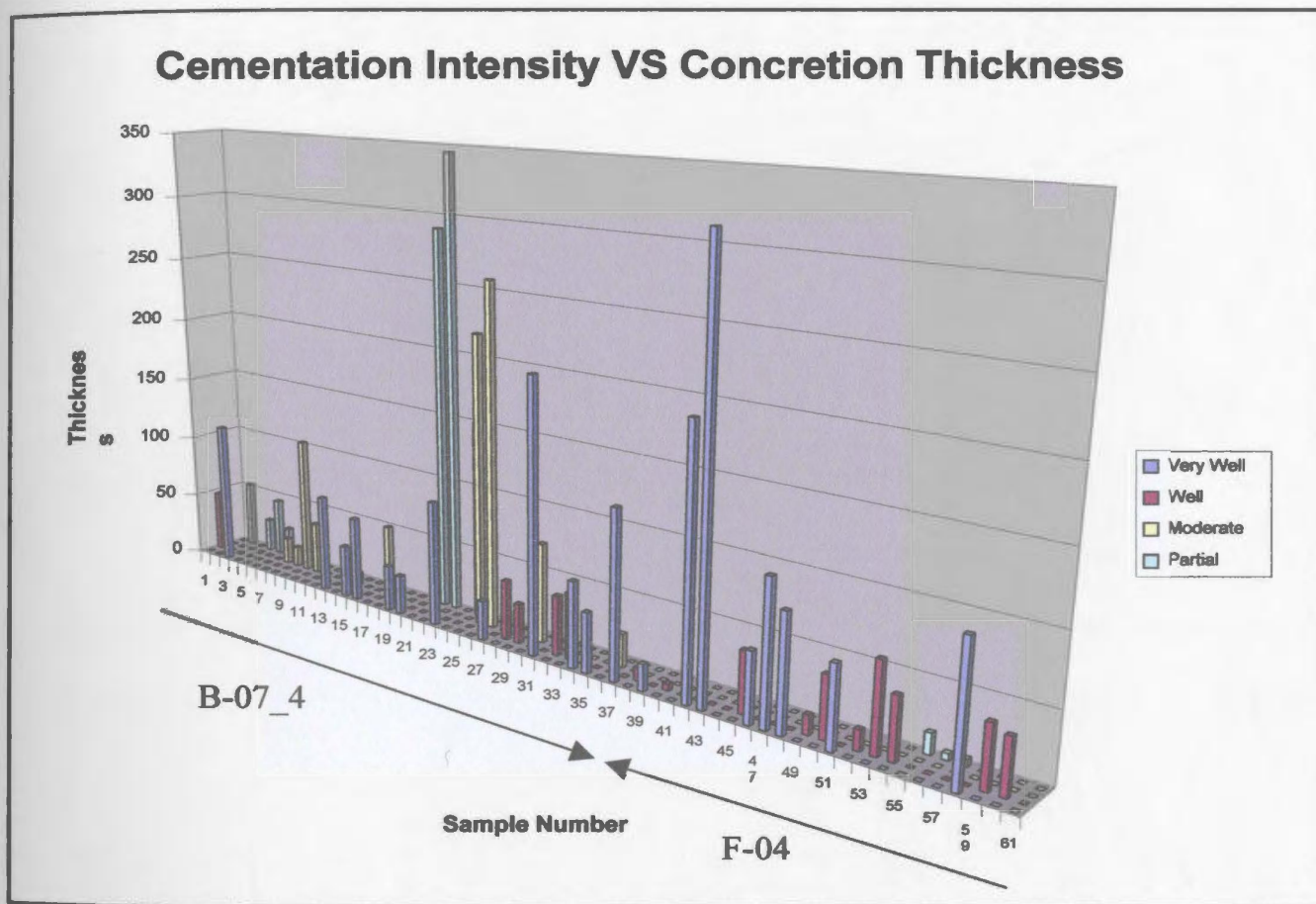


Figure 3.13: Cementation intensity vs. concretion thickness demonstrating decreasing cementation intensity with depth, possibly related to source of calcium carbonate.





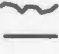




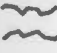
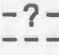

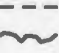



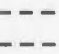
calcareous debris may be early limiting factors affecting the degree of cementation. A possible late stage event resulting in the decrease of cementation intensity in the lower portion of the Ben Nevis Formation may be the result of dissolution in the lower section while the upper section preserves concretions due to a “freeze” on diagenetic processes, as oil or gas emplacement can exclude the water needed to transport ions (Parnell, 1994).

3.3.6.3. Concretion Boundaries

Further refinement of concretion classes was based on the nature of upper and lower concretion contacts, resulting in 17 different classes for intensity types A through D (Table 3.3). The basic contacts dividing these classes are curved (concave or convex), linear, irregular, sharp or gradational and can be conformable or cross-cutting. The curved contacts illustrate the spherical nature of the concretions while the sharp and irregular contacts indicate the influence that lithological change may have on concretion development. Sharp versus gradational contact may also have unique diagenetic pathways.

The only correlation between cementation intensity and concretion contacts occurs when both upper and lower boundaries are sharp and irregular (Figure 3.14). This category of contact represents approximately 20 % of the concretion population and is represented by all concretion intensity types. This contact type may reflect a dominant lithological characteristic created by irregular unconformable beds deposited during storm deposition.

Table 3.3: Concretion Boundary Divisions

	Upper	Lower		Upper	Lower
1	 Sharp convex	Sharp concave			
2	 Sharp linear	Sharp concave	10	 Gradational	Sharp linear
3	 Sharp irregular	Sharp concave	11	 Sharp irregular	Sharp linear
4	 Sharp concave	Sharp concave	12	 Sharp concave	Sharp irregular
5	 Sharp linear	Sharp linear	13	 Sharp irregular	Gradational
6	 Sharp irregular	Sharp irregular	14	 Unknown	Gradational
7	 Sharp convex	Sharp convex	15	 Sharp irregular	Sharp irregular
8	 Sharp convex	Sharp linear	16	 Sharp convex	Sharp convex
9	 Gradational	Sharp irregular	17	 Gradational	Gradational

Concretion Types

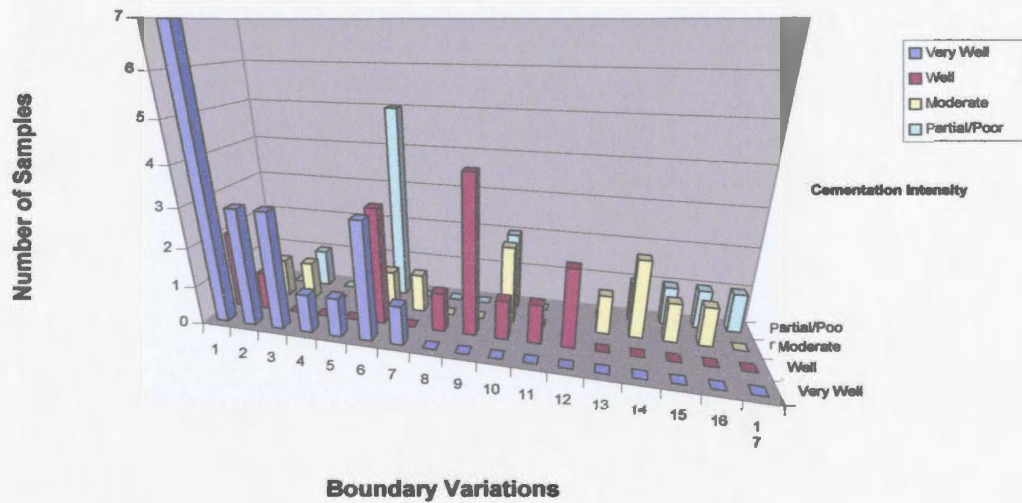


Figure 3.14: Cementation intensity vs. concretion boundary divisions demonstrating sharp boundaries for well cemented concretions and gradational boundaries for moderate to partially cemented concretions.

Boundary types reveal a huge amount of information about the concretion forming process. Over two-thirds of concretions have sharp boundaries suggesting the dominant concretion forming system is not a gradual process. Well to very well cemented concretions were most likely to have convex upper and concave lower boundaries confirming the stability of sub-spherical bodies. The “well” cemented types appear mostly in boundary types 9, 6, and 12. These boundary types all have sharp irregular lower boundaries possibly involve the fluid flow responsible for well cemented concretions to originate from below.

3.3.6.4. Concretion Nucleation Sites

Final grouping of concretions was attempted by using the cementation intensity and relative location of apparent nucleation sites, which are considered to be mutually exclusive of the boundary designations. This produced eight additional subdivisions for each concretion type (Table 3.4). Nucleation sites include shell debris, worm tubes and calcite veins around which the concretion will develop. The apparent location of these nucleation sites may indicate the direction of fluid flow or the merger of concretions as may be the case with more than one nucleation site within one concretion. The dominant nucleation site for the well to poorly cemented concretions is the homogeneous nucleation site while the very well cemented concretions are dominated by no apparent nucleation site (Figure 3.15).

Table 3.4: Various types of nucleation sites.

	Nucleation Site Type
1) UNS	Upper Nucleation Site
2) CNS	Central Nucleation Site
3) LNS	Lower Nucleation Site
4) U & LNS	Upper and Lower Nucleation Sites
5) HNS	Homogeneous Nucleation site
6) None	No Nucleation Site
7) CV	Calcite Veins
8) SS	Single Shell

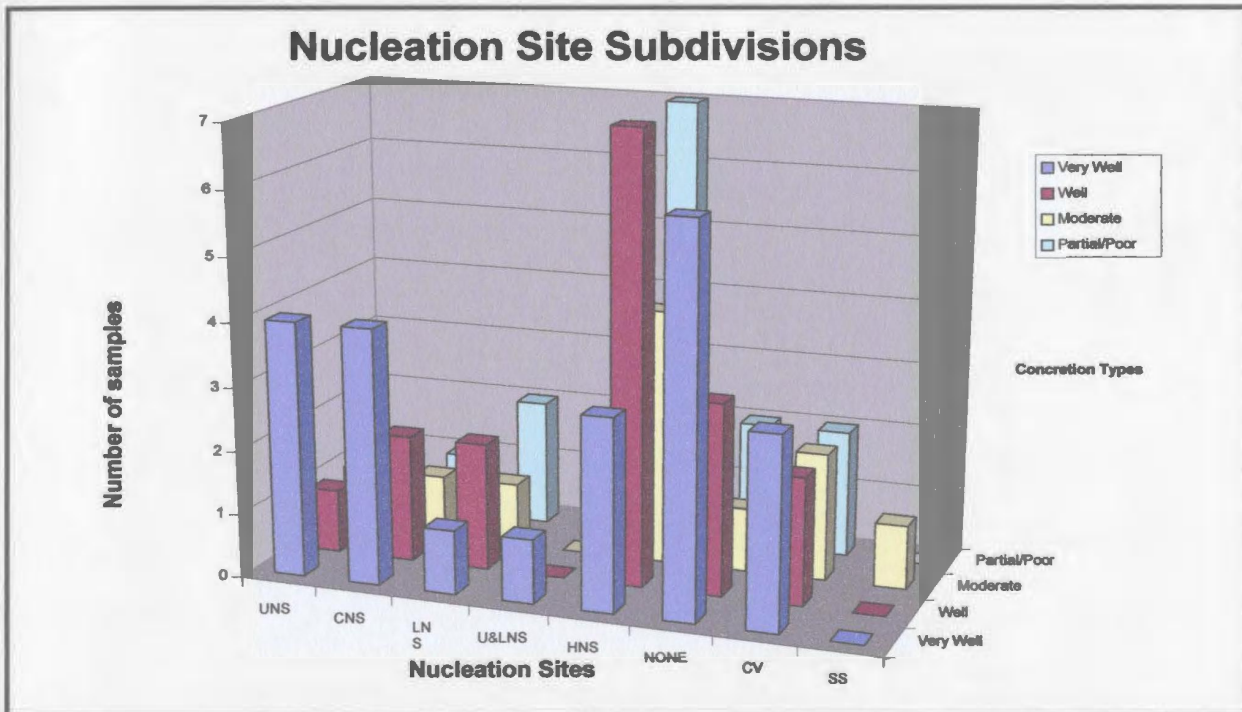


Figure 3.15: Types of nucleation sites for varying degrees of cementation. UNS (Upper Nucleation Site), CNS (Central Nucleation Site), LNS (Lower Nucleation Site), U&LNS (Upper and Lower Nucleation Sites), HNS (Homogeneous Nucleation site), NONE (No Nucleation Site), CV (Calcite Veins) and SS (Single Shell).

3.3.7 Calcite Veins

Zoned calcite veining represents a late stage, continuously evolving fluid that has penetrated small fractures precipitating calcite cement (Figure 3.16). They are more common in the lower portion of the core but there are also rare occurrences in the F-04 well. The zoned calcite veins found in the B-07_4 seem to be stratigraphically confined. They range from white to orange in color and demonstrate multiple pulses of fluids according to their color change.

3.3.8 Siderite Concretions

Siderite concretions range in size from mm scale to a 35 cm concretion located at the top of White Rose F-04 (Figure 3.17). The majority of siderite is located almost exclusively in the F-04 well and consists of thirty-three occurrences of which, over 63 % are five to fifteen mm size spherical siderite clasts. The remainder of the siderite concretions, in descending order of incidence include moderate cementation with gradual upper and lower boundaries, partial cementation with siderite disseminated throughout, very well cemented with sharp upper and lower boundaries and two occurrences have siderite cement following bioturbation. Siderite is a rare occurrence in the B-07_4 well, consisting mainly of mm scale isolated siderite clasts.

3.4 Discussion

To understand the diagenetic sequence of any sedimentary rock unit, it is important to determine physical, geochemical and biological variations in depositional environment,

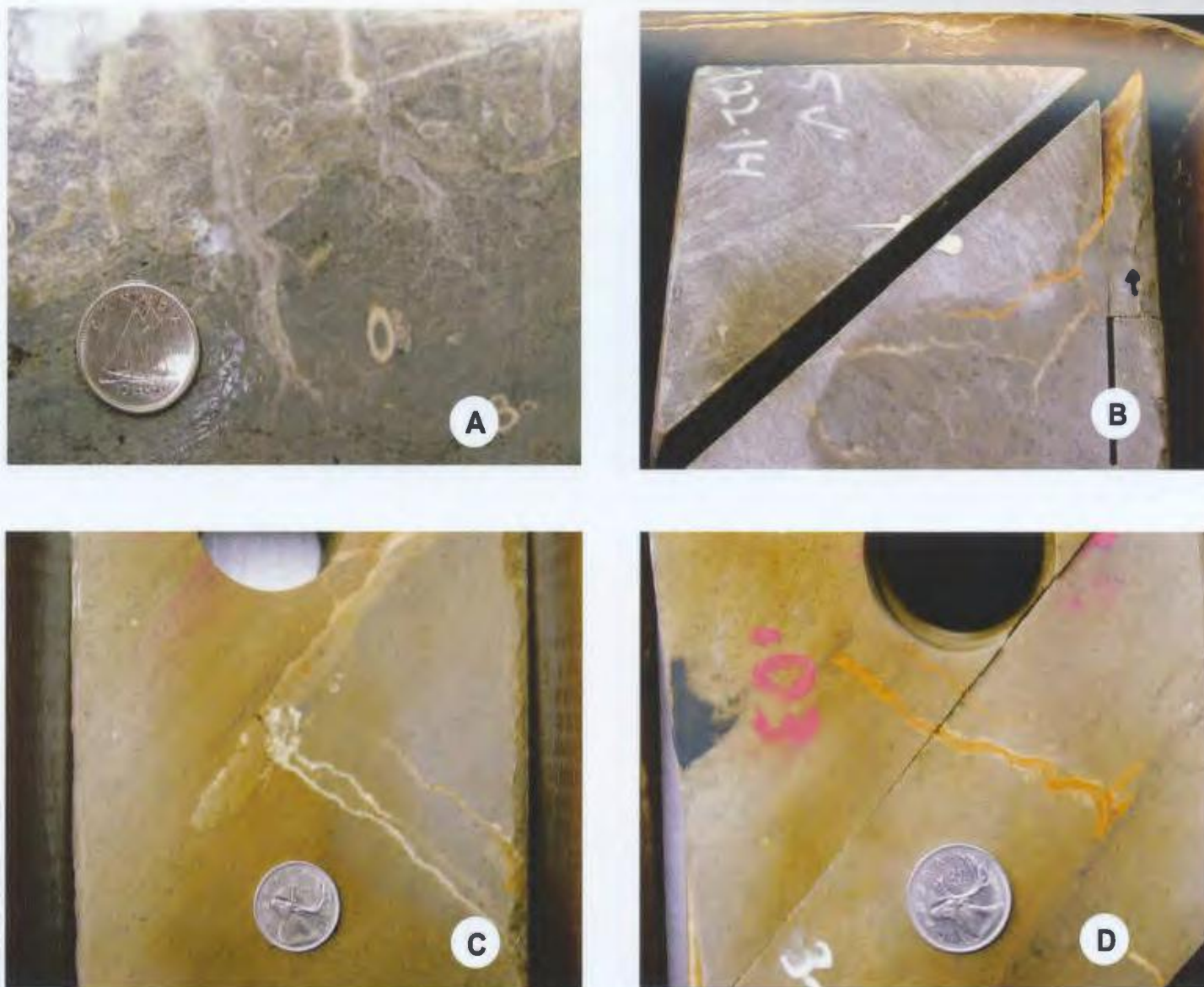


Figure 3.16: Calcite Veining. **A.** F-04, Core 1, Box 35, **B.** B-07_4, Core 2, Box 10, **C.** Stratigraphically confined calcite cement, B-07_4, Core 3, Box 5; and **D.** Zoned calcite cement, B-07_4, Core 3, Box 3.

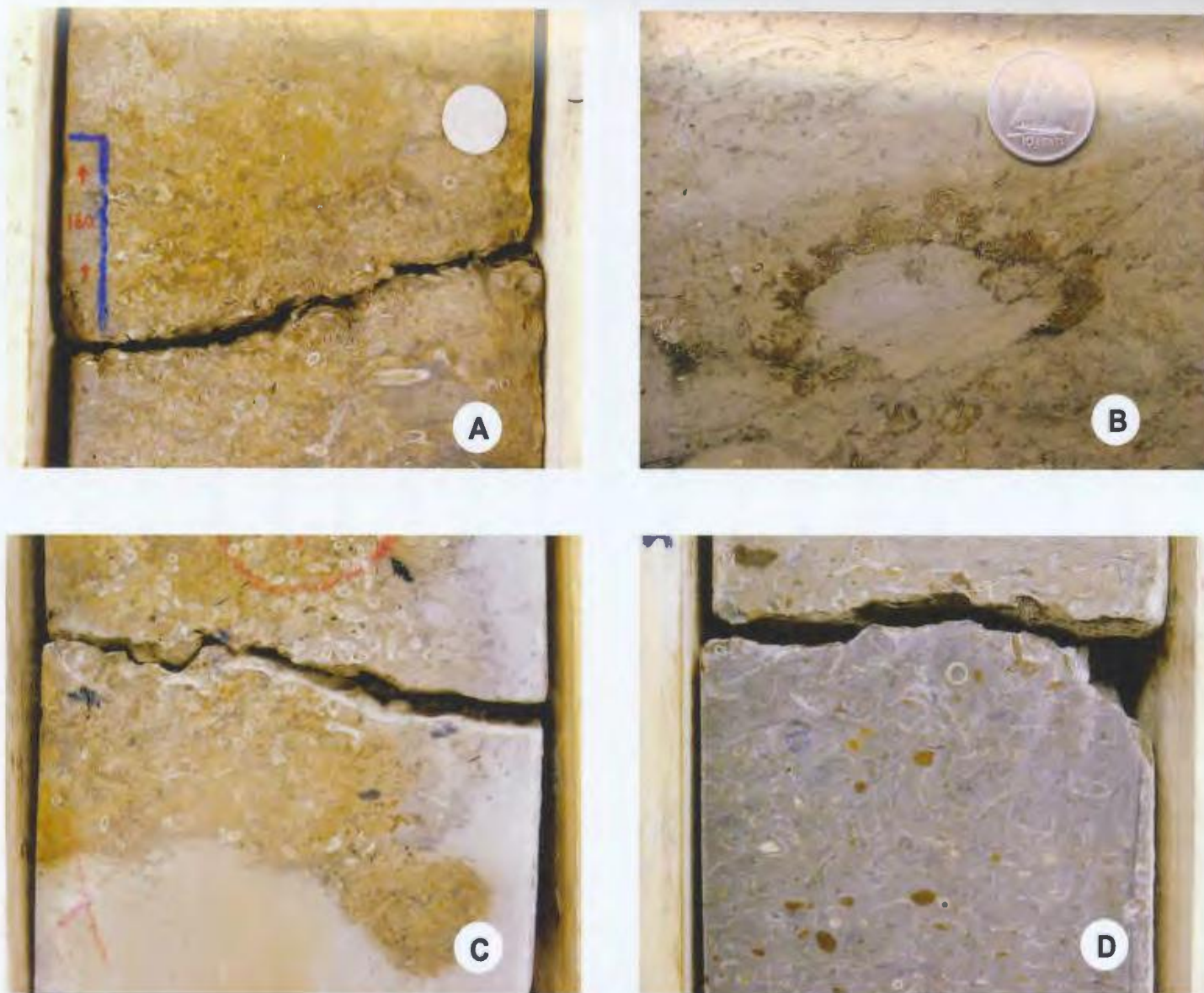


Figure 3.17: Siderite cementation in various forms. **A.** Siderite concretion at bioclastic horizon, F-04, Core 1, Box 5; **B.** Siderite cement replacing organic lining of *Ophiomorpha* trace, F-04, Core 1, Box 20; **C.** Siderite cement following bioturbation, F-04, Core 1, Box 25; and **D.** Siderite concretions, F-04, Core 1, Box 56.

as the compounded effect of all these may lead to divergence in diagenetic evolutionary pathways.

Some physical elements of the original depositional environment that directly affect diagenesis include, provenance, climate, sand/shale ratio, rate of sedimentation, proximity to shoreline, sand body geometry, sedimentary structures, and fluid flux (Mckay *et al.*, 1995).

Geochemical factors may include detrital mineralogy, fluid composition, and iron, sulphur and oxygen content, while biological factors include organic content, oxygen content and bioturbation (Longstaffe, 1987). These characteristics direct diagenetic processes such as cementation, dissolution, recrystallization, replacement and compaction which ultimately are the factors that control whether the porosity and permeability will be reservoir quality or not.

Morad (1998) breaks down diagenesis in timeframes of eodiagenesis (early), mesodiagenesis (middle) and telogenesis (late/uplift) rather than physical, geochemical and biological. Eogenesis is controlled by depositional setting (climate, latitude, hydrogeology, sea level fluctuation, pore water composition and rate of deposition,), organic matter content and the textural and detrital components of the host rocks. Mesogenesis is influenced by temperature, residence time, chemistry and flow rates of subsurface waters and the distribution of eogenetic carbonate cements. Telogenetic alteration and dissolution during uplift and erosion is not applicable to the Ben Nevis Formation at White Rose.

Core description has revealed some interesting evidence into the original depositional environment which may provide some insight for diagenetic interpretations. The general transgressive nature of the Ben Nevis Formation provides a systematic change from a shallow shoreface environment to a deeper shelf environment. This will decrease the rate of deposition, bioclastic content and sand/shale ratio, while increasing mud content, distance from shoreline and bioturbation.

A slower rate of sedimentation allows for a longer period of exposure in the near surface diagenetic setting possibly resulting in early cements. Decreasing bioclastic content reduces the calcium carbonate available as a source for authigenic cement. Decrease in sand/shale ratios will reduce permeability, slowing down fluid flow and possibly inhibiting concretion formation.

Increasing mud content causes blocking of pore throats, reducing porosity and permeability, thereby reducing pore fluid flow and subsequent diagenesis. Increasing the distance to the shoreline can lessen the impact of hydrologic drives pumping meteoric fluids into the offshore setting. Finally an increase of bioturbation up-section may increase homogeneity in the upper portion of the Ben Nevis Formation allowing more efficient fluid flow and therefore increased cementation.

A variety of modifiers were used to categorize the calcite "concretions" found during core description of the B-07_4 and F-04 wells. Size, distribution, cementation intensity, boundary type and nucleation sites each provide evidence to the formation of calcite concretions within the Ben Nevis Formation. Concretion size and shape limit the concretions to relatively small spherical masses, implying outward growth from a central

site. Even though the average thickness is approximately 56 cm, many of the larger concretions may be amalgamations of two or more that are now “one”, thereby reducing the calculated average size. Amalgamation of concretions implies growth across bedding as a result of ideal conditions in restricted intervals.

Before interpreting the differences found between the F-04 and B-07_4 core it is important to reconsider the stratigraphic positions of each well. The F-04 well cores the top contact of the Ben Nevis Formation while the B-07_4 well cores the lower contact, with approximately 10 m of stratigraphic overlap. The subtle trends of decreasing concretion size moving up section may be influenced by amalgamation or it may indicate an underlying source, resulting in depleted source fluids in higher stratigraphic sections as concretions form below. Upward compaction induced flow may be a key component in moving calcium carbonate saturated fluids, resulting in precipitation of cement. This would result in a vertical aspect to evolving pore fluids as they become less saturated with respect to calcite, creating smaller concretions up section. This may also reflect the cyclicity of tempestites depositing shelly horizons, or the formation of first generation carbonate cement which help nucleate concretionary horizons during periods of minimal sedimentation (Wilkinson, 1991).

The irregular distribution of bioclastic carbonate debris is also an important factor in the formation of concretions. Hudson (1978) and Walderhaug (1994) proposed the formation of scattered concretions to be directly related to original depositional scattering of biogenic carbonate providing preferential sites of nucleation. Biogenic carbonate (especially aragonite) is chemically unstable compared with calcite cement. Once a

calcite concretion nucleus forms it begins removing carbonate ions from the pore water reducing the level of dissolved ions around the nucleus and stopping the formation of new nuclei adjacent to the original site (Walderhaug, 1994). At this point the reduction of carbonate ions will rejuvenate dissolution of the less stable biogenic carbonate which will create a diffusion gradient towards the concretion and result in precipitation on its surface.

Cementation intensity also revealed some interesting differences between both wells. The majority of very well to well cemented concretions occur in the upper portion of the Ben Nevis while the moderate to partially cemented horizons are found in the lower Ben Nevis. Does this reflect the different depositional environments from lower to upper, lateral facies change between wells or the “diagenetic freeze” that hydrocarbon emplacement may induce (Parnell *et al*, 2001)? One possibility for the decrease of cementation intensity in the lower portion of the Ben Nevis formation is late stage dissolution of the concretions in the higher permeable portions of the formation. The decrease in both sand/shale ratio and grain size up section reduces the permeability thereby decreasing the volume of calcite dissolving fluids acting on the concretions. This may also have implications on location of cement source and pore fluid flow. Reduction in bioclastic debris as the Ben Nevis Formation transgresses into a deeper water setting, lessens the number of nucleation sites, but super-saturated pores fluids pushed up from below create very well to well cemented concretions.

The upper and lower contacts give a sense for the geometry of the concretions. The concave and convex boundaries imply a rounded, sub-spherical shape. There are also

a wide variety of sharp erosional contacts which make excellent boundaries where a steep change in the original depositional ϕ and k could prevent flow-through of cementing fluids.

The various nucleation sites observed in core also helps with the interpretation of concretion formation. The absence of a nucleation site was the most common occurrence for the very well cemented concretions. This observation may have implications on the creation of very well cemented concretions by utilizing the entire bioclastic horizon that was originally the nucleation site for the concretion. The homogeneous nucleation site occurs in the majority of well to partially cemented concretions, providing a thick bioclastic unit with more than enough carbonate to act as a source. If the concretion development is fast enough, preservation of the bioclastic debris can be accomplished as the enveloping calcite cement occludes all porosity thereby removing possible dissolving fluids. Morad (1998) discussed the impact shell dominated layers have on carbonate cementation. Bioclastic lags indicate a wave and storm dominated, shallow marine environment, reworking into the slope apron (Hendry, 1996) with short-term mortality due to catastrophic events, primarily due to water column turbidity and a decrease in dissolved oxygen content.

The final and maybe one of the most important elements revealed by core description to help understand concretion development is siderite cement. Siderite is a typically early authigenic cement often associated with mica. Distribution is often controlled by bedding features such as ripple marks (Wilkinson *et al.*, 2000). The relative increase in siderite moving up through the Ben Nevis Formation permits some constraints

on siderite precipitation as well as possible siderite relationships with other authigenic cements. Slowing the rate of sediment accumulation by moving into deeper water shelf environments may prolong the duration of sediments through the oxic, sub-oxic (manganese and iron reduction), sulphate reduction and methanogenic zones directly impacting the precipitation of siderite and subsequent authigenic cements (Wilkinson, 1991). Siderite may also be linked to late ferroan calcite cements as a source of iron. Petrography and geochemical analyses may help elucidate some of the questions raised in this chapter.

CHAPTER 4

PETROGRAPHY

4.1 Introduction

Petrography, pioneered by Henry Clifton Sorby in 1849 (Sorby Natural History Society, website 2005) is the methodical description of 30 μm slabs of rock with the aid of a microscope. An invaluable tool for explorationists, petrography reveals information on the detailed composition and texture of a rock, as well as its post-depositional history of alteration (Scholle, 1979).

This chapter will systematically deal with the primary composition and texture of the detrital framework grains and matrix before moving on to authigenic components. Complete listings of modal analyses for all thin sections are found in Appendix B. Forty-six (46) thin-sections from core of well WR F-04 and fifty-nine (59) thin-sections from core of well WR B-07_4 were selected with an irregular distribution throughout the cored intervals to focus on calcite-cemented horizons.

4.2 Rock Classification

The Ben Nevis Formation sandstones in the WR F-04 and WR B-07_4 wells are quartz arenites, composed mainly of monocrystalline quartz grains, with relatively minor amounts of feldspar and rock fragments. A further refinement is made in this study based on the presence of bioclasts, matrix or carbonate cements. Sandstones are termed 'bioclastic' when 15% or more of the modal analysis is bioclastic debris. Argillaceous

modifiers require clay content between 8 and 14 %. Sandstones classified as slightly calcareous contain 5–14 % calcite cement. Calcite cemented sandstones contain ≥ 15 % calcite cement. Slightly sideritic sandstones contain 5-14 % siderite cement and siderite cemented modifiers have 15 % or greater modal analysis siderite.

4.3 Sandstone mineralogy

The above classification scheme exposes several compositional differences between the WR F-04 and WR B-07_4 wells. This is not surprising as the cored intervals are from different stratigraphic intervals. The intervals studied display a stratigraphic transition from offshore environments in the upper portion of WR F-04 to the relatively shallow-water shoreface in the lower section of WR F-04 and the top of WR B-07_4.

The transgressive nature of the Ben Nevis (McAlpine, 1990), with subsequent interpretation of depositional environment (Plint, 1999; Ferry, 2005) have been used with only slight variations identified in this study. The cyclic nature of fining upward beds, as well as the maturity and sorting of sandstones represent deposition in a high-energy, shoreface setting, which experienced intense and/or frequent storm activity with a subordinate amount of normal, fair-weather activity

Argillaceous and sideritic quartz arenites are found in the upper portion of the Ben Nevis Formation (core of well WR F-04), whereas bioclastic and calcite cemented sandstones are distributed irregularly throughout the entire formation. Bioclastic conglomeratic sandstone is present near the base of the Ben Nevis sandstone.

4.3.1 Framework/Detrital Minerals

Framework mineralogy has a significant impact on diagenesis. Dissolution of chemically immature detrital components creates secondary porosity but also provides ions into an evolving pore fluid that can later be precipitated as authigenic cement. Framework minerals control the availability of nucleation sites for authigenic cements. The sandstones of the Ben Nevis Formation consist primarily of very fine grained, well-sorted quartz arenites, containing shell debris concentrated in discrete horizons or disseminated across broad intervals.

4.3.1.1 Quartz

Quartz content averages 59 % of the modal analyses of all sandstones in this study and ranges from 10 to 100 %. Detrital quartz grains are predominately very fine sand size: (62-125 μm), fining upwards to coarse silt, sub-angular to sub-rounded, decreasing in roundness with decreasing grain size (Figure 4.1 A-D). Very rare coarse grains are also found in this generally very well-sorted sandstone. Quartz grains are predominately monocrystalline and normally demonstrate straight extinction. Quartz grains exhibit a wide variety of boundary types and grain-to-grain relationships, from floating grains in poikilotopic calcite cement (Figure 4.1 A), to point, planar, sutured and concavo-convex contacts (Figure 4.1 B-D).

Quartz grains are sometimes covered by quartz overgrowths, at times with sub-rounded to rounded boundaries taken to be indicative of recycling (Figure 4.2 A-C). Fewer quartz overgrowths have sharp euhedral boundaries consistent with authigenic

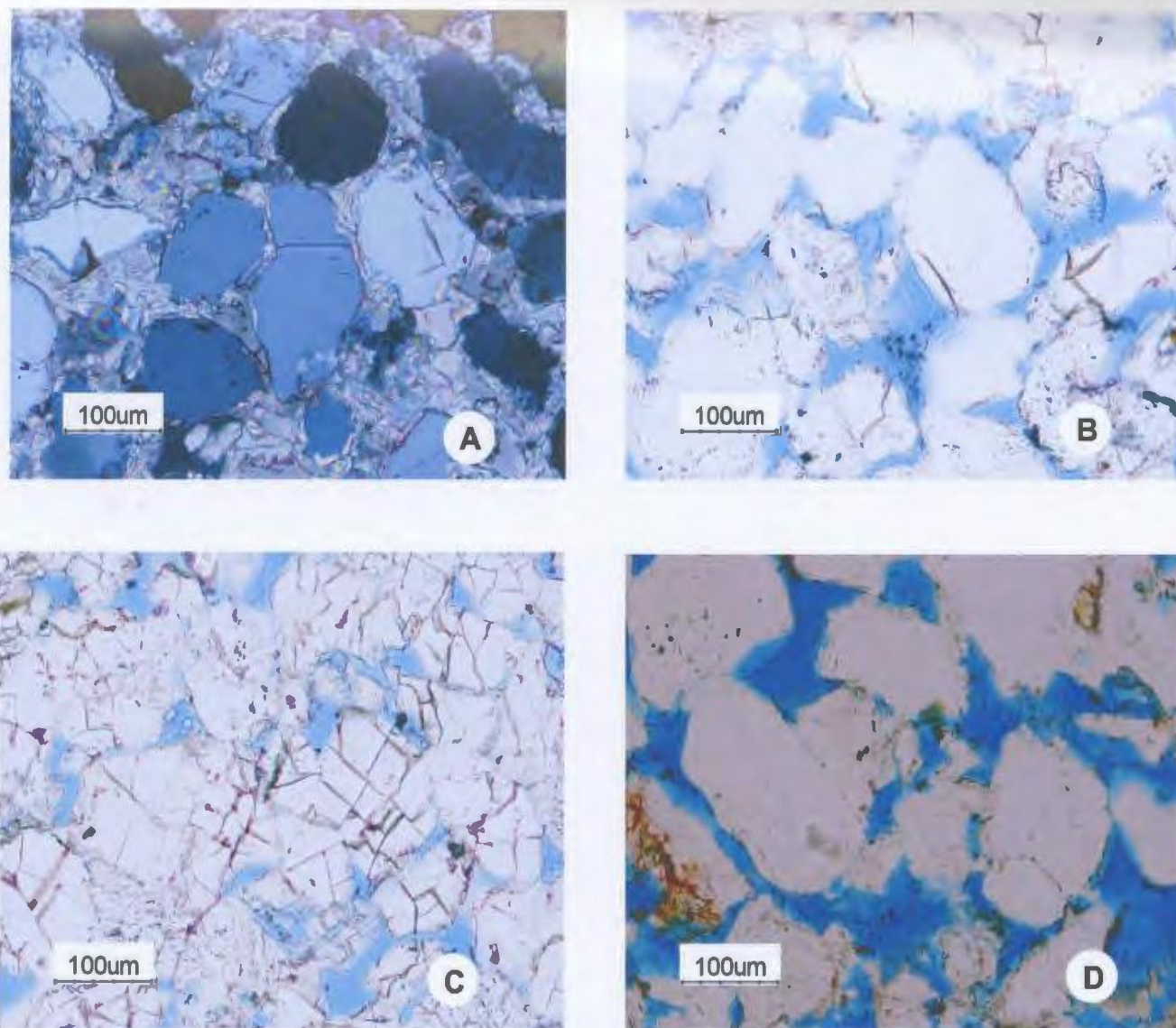


Figure 4.1: Quartz grains are the dominant framework grains **A.** Quartz grains surrounded by poikilotopic calcite cement, Cross Polars (B-07_4 Core 2, Box 10, TS 124; **B.** Sutured grain boundaries (B-07_4, Core 1, Box 73, TS 132); **C.** Fracture of quartz grains due to compaction (B-07_4, Core 1, Box 35, TS 149); and **D.** Sub-angular to sub-rounded, good porosity and permeability (B-07_4 Core 1, Box 65, TS 207).

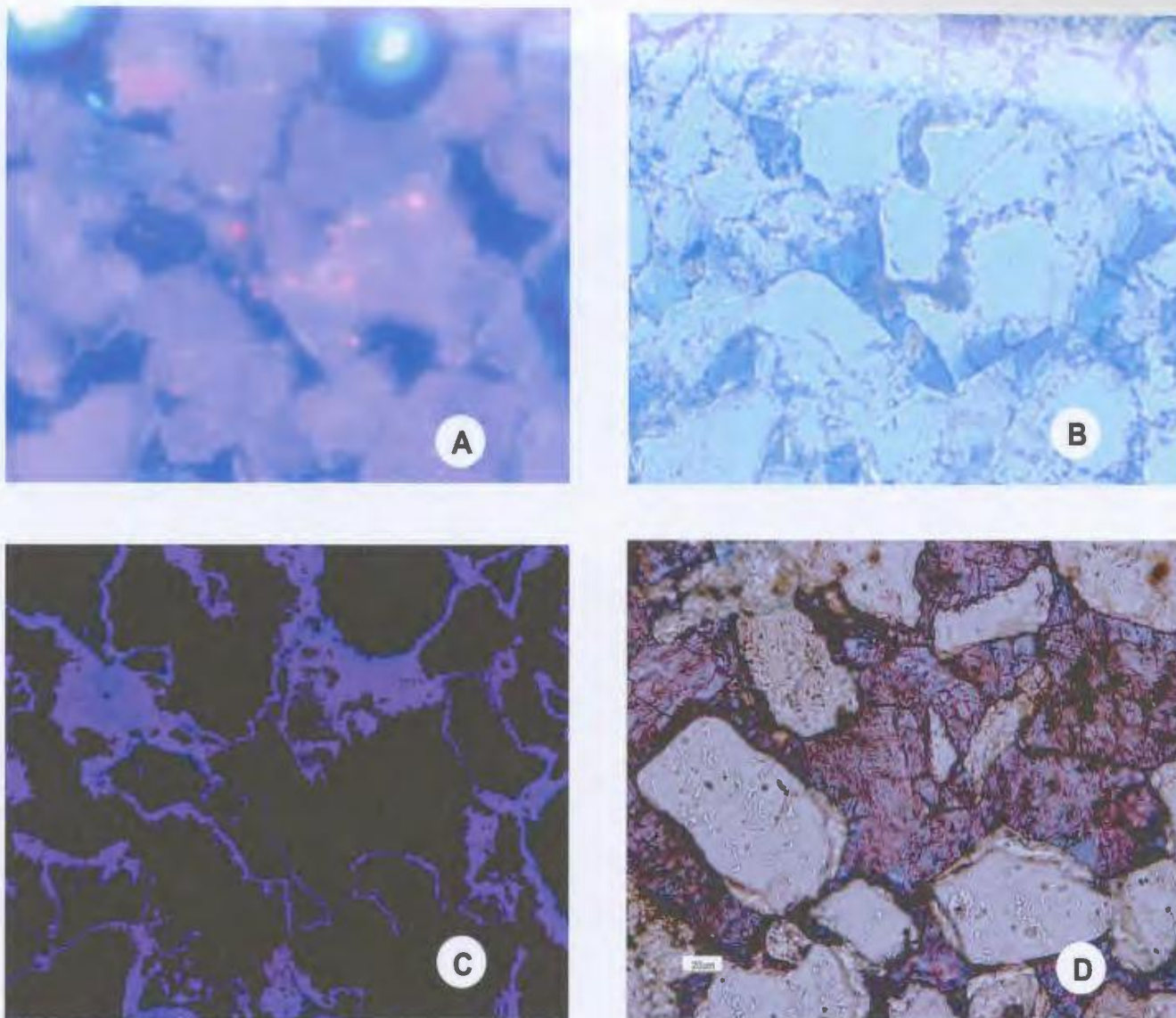


Figure 4.2: Quartz Overgrowths. A. Cathodoluminescence demonstrating two separate episodes of quartz precipitation (B-07_4 Core 1, Box 39, TS 144), B. Same as A in PPL, C. Same as A using ICP digital analysis to highlight quartz overgrowths; and D. Well developed quartz overgrowth prior to early calcite cementation, (F-04, Core 1, Box 73, TS 173).

formation (Figure 4.2 C). When surrounded by poikilotopic ferroan calcite cement, quartz grains commonly exhibit sharply embayed grain boundaries, corrosive textures and small islets next to the original grain (Figure 4.3 A-C).

4.3.1.2 Feldspar

Detrital feldspar is a minor component of the Ben Nevis sandstone, representing less than 1% of the overall modal analysis (Figure 4.4). However, because of the relative instability of feldspars their degree of preservation may be important in establishing the timing of calcite cementation. The majority of feldspar found in this study has been partially or almost entirely dissolved (Figure 4.5 A and C) and a few intact grains reveal albite twinning. Other feldspar grains have been strongly calcitized (Figure 4.5 B and D).

4.3.1.3 Rock Fragments

Rock fragments also make up less than 1 % of the Ben Nevis sandstone. Its absence provides an indication of provenance and environment of deposition. A high energy shoreface environment will remove rock fragments from the system providing texturally mature sandstones. The majority of lithic rock fragments found in WR F-04 and WR B-07_4 are detrital carbonate grains, chert and opaques (Figure 4.6). Detrital carbonate grains (Figure 4.7) may be sourced from the Rankin Formation, which lies unconformably below the Ben Nevis at the WR F-04 well (Dearin, 2005, pers. comm.). Rounded rock fragments imply transportation from the source rock with a high current energy providing abrasion of grains.

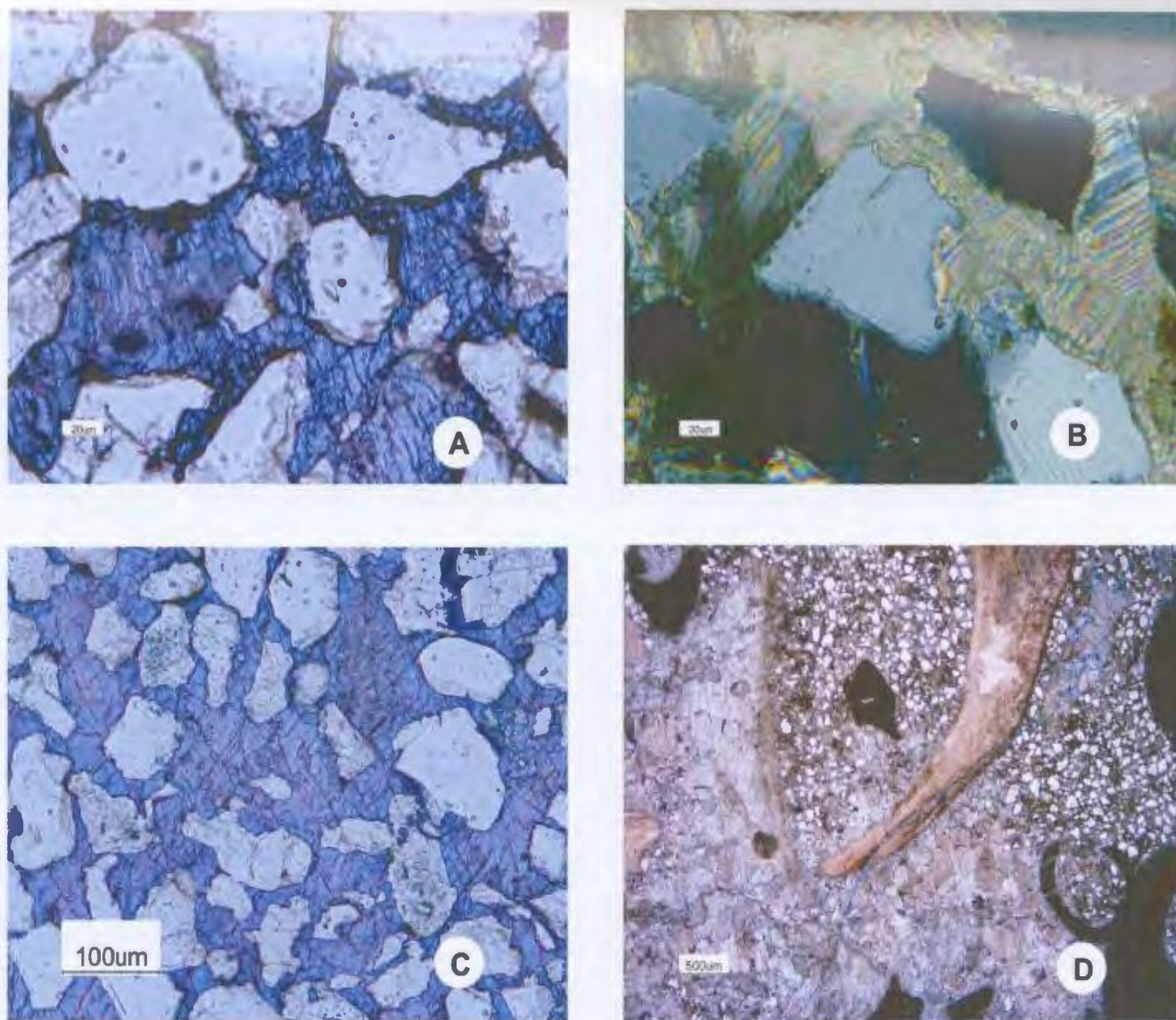


Figure 4.3: Quartz Dissolution A.Quartz islets (F-04 Core 1, Box 37, TS 171), B. Embayments in quartz grains (F-04 Core 1, Box 47, TS 176), C. Quartz dissolution with embayments and quartz islets (F-04 Core 1, Box 48, TS 177) and D. Quartz dissolution and replacement by calcite cement? (F-04 Core 1, Box 48, TS 178).

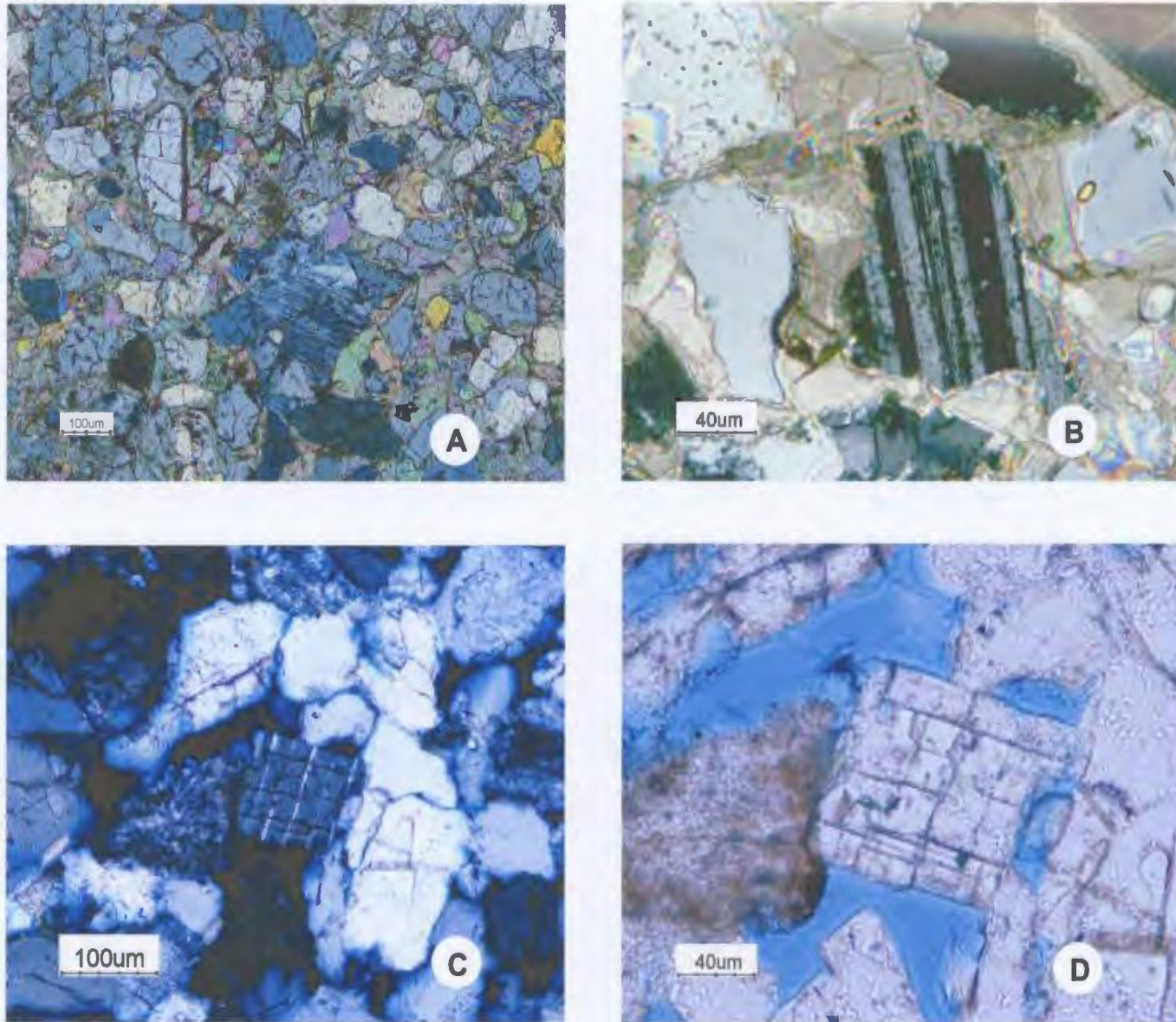


Figure 4.4: Feldspar Grains . A. F-04 Core 1, Box 28, TS 151 B. F-04 Core 1, Box 35, TS 148 C. F-04 Core 1, Box 4, TS 158 ; and D. F-04 Core 1, Box 4, TS 158.

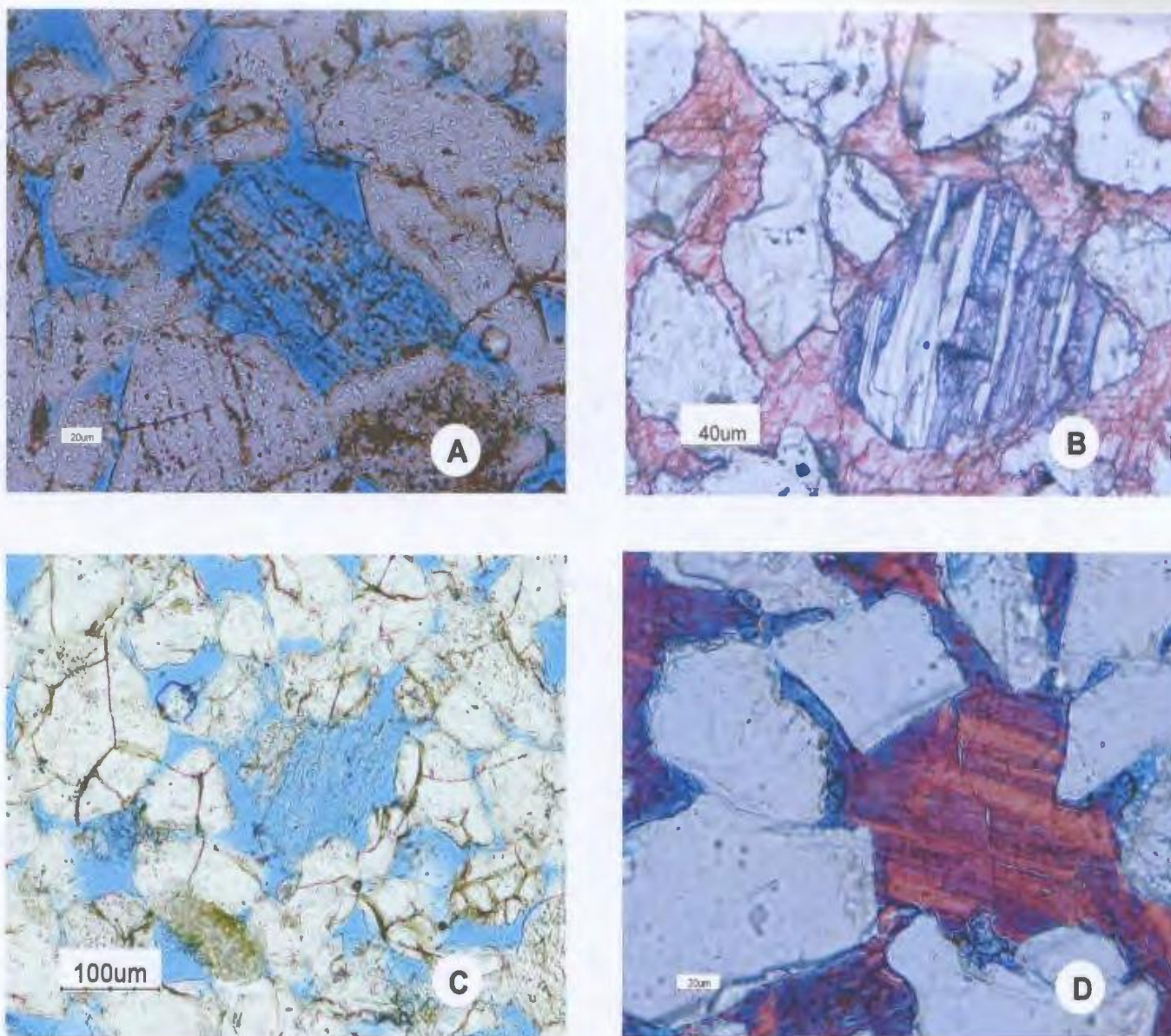


Figure 4.5: Feldspar Dissolution and replacement. A. Feldspar dissolution, (F-04, Core 1, Box 13, TS 162), B. Feldspar replacement with ferroan calcite cement, (F-04, Core 2, Box 65, TS 205), C. Feldspar dissolution (B-07_4, Core 1, Box 25, TS 152), and D. Feldspar replacement (B-07_4, Core 2, Box 10, TS 123).

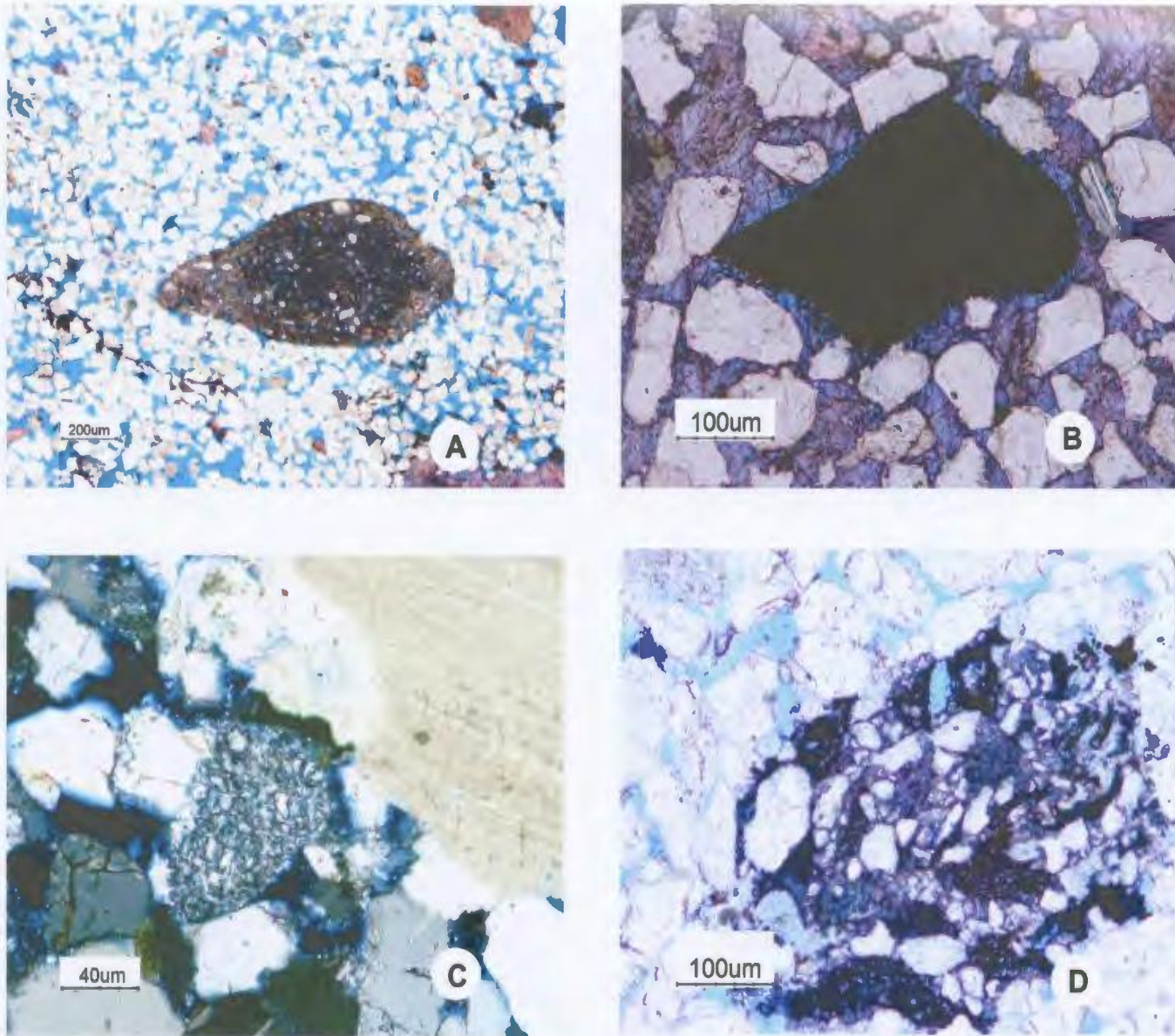


Figure 4.6: Lithic Rock Fragments A. Silty carbonate grain, well rounded and eroded, possibly from the underlying Rankin Formation (B-07_4 Core 2, Box 24, TS 209) B. Opaque grain (F-04 Core 1, Box 37, TS 170), C. Chert grain (F-04 Core 1, Box 35, TS 149); and D. Chert grain (F-04 Core 1, Box 59, TS 140).

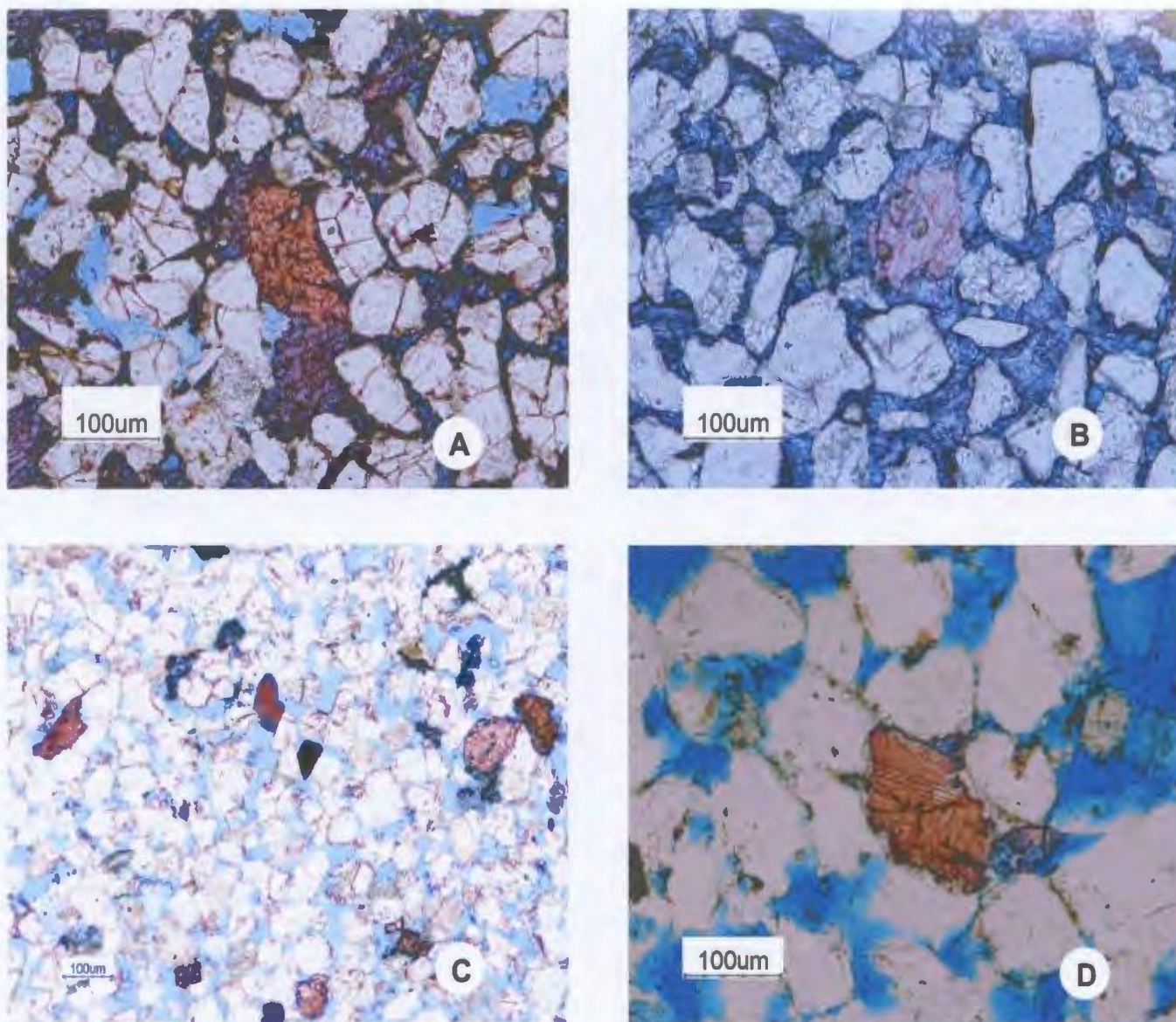


Figure 4.7: Detrital Carbonate grains A. F-04, Core 1, Box 28, TS 165 B. F-04, Core 2, Box 44, TS 199 C. F-04, Core 1, Box 47, TS 175 ; and D. B-07_4, Core 1, Box 65, TS 207.

The relative absence of feldspars and lithic grains implies recycling of sedimentary rocks as a source of the Ben Nevis Formation sandstones to thoroughly separate more labile framework elements, and concentrate quartz grains. Mechanical reworking within a wave and storm dominated shoreface likely also contributed to segregation of the framework mineralogy.

4.3.1.4 Accessory Minerals

A small assortment of accessory minerals is found throughout the Ben Nevis sandstone. While only a very minor component of the modal analysis, they can provide information regarding depositional environment, provenance and diagenesis. Accessory minerals found in WR F-04 and WR B-07_4 includes glauconite, carbonaceous material and opaque minerals.

4.3.1.4.1 Glauconite

Rounded pellet-shaped grains of glauconite (Figure 4.8 A and B) are rare in the lower part of the Ben Nevis sandstone increasing to trace amounts towards the top, perhaps reflecting the change to deeper water environmental conditions. Optimum depth of glauconite formation is thought to be approximately 200 m, near the top of the continental slope (Odin and Fullagar, 1988).

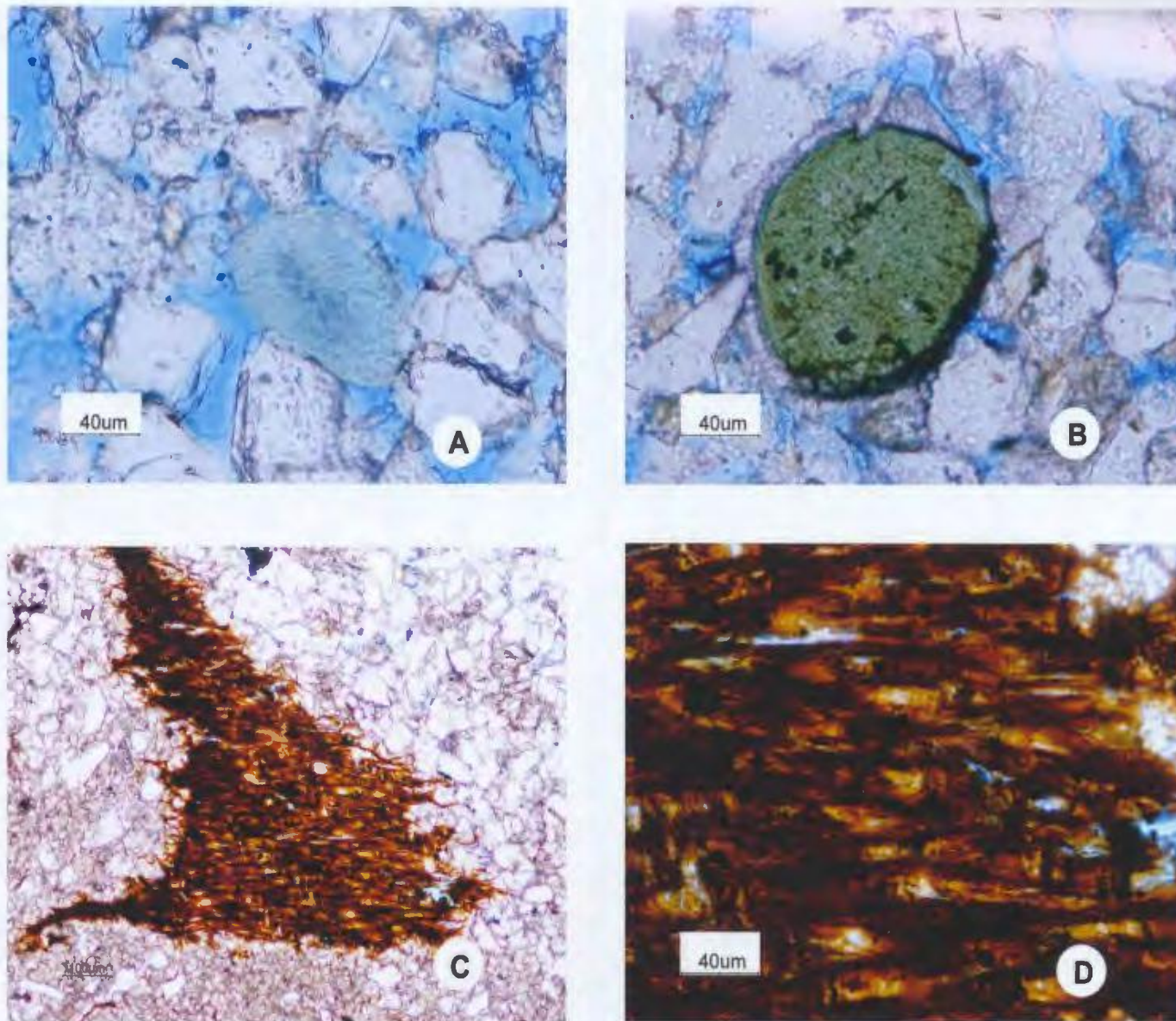


Figure 4.8: Accessories A. Glauconite Grain (F-04 Core 1, Box 13, TS 162) B. Glauconite with cement rim (F-04 Core 1, Box 5, TS 160) C. Wood fragment (F-04 Core 1, Box 9, TS 161); and D. Close-up of wood fragment. (F-04 Core 1, Box 9, TS 161).

4.3.1.4.2 Carbonaceous Material

Carbonaceous debris is rare in the top section occurring as irregularly shaped carbonized woody tissue, with well preserved cellular structure (Figure 4.8 C and D). The proximity to a paleo-shoreline could be implied from the presence of wood, but floating wood and plant debris may be carried far offshore during large storm events, which are the primary depositional environment for this sandstone.

4.3.1.4.3 Opaques

Opaque mineral grains represent up to 2 % of the modal analysis of the Ben Nevis sandstones. This mineral type (possibly pyrite or, hematite) is often associated with thin, compacted and often discontinuous residues of a micro-crystalline textured curved shell fragment of indeterminate affinity (Figure 4.9 D). These concentrations of opaques are occasionally found as a component of pelecypod shells (Figure 4.9 B), and may be associated with processes of shell alteration, and appear to be remnants of nearly complete dissolution of certain shell species. These unidentified shell types may provide the necessary calcite for precipitation of the calcite cemented concretions.

4.3.1.5 Bioclastic Fragments

Bioclastic debris is represented by the intact or disarticulated skeletons of marine organisms and may be the most important controlling factor affecting the precipitation of authigenic cement in the Ben Nevis sandstone. Bioclasts are recognized as bivalves, serpulid worm tubes, gastropods, corals, bryozoans, brachiopods and unidentifiable shell

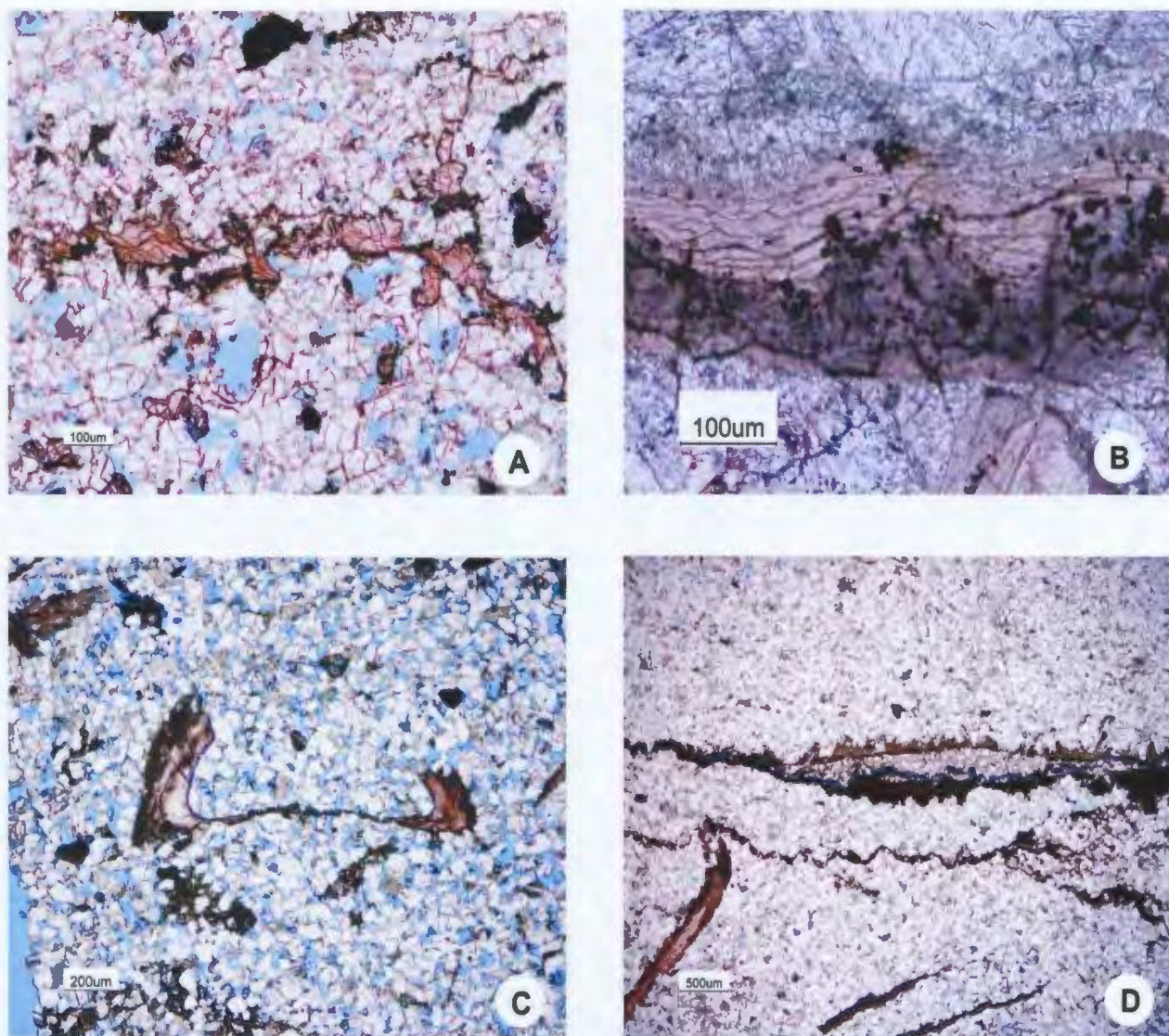


Figure 4.9: Shell Dissolution, source of carbonate. A. Dissolution and stylolization features; (F-04, Core 1, Box 44, TS 172), B. Opaques are commonly found within shells producing thin discontinuous intervals when shell is completely dissolved; (F-04, Core 1, Box 49, TS 179), C. Preferential dissolution in the direction of compaction; (F-04, Core 1, Box 60, TS 186), and D. Nearly complete dissolution of shells leaving behind opaques (F-04, Core 2, Box 29, TS 194).

species, and can locally represent up to 39 % of the modal analysis but overall average is 8.6 %.

4.3.1.5.1 Pelecypods (Bivalves)

The class Bivalvia occupy a wide geological time range from Lower Ordovician to Recent and poorly constrain depositional environment as they can live in marine, brackish or fresh water (Majewske, 1969). They can be mobile or sedentary with two convex valves and the shell microstructure can develop up to three distinct layers with mineralogy varying between entirely calcite, entirely aragonite or a combination of both minerals (Majewske, 1969). Common calcitic microstructures include foliated, prismatic, and homogeneous, while aragonitic structures are usually lost during replacement with possible relict microstructure within sparry calcite cement or a mosaic of irregularly grained calcite may suggest the former presence of aragonite (Majewske, 1969). Bivalves found in WR F-04 and WR B-07_4 display foliated and complex cross laminated microstructure as well as a multi-layered fabric (Figure 4.10). One distinctive species found in the Ben Nevis formation is *Exogyra* (McIlroy, 2005, pers comm.).

4.3.1.5.2 Serpulid Worm Tubes

Serpulid worm tubes are sedentary polychaetes of the phylum Annelida which secrete a calcareous habitation tube attached to a hard substrate in a marine environment (ten Hove and van den Hurk, 1993). Lowenstam (1954) was the first to investigate the mineralogy and composition of serpulid worm tubes, demonstrating how cold water

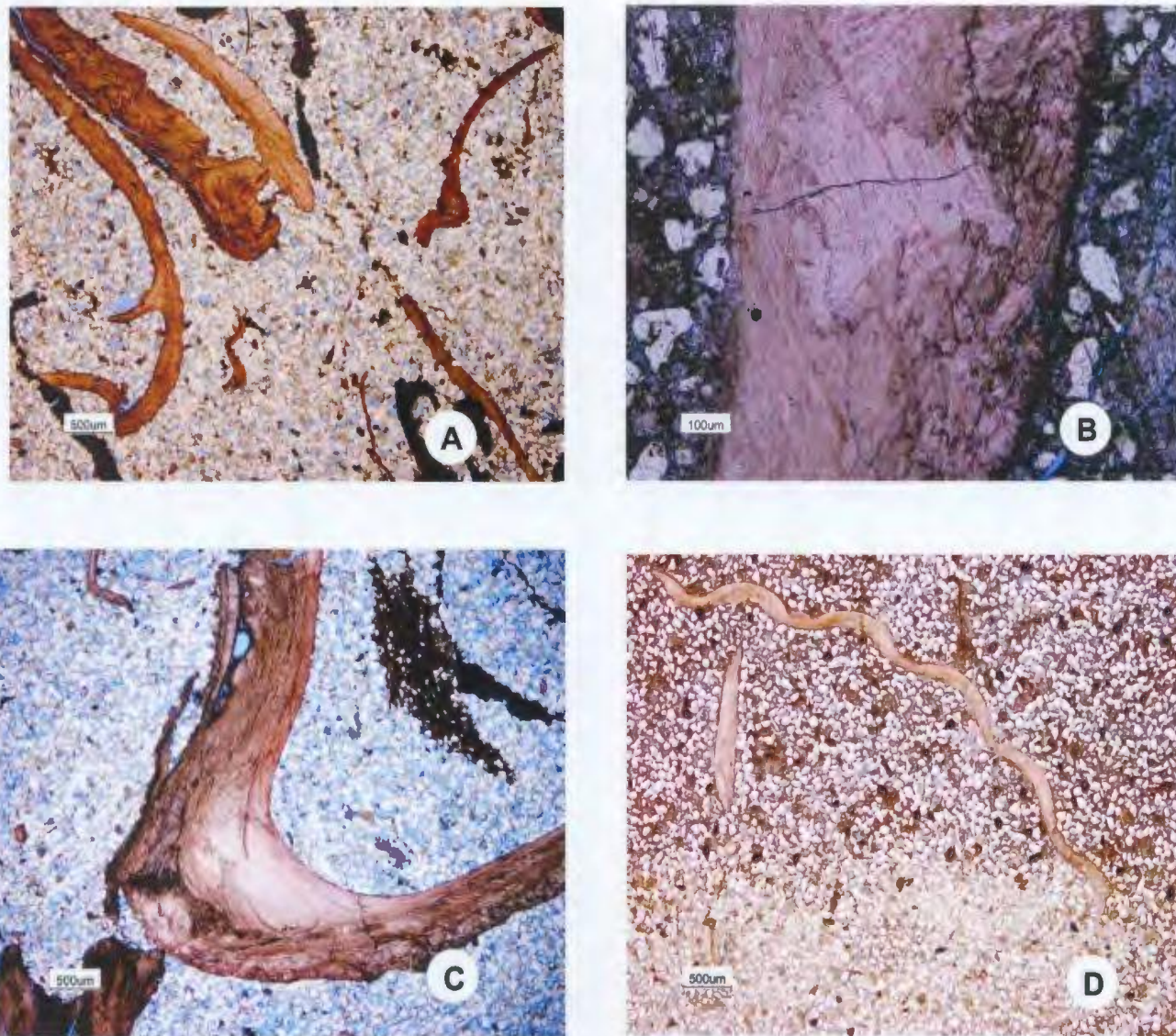


Figure 4.10: Bivalve Shells A. Foliated microstructure composed of random oriented bundles of thin calcite lamellae (F-04 Core 1, Box 28, TS 164) B. Complex crossed lamellar microstructure (F-04 Core 1, Box 37, TS 170) C. Multi-layer, foliated microstructure bivalve shell (F-04 Core 1, Box 37, TS 178) ; and D. Three layered foliated ridged bivalve shell (B-07_4 Core 1, Box 28, TS 151).

worm tubes secreted calcitic tubes and tropical species secreted aragonitic tubes. The proportional increase of aragonite with temperature has since been questioned by Bornhold and Milliman (1973), demonstrating compositional variations in calcite-to-aragonite ratios within the same tube. Varying ratios at this scale may represent seasonal variation but a more relevant question may be the change from calcite to aragonite in transverse cross-sections from inner to outer tube to determine any mineralogical changes during a single growth season.

Although serpulid worm tubes are not the most volumetrically significant portion of bioclastic debris found in the Ben Nevis Sandstone, they are possibly one of the sources of calcite cement and their presence could also help interpret depositional paleoenvironments. Typically a shallow water fauna (2 to 30 m depth), serpulid worm tubes inhabit unstable marine environments such as mixed saline (brackish 0.5 to 30 ppt) or hypersaline waters (>30 ppt), (Majewske, 1969). Serpulid ‘reefs’ are deposited on continental shelves at intertidal and sub-tidal depths in temperate to tropical seas around the world.

Ten Hove and van den Hurk (1993) indicate that the Serpulidae (Order Sabellida) are composed of calcite and/or aragonite. Neff (1969) recognized that aragonite is secreted by the lumen of what was previously known as the calcium secreting gland while high-Mg calcite is secreted from the ventral shield epithelium. Some worm tubes found in the Ben Nevis sandstone (Figure 4.11) reveal partial dissolution and recrystallization on the outer layer with very little dissolution on the inner layer.

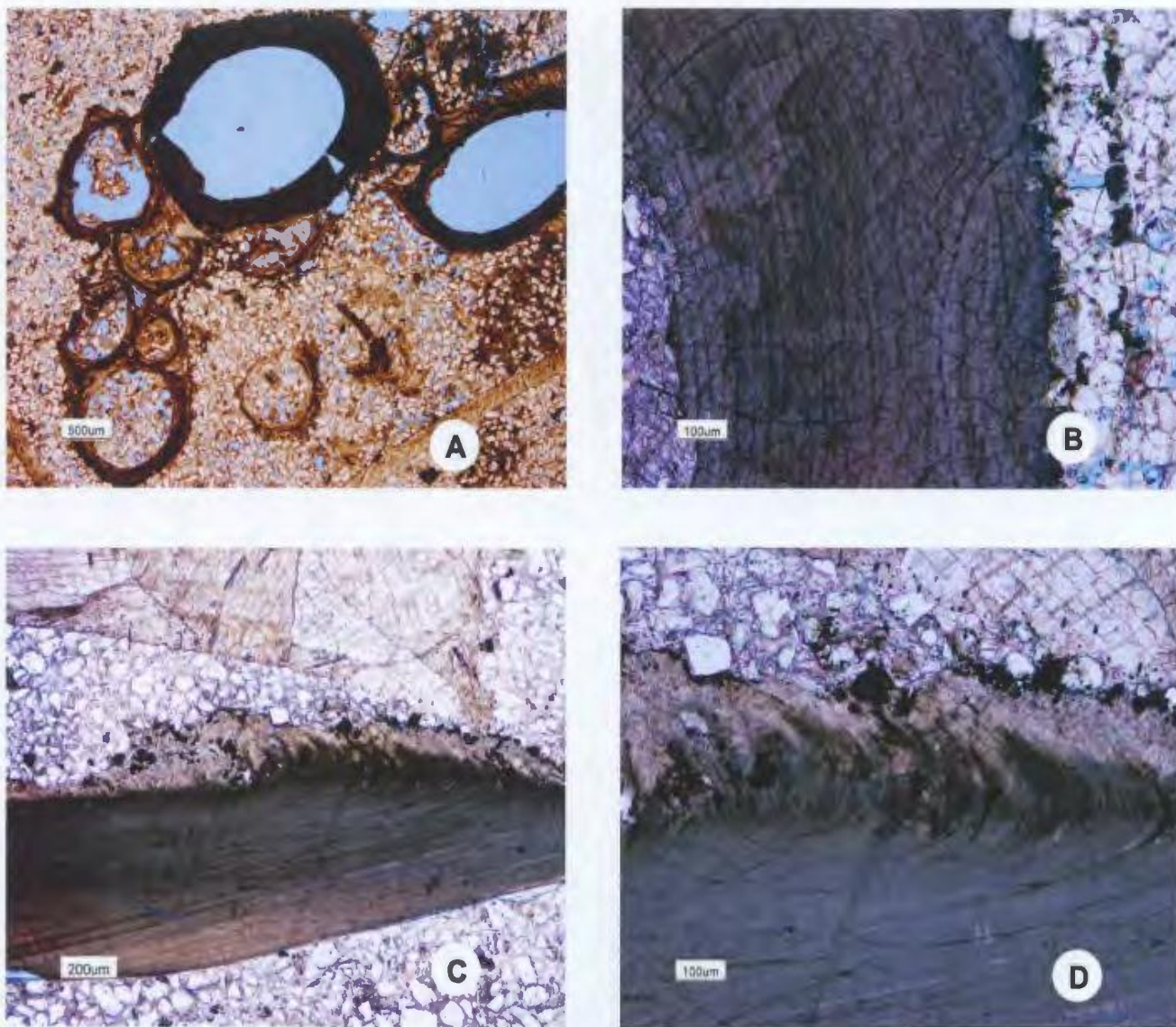


Figure 4.11: Serpulid Worm Tubes . A. Transverse cut through a colony of worm tubes (F-04 Core 1, Box 28, TS 165), B. Dissolution on the outer edge of worm tube (F-04 Core 2, Box 10, TS 190), C. Oblique cut through worm tube possibly identifying cone in cone structure of outer layer (F-04 Core 2, Box 45, TS 200; and D. Same as C with increased magnification (F-04 Core 2, Box 45, TS 200).

Assuming that the outer layer was originally aragonite, it has since been dissolved and may be a source for calcite cementation (See Chapter 5: Carbon and Oxygen Isotopes).

4.3.1.5.3 Gastropods

Gastropods range from the Cambrian to Recent and can be found in virtually any environment from marine and brackish, to fresh, terrestrial. The univalved cone of gastropods consists of a series of “whorls” wrapped around a central cavity and may contain up to five layers of calcium carbonate. The mineralogy of gastropods consists of calcite and aragonite or entirely aragonite. The mixed layer mineralogy consists of an external calcite layer and internal aragonite (Majewske, 1969). Figure 4.12 reveals the size and shape of gastropods found in the Ben Nevis Formation and occasionally demonstrates calcite replacement.

4.3.1.5.4 Brachiopods

Brachiopods range from Cambrian to Recent but occur in decreasing numbers in the late Mesozoic and Cenozoic. They are sessile and bivalved and exist mainly in marine environments. Generally composed of chitinophosphatic and calcareous shells, brachiopods distinguish themselves from bivalves based on their elaborate internal structure. Brachiopods can have external hollow spines on one or both valves (Majewske, 1969). The rare examples found in the WR F-04 and WR B-07_4 wells appear to be transverse sections of calcitic pentamerid brachiopods showing the pedicle and brachial valves with the spondylium in the center (Figure 4.13 A and B).

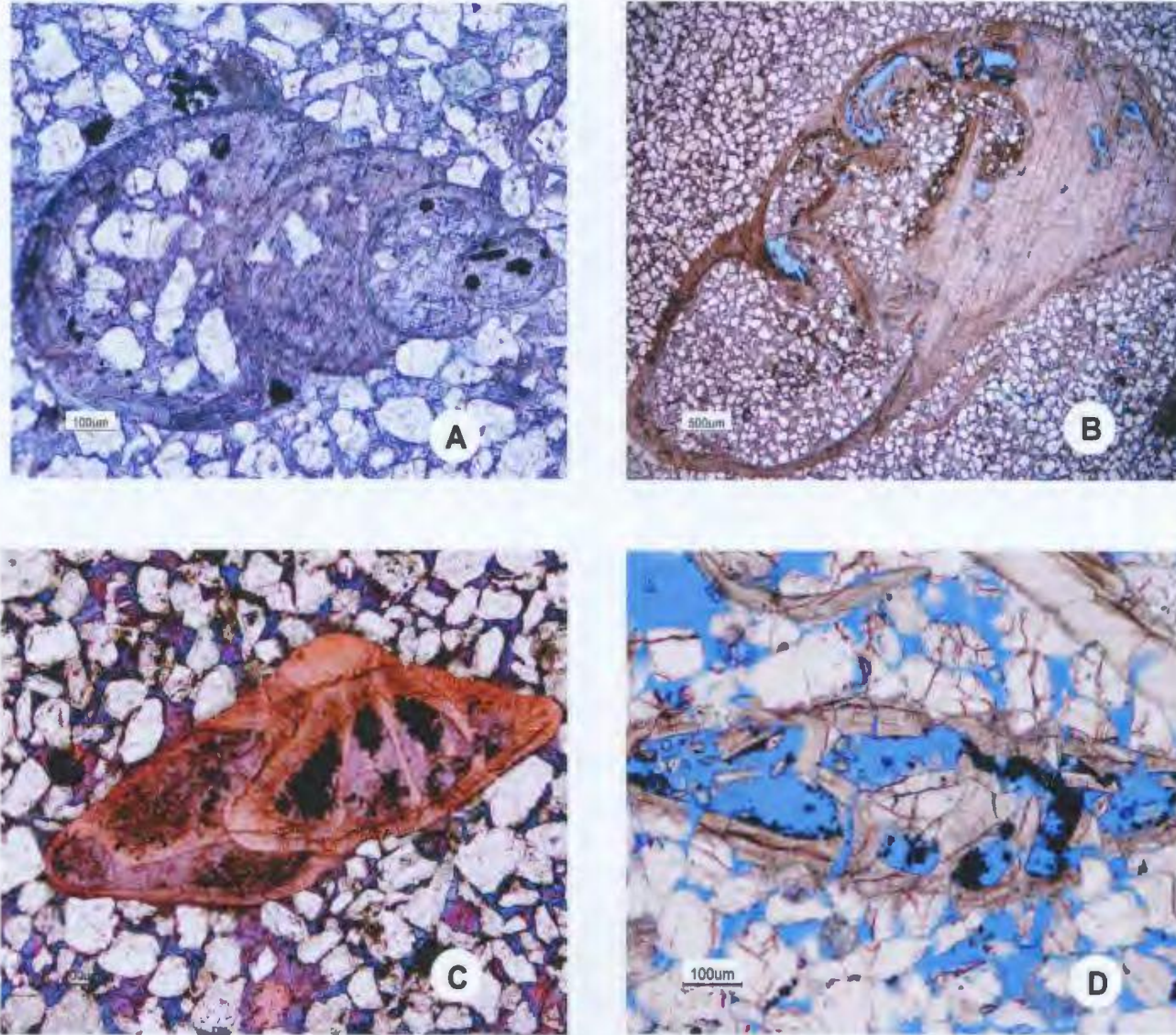


Figure 4.12: Gastropods. A. Gastropod shell replaced with ferroan calcite cement (F-04 Core 2, Box 10, TS 188), B. Gastropod shell (F-04 Core 2, Box 30, TS 195), C. Gastropod shell partially replaced but retaining the original structure (B-07_4 Core 1, Box 3, TS 159); and D. Gastropod shell under compaction (B-07_4 Core 1, Box 8, TS 157).

4.3.1.5.5 Corals

Rugose corals are solitary invertebrates found exclusively in marine environments and have been found in the rock record since the Ordovician (Majewske, 1969). Made-up of fibrous aragonite crystals, rugose corals are recognized by multiple septa projecting into a solid club shaped columella (Majewske, 1969). Corals are rare in the cores of this study, possibly sourced from a very distant reef or carbonate bank eroded during larger storm events (Figure 4.13 C).

4.3.1.5.6 Bryozoa

The colonial Bryozoa range from Ordovician to recent and are confined to a marine environment. Colonies consist of densely packed tubes (< 1 mm) and may appear as a lacy network of irregular polygons (Figure 4.13 D). They are generally composed of calcite in the form of granules or tiny imbricating plates (Majewske, 1969).

4.3.1.5.7 Unidentified Shell Species

Some ‘problematic’ shell fragments were too broken or fragmented to be identified petrographically (Figure 4.14), possibly representing cricoconarids, scaphopods, bivalves or gastropods. The variety of fauna preserved in very small abundance suggests a of fair weather shallow water environment capable of supporting an extensive communal ecosystem.

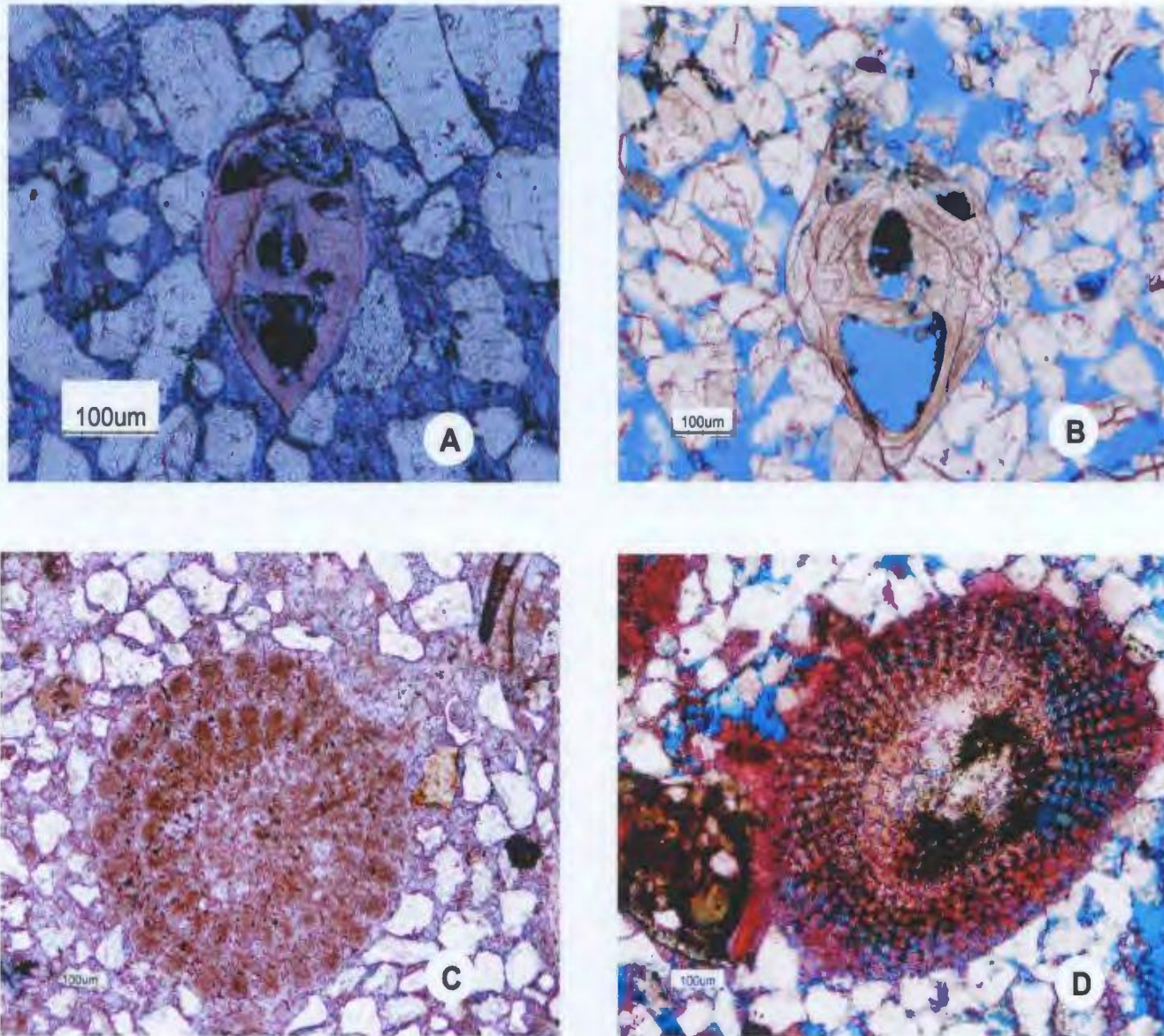


Figure 4.13: Brachiopods and Corals A. Transverse section through a pentamerid Brachiopod (F-04 Core 2, Box 10, TS 188), B. Pentamerid Brachiopod (B-07_4 Core 1, Box 8, TS 165), C. Transverse section through a solitary rugose coral (F-04 Core 1, Box 35, TS 167); and D. Coral? (B-07_4 Core 1, Box 17, TS 208).

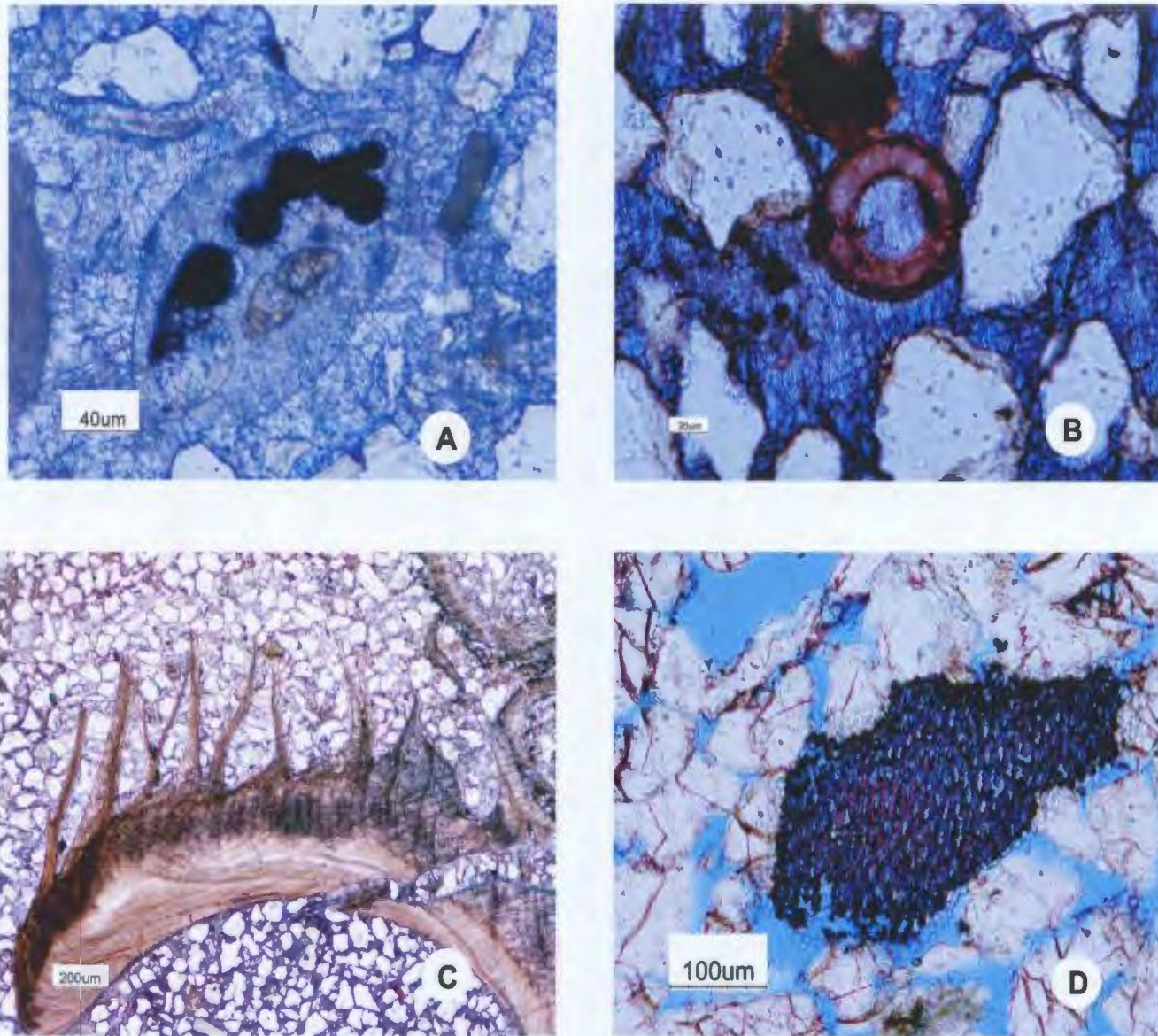


Figure 4.14: Unidentified shell species. A. Gastropod? (F-04 Core 1, Box 35, TS 167) B. Cricoconarid or Scaphopod (F-04 Core 1, Box 37, TS 171), C. Bivalve? (F-04 Core 2, Box 10, TS 189); and D. Echinoid Fragment? (B-07_4 Core 1, Box 59, TS 140).

4.3.2 Matrix

Matrix is detrital clay and other particulate fines deposited at the same time as the framework grains, which partly or completely infill the intergranular space. The majority of samples are clean arenites without any trace of matrix, with the majority of matrix-rich samples (Figure 4.15) occurring in the upper portion of the Ben Nevis Formation as it appears to grade into clay dominated mudstones of the deep-water Nautilus Formation. Clay minerals may occur as irregular, discontinuous laminae and may be associated with opaque minerals.

Clay minerals occupy approximately 1 % of the modal analysis of the samples selected in this study. Their presence is more pronounced in WR F-04 as the Ben Nevis sandstones become interbedded with muddy siltstones and finally silty mudstones during the transition into the overlying Nautilus Formation. Clay minerals provide information on the energy of the depositional environment, reduced current energy allows clay minerals carried in suspension the opportunity to settle. Compaction of clay minerals may be important during diagenesis, when clays are squeezed and deformed within pore networks, possibly occluding pore space. Another potentially important aspect relative to clay compaction is the release of structural or adsorbed water which can help to move fluids through the system directly influencing diagenesis.

Authigenic/Diagenetic Components

Authigenic minerals precipitate from solution or replace pre-existing minerals after deposition, representing the effect of diagenesis over the course of sediment burial

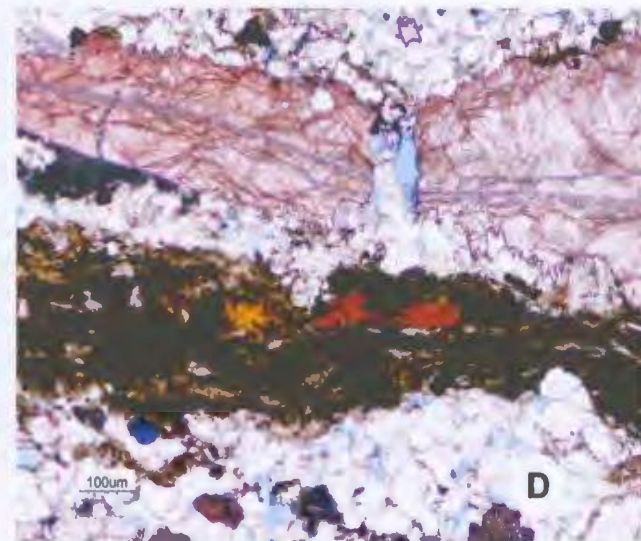
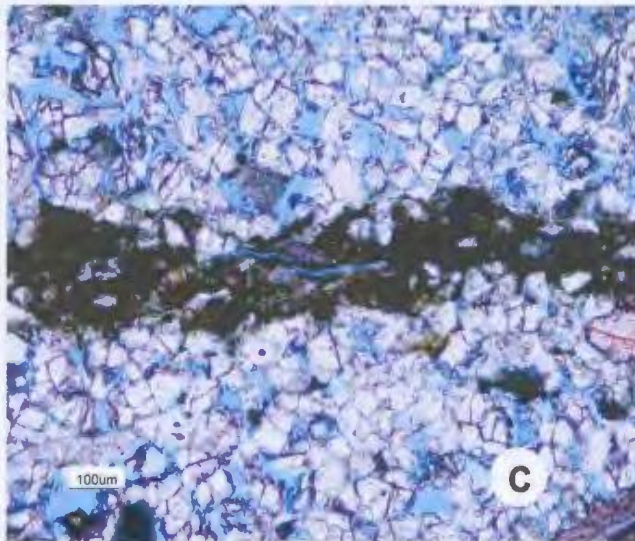
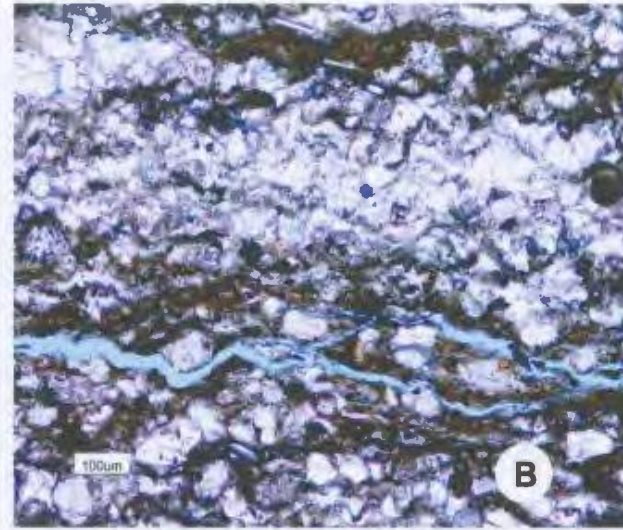
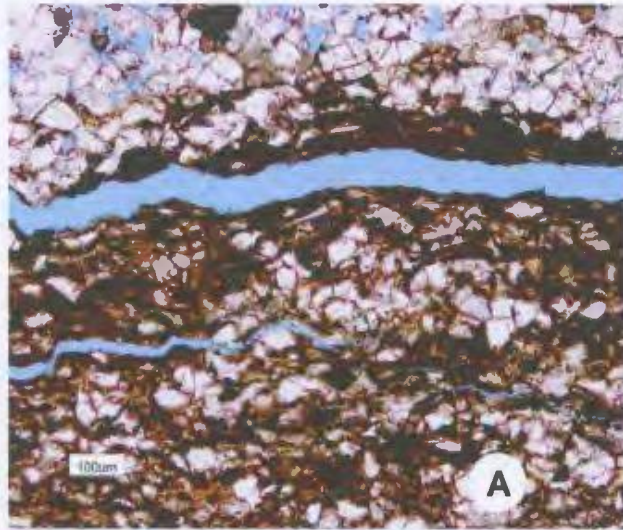


Figure 4.15: Clay Minerals A. F-04 Core 1, Box 44, TS 172 B. F-04 Core 1, Box 49, TS 180 C. F-04 Core 1, Box 57, TS 181 ; and D. F-04 Core 1, Box 57, TS 182.

and compaction. The major authigenic components identified in WR F-04 and WR B-07_4 cores of the Ben Nevis Formation are, in general order of decreasing frequency of occurrence, ferroan calcite, non-ferroan calcite, siderite, and quartz.

4.3.2.1 Calcite Cement

Calcite is the dominate authigenic cement, ranging from 0 to 50 %, averaging approximately 17.3 % of the modal analysis in the 88 samples analysed for this study, Calcite cement is primarily found as clearly defined, discrete horizons where it occurs as pore-filling cement, veins, or as recrystallization or replacement of bioclasts but it is also found as partially or weakly cemented horizons. This cement can be separated into non-ferroan and ferroan and occurs in several habits; coarse poikilotopic cements, pervasive micritic cements, syntaxial sparry cements on bioclasts and isolated subhedral crystals.

4.3.2.1.1 Non-Ferroan Calcite Cement

Non-ferroan calcite cement accounts for 2.5 % of the modal analyses of the samples in this study. This non-pervasive cement occurs as syntaxial overgrowths on coarsely crystalline calcite bioclasts (Figure 4.16 A), and tends to be irregularly distributed as poikilotopic patches (Figure 4.16 B-C). Where the host grain is iron-free, the calcite cement shows distinct zoning with an early slightly-ferroan calcite core followed by outer, clearly later strongly-ferroan calcite (Figure 4.17 A-D). Irregular boundary suggests neomorphic processes inconsistent with dolomitization. This boundary appears irregular possibly implying a gradational increase of Fe concentration in pore

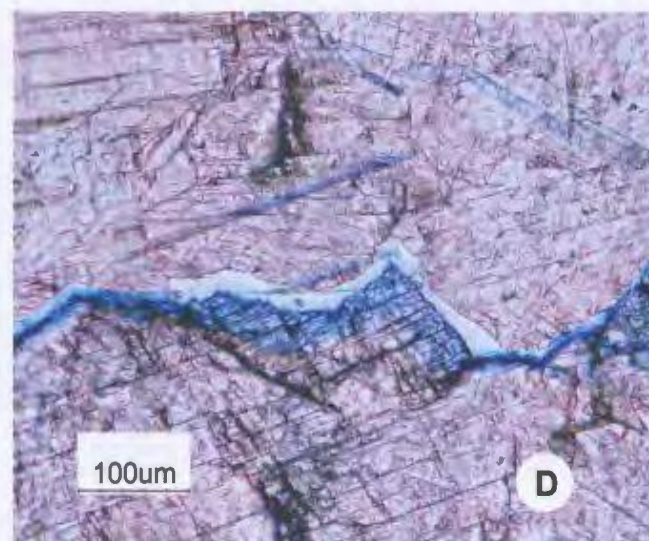
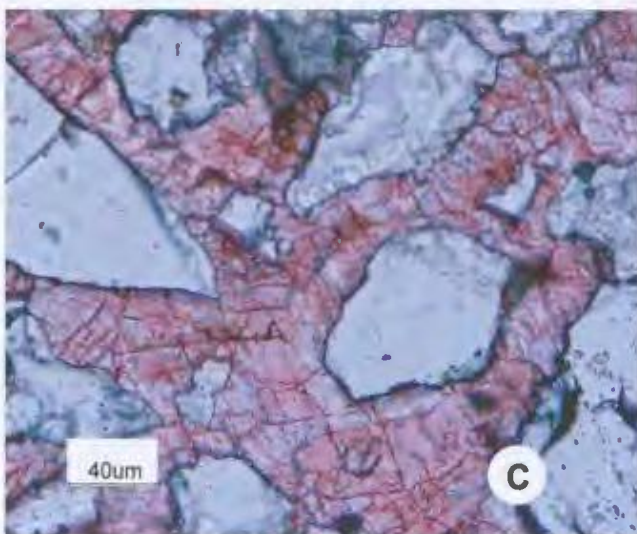
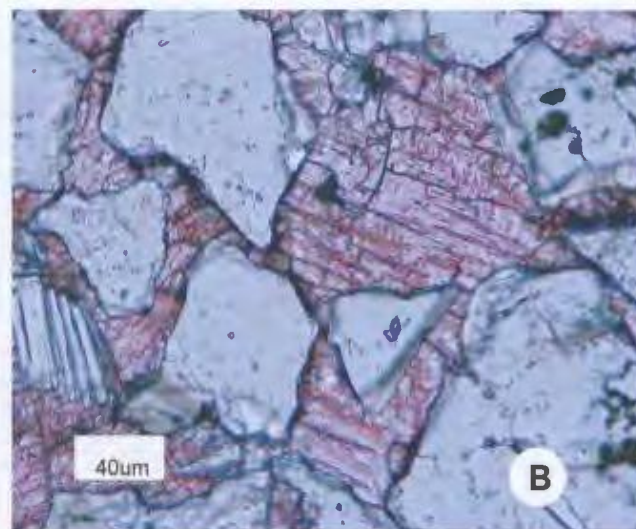
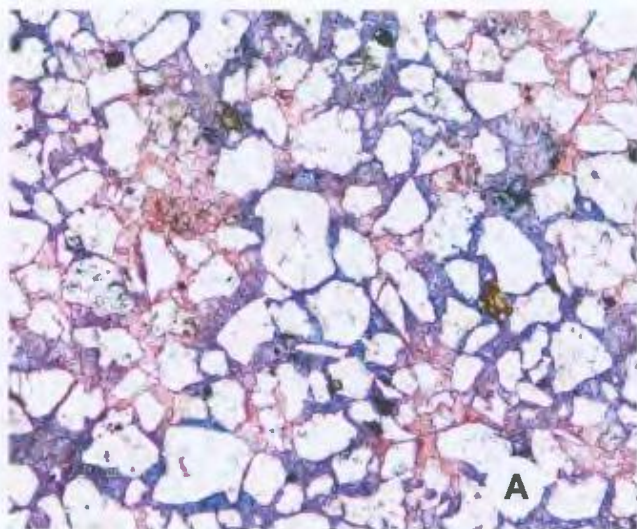


Figure 4.16: Non Ferroan Calcite Cement. A. F-04 Core 2, Box 59, TS 204 B. F-04 Core 2, Box 65, TS 205 C. F-04 Core 2, Box 65, TS 205 ; and D. F-04 Core 1, Box 35, TS 168.

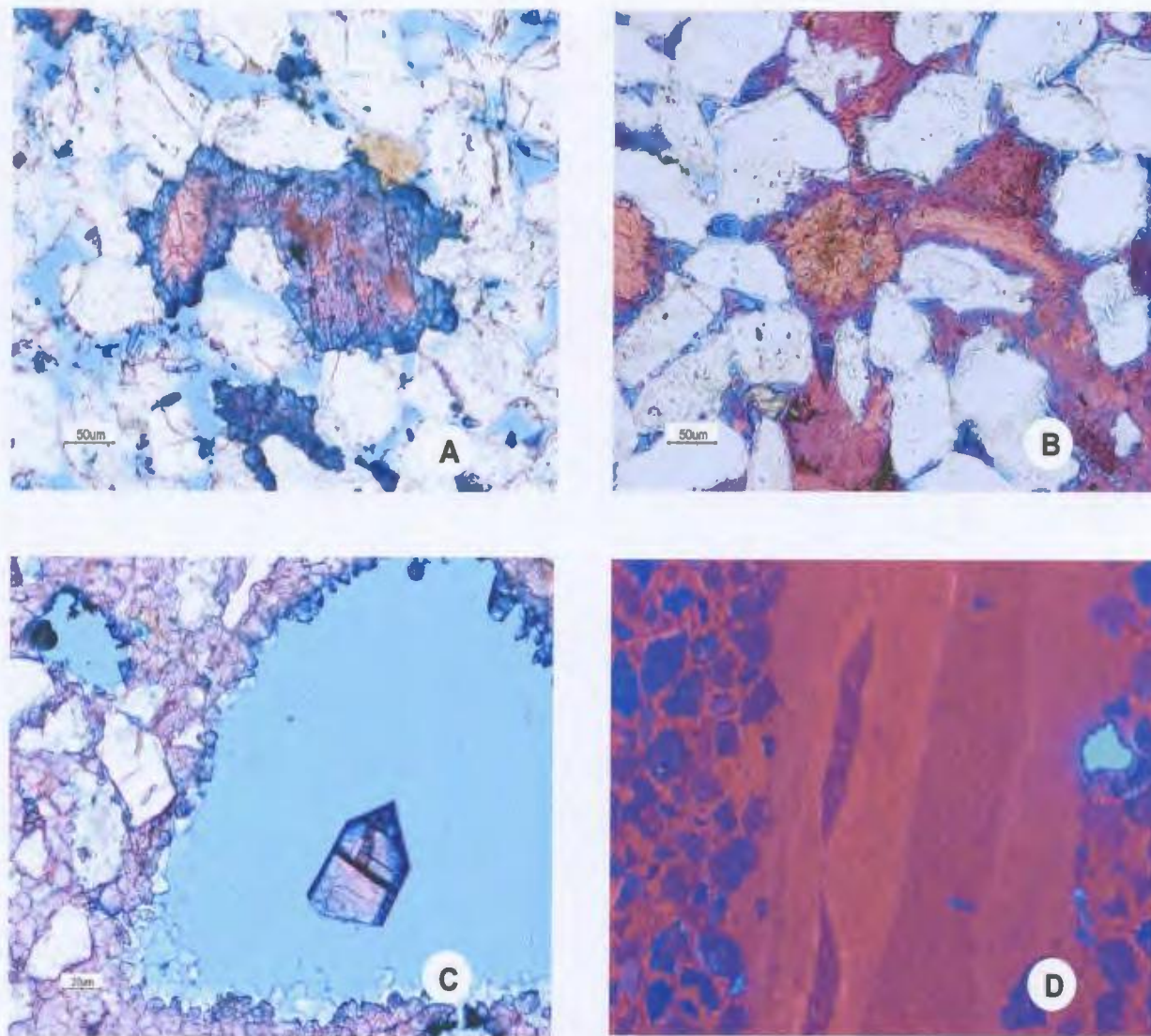


Figure 4.17: Distinct zonation between non-ferroan bioclasts, slightly ferroan cement and strongly ferroan calcite cements. A. Predominantly ferroan calcite cement, (B-07_4, Core 2, Box 11, TS 122), B. Non ferroan bioclast surrounded by slightly ferroan calcite cement (mauve) gradually converting to strongly ferroan calcite cement, (B-07_4, Core 2, Box 10, TS 123), C. Strongly ferroan calcite cement precipitating on slightly ferroan calcite cement (B-07_4, Core 2, Box 5, TS 126); and D. Calcite veins under catholuminescence showing four stages of cementation, (B-07_4, Core 2, Box 10, TS 124).

fluids or some hiatus between non-ferroan and ferroan calcite cementation during which limited dissolution of the non ferroan calcite cement occurred.

4.3.2.1.2 Ferroan Calcite Cement

Ferroan calcite cement is the dominant pore-occluding cement found in this study. It appears to have four distinct fabrics: poikilotopic, drusy spar mosaic, veins and small euhedral dog tooth crystals (Figure 4.18). This cement type occupies 14.8 % in the thin sections analysed but ranges from 30 to 46 % for the cemented samples. While there are various fabrics for the ferroan calcite cement, it is unclear whether they represent distinct events in a paragenetic sequence. These fabrics are usually mutually exclusive of each other denying petrographic analyses of cross-cutting relationships, but the various textures may reflect differences in the degree of super-saturation, distribution of shells, grains available for nucleation or available pore space.

Poikilotopic fabrics are characterized by very large crystals, several millimetres to more than one centimetre in size enclosing hundreds of framework grains. Poikilotopic cements exhibit under-compacted grain fabrics (Figure 4.18 A), corrosion (Figure 4.18 B) and replacement of silicate grains (Figure 4.18 C & D). This cement type generally occludes all porosity.

Drusy spar calcite mosaic crystals range from 100 to 500 μm mainly as replacement of shell fragments exhibiting an increase in crystal size towards the center of the shell. This type of cement occurs mainly in the bioclastic intervals and is typically very well cemented.

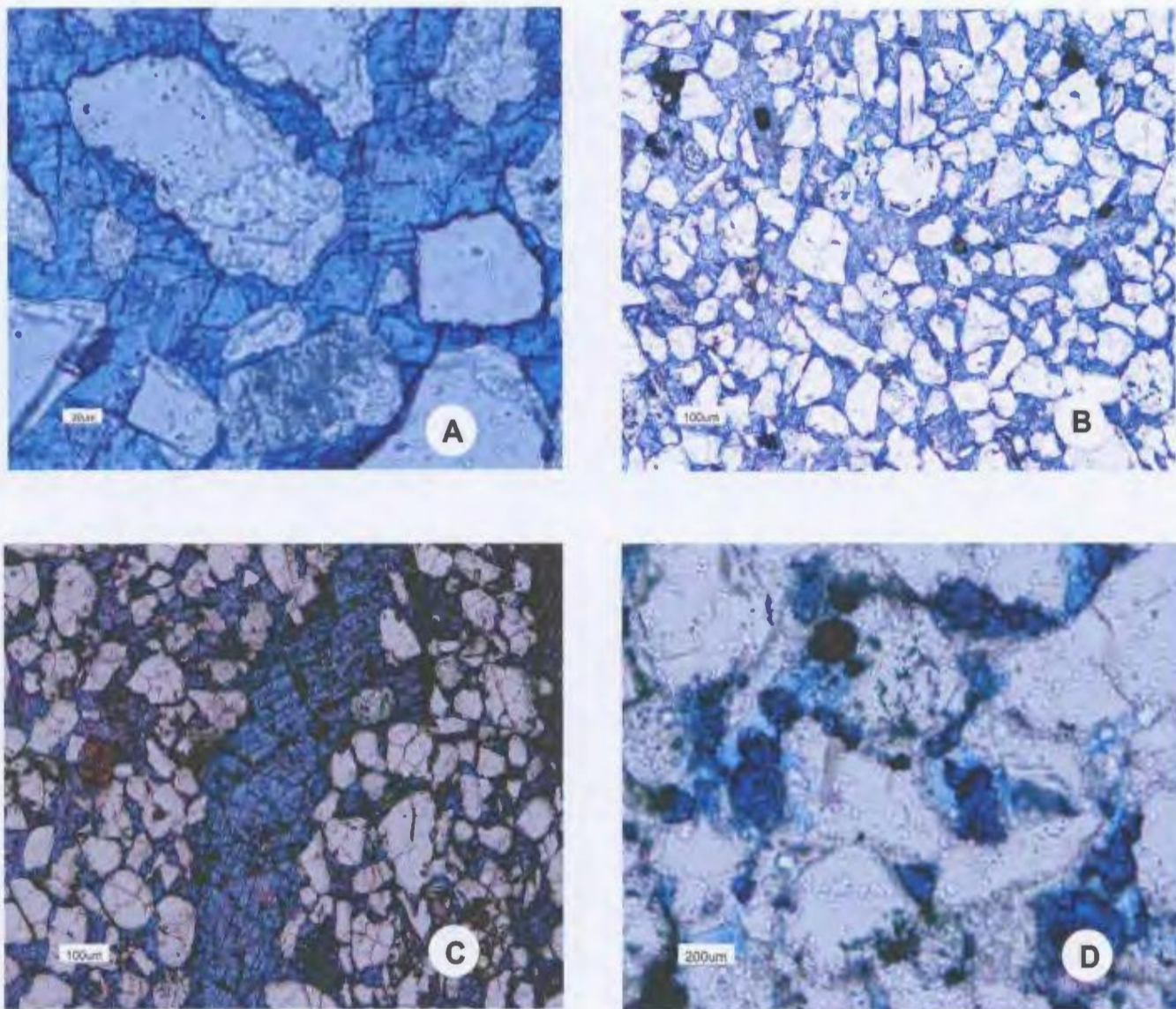


Figure 4.18: Ferroan Calcite Cement. A. F-04 Core 1, Box 58, TS 183 B. F-04 Core 2, Box 44, TS 199 C. F-04 Core 2, Box 45, TS 200 ; and D. F-04 Core 2, Box 65, TS 205.

Calcite veins are rare throughout the Ben Nevis Formation with six zones found within the WR F-04 core and four zones occurring towards the base of the WR B-07_4 core. The lower occurrences may be associated with slumping, which was identified towards the base of WR B-07_4 during core description. Calcite veins are white to orange, displaying four zones of distinct colours and intensity under cathodoluminescence, responding to phases of calcite precipitation (Figure 4.17 D). Calcite veins are up to 20 cm long, 3 mm wide, sub-vertical, with varying thicknesses and are sometimes stratigraphically confined to single beds. Calcite veins are generally located within the very well cemented concretions but are occasionally found on the edges of concretions or within uncemented sandstones. They are thought to record extensional forces after the formation of concretions providing timing for the paragenetic sequence.

The small euhedral dog tooth/bladed crystals have a more intense dark blue iron staining, range from 5 to 30 μm in size and have an elongate growth pattern. They occur primarily in the partially cemented intervals and may be extensions of the typical zoned calcite cement that have access to open pore space (Figure 4.19).

4.3.2.2 Siderite Cement

Siderite (Figure 4.20) content is highest in the upper portion of the WR F-04 well in the deeper water depositional setting. Siderite crystals are yellowish brown in color, flattened, rhombohedrons in shape and approximately 30 to 50 μm in length. The general association of siderite in most thin-sections is within the mold of a shell (Figure 4.20 A

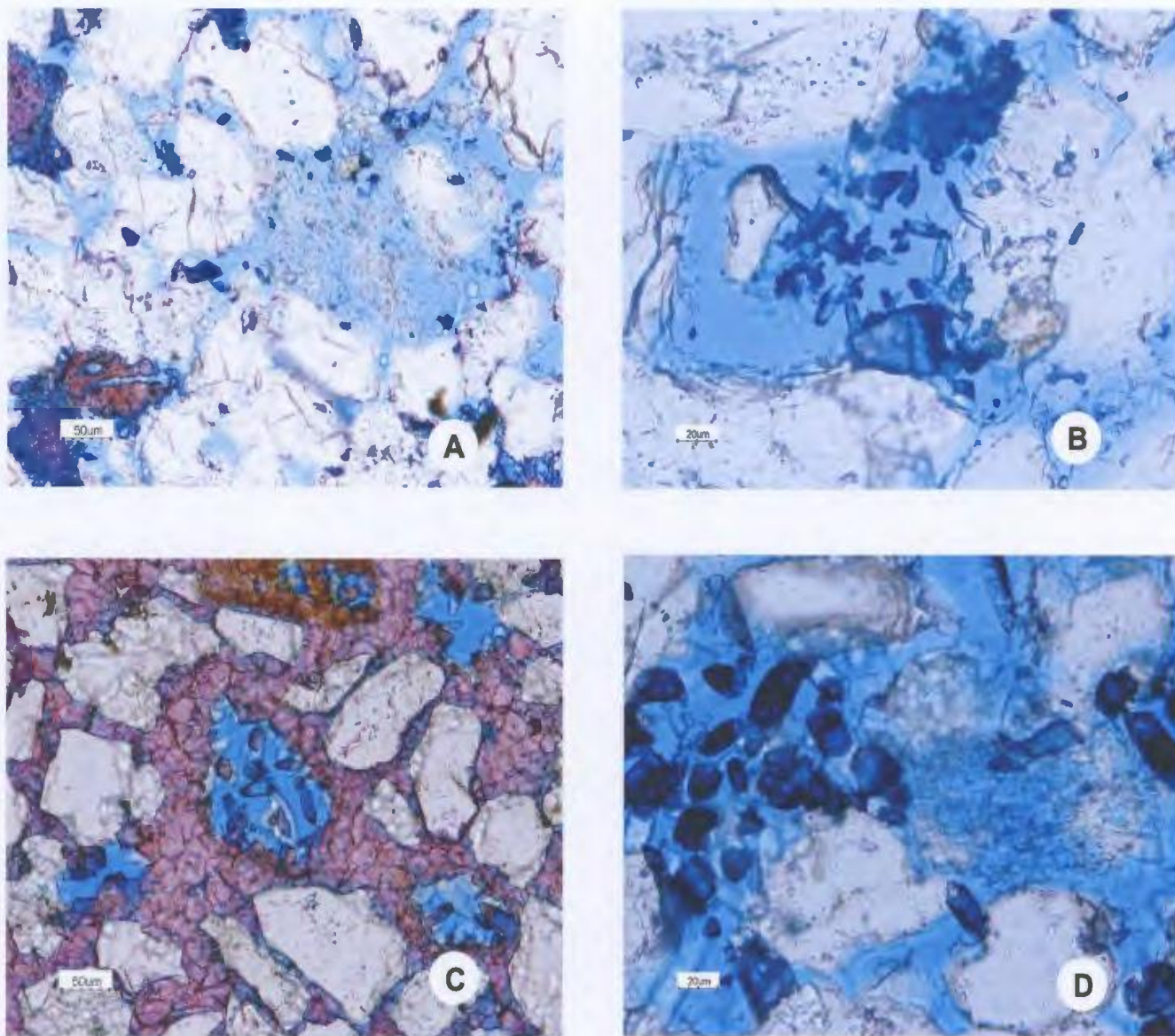


Figure 4.19: Late ferroan calcite cement. A. (B-07_4, Core 2, Box 11, TS 122), B. (B-07_4, Core 2, Box 11, TS 122), C. (B-07_4, Core 2, Box 5, TS 126) and D. (B-07_4, Core 1, Box 82, TS 130).

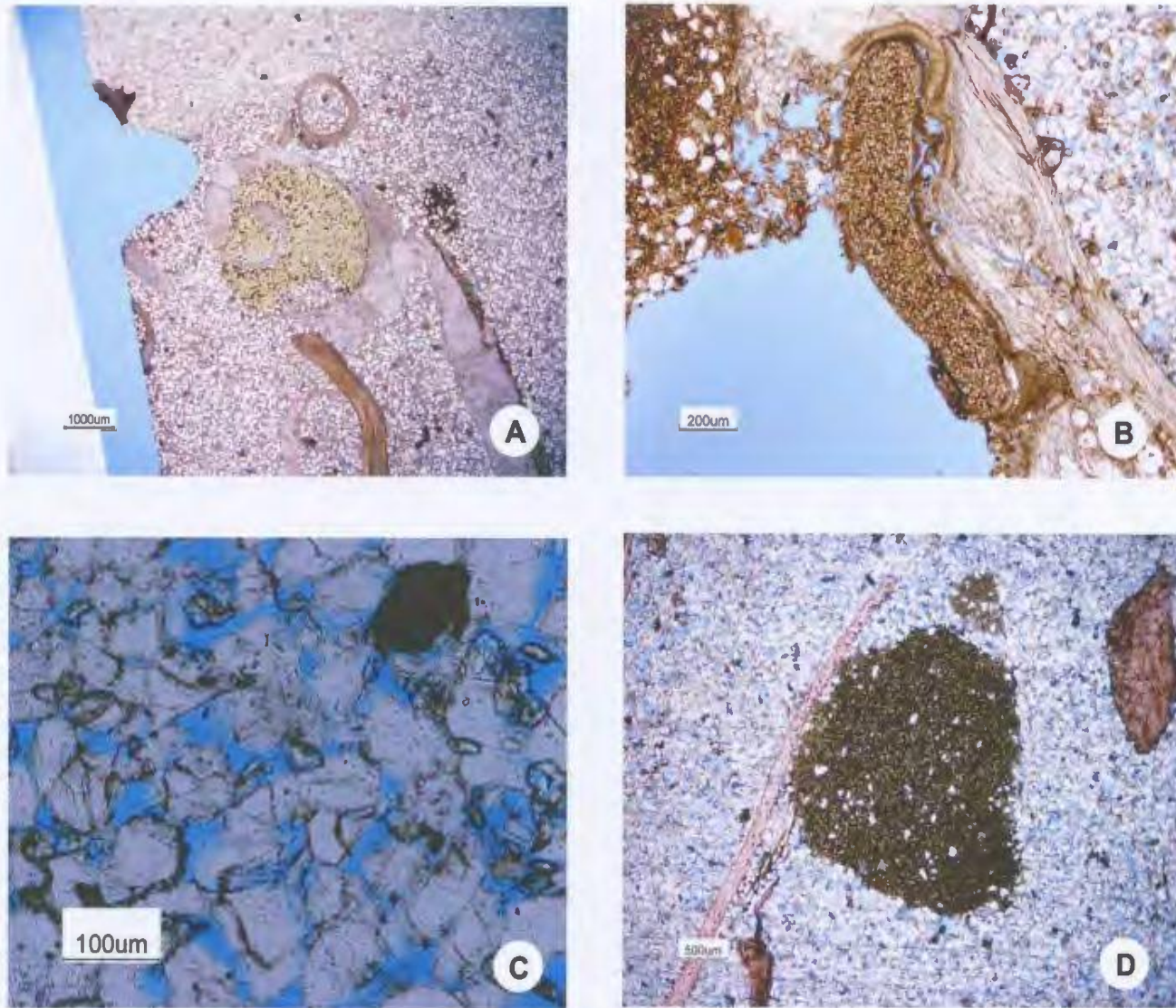


Figure 4.20: Siderite cementation in various forms. A. Siderite infilling gastropod shell, possibly developing on an organic substrate; (B-07_4, Core 1, Box 37, TS 146), B. Siderite infilling shell opening; (F-04, Core 1, Box 22, TS 163) C. Siderite crystals growing individually within open pore space; (F-04, Core 1, Box 60, TS 186) and D. Siderite cement completely replacing bioclastic material; (F-04, Core 1, Box 60, TS 186).

and B), as patches of isolated euhedral crystals (Figure 4.20 C) or disseminated throughout as individual crystals (Figure 4.20 D).

4.3.2.3 Quartz Overgrowths

Some quartz grains reveal multiple episodes of quartz overgrowths which clearly demonstrate the eroded nature of the early overgrowths suggesting derivation from an earlier sedimentary rock (Figure 4.2). Possible sources for the Ben Nevis sandstone are derived from previous cycles of erosion, transport, and re-sedimentation from the Avalon Uplift to the south or Central Ridge Complex to the east where much of the sediments have been eroded down to the Rankin Formation (Dearin, 2005, pers. comm.). The fine-grained nature and multiple quartz overgrowths can be interpreted to suggest erosion and reworking of underlying sandstones, possibly the Eastern Shoals, Catalina, Hibernia or Jeanne d'Arc Formations.

4.4 Diagenetic Sequence based on petrographic observations

4.4.1 Introduction

The diagenetic evolution of a sedimentary package includes the various stages of fluid flow responsible for the precipitation of authigenic cements and the dissolution of detrital framework grains as well as previously formed authigenic minerals. To fully understand this evolutionary pathway, it is critical to examine the influence of the original depositional environment, stratigraphy, sediment composition and texture (Burley *et al*, 1985 and Morad, 1998).

The depositional environment of the Ben Nevis sandstone ranges from lower shoreface to inner shelf and finally outer shelf at the top of this transgressive sequence (McAlpine, 1990). This texturally mature sandstone is relatively resistant to chemical alteration during diagenesis. However, deposition was dominated by a storm environment, adding large volumes of bioclastic debris which depending on the calcium carbonate content and alkalinity of marine waters may have been in the process of dissolution prior to deposition and surely would continue to dissolve during burial.

The high rate of deposition produced by a storm dominated environment, and the rapid subsidence inferred to be responsible for this very thick succession (350 m in the South Avalon pool), forced the sediment column to pass quickly through the oxic, sub-oxic, bacterial sulphate reduction and microbial methanogenesis zones in the sub-surface. The geochemical classification of sedimentary environments based on oxygen and sulphur variables was originally introduced by Berner (1981). After dividing sedimentary

environments into oxic and anoxic sub-environments, the anoxic environment is further subdivided into sulphidic and non-sulphidic and the final division is anoxic-nonsulfidic into post-oxic and methanic.

The volume of clays is also very important, as clay grains are responsible for reducing permeability by blocking pore throats during compaction. The limited amount of feldspar has little effect on authigenic cementation as it provides insufficient ions for subsequent precipitation.

Regarding fluid flow properties within shallowly buried, uncemented Ben Nevis sands, the data of Beard and Weyl (1973) can be used to estimate permeability and porosity. Beard and Weyl (1973) used artificially packed sand to determine that a decrease in permeability results from decrease in grain size and a decrease in sorting, while sphericity and angularity are of second-order importance. Accordingly, using Beard and Weyl's (1973) size-sorting tables, the fine grained, very well sorted Ben Nevis sandstones may have had an original porosity of 39.8-40.8 % and permeability of 14-29 Darcys.

The nature of the stratigraphic succession may also provide insight on possible sources of authigenic cements, ultimately affecting the diagenetic history. Erosion of the underlying sediments on horst blocks or halokinetic structures resulted in a disconformity between the Ben Nevis Formation and the Rankin Formation (Dearin, 2005, pers. comm.), and this relationship is illustrated on a seismic section across the WR F-04 location (Figures 4.21 and 4.22). This lime rich formation which also contains the Egret

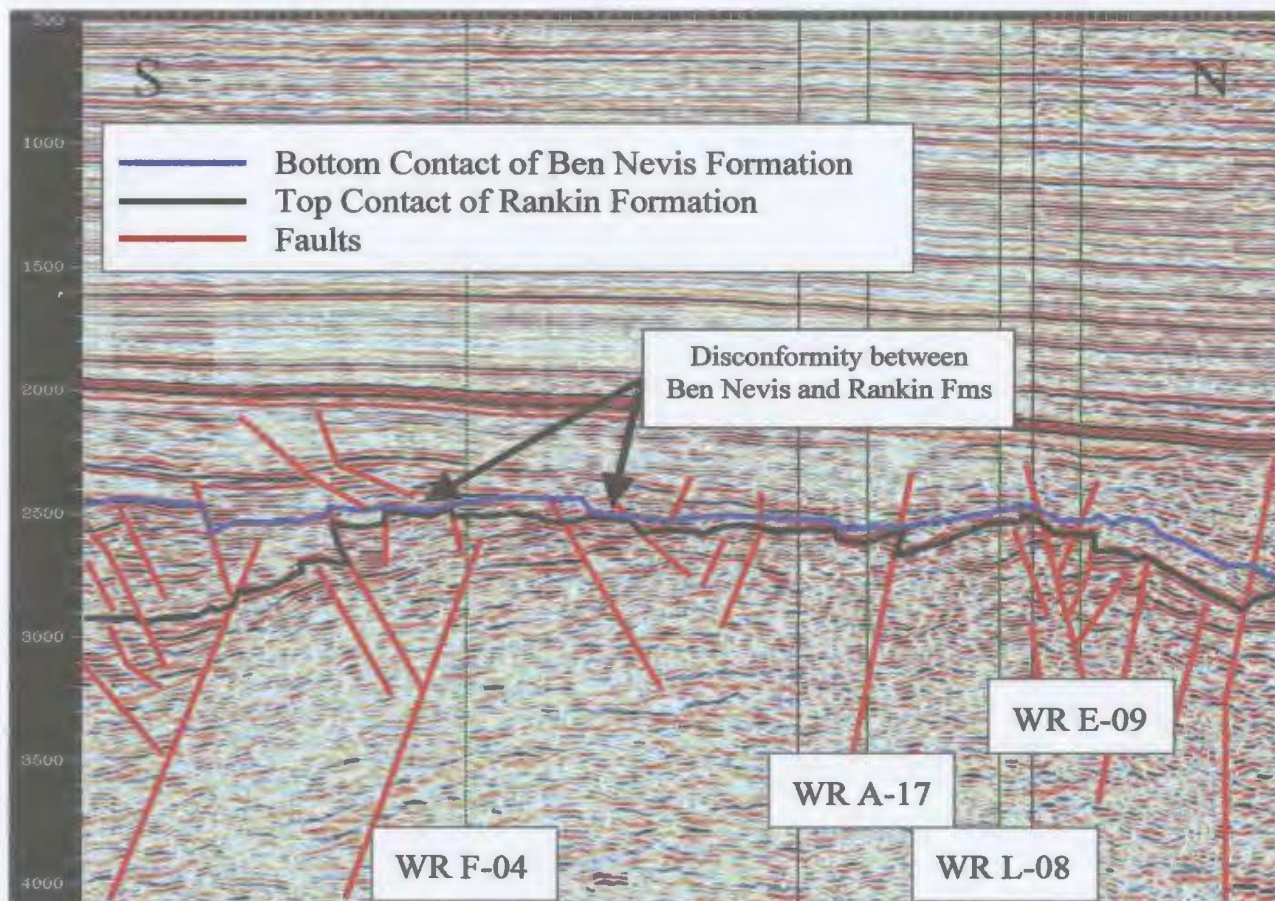


Figure 4.21: Seismic line North – South through White Rose Field, demonstrating the erosion of sediments allowing the Ben Nevis Formation to lie unconformably above the Rankin Formation.

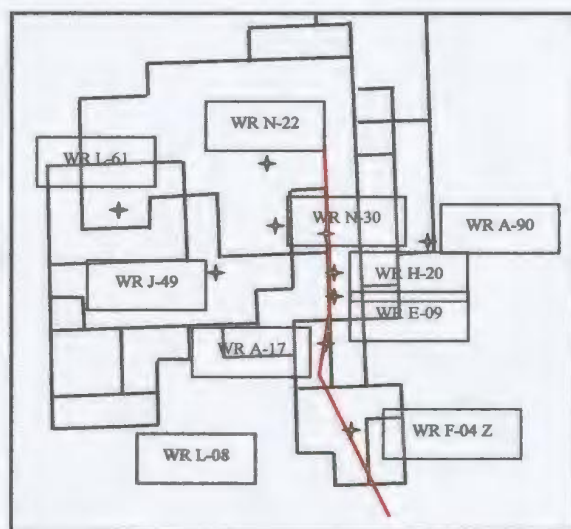


Figure 4.22: Location map of seismic line (Figure 4.21) through White Rose Field

member source rock could easily develop a diffusion gradient with the Ben Nevis paleo-aquifer providing an abundant source of calcium carbonate. A similar relationship could arise between the Ben Nevis and the underlying marlstones found at the WR B-07_4 location.

Subsequent petrographic observations will use the same guidelines as those applied to planar features in bedrock geological mapping such as superposition or cross-cutting relationships. Also very important is the nature of grain and crystal boundaries to distinguish conditions of growth and/or dissolution. Textural relationships are interpreted from petrography to estimate relative timing of the paragenetic sequence of the Ben Nevis Formation at the White Rose Field in terms of early, middle or late. The proposed paragenetic sequence is presented in Figure 4.23 and each of the mineral phases and diagenetic events are discussed in chronological order.

4.4.2 Recycled Quartz Overgrowths

Observations with optical cathodoluminescence provide some useful information regarding the secondary and even tertiary nature of quartz overgrowths. Figure 4.2 (A) clearly shows two separate stages of quartz overgrowths that have been truncated and both demonstrate a rounded to sub-rounded texture. These overgrowths were most likely present prior to burial and could represent the recycling of underlying sandstones such as the Catalina, Hibernia, or Jeanne d'Arc Formation sandstones.

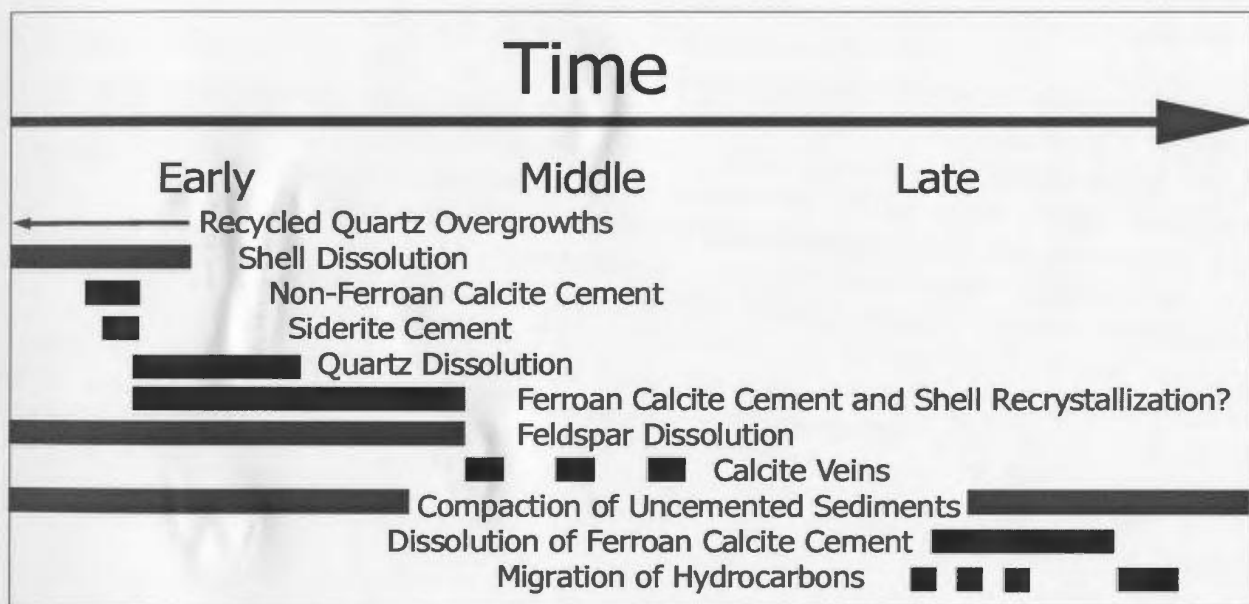


Figure 4.23: Paragenetic Sequence for the Ben Nevis Formation at the White Rose Field.

4.4.3 Early Shell Dissolution

Bioclasts are typically stable in the shallow subsurface near the sediment-water interface because they formed in equilibrium with seawater. However, shells made of metastable aragonite and high Mg calcite may begin to dissolve in the meteoric, sub-oxic and bacterial sulphate reduction zones (Morse and Mackenzie, 1990). As burial increases and pore waters evolve, calcium carbonate ions increase to a point of super-saturation and calcite may precipitate as cement. Since shell debris provides the largest volume of calcium carbonate within the Ben Nevis sandstone, it is the primary target as a source of calcite cement. The preservation of original depositional porosity in well to very well cemented concretions as minus cement porosity close to that estimated by Beard and Weyl (1973) would place shell dissolution (potential source of calcite cement) prior to significant burial and early in the paragenetic sequence. Another important aspect is the intimate relationship between bioclasts and calcite concretions, as most concretions contain a central layer of bioclasts, and the latter can be assumed to provide ideal nucleation sites for calcite cement.

Thin sections from the Ben Nevis Formation illustrate varying stages of shell dissolution (Figure 4.9) as well as the complete dissolution of shells resulting in moldic porosity (Figure 4.24). Consistent with isotope results (Chapter 5) and the transgressive nature of the Ben Nevis Formation, shell dissolution is not a result of fresh water influence. Instead, original shell composition is deemed to be aragonite that became unstable early on with progressive burial. Also notable concerning shell dissolution is the occurrence of framboidal pyrite, within thin, compacted and often discontinuous residues

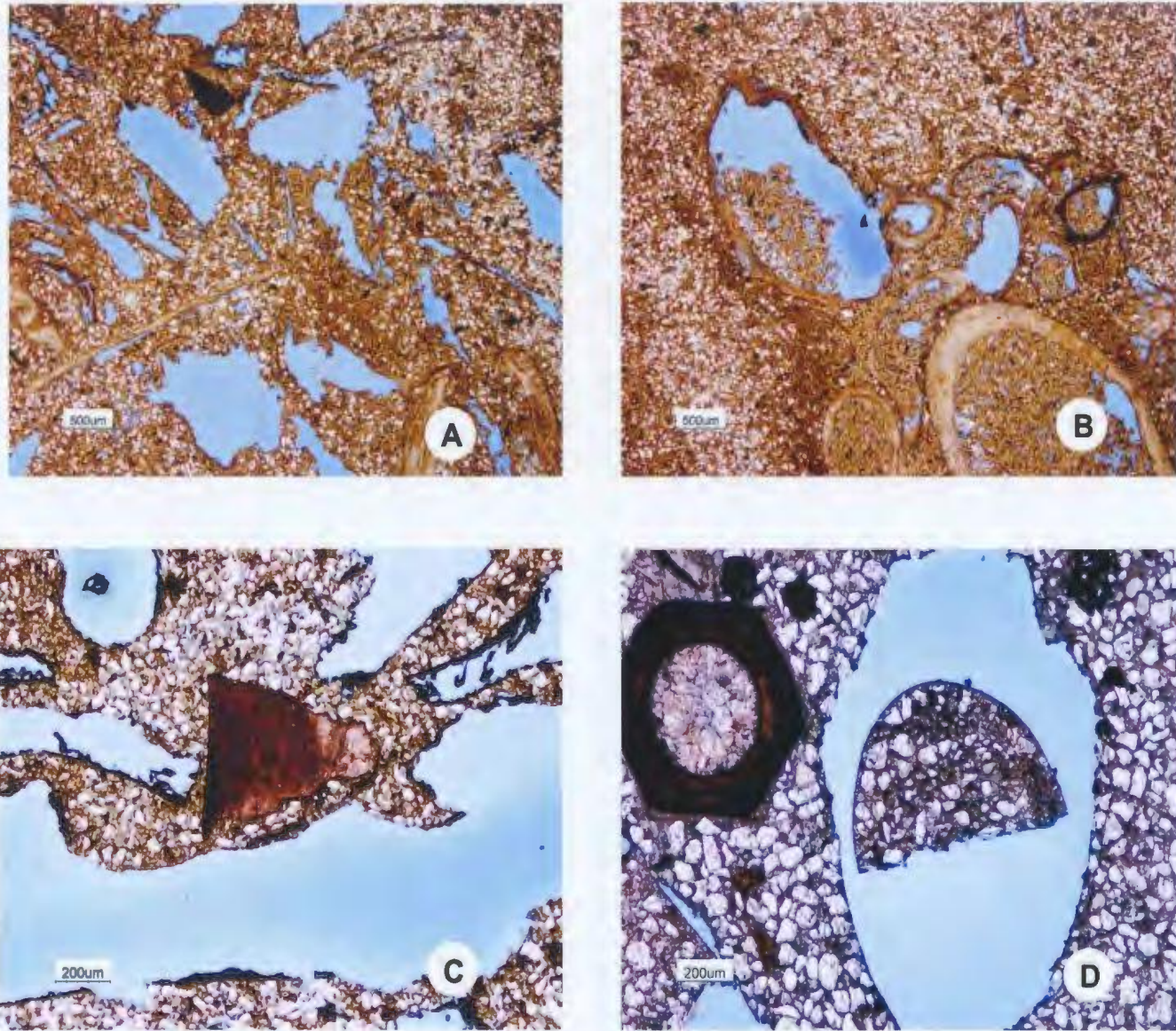


Figure 4.24: Moldic Porosity A. F-04, Core 1, Box 5, TS 160, B. F-04, Core 1, Box 5, TS 160, C. F-04, Core 1, Box 5, TS 160 and D. F-04, Core 2, Box 28, TS 193.

of a micro-crystalline textured curved shell fragment of indeterminate affinity (Figure 4.9 D). These concentrations of pyrite are occasionally found in pelecypod shells as well as on their own, suggesting it is associated with shell alteration and appear to be remnants of nearly complete dissolution of a certain shell species. These completely dissolved shells may provide the necessary calcite for precipitation of calcite-cemented concretions.

Wright *et al.*, (2003) discuss the ‘loss of taphonomy’ in clastic sediments as the result of selective dissolution of aragonite shells. Lower energy offshore settings dissolve aragonite shells through microbial decay and acidity in the upper sediment column. Mollusk shells are sometimes composed of calcite and aragonite layers (Lowenstam and Weiner, 1989). Class Gastropoda and Class Bivalvia contain members that are entirely aragonite (Palmer and Wilson, 2004), while other taxa have both aragonite and calcite layers (Majewske, 1969). Keith *et al.*, (1963) noted that all mollusc ligament fibers are aragonite and most mollusc shells consist mainly of aragonite. Serpulid worm tubes have shown various calcite/aragonite ratios (Bornhold and Milliman (1973). Hendry *et al.*, (1995) discuss the instability of aragonite and suggest that it will normally be removed during diagenesis. The presence of sparry calcite molds (Figure 4.25 B and C) and multiple layered shells in thin section (Figure 4.25 D) are consistent with the widespread presence of aragonite in the Ben Nevis Formation.

4.4.4 Early Non-Ferroan Calcite Cement

Early non-ferroan calcite cement is a non-pervasive cement type which occurs mainly as coarsely crystalline overgrowths that appear to nucleate on and around the

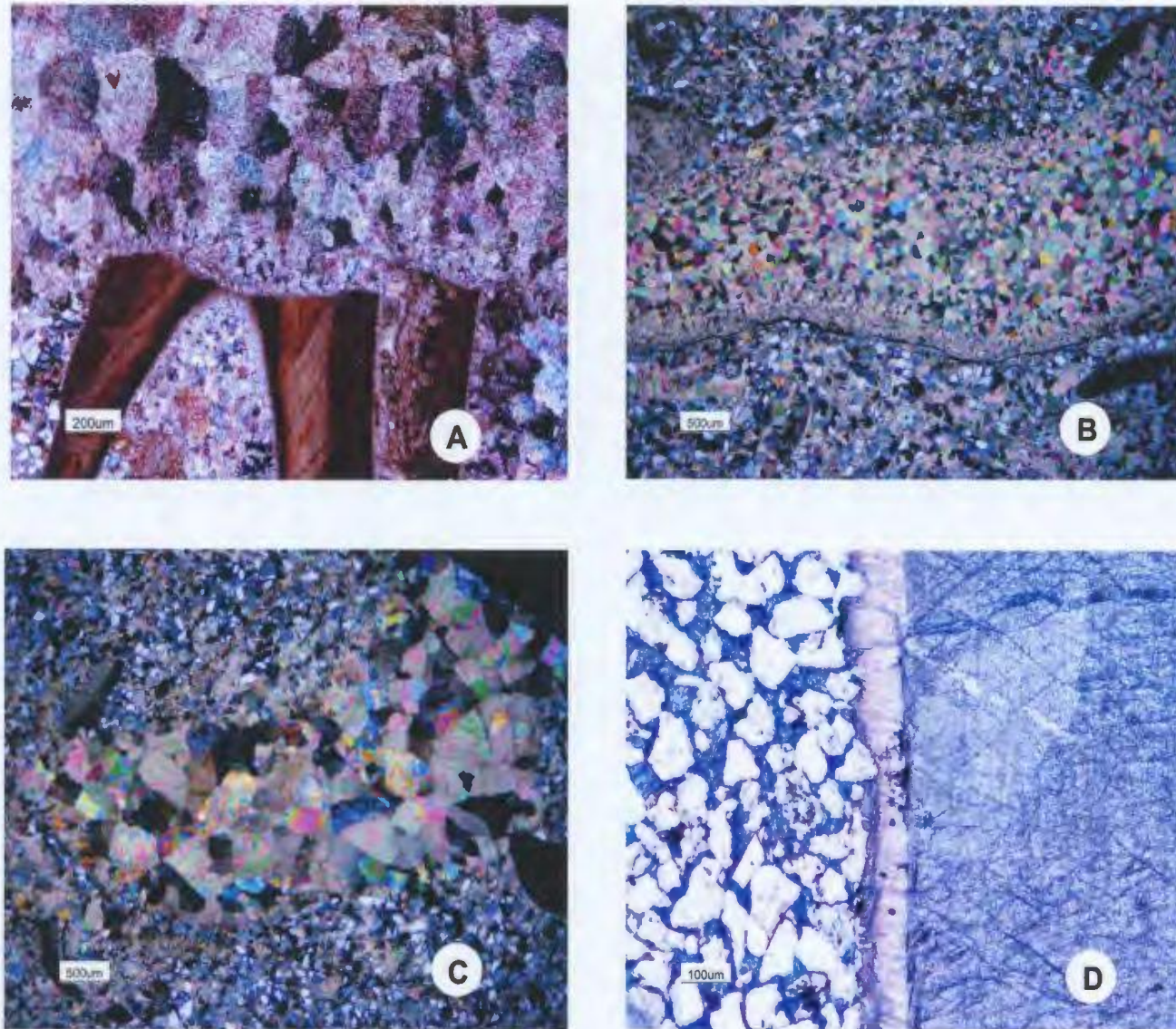


Figure 4.25: Recrystallized Shells. A. Partially recrystallized serpulid worm tube (F-04 Core 1, Box 35, TS 168), B. Recrystallization of large shell demonstrating an increase in crystal size towards the center (F-04 Core 1, Box 47, TS 176), C. Close-up of sparry calcite (F-04 Core 1, Box 47, TS 176); and D. Selective recrystallization of one shell layer (F-04 Core 2, Box 32, TS 196).

remains of calcite bioclasts and tends to be irregularly distributed as disseminated patches (Figure 4.17). Bioclasts clearly acted as nuclei for calcite precipitation, consistent with the study by Bjorkum and Walderhaug (1990). Wilkinson (1991) also acknowledged that burial cements are likely sourced from dissolution of detrital carbonates and bioclasts.

Based on the law of superposition, the slightly ferroan calcite cement is designated as the earlier authigenic cement which possibly experienced a minor period of neomorphism based on irregular, strongly embayed boundaries between the cement types before the pore fluids evolved their iron enhanced character. Veins of calcite cement also have a non-ferroan outer layer with a later stage core of ferroan calcite. This may imply that vein-filling cement was also during early stage diagenesis when pore fluids were non-ferroan. This would suggest early non-ferroan cement to develop after sufficient lithification occurred to develop fracturing.

One possible explanation for the evolving pore fluids resulting in the transition from non-ferroan to ferroan calcite could be the rate of deposition. Controlling rate of burial will affect the progressive change in redox conditions. Raiswell (1987), studied calcium-rich shales, concluding that a prolonged pause in sedimentation allows time for cement precipitation, making sedimentation rate the limiting factor for authigenic cements. Sedimentation rate and the oxygenation state of bottom waters influenced the preservation of organic matter within the sediments (Didyk *et al.*, 1978) and therefore were a control on the course and duration of early diagenetic reactions. Calcareous concretions are confined to specific areas deposited under lower sedimentation rates, forming in the sulphate reduction zone during lulls in sedimentation along favourable

horizons (Scotchman, 1991). Concretions generally form within the first few meters of the sediment water interface (Mozley and Burns, 1993) and rate of sedimentation may be correlated to concretion mineralogy. While the above studies are primarily based on anoxic bottom waters above organic rich shales, the rapid deposition of the thick Ben Nevis Formation will preserve sufficient soft shell tissue and burrow linings while accomplishing rapid burial into the microbial methanogenesis zone.

Slow sediment accumulation allows active sulphate reduction, providing abundant sulphate and H_2S , which results in the precipitation of pyrite and iron-free carbonate (Curtis and Coleman, 1986). This would imply that localities of slightly and non-ferroan calcite cementation are the result of a relative decrease in sedimentation removing iron from the system and/or relevant oxidizing conditions. Crystal size is consistent with this. As the rate of deposition increases, sulphate reduction slows down, preventing pyrite precipitation and precipitating ferroan calcite cement. The only evidence for significant changes in sedimentation rate for the Ben Nevis Formation is the episodic nature of storm deposits with inferred periods of comparatively much slower sediment accumulation during fair-weather periods.

4.4.5 Early Pyrite and Siderite Cement

The concept of depth-controlled processes producing a sequence of marine sediment zonation from oxic to sub-oxic (Mn reducing, Fe reducing) to sulphate reduction and finally to methanogenesis is well established (Irwin *et al.*, 1977; Froelich *et al.*, 1979). Various researchers have worked on determining the environmental conditions

required for the formation of siderite. Roh *et al.*, (2003) indicate that bacterial respiration of organic material is required for siderite precipitation. Ellwood *et al.*, (1988) suggest that bacterial dissimilatory iron reduction produces the source of iron for siderite precipitation in an anoxic environment, after considerable burial. Gautier and Claypool (1984) concluded that siderite forms after the sulfidic diagenesis of pyrite, in a bacterial methanogenic regime, while Berner (1980) stated that siderite is created in conditions of low oxygen and low eH, and is controlled biogenically.

Siderite experiences chemical transitions as it evolves through the sub-oxic, sulphate reduction and methanogenic biogeochemical zones within the sediment column (Wilkinson *et al.*, 2000). They suggest the formation of pyrite favours the development of a strong sulphate reduction zone, where as siderite precipitation is mainly affected by microbial activity. Wilkinson *et al.*, (2000) also acknowledged the difficulty in determining the depth of burial of siderite precipitation but geochemical results imply burial depths of cm to 10s of m in sandstones.

In most thin-sections siderite is present within the mold of a shell formerly occupied by soft tissue (Figure 4.20 A & B). This association may suggest that local siderite precipitation depends on organic remains to pass through the sulphate reduction zone (producing pyrite), and into the bacterial methanogenesis zone. Slower burial rates associated with offshore depositional environment allowed the time necessary in the bacterial methanogenic zone for siderite precipitation to proceed. The faster rates of the lower shoreface environment coupled with the geologically instantaneous deposition of

storm deposits would allow only a brief period in the sulphate reduction and bacterial methanogenic zones, thereby reducing siderite content in the lower Ben Nevis Formation.

4.4.6 Dissolution of Quartz Grains

The corrosion of quartz grains primarily occurs in the very well cemented concretions and is generally associated with the poikilotopic cement. Corrosion of quartz is identified in thin-section by the irregular grain boundaries, free floating nature of the grains and the less than 20 μm islets found encased in calcite cement (Figure 4.3 A-C).

Quartz dissolution appears to be associated with the fluids responsible for precipitating calcite cement as all pore space is occluded, removing all fluids from the system and bringing a halt to diagenesis. As lithostatic pressure builds up at load bearing grain to grain contacts, the solubility of quartz increases, dissolving silica (Walderhaug, 1994).

Bjorlykke and Egeberg (1993) estimate a temperature range of 80 to 100 °C to initiate quartz cementation in the North Sea Basin based on fluid inclusion studies. Gluyas *et al.*, (1993) indicates quartz cementation occurred over a wide depth range in a relatively short period of time during rapid subsidence (>100 m/m.y.) and heating (>2 °C/m.y.). Temperature is not the only factor regulating the precipitation and dissolution of quartz as the low temperatures concluded for precipitation of calcite cement (25 to 30 °C) were also those responsible for dissolution of quartz cement in the Ben Nevis Formation.

Low temperature quartz solubility has been proven experimentally predicting 11.0 +/-1.1 ppm at 25°C (Rimstidt, 1997). Dissolution of quartz and precipitation of carbonate are largely controlled by pH (Friedman *et al*, 1976). Ph above 9 increases the dissolution of quartz, possibly resulting from an increase as a result of biological activity (Friedman *et al*, 1976). Biofilm growth dramatically increases pH from 3.4 to greater than nine and plays a major role in the breakdown of quartz (Brehm, *et al.*, 2005). It is therefore the authors assumption that a high energy, well oxygenated shoreface environment, will have a heightened biological activity, increasing the pH and promoting the dissolution of detrital quartz grains in conjunction with precipitation of authigenic calcite cement.

4.4.7 Ferroan Calcite Cement

Hutcheon *et al.*, (1985) conducted geochemical analyses of carbonate cements of the Avalon sand, Hibernia field, concluding calcite cementation, recrystallization and veining developed from the same fluids. The poikilotopic ferroan calcite cement is a very early episode of cementation based on minus-cement porosity up to 40 %, similar to paleo-porosity values of Beard and Weyl (1973), (Figure 4.26). Gautier and Claypool (1984) used minus-cement porosity to indicate the amount of compaction prior to concretion formation. As pore fluids evolved to precipitate non-ferroan calcite cements, this early cementation allowed the framework grains to maintain their original packing and prevent further compaction (Figure 18 A and B).

Sparry ferroan calcite appears to develop directly from recrystallization of shells (Figure 4.25 A, B and C), with crystal size decreasing from the center of shells outward,

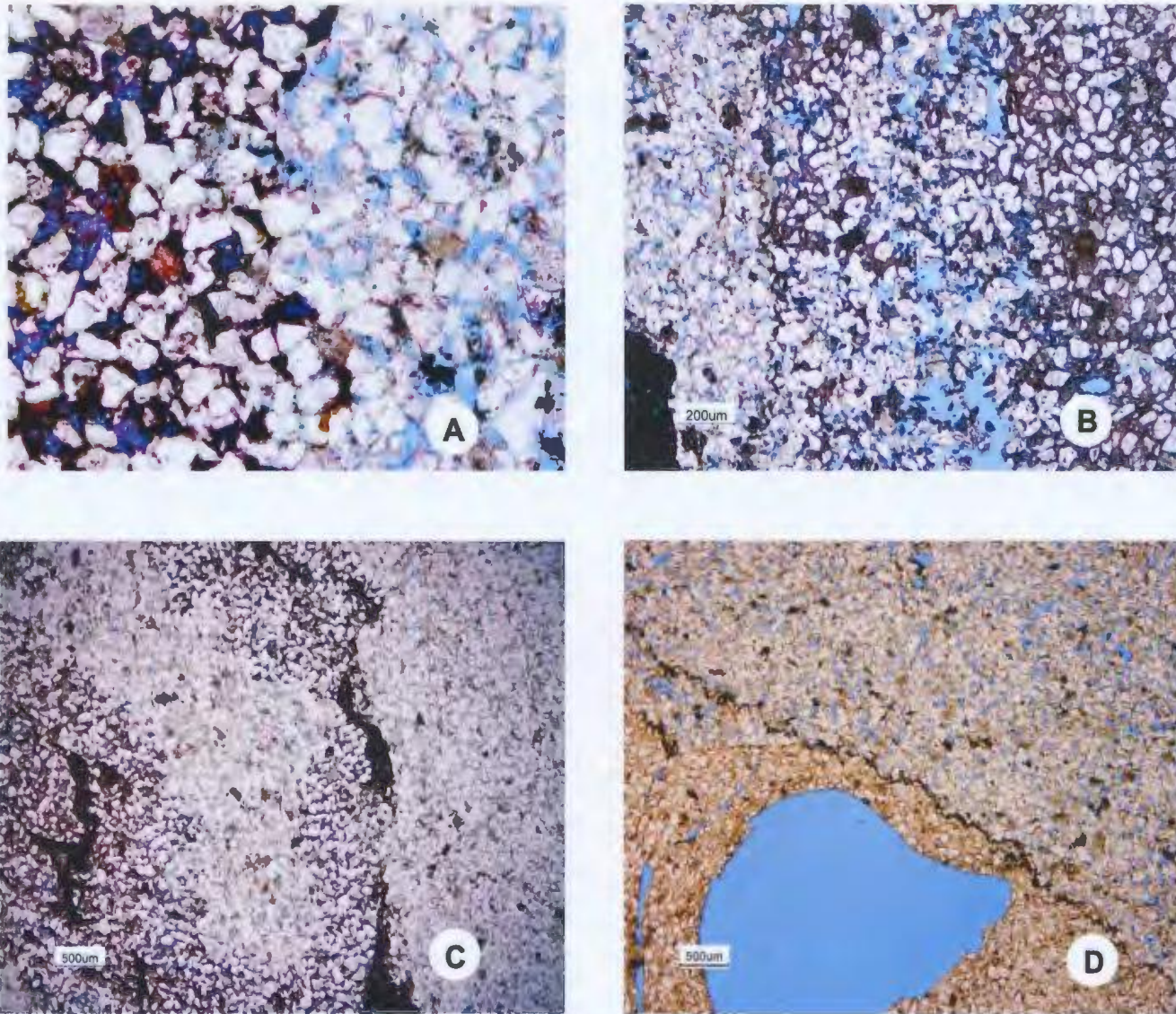


Figure 4.26: Dissolution Boundaries. A. Sharp irregular dissolution boundary (F-04, Core 1, Box 31, TS 166 , B. Gradual dissolution boundary (F-04, Core 2, Box 28, TS 193, C. Breached dissolution boundary (F-04, Core 2, Box 29, TS 194) and D. Remnants of a shell acting as a dissolution boundary (F-04, Core 2, Box 59, TS 204).

perhaps as a function of depth (e.g., temperature of recrystallization) as reducing conditions increase with progressive burial providing more Fe in the Fe^{+2} state. The most likely explanation is that Fe^{+2} iron has become available at progressive more strongly reducing conditions at depth. Other possibilities of a Fe source include dissolution of siderite cement (Figure 4.27) in the upper section of the Ben Nevis Formation or from the compaction of shales and marlstones releasing Fe ions into the system. The illite/smectite transition provides a mass transfer of structural H_2O and SiO_2 with minor Na, Mg, Ca and Fe transfers (Abid, 1996). This ion transfer may result in sandstone cementation, possibly sourcing enough iron for the ferroan calcite cement.

Recrystallization begins on the outer edge of the shell, moving towards the center resulting in an increase in crystal size (Milliken, 2006, pers. comm.). Palmer and Wilson (2004) indicate that aragonite taxa are most commonly preserved as molds or sparry calcite casts (Figure 4.25 B and C). This same pattern can also develop when there is open space available to be filled by calcite cementing crystals. Coarsening crystal size into a fracture is indicative of growing into a void (Bathurst, 1975). Morad (1998) also noted how drusy carbonates increase crystal size from pore wall to pore center.

Sharp crystal faces demonstrate development of these crystals into open pore space, and are isolated from external corrosive solutions and/or stable relative to subsequent and present formation fluids, which would have begun the deterioration process, etching and rounding euhedral crystal surfaces. Ferroan calcite as small isolated crystals is rare (Figure 4.19) but may have implications on porosity / permeability

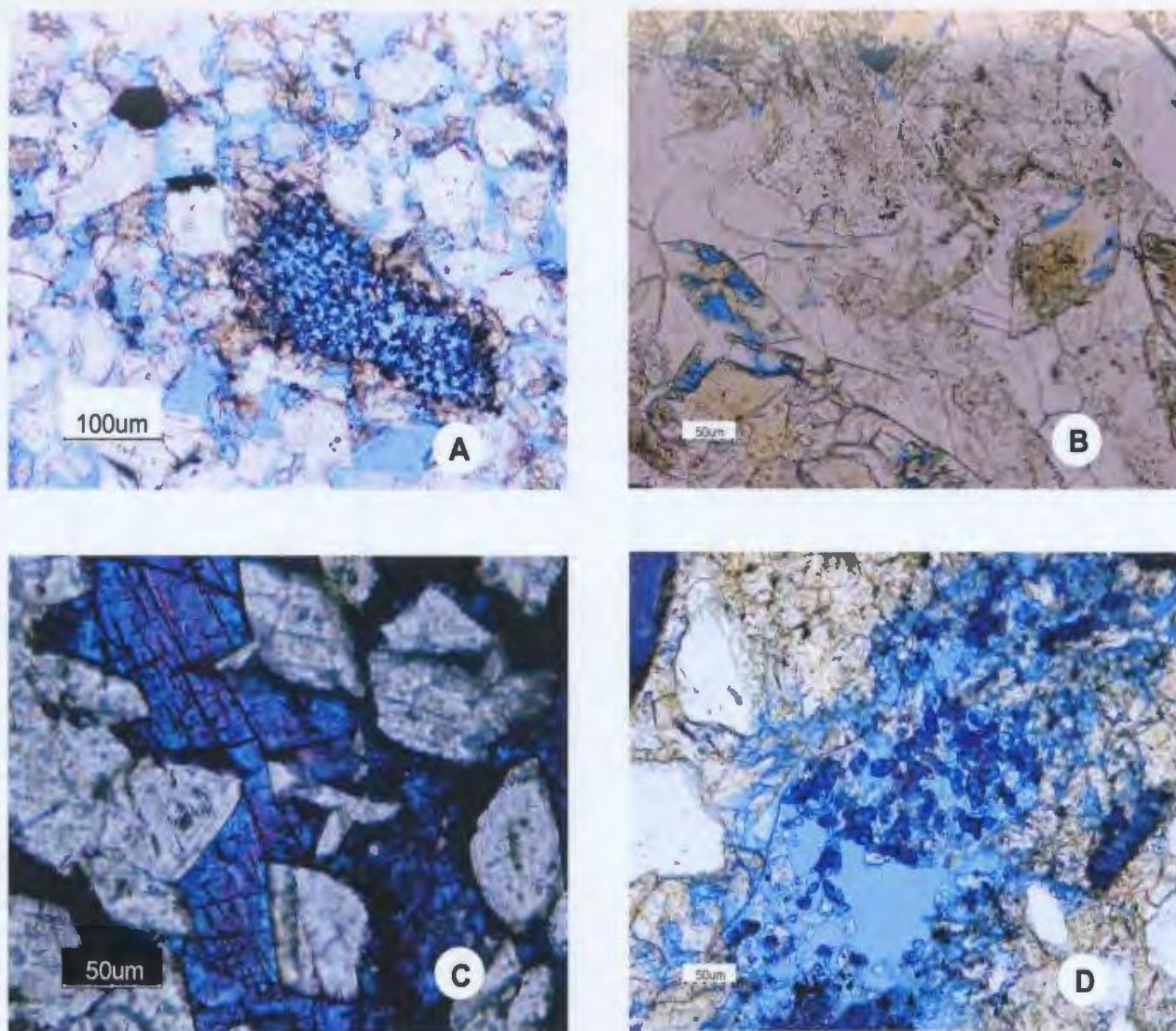


Figure 4.27: Siderite dissolution and possible source for late stage ferroan calcite cement. A. Dissolution of siderite and precipitation of late ferroan calcite cement, (F-04, Core 1, Box 13, TS 162), B. Dissolution of euhedral siderite crystal, (B-07_4, Core 2, Box 6, TS 125), C. Siderite dissolution and precipitation of ferroan ferroan calcite cement (B-07_4, Core 1, Box 37, TS 146) and D. Dissolution of siderite and precipitation of ferroan calcite cement (B-07_4, Core 2, Box 6, TS 125).

relationships. These small euhedral ferroan calcite crystals allow a higher percentage of porosity but the location of the crystals in pore throats drastically reduces permeability. This type of cement is characteristic of the partially to poorly cemented sandstones and predominates in lower stratigraphic intervals of the Ben Nevis Formation.

4.4.8 Early Feldspar Dissolution

The occurrence of partially dissolved feldspars gives a sense of the relative timing of early calcite cementation (Figure 4.5). Paces (1983) suggests dissolution of a 0.5 mm diameter feldspar grain to require at least eight million years. If the rare feldspar grains found in the Ben Nevis Sandstone are not exposed to pore fluids long enough to become completely dissolved, it can be assumed that these grains were sealed off from further dissolution by the precipitation of calcite cement completely occluding pores. This could imply that early calcite cementation occurred before the first eight million years after burial. "If dissolution of feldspar took place after deposition of the sediment, this would provide a minimum estimate of the time interval between sedimentation and concretion growth (Wilkinson, 1991)." The fact that most of the feldspar grains observed within calcite cement were only partially dissolved could place precipitation of calcite cement within a few million years after deposition.

A net reduction in total feldspar content as a result of dissolution can have a big impact on rock classification, concepts of provenance and reservoir quality factors. Dissolution of feldspar creates secondary porosity with oversized pores and provides a

source for precipitation of quartz overgrowths. The rare nature of feldspars in this sandstone would provide a negligible source for quartz cement.

4.4.9 Calcite Veins

Calcite veins are found in the Ben Nevis Formation in both WR F-04 and WR B-07_4 wells, occurring in partially cemented sandstones lower in the formation and in well-cemented concretions in the upper part of the formation (Figure 4.17 D). Calcite veins may have developed early as rapid sedimentation caused slumping of unconsolidated sediments or later when sediments consolidated and fracturing occurred with progressive burial releasing pore fluids from above. Fluids enriched in calcium carbonate could then have accessed fractures to precipitate calcite cement. Crude timeframes such as “early diagenetic” or “tectonic” are normally used regarding the opening of fractures and subsequent precipitation of calcite cement, [Falcon.tamucc.edu/.../ Montereydiagenesis.html](http://Falcon.tamucc.edu/.../Montereydiagenesis.html), (January, 2006). Micro-fractures are occasionally found in thin section of the Ben Nevis core (Figure 4.28) but these observations require a note of caution as the process of grinding down thin sections can sometimes induce micro-fracturing.

4.4.10 Siderite Dissolution

Dissolution of siderite appears to be rare, but these rare occurrences seem to be associated with ferroan calcite cement (Figure 4.29). The dissolution of siderite would

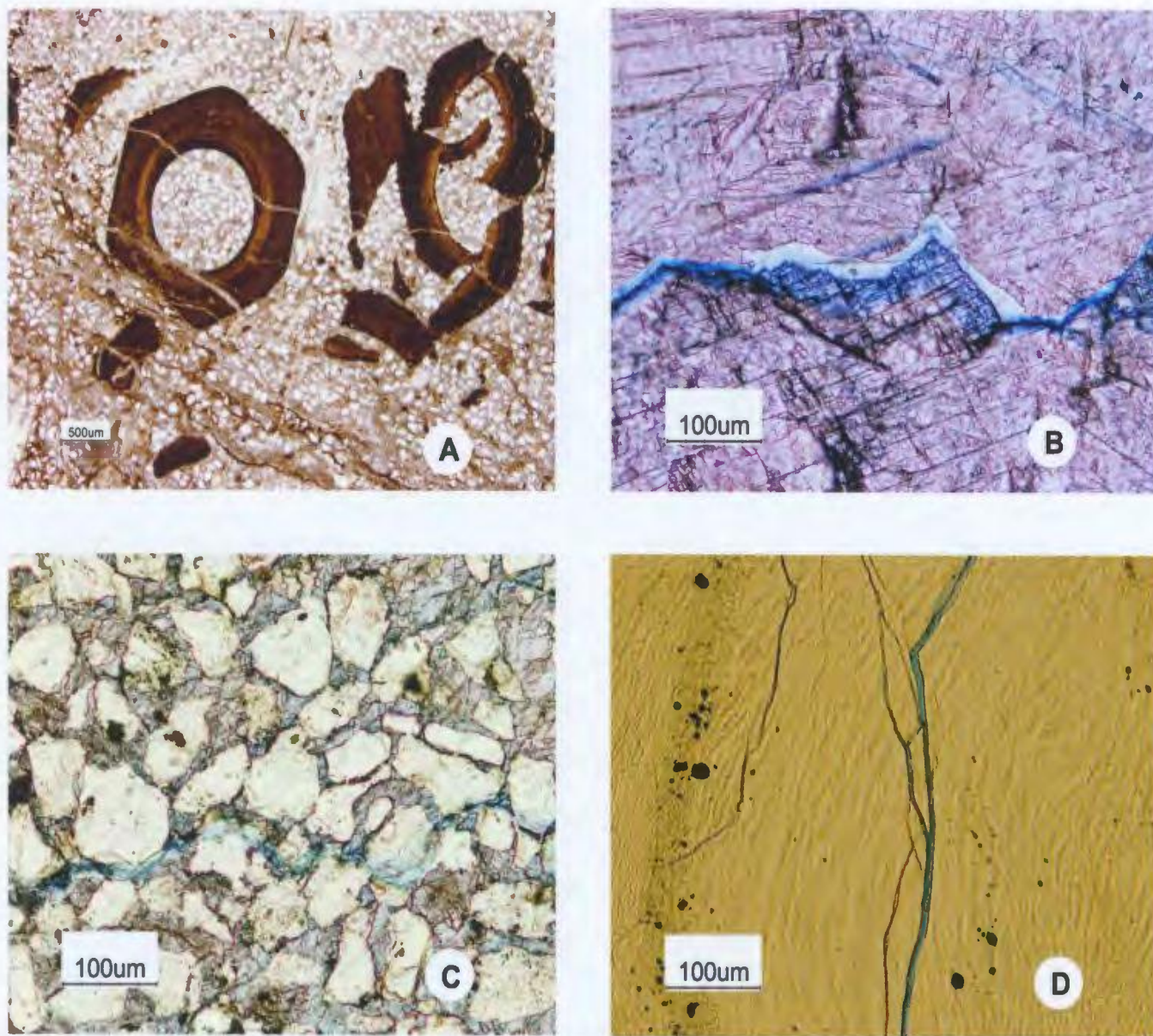


Figure 4.28: Micro-Fractures. A. F-04, Core 1, Box 35, TS 167, B. F-04, Core 1, Box 35, TS 168 C. F-04 Core 1, Box 47, TS 176 and D. F-04, Core 2, Box 44, TS 199.

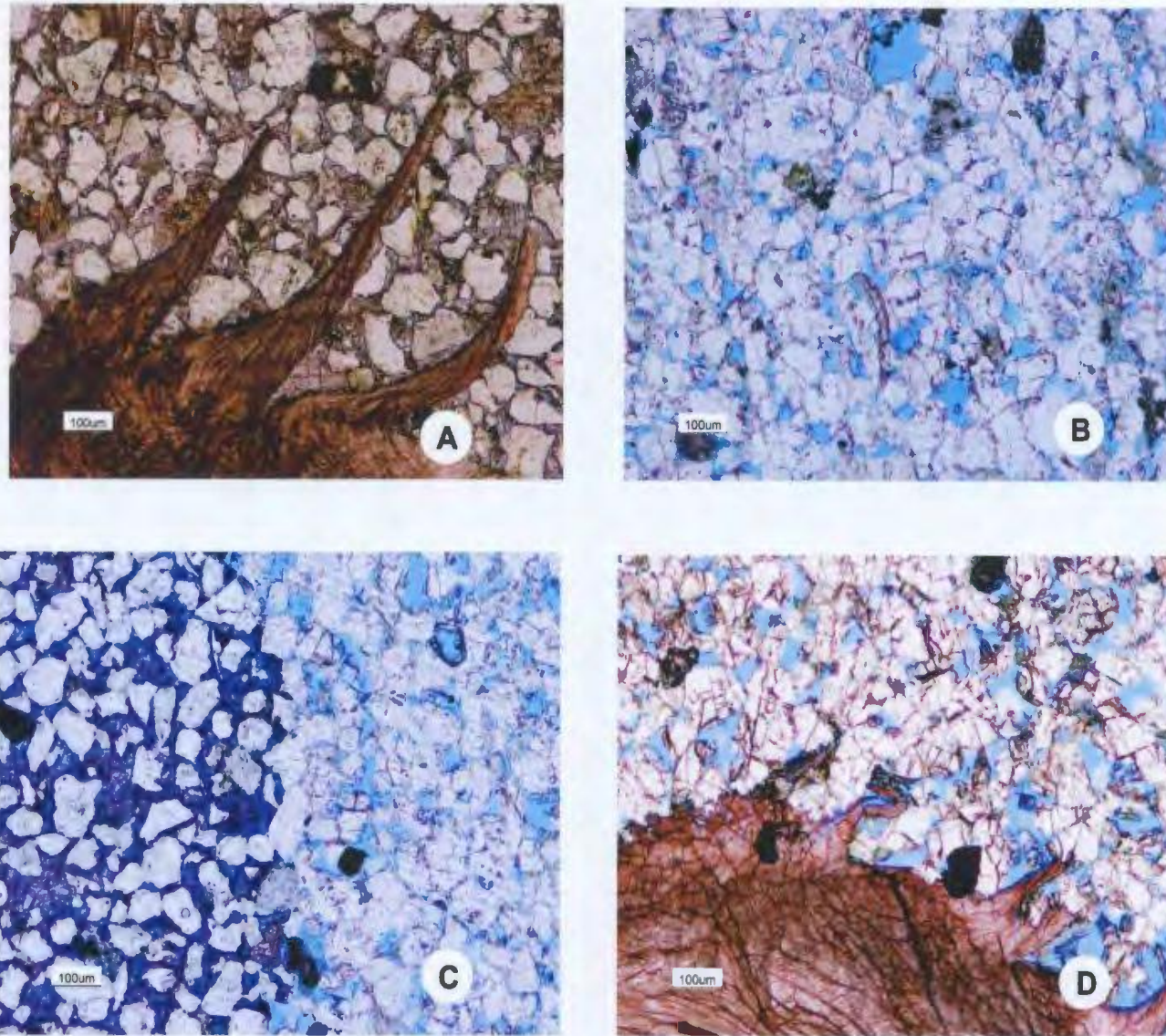


Figure 4.29: Compaction. A. Early compaction preserving the delicate shell structure, (F-04, Core 1, Box 58, TS 188). B. Planar grain boundaries, (F-04, Core 1, Box 58, TS 184). C. Difference in compaction between the cemented and uncemented sandstone, (F-04, Core 2, Box 7, TS 187) and D. Slight compaction of shell structures demonstrating the variable nature of compaction, (F-04, Core 2, Box 16, TS 192).

provide iron ions into the evolving pore fluid system that could subsequently act as a source for authigenic ferroan calcite cement.

4.4.11 Compaction of uncemented sediments

As deposition continues and sediment load builds, the load of overlying sediments causes compaction of the framework grains and matrix in uncemented intervals, decreasing porosity and permeability (Figure 4.29). The rounded nature of the concretions does not create protective load bearing columns to prevent compaction of uncemented sandstones. This provides evidence of non-compartmentalization of the reservoir. Quartz grains exhibit a wide variety of boundaries and grain-to-grain relationships, from floating grains in poikilotopic calcite cement, to point, planar, sutured and concavo-convex contacts. Generally, the sutured and concavo-convex contacts are found in uncemented sandstones exposed to compaction.

4.4.12 Dissolution of Ferroan Calcite Cement

Dissolution of ferroan calcite cement is subtly revealed by petrographic analysis based on the corroded nature of crystal boundaries (Figure 4.30 B, C and D). Dissolution of both early poikilotopic and sparry ferroan calcite cements may result from changes in pore fluid chemistry (Veizer, 1983), primarily organic and carbonic acids associated with hydrocarbon generation and migration into the reservoir pubs.usgs.gov/.../USGS_3D/ssx_txt/diagenes.htm (Feb, 2006). Timing of this episode of dissolution is very beneficial to reservoir production by increasing porosity and permeability.

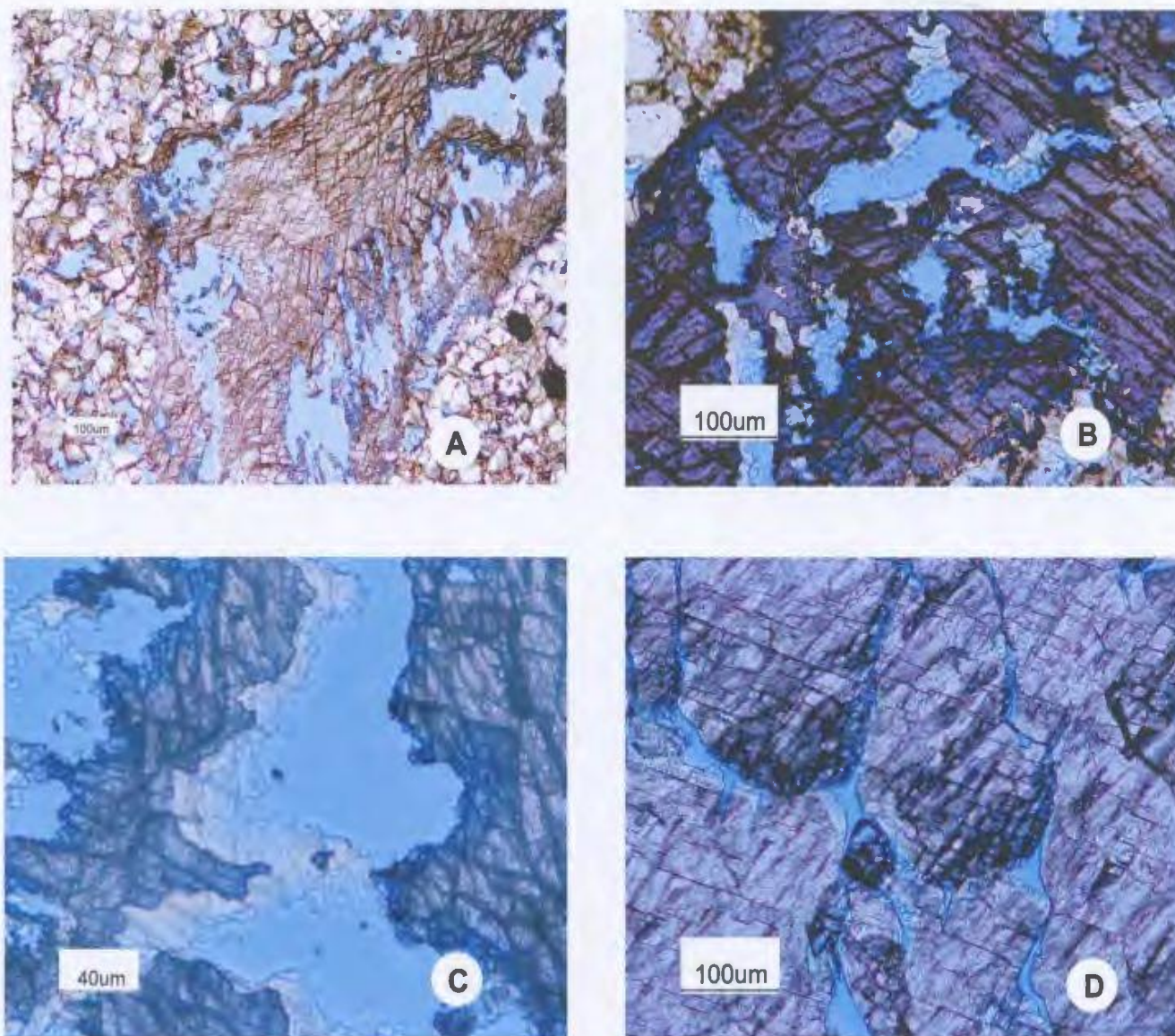


Figure 4.30: Calcite Dissolution A. Dissolution of Non-Ferroan calcite cement (F-04, Core 1, Box 5, TS 160), B. Dissolution of Ferroan calcite cement (F-04, Core 1, Box 5, TS 160), C. Dissolution of Ferroan calcite cement (F-04, Core 1, Box 5, TS 160) and D. Dissolution of Ferroan calcite cement (F-04 Core 1, Box 49, TS 179).

CHAPTER 5: STABLE ISOTOPE GEOCHEMISTRY: CARBON AND OXYGEN ISOTOPES

5.1 Introduction to Isotopes and Stable Isotope Geochemistry

Anderson and Arthur (1983) discuss the value of stable isotopes of oxygen and carbon for understanding processes of diagenetic alteration of sedimentary rocks. Longstaffe (1987) used isotopic compositions to reconstruct pore-water evolution in a sedimentary system. Carbonate cements and shells act as carrier phases for studies of isotopic composition of past seawater (Veizer *et al.*, 1999). Carbon and oxygen isotopes are used in this study to provide insight on the source and evolution of sub-spherical calcite cemented concretions in Ben Nevis Formation sandstones. Isotopic analysis of authigenic carbonates will attempt to identify carbon and oxygen sources associated with specific diagenetic environments.

5.2 Limitations of Carbon and Oxygen Isotopes

Carbon and Oxygen isotopes are useful in determining environmental conditions during precipitation of authigenic cement but they have a number of limitations which should be considered before applying results. Spatial variability of oceanic $\delta^{13}\text{C}$ CO_2 (Kroopnick, 1985), diagenetic resetting of the signal, as well as biological factors of shell formation (McConnaughey and Whelan, 1997) can give rise to a substantial spread of values. Variations of oceanic $\delta^{13}\text{C}$ CO_2 are a direct result of organic productivity and mixing caused by global circulation of currents (Kroopnick, 1985). Resetting of

diagenetic signals can occur when recrystallization of cements cause isotope compositions to equilibrate with ambient diagenetic fluids (Mozley and Burns, 1993).

Paragenetic interpretations are difficult whenever there is recrystallization of carbonates (Hutcheon *et al.*, 1985). Recrystallization of carbonates can produce a resetting of isotopic signature masking original carbonate signature, thereby adjusting the paragenetic sequence. Handford *et al.*, (1989) recognized problems with non-distinctive bulk isotopic compositions. Can not distinguish between different phases of cements and in some cases the isotope signature will be a mixture of bioclasts and cements, nonetheless the signature will be dominated by the more abundant component. Based on sampling limitations, cement and bioclast isotopic signatures can be distinguished.

Keith *et al.*, (1963) used modern mollusk shells from marine and continental environments to prove that the difference in carbon and oxygen isotopes are clearly environmentally controlled, due mainly to land plant and humus effect in continental waters which should be valid back to the Carboniferous when land plants evolved.

5.3 Carbon Isotopes

Various diagenetic processes produce distinctive carbon isotopic compositions (Figure 5.1). Before trying to decipher diagenetic isotopic conditions, it is important to understand current isotopic conditions in different environmental settings. Mook and Tan (1991) concentrate on freshwater sources, noting that depending on rock type and vegetation cover, $\delta^{13}\text{C}$ values can range from -27 to -7 ‰, but also discuss other sources: atmospheric $\delta^{13}\text{C}$ (-8 ‰ to -9 ‰ for continental, -7.5 ‰ over oceans), land plants (-29 ‰

to -9 ‰ depending on the photosynthetic pathway) and sea water (0 to +2 ‰). Irwin *et al.*, (1977) analyzed isotopes in the Kimmeridge Clay to test a model of subsurface zones characterized by bacterial oxidation to produce a depleted $\delta^{13}\text{C}$ signature ~ -25 ‰, bacterial sulphate reduction ~ -25 ‰, bacterial fermentation $\sim +15$ ‰ and abiotic reactions ranging from -10 to -25 ‰.

Possible sources of authigenic carbonate cements as determined from $\delta^{13}\text{C}$ have been well documented by Macaulay *et al.*, (1998). It is well established that marine bicarbonate has a $\delta^{13}\text{C}$ signature of approximately 0 ‰ (Keith and Weber, 1964);

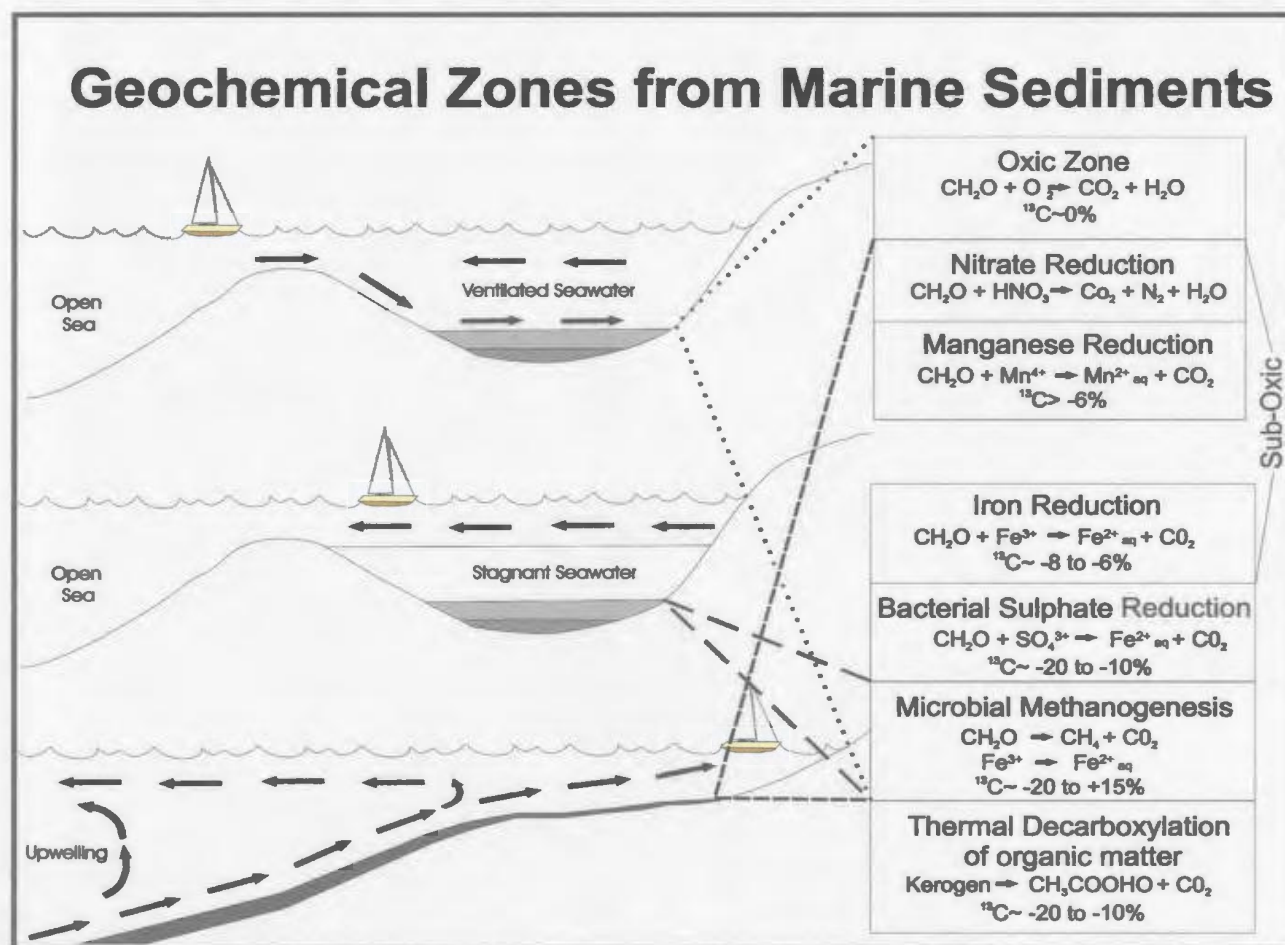


Figure 5.1: Geochemical Zones from Marine Sediments during progressive burial. Diagenetic carbonates can become imprinted during precipitation allowing recognition of the particular geochemical zone within which they formed. As burial begins, sediments move from the oxic zone to the sub-oxic zone which includes manganese, iron and bacterial sulphate reduction, followed by microbial methanogenesis and finally at temperatures greater than 75°C into the thermal decarboxylation zone, (Modified from Morad, 1998).

Schidlowski, 1988). Hoefs (1987) studied dissolved inorganic carbon in meteoric waters, suggesting $\delta^{13}\text{C} \sim -25 \text{ ‰}$ for CO_2 from organic carbon, $\delta^{13}\text{C} \sim +2 \text{ ‰}$ for carbon from dissolution of carbonates, and $\delta^{13}\text{C} \sim -7 \text{ ‰}$ for atmospheric CO_2 . MaCaulay *et al.*, (1993) analysed unaltered shell material to determine $\delta^{13}\text{C} \sim 0 \text{ ‰}$ for dissolution of shell debris in sediments. Mozley and Burns, (1993) also noted that calcite concretions are considerably lower than that expected of marine carbonate at low temperature ($\delta^{13}\text{C} = -22$ to 3 ‰ VPDB; $\delta^{18}\text{O} = -10$ to 0 ‰ VPDB). James and Choquette (1990) argue that diagenetic stabilization occurs very early in the post-depositional history of rocks, transforming metastable polymorphs (aragonite and high-Mg calcite) into stable ones (low-Mg calcite). It is important to note that this applies to limestones and may be similar but not the same as calcite cement in sandstones.

Carbon isotopes for WR F-04 range from -13.9 to $+8.8 \text{ ‰}$ $\delta^{13}\text{C}$ (majority lying between 0 to $+5 \text{ ‰}$ $\delta^{13}\text{C}$), throughout a depth interval of 2766m-2870m TVD (Figure 5.2). The WR B-07_4 well had a smaller carbon isotope range from -2.6 to $+6.8$ and a slightly deeper interval at the base of the Ben Nevis Formation from approximately 2897m-2958m TVD (Figure 5.3).

5.3.1 Carbonate Source

Carbon isotopes can be used to distinguish the source of calcite for Ben Nevis concretions. Several carbonate sources were hypothesized in the initial stages of this study:

WHITEROSE F-04

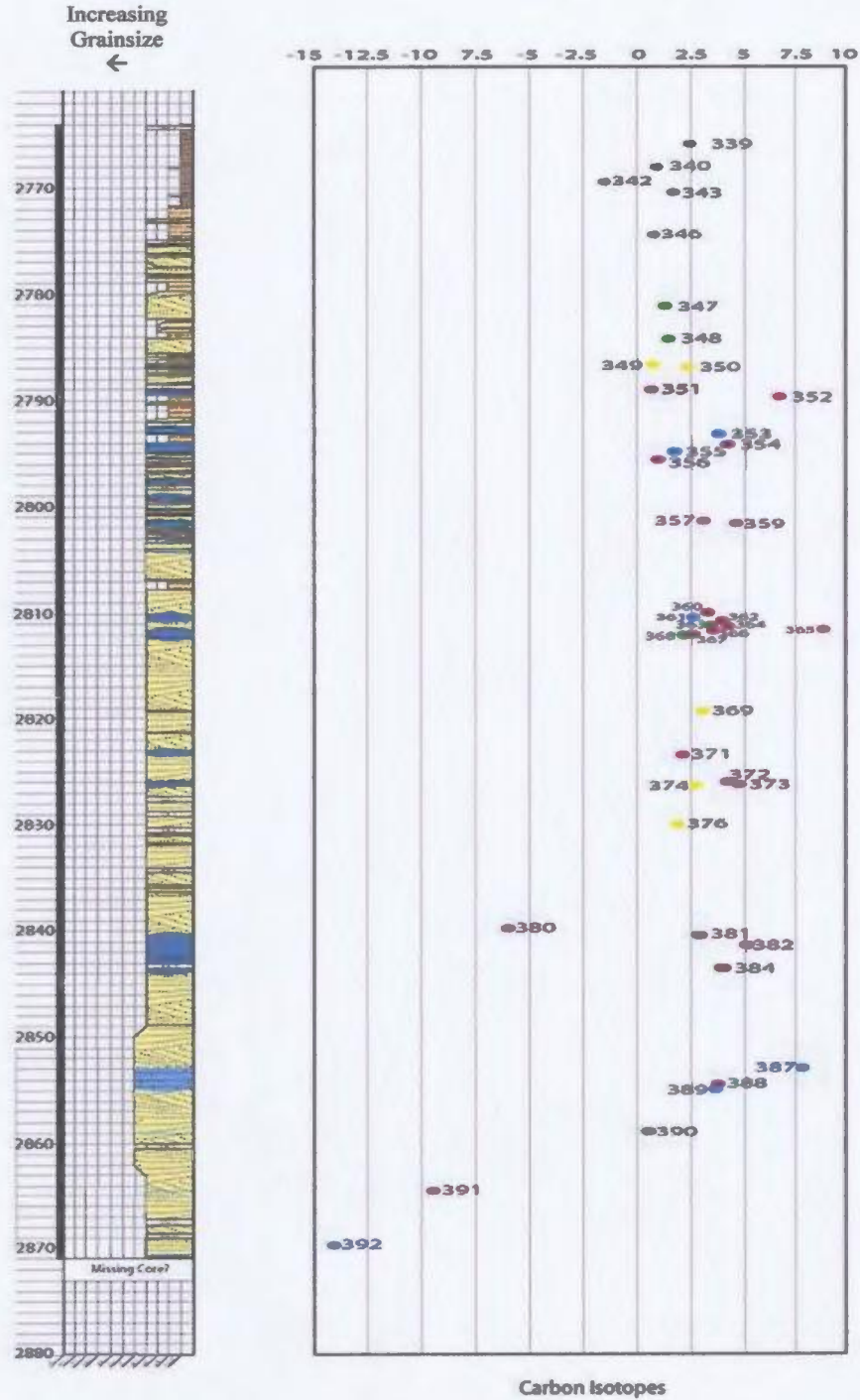


Figure 5.2: Location of carbon isotopes relative to core of WR F-04.

WHITEROSE B-07_4

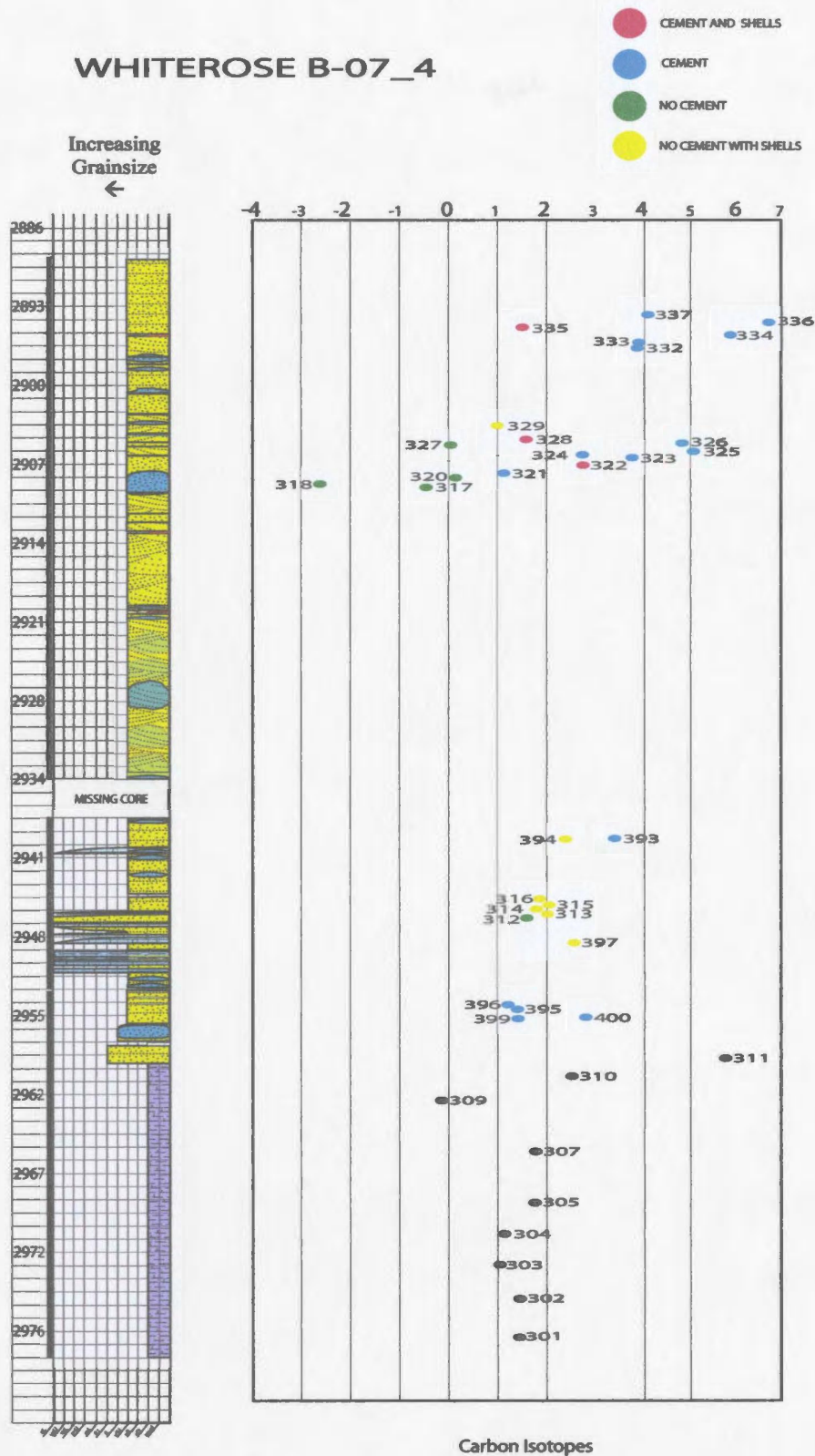


Figure 5.3: Location of carbon isotopes relative to core of WR B-07_4.

1) Diffusion boundaries with underlying limestones such as the Rankin Formation and Eastern Shoals Formation;

2) Ion transport from compaction of underlying marlstones identified at the base of B-07_4;

3) Dewatering of overlying Nautilus shales; Land (1983) notes that shale occupies over 50 % of sedimentary rocks in a basin and shale diagenesis and water expulsion can control the diagenesis of adjacent sediments;

4) Dissolution of skeletal shell debris and carbonate grains within the Ben Nevis Fm.

5.3.2 Results

To understand the results of carbon isotope geochemistry, a baseline must be established for original $\delta^{13}\text{C}$ conditions under which marine biogenic carbonate formed. Today's marine biogenic carbonate has a $\delta^{13}\text{C}$ of 0 ‰ (MaCaulay *et al.*, 1993) but variations over geologic time must be taken into account. Veizer *et al.*, (1999) developed trends throughout the entire Phanerozoic, showing a steady increase throughout the Paleozoic, followed by a general decline through the Mesozoic and fluctuations around the present day value for the Cenozoic (Figure 5.4). A range of +1.5 to +3.3 ‰ $\delta^{13}\text{C}$ (VPDB) of marine biogenic calcium carbonate of Albian age was extrapolated from the overall Phanerozoic $\delta^{13}\text{C}$ trend (Veizer *et al.*, 1999). A complete listing of Carbon and Oxygen results is presented in Appendix C.

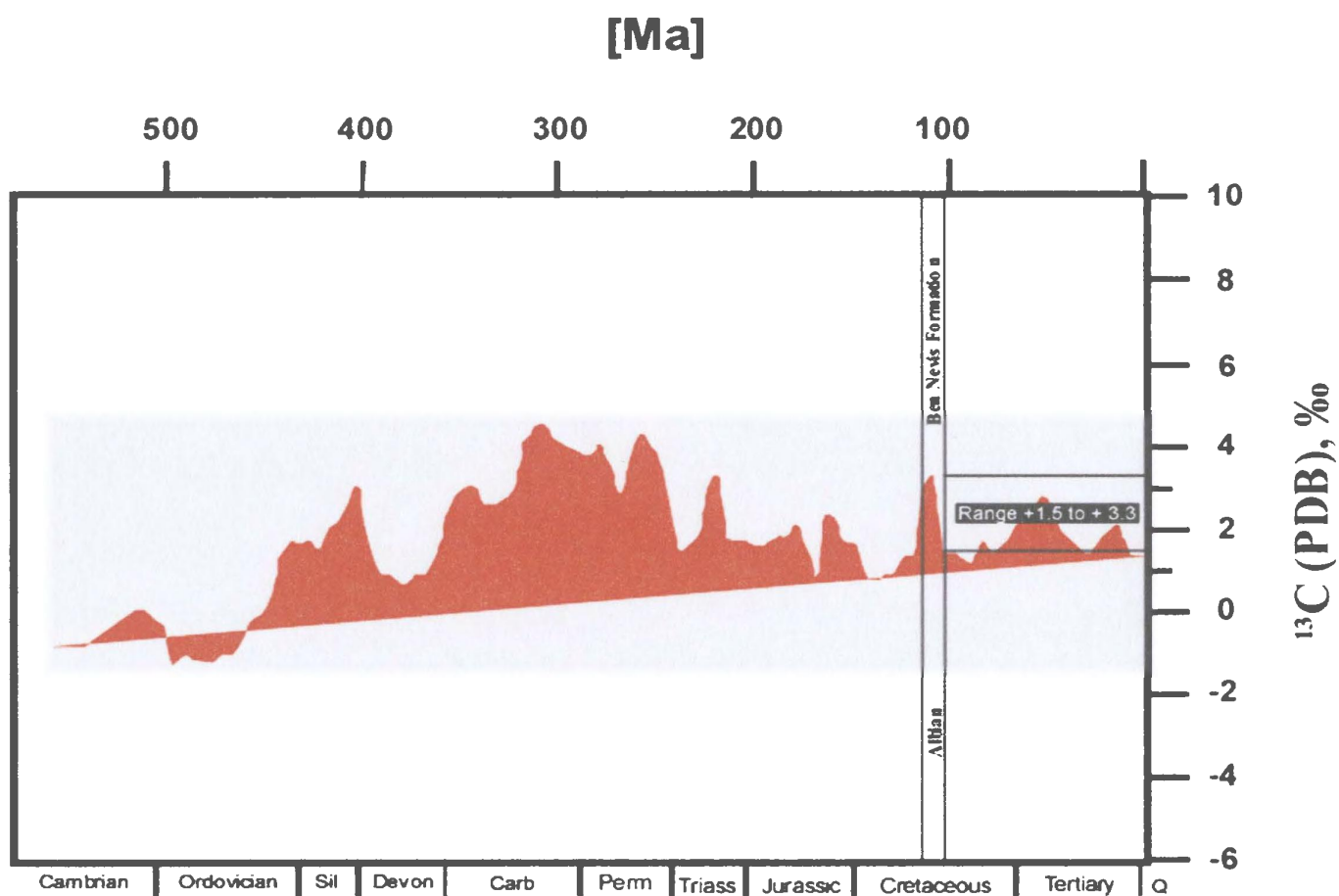


Figure 5.4: Variation of $\delta^{13}\text{C}$ (VPDB) values throughout the Phanerozoic, demonstrating a range of +1.5 to +3.3 during the Albian when the Ben Nevis Formation was deposited. Modified from Veizer *et al.*, (1999).

The overall trend of $\delta^{13}\text{C}$ throughout the Ben Nevis Formation displays an increase from 1-3 ‰ $\delta^{13}\text{C}$ at the base of WR B-07_4 to 2.5-7.5 ‰ $\delta^{13}\text{C}$ in the upper portion of the B-07-4 and the entire interval in WR F-04. This enrichment in carbon isotopes in the upper part of the Ben Nevis Formation may be due to longer term residence in the zone of microbial methanogenesis (Figure 5.1) as the rate of burial slows down in the upper part of the formation.

5.3.2.1. Muddy siltstones above the Ben Nevis Formation

Nine samples of muddy siltstone were taken above the Ben Nevis Reservoir sandstone, of which only five provided enough calcium carbonate to obtain isotopic results (Figure 5.5). Excluding the notable outlier (sample 342), $\delta^{13}\text{C}$ values average 1.6 ‰. This overlaps the lower limit of Albian marine carbonate (+1.5 to +3.3 ‰ $\delta^{13}\text{C}$ VPDB) as extrapolated from Veizer *et al.*, (1999). Samples 343 and 346 correspond to thin sections 161 and 162 which are dominated by siderite cement occupying approximately 40 and 35 ‰ of the modal analysis respectively.

These $\delta^{13}\text{C}$ values are very similar to the expected range and may be influenced by biogenic precipitation from Albian seawater (Veizer *et al.*, 1999), an increase in organic content (Hoefs, 1987) or a longer residence time in the bacterial sulphate reduction zone (Irwin *et al.*, 1977). The association of siderite with organic material (4.4.5) suggests an influence of organic content on the $\delta^{13}\text{C}$ values in this muddy siltstone interval. The outlying sample exhibits a much more depleted $\delta^{13}\text{C}$ value than the rest of this group ($\delta^{13}\text{C} = -1.7$ ‰) and may represent a longer period of non-deposition during the time it

spent in the bacterial sulphate reduction zone or it may be exceptionally high in organic content. $\delta^{13}\text{C} = -1.7\text{‰}$ is also a typical value for recrystallized cement during later burial stages (Al-Aasm and Azmy, 1996).

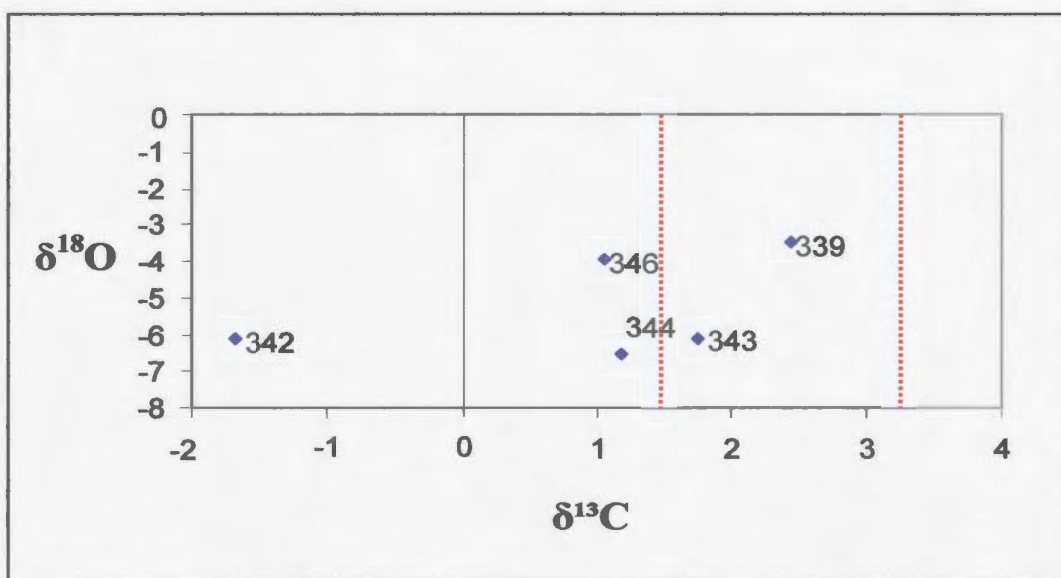


Figure 5.5: Plot of $\delta^{18}\text{O}$ versus $\delta^{13}\text{C}$ above the Ben Nevis Reservoir in muddy siltstones, dashed lines represents marine biogenic calcium carbonate of Albian age.

5.3.2.2 White Rose Shale below the Ben Nevis Formation

Nine of eleven samples taken from the marlstone below the Ben Nevis Formation provided a close grouping with an average value of 1.8‰ (Figure 5.6) indicating biogenic precipitation from Albian seawater (Veizer *et al.*, 1999). Sample 311 is anomalously high relative to its subset, possibly as a result of a period of bacterial fermentation (Irwin *et al.*, 1977). The other two samples did not release enough CO_2 for analysis.

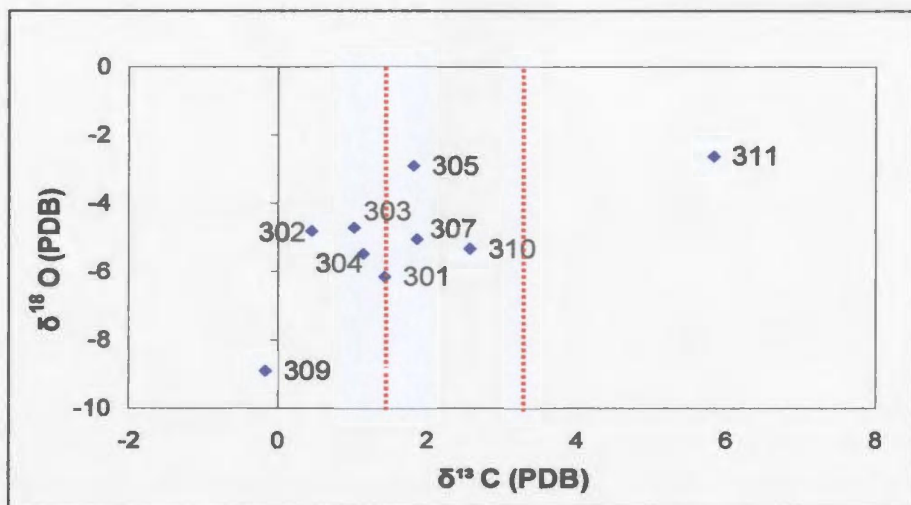


Figure 5.6: Plot of $\delta^{18}\text{O}$ versus $\delta^{13}\text{C}$ for samples below the Ben Nevis Formation, White Rose B-07_4, dashed lines represents marine biogenic calcium carbonate of Albian age.

5.3.2.3 Rankin Formation

Seventeen samples of cuttings (fourteen limestone and three calcareous shales) assigned to the Rankin Formation in wells Mobil *et al.*, Rankin M-36 and Husky-Bow Valley *et al.*, Archer K-19 yielded range for these samples is -2.8 to 2.7 ‰ $\delta^{13}\text{C}$ with an average of -0.56 ‰ $\delta^{13}\text{C}$. The results were ordered based on stratigraphic position within the Rankin Formation;

Rankin Formation: M-36 (Lower Unit) = 1.1 to 2.7 ‰ $\delta^{13}\text{C}$

M-36 (Middle Unit) = -2.8 to 1.1 ‰ $\delta^{13}\text{C}$

M-36 (Upper Unit) = -0.7 ‰ $\delta^{13}\text{C}$

Egret Member = 1.3 to 2.6 ‰ $\delta^{13}\text{C}$

K-19 (Lower Unit) = -2.4 to 0.6 ‰ $\delta^{13}\text{C}$

These wells were selected based on McAlpine (1990) well type section (Rankin M-36) and the well in closest proximity to the White Rose Field that also contained the

Rankin Formation (Archer K-19). It is important to note that the Egret member of the Rankin Formation is the organic-rich source rock for the Jeanne d'Arc Basin (Swift and Williams, 1980).

These samples provide a larger $\delta^{13}\text{C}$ spread than preceding samples, from -2.8 to $+2.7$ possibly representing a mixture of calcium carbonate sources or a bulk sample consisting of shells and different types of cements (Figure 5.7). The three samples from the organic rich Egret Member would be expected to have high organic content with a depleted $\delta^{13}\text{C}$ (Hoefs, 1987), but instead have some of the highest $\delta^{13}\text{C}$ in the Rankin Formation. The higher $\delta^{13}\text{C}$ for the Egret Member and the M-16 lower unit may represent exposure to bacterial fermentation (Irwin *et al.*, 1977) or have a larger component of marine sourced calcium carbonate (Veizer *et al.*, 1999). Expected range for Late Jurassic marine biogenic calcium carbonate as extrapolated from Veizer *et al.*'s (1999) Phanerozoic trend is 1.4 to 2.2 ‰ $\delta^{13}\text{C}$, corresponding to the Egret Member and lower unit of the Rankin Formation found in the M-16 well. Slower sedimentation rates causing longer periods of time in the sulphate reduction zone may cause depletion of $\delta^{13}\text{C}$ found in K-19 and M-36 middle unit samples.

This section is broken down into the following sample groups to distinguish isotopic difference between shells of mid-Cretaceous age and authigenic calcite cements:

- 1) calcite cement and shells (Figure 5.8);
- 2) calcite cement only (Figure 5.9);
- 3) shells only (Figure 5.10) or
- 4) without appreciable shells or cement (Figure 5.11).

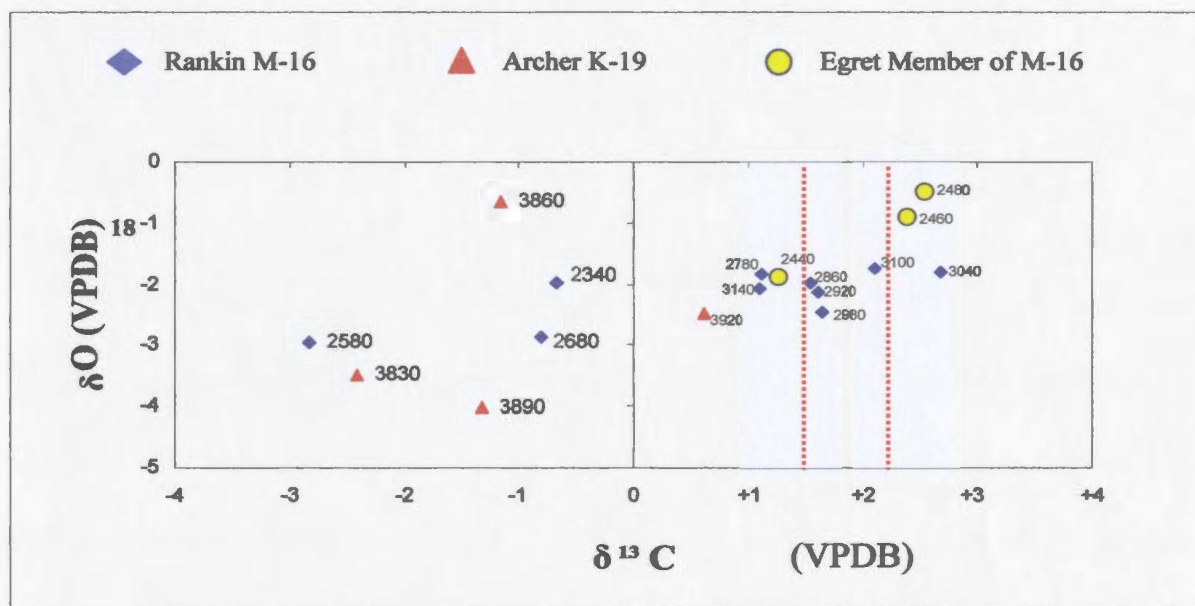


Figure 5.7: Plot of $\delta^{18}\text{O}$ versus $\delta^{13}\text{C}$ for samples from Rankin M-16 and Archer K-19 within the Rankin Formation, dashed red lines represents marine biogenic calcium carbonate of Kimmeridgian age.

5.3.2.4 Skeletal shell debris and detrital carbonate grains of the Ben Nevis Formation

Table 5.1 lists the four sample groups with the number of samples, mean and standard deviation for $\delta^{13}\text{C}$. Calcite cement is predominantly ferroan calcite cement and no divisions were attempted on shell type.

Table 5.1 $\delta^{13}\text{C}$ values for wells B-07_4 and F-04

Group	Number of Samples	Mean \pm S.D.
A) Calcite cement and shells	21	+3.2 \pm 1.4
B) Calcite cement only	19	+3.8 \pm 1.8
C) Shells only	6	+2.6 \pm 0.4
D) Without appreciable shells or cement	14	+1.2 \pm 1.6

Using Veizer *et al.*, (1999) $\delta^{13}\text{C}$ range of +1.5 to +3.3 ‰ for the Albian time period (Figure 5.2), the selected shells fall within the boundaries (+2.6 to +3.3 ‰), supporting this range to be correct for marine biogenic carbonate precipitated during the mid-Cretaceous. When analyzing calcite cement alone, a slight increase is observed on average of 1.2 ‰ $\delta^{13}\text{C}$. The combination of shells and calcite cement gives an average that is located between the two individual populations. This would be expected if groups A and B were combined. The lowest $\delta^{13}\text{C}$ values are from samples representing detrital carbonate grains (+1.2 $\delta^{13}\text{C}$) and may indicate a slightly earlier $\delta^{13}\text{C}$ value of marine bicarbonate (Veizer *et al.*, 1999), previous diagenetic influences in its original depositional setting or effects of continental weathering.

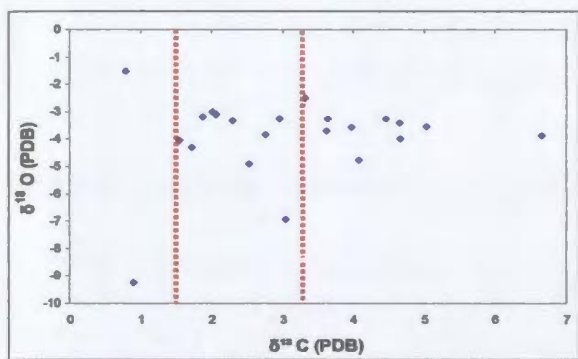


Figure 5.8: Plot of $\delta^{18}\text{O}$ versus $\delta^{13}\text{C}$ for samples containing *both calcite cement and shell debris* from wells F-04 and B-07_4, dashed lines represent marine biogenic calcium carbonate of Albian age.

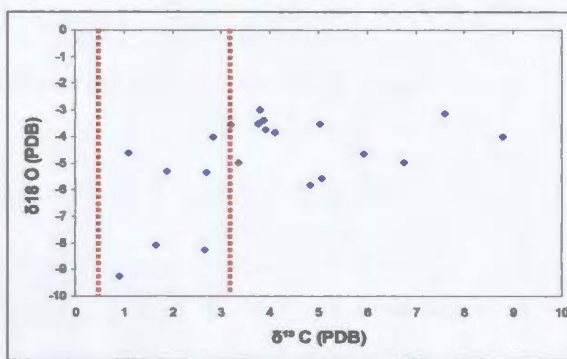


Figure 5.9: Plot of $\delta^{18}\text{O}$ versus $\delta^{13}\text{C}$ for samples containing *calcite cement* from wells F-04 and B-07_4, dashed lines represent marine biogenic calcium carbonate of Albian age.

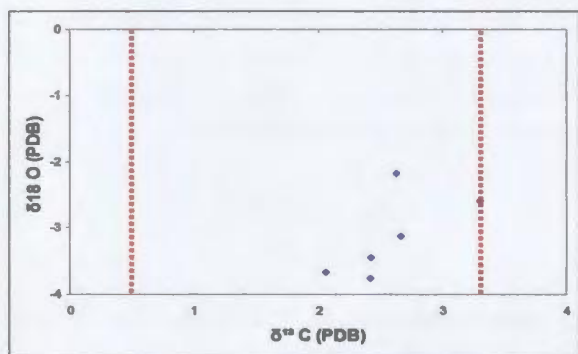


Figure 5.10: Plot of $\delta^{18}\text{O}$ versus $\delta^{13}\text{C}$ for samples containing *shells* from wells F-04 and B-07_4, dashed lines represent marine biogenic calcium carbonate of Albian age.

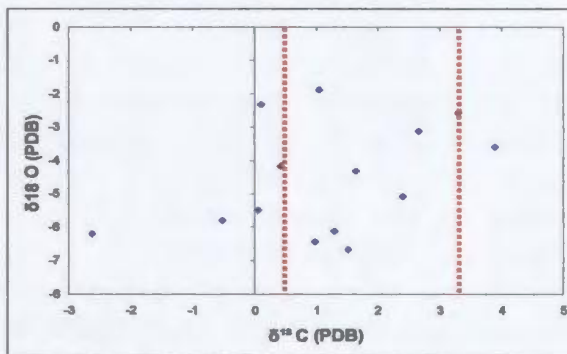


Figure 5.11: Plot of $\delta^{18}\text{O}$ versus $\delta^{13}\text{C}$ for samples *not containing shells or calcite cement* from wells F-04 and B-07_4, dashed lines represent marine biogenic calcium carbonate of Albian age.

As noted in Chapter Four, the primary source for authigenic calcite cement is proposed to be the abundant shell debris found throughout the Ben Nevis Formation. While there is a significant volume of serpulid worm tubes, bivalves and gastropods, it may be thin, compacted and often discontinuous residues of micro-crystalline textured curved shell fragments of indeterminate affinity that are the primary source for calcite cement. These 'thin black shells' have been reduced by dissolution to their current state representing multi-fold volume reduction and must have supplied enormous amounts of

calcium carbonate to formation fluids, which subsequently yielded calcite cement when proper conditions existed.

It is now necessary to determine what causes enrichment in $\delta^{13}\text{C}$ from the time of shell dissolution to subsequent precipitation as authigenic calcite cement. The basis for apparent enrichment may be derived from the fact that aragonite is slightly enriched in $\delta^{13}\text{C}$ relative to calcite (Faure and Mensing, 2005). Unstable aragonite is first to be dissolved in the burial process providing an excellent source of enriched $\delta^{13}\text{C}$, to then precipitate as calcite cement.

Sommer and Rye (1978) developed the aragonite-calcite equation:

$$10^3 \ln \alpha_{\text{cal}}^{\text{ar}} = 2.56 - 0.065T \quad (1)$$

At a temperature of 15 °C, $\alpha_{\text{cal}}^{\text{ar}} = 1.001586$ and calcite of $\delta^{13}\text{C}_{\text{cal}} = +2.45 \text{ ‰}$, the value of $\delta^{13}\text{C}_{\text{ar}}$ in equilibrium with calcite is:

$$\begin{aligned} 1.001586 &= \frac{\delta^{13}\text{C}_{\text{ar}} + 1000}{2.45 + 1000} \\ \delta^{13}\text{C}_{\text{ar}} &= +4.04 \text{ ‰ (VPDB)} \end{aligned} \quad (2)$$

This represents an enrichment of + 1.59 ‰ (VPDB) from aragonite to calcite (4.04 - 2.45 ‰) at these parameters. Average enrichment calculated from original shells (+2.6 ‰) to authigenic calcite cement (+3.8 ‰) in this study is +1.2 ‰ (VPDB). These results are taken to indicate that the aragonite/calcite relationship to be the definitive answer to isotopically $\delta^{13}\text{C}$ enriched calcite cement, thereby supporting and strengthening the petrographic assessment.

Rubinson and Clayton (1969) used theoretical calculations to yield a 0.9 ‰ $\delta^{13}\text{C}$ enrichment from aragonite to calcite at 25°C, although their experimental analyses revealed 1.8 ‰ $\delta^{13}\text{C}$ enrichment. Using the aragonite-calcite equation (3) in conjunction with the calcite equilibrium equation (4), an increase in temperature reveals a decrease in the enrichment of aragonite relative to calcite. A temperature of 20°C reduces the enrichment:

$$10^3 \ln \alpha_{\text{cal}}^{\text{ar}} = 2.56 - 0.065T \quad (3)$$

$$\alpha_{\text{cal}}^{\text{ar}} = 1.001261$$

$$1.001261 = \frac{\delta^{13}\text{C}_{\text{ar}} + 1000}{2.45 + 1000}$$

$$\delta^{13}\text{C}_{\text{ar}} = +3.71 \text{ ‰ (VPDB)}$$

$$\text{Aragonite enrichment} = 3.71 - 2.45 = 1.26 \text{ ‰ } \delta^{13}\text{C} @ 20^\circ\text{C}$$

$$\text{Using } T = 25^\circ\text{C}$$

$$\text{Aragonite enrichment} = 3.39 - 2.45 = 0.94 \text{ ‰ } \delta^{13}\text{C} @ 25^\circ\text{C}$$

The value established from isotopic results of this study, +1.20 ‰ average enrichment, is well within fractionation factors of biogenic aragonite (*e.g.* Grossman and Ku, 1986). In addition, the value is consistent with dissolution of slightly enriched aragonite to provide the source for calcite cement that is enriched relative to biogenic marine calcite may occur between 20 °C (+1.26 ‰) and 25°C (+0.94 ‰), implying very early diagenesis directly below sediment-water interface, again supporting the petrographic assessment of very early concretion formation. Since carbon isotopes have not traditionally been widely used as paleothermometers, additional aspects regarding paleo-temperatures will be addressed in the section on oxygen isotopes below. The

temperature dependence of aragonite-bicarbonate fractionation may not be sufficiently established with carbon isotopes to distinguish 5 °C changes.

5.3.2.5 Isotopic pattern across concretions.

Concretion C (well B-07_4, core 1, boxes 15 and 16) was sampled for isotope analysis from the lower boundary across to the top. Results revealed a distinct pattern of relative depletion in the center, enrichment in the middle and depletion towards the edges (Figure 5.12). The relative depletion at the center of the concretion may represent the signature of the Albian shells which are concentrated at the nucleation site (Figure 5.13). The intermediate zone of enrichment is consistent with enrichment of authigenic calcite cement derived from shell dissolution. The subsequent depletion at the edge of the concretion may indicate reduction of $\delta^{13}\text{C}$ in pore waters by selectively removing $\delta^{13}\text{C}$ as calcite precipitates (Mozley and Burns 1993).

5.4 Oxygen Isotopes

Measurement of oxygen isotopes of authigenic cements can also reveal much about their origin and evolution. Several hypotheses are found in the literature concerning changing $\delta^{18}\text{O}$ values. Isotopic exchange of formation water with $\delta^{18}\text{O}$ rich mineral phases such as calcite are controlled by the isotopic composition of the calcite, the water/rock ratio and the temperature, (Clayton *et al.*, 1966 and Knauth *et al.*, 1980).

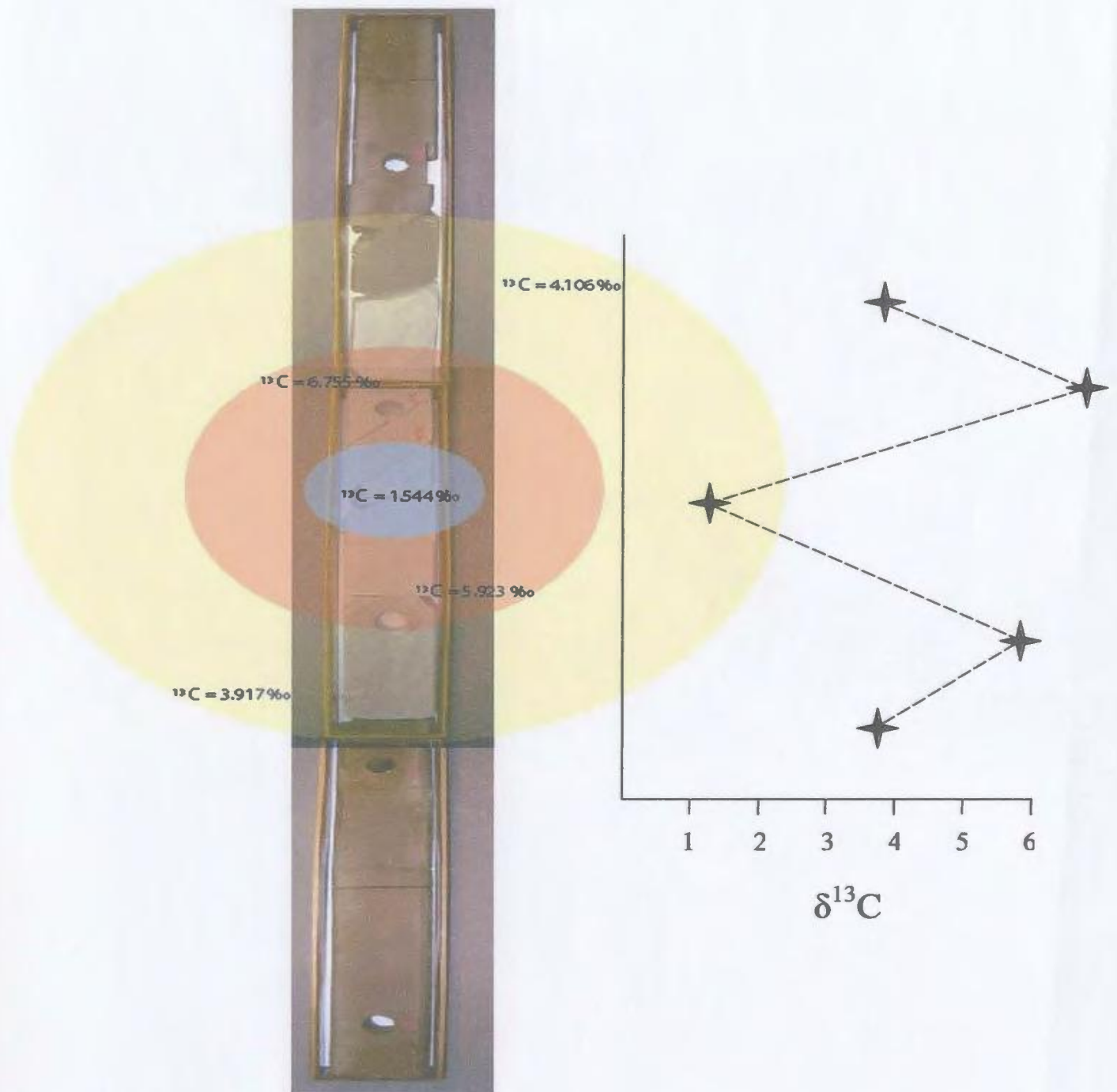


Figure 5.12: Distribution of carbon isotopic results across a concretion demonstrating the relatively depleted central nucleation site, subsequent enrichment outside the center and minor relative depletion towards the edge of the concretion. Graph to the right demonstrates the symmetric pattern of carbon isotopes within the concretion.



Figure 5.13: Central nucleation site of the above concretion. The relative depletion of carbon isotopes may represent the preservation of Albian shells and their marine biogenic calcium carbonate signature.

Others suggest that shale sequences dominate oxygen isotope signatures because of their large volumes and water expulsion properties (Powers, 1967; Bruce, 1984). Smectite membrane filtration has been experimentally proven to enrich $\delta^{18}\text{O}$ values at high temperatures (Hayden and Graf, 1986). Another possibility for the variability of $\delta^{18}\text{O}$ values is the mixing of meteoric fluids with evaporite brines (Knauth and Beeunas, 1986).

Longstaffe (1987) discusses the unidirectional increase of $\delta^{18}\text{O}$ over the Phanerozoic which may be caused by a reduction in oceanic hydrothermal systems and declining ratio of low temperature / high temperature alteration processes (Veizer, 2003). Veizer *et al.*, (1999) provides $\delta^{18}\text{O}$ trends over the entire Phanerozoic demonstrating the cyclic nature and increasing trend through time (Figure 5.14). For the Albian-age Ben Nevis Formation a range of -1.25 to -0.75 $\delta^{18}\text{O}$ (VPDB) of well preserved marine biogenic Ca-carbonate is extrapolated from the Phanerozoic $\delta^{13}\text{C}$ trend of Veizer, *et al.*, (1999).

Various authors provide diverse results regarding the source of $\delta^{18}\text{O}$ values. Unique conditions result in distinct $\delta^{18}\text{O}$ signatures such corresponding, for example, to meteoric water $\delta^{18}\text{O} \sim -5$ to 0 ‰, pore water in oceanic sediments $\delta^{18}\text{O} -2.5$ to $+2.5$ ‰, and marine carbonate from oceanic reservoirs 0 ± 4 ‰ (Longstaffe, 1987). Wilkinson (1991) interprets -10 to -6 ‰ VPDB for $\delta^{18}\text{O}$ of cement from meteoric waters, -6 to -4 ‰ VPDB for $\delta^{18}\text{O}$ of cement from mixed marine-meteoric waters and -1 to -4 ‰ VPDB for $\delta^{18}\text{O}$ of cement from marine pore waters. For modern environments of warm conditions and low latitudes, $\delta^{18}\text{O}$ of seawater is 0 ‰ and meteoric water is -4 ‰ (Clark and Fritz, 1997). Veizer *et al* (1999) used Silurian brachiopod data and whole rock data

to establish $\sim 2 \text{ ‰ } \delta^{18}\text{O}$ VPDB depletion through diagenetic stabilization of aragonite and high Mg-calcite to low Mg-calcite, in much the same way as the $\delta^{13}\text{C}$ stabilization discussed previously. Veizer (2003) modified the earlier study to conclude a 1 ‰ depletion of $\delta^{18}\text{O}$ during the aragonite-to-calcite reaction.

Mozley and Burns (1993) provide several possible explanations for the $\delta^{18}\text{O}$ depletion in carbonate concretions:

- 1) Recrystallization of calcite cement to re-equilibrate at ambient conditions.

- 2) Removal of $\delta^{18}\text{O}$ from pore waters during the precipitation of volumetrically significant authigenic carbonates. Subsequent cements would then be anomalously depleted.

- 3) Mixing with meteoric water as the reason for anomalous depletion of $\delta^{18}\text{O}$ values (Sass and Loldny, 1972; Hudson, 1978; Carpenter *et al.*, 1988; Machemer and Hutcheon, 1988; Thyne and Boles, 1989; Bloch, 1990; Scotchman, 1991). The mixing of marine and meteoric waters may be quite common during early deposition if meteoric water impinges on the offshore (Bjorlykke, 1988). Manheim and Sayles (1974) detected meteoric waters in limestones from DSDP boreholes 120 km off the coast of Florida, clearly demonstrating the influence of meteoric waters in an offshore environment.

- 4) Precipitation at anomalously high temperatures. Scotchman (1991) identified an important product of smectite-illite transition in a closed system with a $\delta^{18}\text{O}$ value of +6 ‰ at 100 to 140 °C as hot pore waters migrate up-dip from the basin center. Overpressure zones can cause the geothermal gradient to increase by as much as 62%

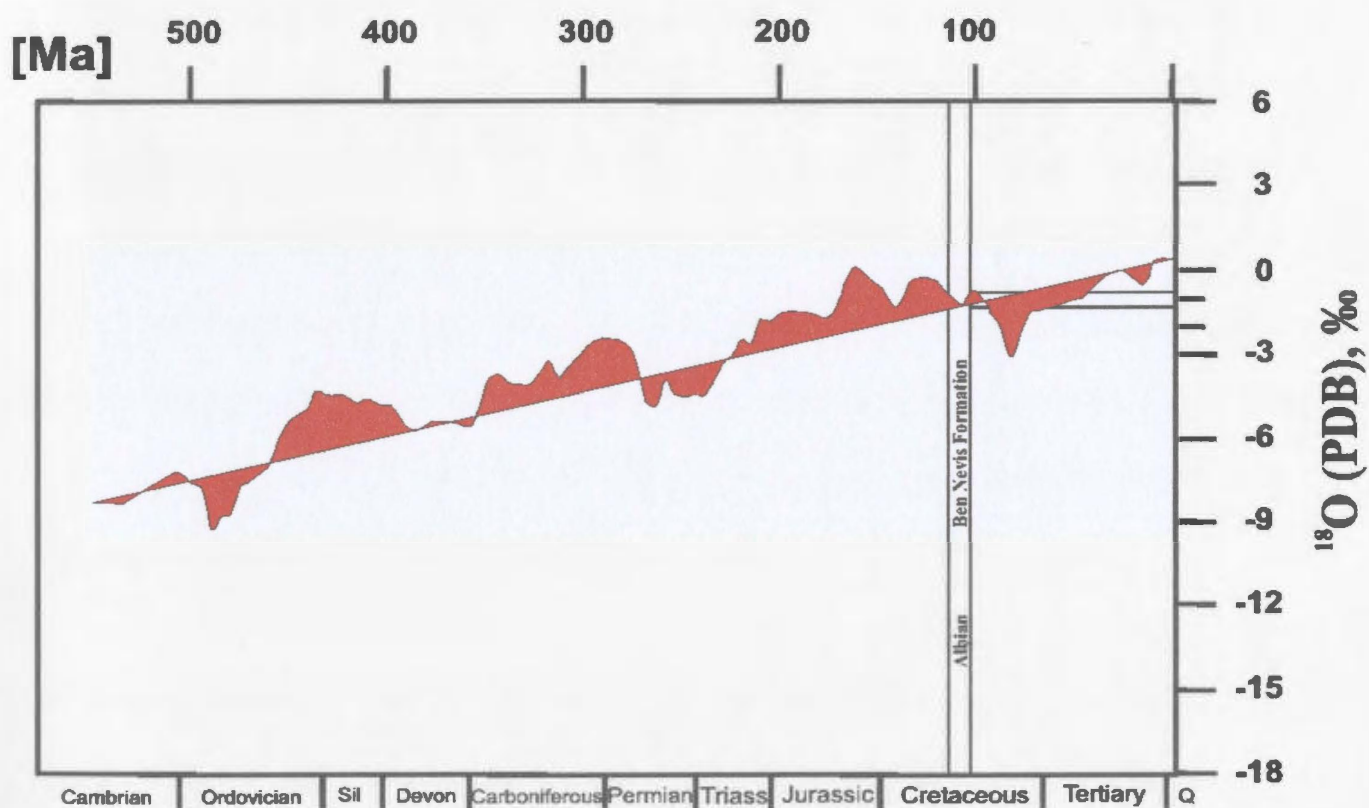


Figure 5.14: Variation of $\delta^{18}\text{O}$ (VPDB) values throughout the Phanerozoic, demonstrating a range of -1.25 to -0.75 during the Albian when the Ben Nevis Formation was deposited. Modified from Veizer *et al.*, (1999).

(Scotchman, 1991). The presence of highly conductive salt structures such as the White Rose diapir can funnel geothermal heat, providing anomalously high temperatures (Nagihara *et al.*, 2002) possibly increasing $\delta^{18}\text{O}$ values, if it occurred prior to cementation, higher.

5) Variation in seawater composition over time.

Oxygen isotope fractionation is temperature dependent. Veizer (2003) discusses oxygen isotopes and their relationship with paleothermometry. An increase of 4 °C during carbonate precipitation depletes the $\delta^{18}\text{O}$ value by approximately 1 ‰. Paleoclimate studies must be utilized to determine the surface temperatures during deposition of the Ben Nevis Formation. Paleogeographic reconstructions would also be helpful to determine the location of the Jeanne d'Arc basin during this period of time, as well as the depth of water at time of deposition to better estimate a temperature for the sediment-water interface.

Voigt and Wiese (2000) provide references both for and against using $\delta^{18}\text{O}$ as a paleoenvironmental indicator. They recognize that the oxygen isotope ratio in calcium carbonate is controlled by temperature and the $\delta^{18}\text{O}$ of ambient water, and by the unique fractionation factors of individual organisms. Voigt and Wiese (2000) show isochronous $\delta^{18}\text{O}$ values in three Cretaceous-age European basins with isotopic signatures that have not been reset by different diagenetic sequences, thereby supporting their use in paleogeographic reconstructions.

Oxygen isotopes for WR F-04 range from -9.2 to -1.5 ‰ $\delta^{18}\text{O}$, throughout a depth interval of 2766m-2870m TVD (Figure 5.15). The WR B-07_4 well had a similar oxygen isotope range from -8.1 to -4.5 ‰ $\delta^{18}\text{O}$ and a slightly deeper interval at the base of the Ben Nevis Formation from approximately 2897m-2958m TVD (Figure 5.16). Overall there is a lack of consistent stratigraphic trends in $\delta^{18}\text{O}$ values, possibly reflecting the homogeneity of such a large storm dominated formation. On the other hand, $\delta^{18}\text{O}$ average values appear to be more depleted toward the top of each core. This indicates a lack of dependency on burial depth.

5.4.1 Paleothermal Reconstructions and Precipitation Temperatures

In this section an attempt will be made to derive paleo-precipitation temperatures. Faure and Mensing, (2005) list the following assumptions that must be satisfied in order to use paleothermometry based on the temperature dependence of the fractionation of oxygen isotopes between marine calcium carbonate and water;

- 1) Isotopic equilibrium between oxygen in the water and the biogenic calcium carbonate;
- 2) The preservation of the isotopic composition of oxygen in the solid state, and
- 3) The constancy of the isotopic composition of water in the oceans.

It is proposed herein that these assumptions can be satisfied for the case of original shells. A precautionary warning regarding $\delta^{18}\text{O}$ results is mentioned by Azmy *et al.*, (2001); homogenization and melting temperatures of primary fluid inclusions should be used to confirm values based on $\delta^{18}\text{O}$.

WHITEROSE F-04

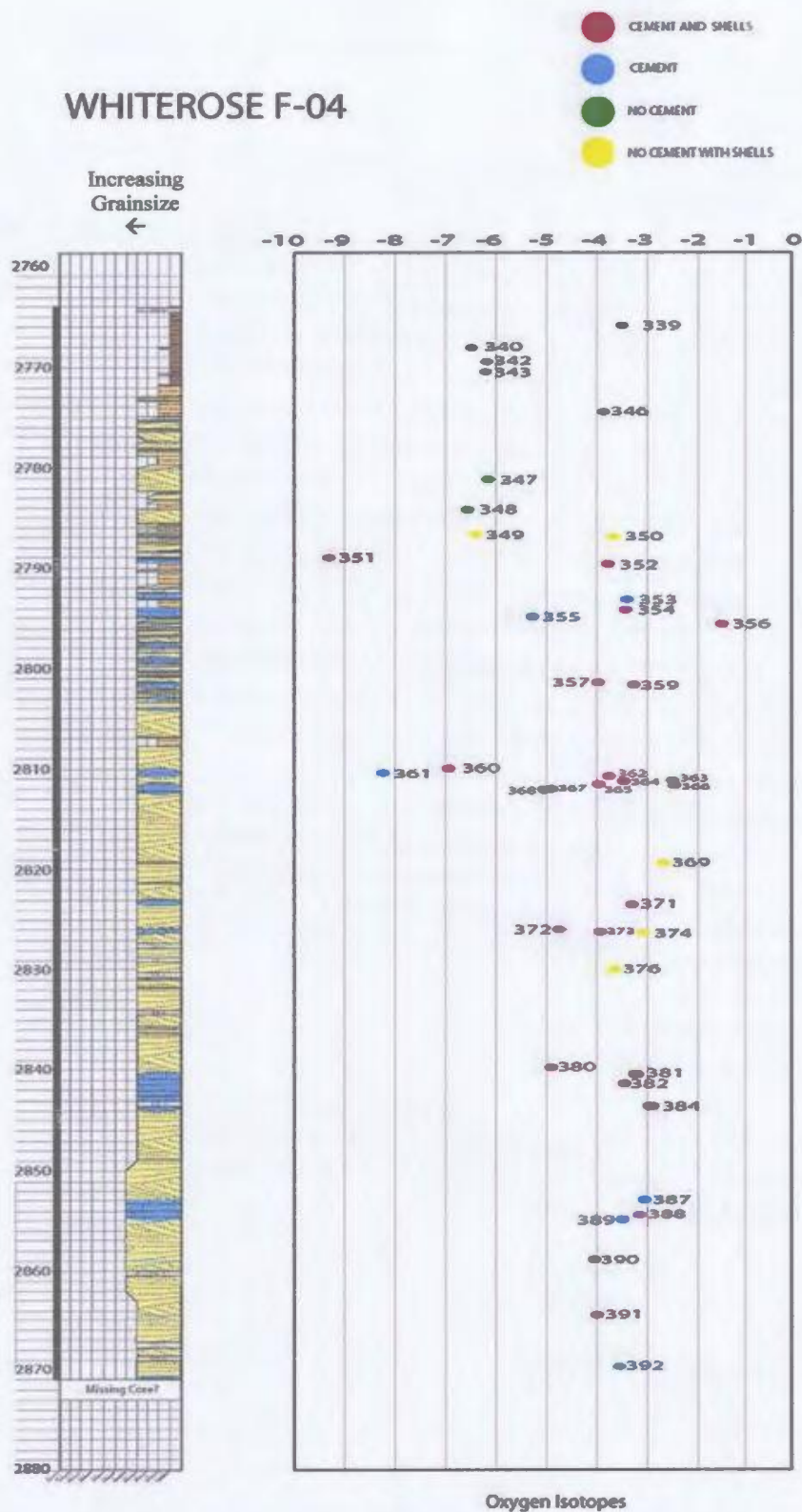


Figure 5.15: Location of oxygen isotopes relative to core of WR F-04.

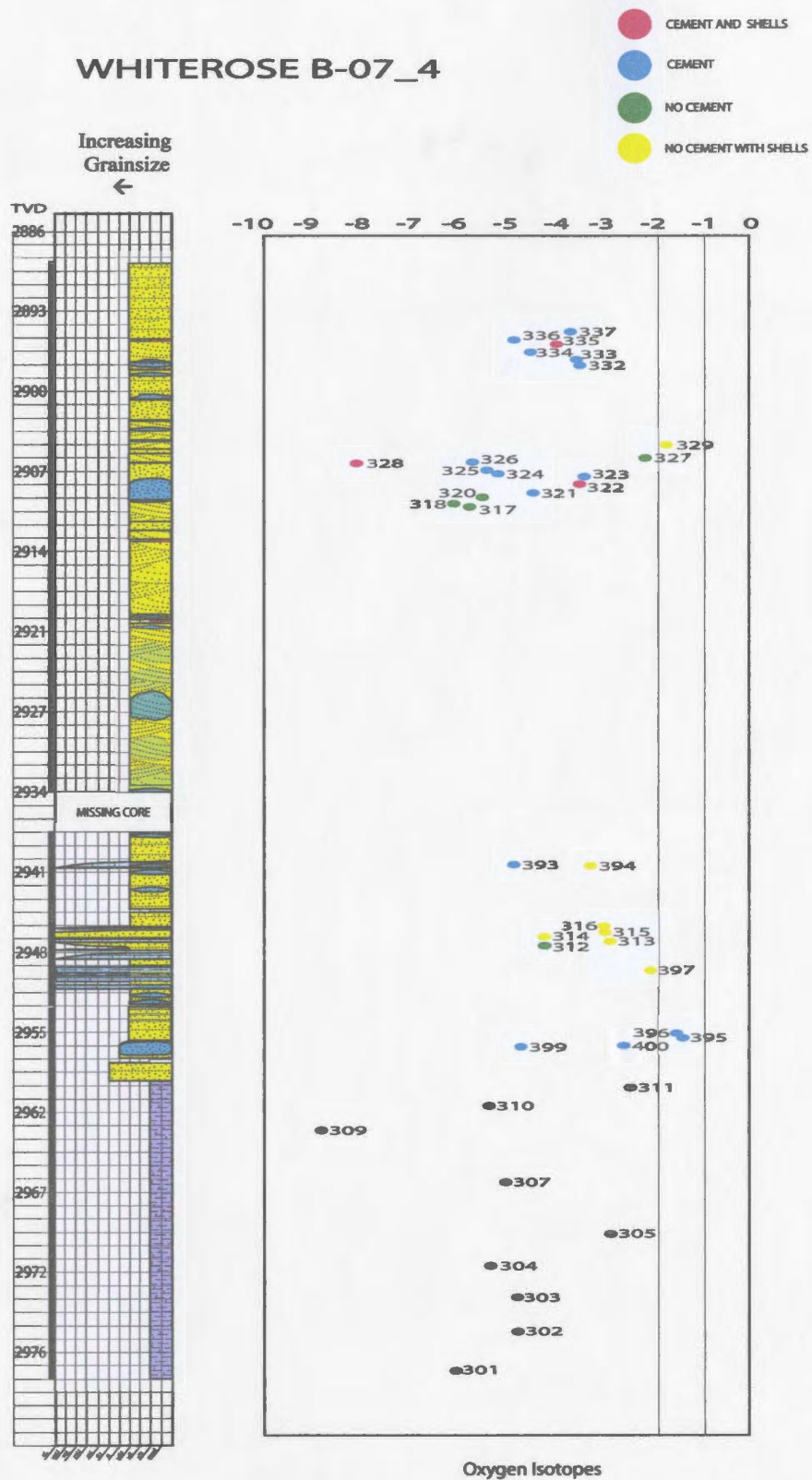


Figure 5.16: Location of oxygen isotopes relative to core of WR B-07_4.

Thompson and Barron (1981) and Barron and Washington (1982) used paleogeographic restoration of Cretaceous continents to develop a climate model which estimated a 2°C global temperature increase compared to today's temperatures. This transforms to a 6-14 °C increase of globally averaged surface temperatures. Using Barron and Washington (1982) paleogeographic reconstructions, the Grand Banks were located approximately 36°N during the Albian-Cenomanian (108-92 Mya), 10.5° to the south of present day Jeanne d'Arc Basin. This latitude is comparable to today's North Carolina which has a mean temperature of 4.4°C in January and 26.7°C in July (<http://www.worldatlas.com/webimage/countrys/namerica/usstates/nc.htm#climate>).

Combining the global temperature increase with the more southerly position will give a possible annual range of 10.4 to 40.7 °C surface temperatures during the time of deposition of the Ben Nevis Formation. To determine the precipitation depth of calcite cement, mid-Cretaceous seawater $\delta^{18}\text{O}$ composition is required to use the paleo-temp equation, as well as assumptions on sediment water interface depth and paleothermal gradient.

Precipitation temperatures derived from (Craig, 1957, modified by Anderson and Arthur,

1983)
$$T (^{\circ}\text{C}) = 16.0 - 4.14 (\delta\text{c} - \delta\text{w}) + 0.13 (\delta\text{c} - \delta\text{w})^2 \quad (4)$$

$$\delta^{18}\text{O water} = \delta\text{w}$$

$$\delta^{18}\text{O calcite} = \delta\text{c}$$

A $\delta^{18}\text{O}$ value of ~ -1 ‰ for precipitation from Cretaceous marine waters was derived by Shackleton and Kennet, (1975). This number has since been confirmed by Veizer *et al.*, (1999) through the development of trends throughout the entire Phanerozoic, showing a steady increase throughout the Paleozoic, followed by a general decline through the Mesozoic and fluctuations around the present day value for the Cenozoic (Figure 5.14). A range of -1.25 to -0.75 ‰ $\delta^{18}\text{O}$ (VPDB) of marine biogenic Ca-carbonate of Albian age was extrapolated from the $\delta^{18}\text{O}$ Phanerozoic trend of Veizer *et al.*, (1999). Using a sample selected from an individual shell may give the diagnostic temperatures of the formation of marine biogenic carbonate during the deposition of the Ben Nevis Formation. The critical assumption for this determination is that the carbonate shell was well preserved and has never been diagenetically re-set.

A thermocline is the sharp decrease in water temperature with depth associated with latitudes between 40°N and 40°S, and ranges from 50 to 500 m, (<http://www.esr.org/outreach/glossary/thermocline.html>). The deposition of the Ben Nevis Formation in an inner shelf to lower shoreface environment in water depths of 20 to 50 m is just above a hypothetical thermocline and would not be exposed to any drastic decrease in temperature associated with a paleo-thermocline.

Using equation (4) for $\delta^{18}\text{O}$ values of sample 397, gave a paleo-temperature of 21.1 °C. These temperatures are well within the range of Ben Nevis depositional temperatures discussed above and also correlate with the temperatures derived from $\delta^{13}\text{C}$ results in the previous section, which suggested between 20 and 25 °C.

Sample 397 $T (^{\circ}\text{C}) = 16.0 - 4.14 (\delta\text{c} - \delta\text{w}) + 0.13 (\delta\text{c} - \delta\text{w})^2$

$$\delta^{18}\text{O water} = \delta\text{w} = -1 \text{ ‰}$$

$$\delta^{18}\text{O calcite} = \delta\text{c} = -2.18 \text{ ‰}$$

$$T (^{\circ}\text{C}) = 21.1 \text{ }^{\circ}\text{C}$$

5.4.2 Results

5.4.2.1 Skeletal shell debris, detrital carbonate grains and cements from the Ben Nevis Formation.

This section is also divided into samples which contain calcite cement and shells, just calcite cement, just shells or detrital carbonate grains to distinguish the difference between unaltered Mid-Cretaceous shells and authigenic calcite cement.

- 1) calcite cement and shells (Figure 5.17);
- 2) calcite cement only (Figure 5.18);
- 3) without appreciable shells or cement (Figure 5.19) or
- 4) shells only (Figure 5.20).

Table 5.2 lists the four sample groups with the number of samples, mean and standard deviation for $\delta^{18}\text{O}$ followed by paleo-temperatures prior to and after the aragonite to calcite conversion where applicable. The calcite cement is predominantly ferroan calcite.

Applying the paleo-temperature equation (4) to these values gives 21.1 $^{\circ}\text{C}$ for shell formation and an 13.0 $^{\circ}\text{C}$ increase during cement precipitation. Correia *et al.*, (1990) used corrected bottom hole temperatures to calculate geothermal gradients for the Jeanne d'Arc Basin. They derived higher geothermal gradients (30-33 $^{\circ}\text{C}/\text{km}$) for the northern portion of the basin with the highest temperatures associated with salt structures. It must be noted that present day geothermal gradients are not necessarily the same as

paleo-geothermal gradients. Taking into account the White Rose diapir, a geothermal gradient of 33 °C/km for the White Rose Field results in a depth of calcite precipitation

Table 5.2: Sample types, average $\delta^{18}\text{O}$ shifts and corresponding paleo temperatures. The addition of cement and shells is a bulk sample analysis which has difficulties in applying $\delta^{18}\text{O}$ shifts but clearly indicates that values for the mixture is found between the two individual populations. The detrital carbonate grains may be harder to interpret as the provenance of such is unknown.

Sample Type	Number of Samples	$\delta^{18}\text{O}$ Mean and standard deviation	Paleo Temperature	Aragonite to Calcite	Arag-Cal Adjusted Paleo Temperature
Shells	1	-2.180 +/- 0.034	21.1°C	-2.180	21.1°C
Cement and Shells?	19	-3.935 +/- 1.5	n/a	n/a	n/a
Cement	21	-4.888 +/- 0.6	34.1°C	-3.888	29.0°C
Detrital Carbonate	14	-4.438 +/- 2.0	31.8°C	-4.438	31.8°C

of about 390 m. This very early diagenesis supports the petrographic evidence presented in Chapter four.

The assumption of a 1 ‰ depletion of $\delta^{18}\text{O}$ for samples subjected to the aragonite calcite transition (Veizer, 2003) could be a complementary application. The 1 ‰ depletion was upgraded from Veizer *et al.*, (1999) who suggested a 2 ‰ depletion of calcite relative to its parent aragonite. If the cement converted from aragonite shells as suggested by the carbon isotopes in the previous section, the cement values can be adjusted.

Incorporating this shift for the authigenic calcite cement would give a reduced paleo-temperature of 29 °C and would represent an increase of 7.9 °C. This lower paleo-temperature reduces depth of cement precipitation to ~ 240 m. This seems to be a realistic result defining the aragonite shells as the source of the calcite cement but it also

requires adjustments for the paleo-temperature calculations above. The $\delta^{18}\text{O}$ depletion can be affected by both an increase in temperature and the aragonite-to-calcite transition.

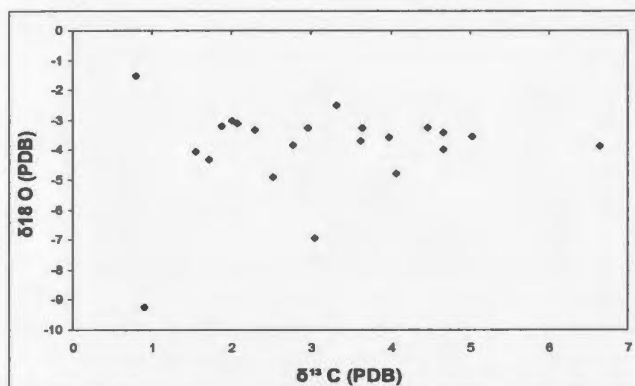


Figure 5.17: Plot of $\delta^{13}\text{C}$ versus $\delta^{18}\text{O}$ for samples containing *both calcite cement and shell debris* from wells F-04 and B-07_4.1

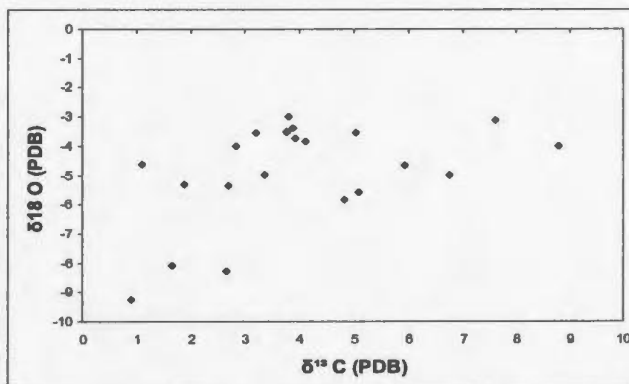


Figure 5.18: Plot of $\delta^{13}\text{C}$ versus $\delta^{18}\text{O}$ for samples containing *calcite cement* from wells F-04 and B-07_4.

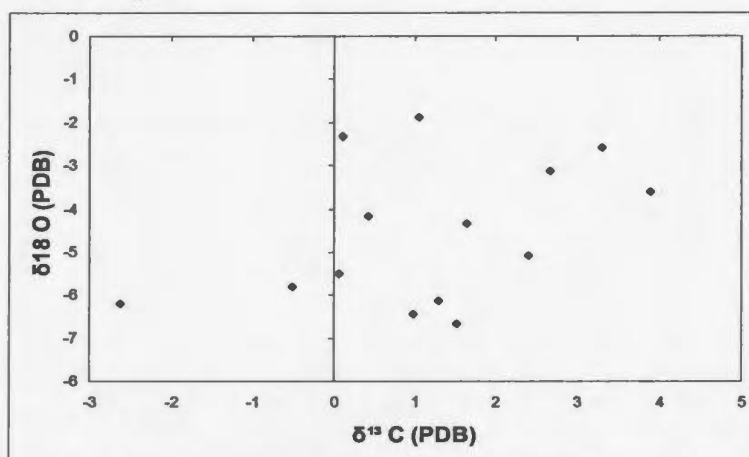


Figure 5.19: Plot of $\delta^{13}\text{C}$ versus $\delta^{18}\text{O}$ for samples *not containing unaltered shells or calcite cement* from wells F-04 and B-07_4.

Temperature varies with depth, pressure and formation water composition, all of which act to destabilize aragonite. Additional work is required to thoroughly investigate this association.

The detrital carbonate samples are slightly more depleted implying a higher paleo-temperature or possibly a shift for these samples, the resulting $\delta^{18}\text{O}$ values fall within

Wilkinson's (1991) definition of marine pore waters (-4 to -1 ‰ $\delta^{18}\text{O}$), thereby eliminating the problem of how meteoric waters enter into a lower shoreface environment.

5.4.2.2 Muddy siltstones above the Ben Nevis Formation

Nine samples of muddy siltstone were taken from above the Ben Nevis reservoir sandstone, of which only five yielded enough calcium carbonate to provide isotopic results (Figure 5.20). $\delta^{18}\text{O}$ values average -5.2 ± 1.2 ‰. Applying the paleo-temperature equation gives a value of 35.9 °C. Using this value with Correia *et al.*, (1990) geothermal gradient of 33 °C/km would result in an approximate depth of calcite formation of 320 m. The depleted $\delta^{18}\text{O}$ values may also represent a slightly meteoric input into this formation. The slight depletion of $\delta^{18}\text{O}$ values also helps to eliminate this unit as a source for the calcite cement.

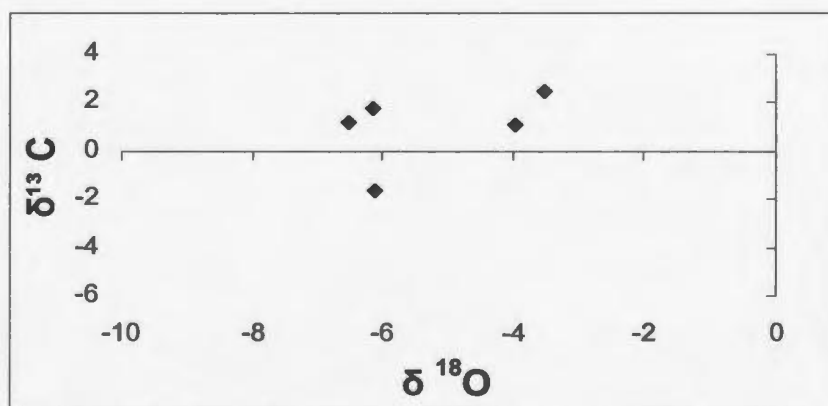


Figure 5.20: Plot of $\delta^{13}\text{C}$ versus $\delta^{18}\text{O}$ above the Ben Nevis Reservoir in muddy siltstones.

5.4.2.3 White Rose Shale below the Ben Nevis Formation

Nine of the eleven samples taken from below the Ben Nevis Formation within the Hibernia Formation distal equivalent marlstone provided the following $\delta^{18}\text{O}$ results (Figure 5.21). Samples were taken from this formation because it is highly calcareous, in direct contact with the somewhat meteoric influenced environment during their formation which is still in question because of their unknown affinities. The range of results from the Ben Nevis Formation is -9.2 to -1.5 ‰ suggesting a slightly meteoric to mixed meteoric regime. The depleted $\delta^{18}\text{O}$ values along with their early diagenetic origin as established by petrography may indicate removal of $\delta^{18}\text{O}$ from pore waters during the precipitation of volumetrically significant authigenic carbonates (Mozley and Burns, 1993). After applying the time and aragonite/calcite overlying Ben Nevis sandstones, and hence a potential source of calcium carbonate. The $\delta^{18}\text{O}$ values average 5.1 ‰ for this section, similar to the muddy siltstones above. Paleo-temperatures from $\delta^{18}\text{O}$ values

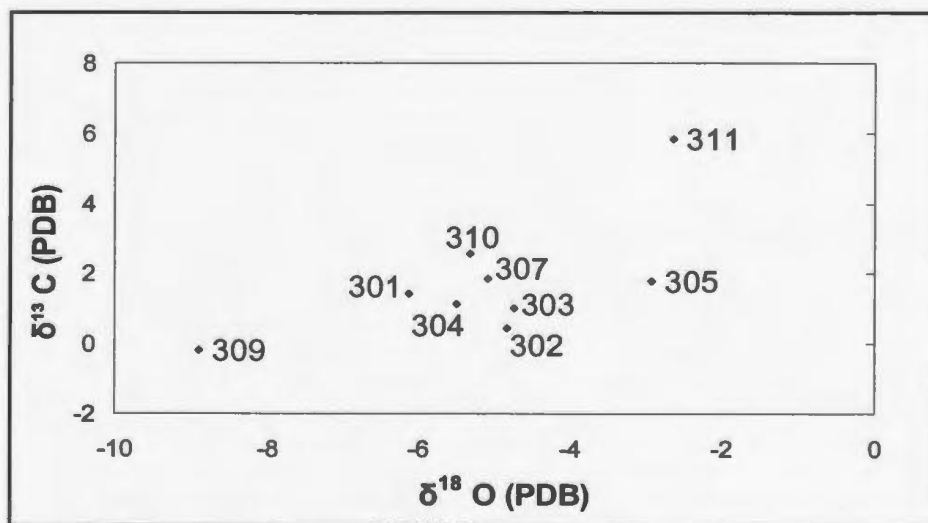


Figure 5.21: Plot of $\delta^{18}\text{O}$ versus $\delta^{13}\text{C}$ for samples below the Ben Nevis Formation, White Rose B-07_4

suggest an approximately 430 m burial depth for precipitation of calcite cement found in this calcareous shale unit. The $\delta^{18}\text{O}$ values may also represent a slightly meteoric input into this formation. The slight depletion of $\delta^{18}\text{O}$ values also helps eliminate this unit as a source for the calcite cement.

5.4.2.4 Rankin Formation

Seventeen samples (fourteen limestone and three calcareous shales) were taken within the Rankin Formation from wells Mobil *et al.*, Rankin M-36 and Husky-Bow Valley *et al.*, Archer K-19 and sampled for oxygen isotopes (Figure 5.22). The range for these samples was -4.0 to -0.5 ‰ $\delta^{18}\text{O}$ with an average of -2.1 ‰ $\delta^{18}\text{O}$. The results were divided based on the stratigraphic position within the Rankin Formation;

Rankin:	M-36 (Lower Unit 2856-3144 m)	= -2.4 to -1.7 ‰
	M-36 (Middle Unit 2533-2856 m)	= -3.0 to -1.8 ‰
	M-36 (Upper Unit 2386-2533 m)	= -2.0 ‰
	Egret Member	= -1.9 to -0.5 ‰
	K-19 (Lower Unit 3825-3942m RT)	= -4.0 to -0.7 ‰

Since these samples are from the Late Jurassic, the paleo-temperature equation must be adapted to incorporate Veizer *et al.*, (1999) paleo $\delta^{18}\text{O}$ depletion of -0.5 ‰.

$$T (^{\circ}\text{C}) = 16.0 - 4.14 (\delta_{\text{c}} - \delta_{\text{w}}) + 0.13 (\delta_{\text{c}} - \delta_{\text{w}})^2$$

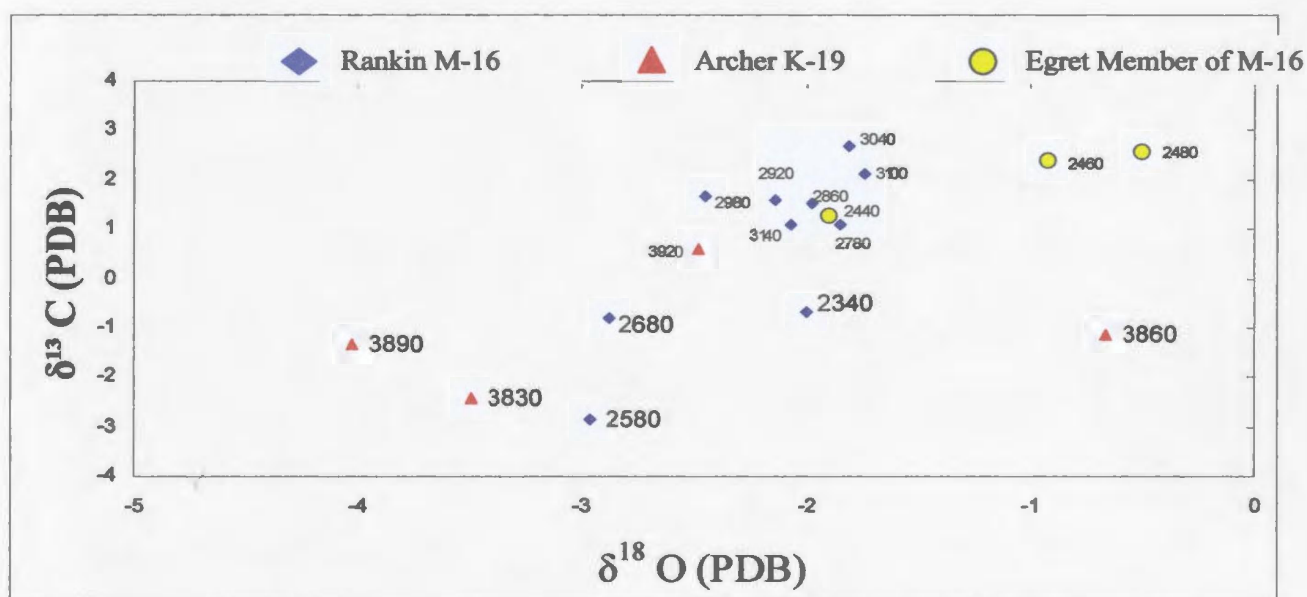
$$\delta^{18}\text{O water} = \delta_{\text{w}} = -0.5 \text{ ‰}$$

$$\delta^{18}\text{O calcite} = \delta_{\text{c}} = -2.1 \text{ ‰}$$

$$T (^{\circ}\text{C}) = 23.0 ^{\circ}\text{C}$$

This results in a paleo-temperature of approximately 23 °C during the deposition of the Rankin Formation.

The range of oxygen isotope results for the Rankin Formation (4 to -0.5 ‰) indicate a more dominant marine environment without meteoric input. The increase of $\delta^{18}\text{O}$ values for the Rankin Formation relative to the calcite cement suggests there is no connection between both entities.



progressive outward depletion in $\delta^{18}\text{O}$ values within concretions suggesting an increase in temperatures during growth, presumably due to progressive burial.

Four different hypotheses are proposed based on these trends. The first is that distinct concretions may have grown together to form what appears to be a single, larger concretion. This may disguise the original nucleation sites where lowest paleotemperatures are expected.

Secondly, different proportions of shells/cement are sampled across the concretion. The nucleation site sample may primarily reflect $\delta^{18}\text{O}$ in shells, whereas the remaining samples are measuring authigenic cement. The aragonite to calcite shift can be applied but the results still demonstrate a decrease in temperature towards the concretion edge, opposite to Wilkinson's (1991) radial increase of temperature with concretion growth and burial. An alternative view of concretion formation was put forward by Mozley and Burns (1993), whereby authigenic minerals may lower $\delta^{18}\text{O}$ in pore waters by selectively removing $\delta^{18}\text{O}$.

A third possibility may be the presence of an active multi-phase thermal history where pulses of hydrothermal fluids are pushed through active faults creating varying temperatures during concretion growth that are not strictly depth dependent. Parnell *et al.*, (2001) applied fluid inclusion data to determine anomalously high temperatures for the Jeanne d'Arc Basin, suggesting episodic pulses of hot deep-seated basinal fluids. Finally, outer samples of concretion may be derived from other dissolution sites and the center and middle samples are locally related via aragonite to calcite transformation.

Much more closely-spaced sampling and comparison between different concretions is required to derive broadly applicable conclusions.

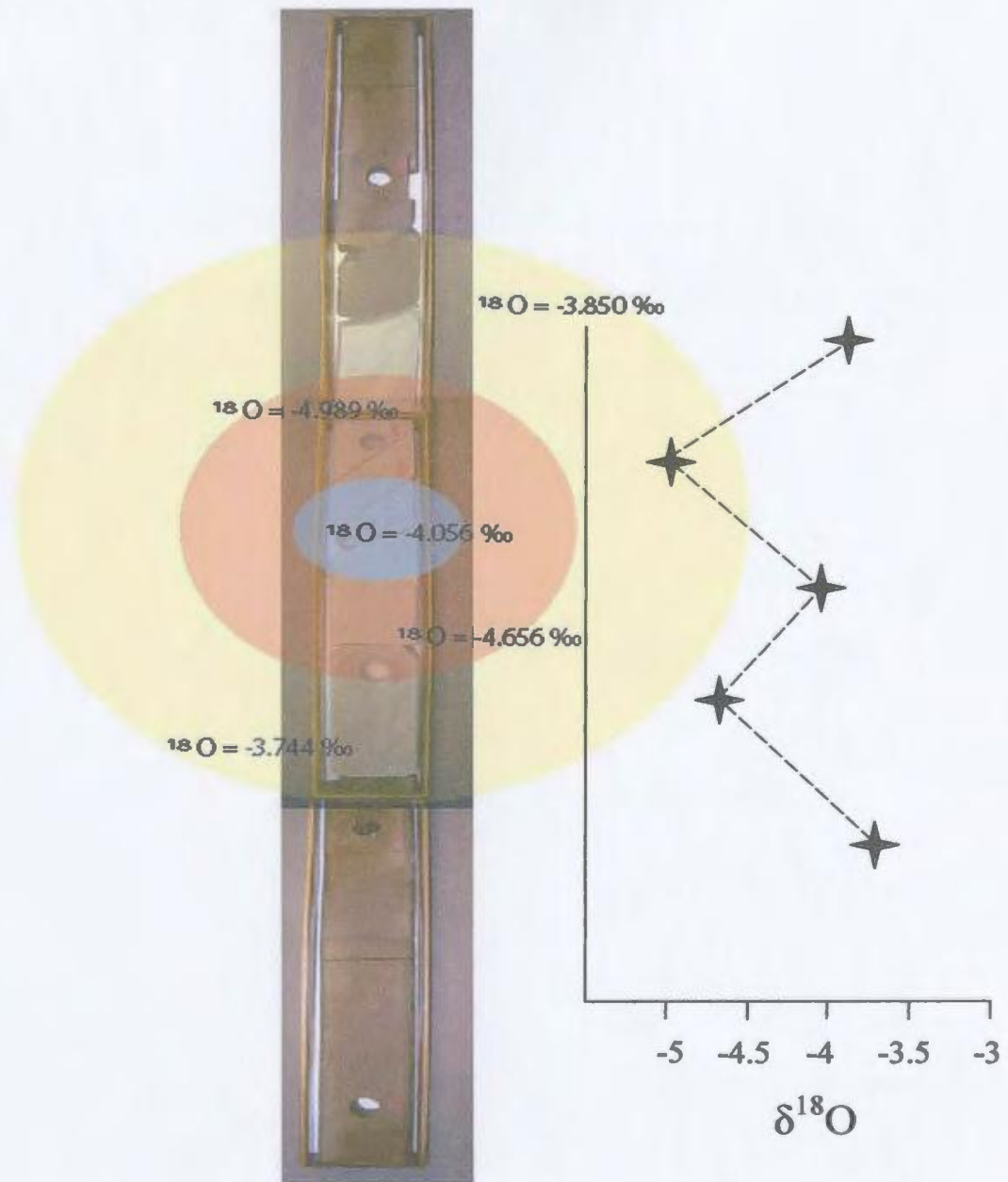


Figure 5.23: Distribution of oxygen isotopic results across a concretion demonstrating an initial increase of paleo-temperature from the center to the middle of the concretion followed by a decrease in paleo-temperature towards the outer edges of the concretion.

CHAPTER 6

INTEGRATION OF RESULTS

6.1 Introduction

The primary aim of this thesis is to develop the diagenetic history of the Ben Nevis Formation sandstone of the White Rose Field, to ultimately comprehend the formation process of calcite cemented concretions. Unravelling a 120 million year diagenetic history requires the amalgamation of several analytical methods to help elucidate the various processes involved. Core description (Chapter 3) and optical petrography (Chapter 4) together with carbon-oxygen isotopes studies (Chapter 5) all provide fundamental components to understanding the formation of authigenic cements in the Ben Nevis Formation. This chapter will provide a geological history of the Ben Nevis Formation at the White Rose Field, starting with the stratigraphy and depositional environment. This is followed by a discussion on the distribution and abundance of bioclastic debris, sedimentation rate, pore fluid composition, fluid transport and their effect on burial diagenesis.

6.2 Stratigraphy and Depositional Environment

The general transgressive stratigraphy of the Ben Nevis Formation provides the starting point for this diagenetic study. The Avalon Unconformity in juxtaposition with structural highs produced during the structural evolution of the White Rose Field created unconformable boundaries between the Ben Nevis Formation and underlying formations as old as the Rankin Formation (Dearin, 2006, pers.comm.). This provides potential fluid

pathways from underlying calcareous formations with higher hydrostatic pressure causing fluids to migrate up and laterally during progressive compaction.

The transgressive character of the Ben Nevis Formation gradually changes depositional environment from lower shoreface to the offshore transition, decreasing sand/shale ratio, bioclastic content, and rate of deposition, while increasing distance to shoreline and bioturbation to eventually become a seal rock in the form of the overlying Nautilus Shale. The capping of the Ben Nevis Formation with the Nautilus Shale will not drastically affect early diagenesis but it will confine pore fluids in the later stages of diagenesis when the shale has undergone complete water expulsion and becomes completely impermeable. These lithological changes will also affect pore composition, fluid flow and the diagenetic history of the upper Ben Nevis Formation.

Reduction in porosity and permeability as a result of decreasing sand/shale ratio diminished the volume of pore fluids in the upper portion of the Ben Nevis Formation slowing down the exchange of ions and the resulting dissolution/re-precipitation. Decreasing bioclastic content reduced the calcium carbonate source. As sedimentation rate slowed down sediments were exposed to a longer duration in the near surface diagenetic environment allowing time for dissolution of shells and formation of cements. When rate of sedimentation was fast enough, a higher volume of bioclastic debris may have been preserved, as is the case with the lower part of the Ben Nevis Formation. Decreasing sand/shale ratio will also reduce porosity and permeability impacting diagenesis.

Increasing the distance to shoreline reduces the affect of hydrologic drives providing meteoric fluids to an offshore setting. Increasing bioturbation may counteract the porosity/permeability reducing affects of increased mud content by increasing homogeneity and allowing more efficient pore fluid flow.

The original depositional environment is one of the most important aspects regarding the subsequent diagenetic history of a sedimentary package. The storm dominated depositional environment of the Ben Nevis Formation deposited a texturally and chemically mature, well sorted, very fine grained sandstone with abundant bioclastic debris. This sandstone has excellent original porosity and permeability, allowing pore fluids easy flow through, dissolving the shelly debris to the point of over-saturation and finally re-precipitating the calcium carbonate as authigenic cements.

6.3 Distribution and abundance of shells and cement

The distribution and abundance of shells accumulated during the deposition of the Ben Nevis Formation are crucial to the development of authigenic cements. Core description (Chapter 3) revealed important trends in cemented intervals directly related to shell volume and location, while isotopic evidence (Chapter 5) clearly defines aragonite shells as the source for calcite cementation.

Emphasis of core description focused on calcite cemented horizons providing categorization based on size, boundary types, distribution, cementation intensity, and nucleation sites. Concretions range from 2 to 316 cm in diameter, averaging approximately 56 cm. A high abundance of concave and convex concretion boundaries

reveal well defined spherical bodies. This would imply outward growth from a central site with no lateral continuity, rather than a distinct calcite cemented horizon that could drastically impact field production. Concave and convex boundaries cross-cut bedding, demonstrating the control of pore fluids during cement precipitation. In contrast to cross-cutting cementation, cement boundaries that coincide with sharp erosional contacts suggest that abrupt changes in original porosity and permeability can impact flow through of cementing pore fluids.

The distribution of concretions show subtle trends of decreasing concretion size moving up-section indicating a vertical aspect to evolving pore fluids. This may result from upward moving super-saturated pore fluids gradually dropping their calcium carbonate ions as they move higher in the formation (Figure 6.1). Fluid transfer will be occurring, as the formation is accumulating not only vertically, but also obliquely upward, sub-parallel to bedding. The absence of a nucleation site was most common in very well cemented concretions and may point to complete dissolution of the original bioclastic debris. This would suggest a slower cementation process in the upper Ben Nevis Formation whereas the preservation of nucleation sites may imply faster cementation as enveloping calcite cement occludes all porosity preventing further dissolution of bioclastic debris.

The lower portion of the Ben Nevis Formation has a higher volume of calcite cement but it is generally partially or poorly cemented compared to the Upper Ben Nevis, which contains less calcite cement but is primarily very well to well cemented. This trend can be understood by incorporating the transgressive development of the Ben Nevis Formation

along with general basin wide fluid flow characteristics. The effects of storm induced deposition and their resulting bioclastic lag deposits become less as water levels increase and the offshore environment gradually overlies the lower shoreface. The lower volume of shell debris will result in less nucleation sites for concretions to develop but a constant supply of calcium rich fluids from the lower Ben Nevis will result in very well to well cemented horizons above. A second mechanism for fluid flow into the upper Ben Nevis is laterally from the co-eval down-dip offshore transition zone where the aragonite factory is actively providing calcium rich fluids and the compaction of the overlying Nautilus Shale is directing fluids towards the shoreline. A combination of these two flow regimes is the cause for variable cementation throughout the Ben Nevis Formation (Figure 6.1).

Parrell (2005) compared the shell horizons of WR A-17 and WR B-07_4, revealing a slightly higher density in the WR B-07_4 well which she concluded to be directly related to lower relative sea-level and closer proximity to the shallow-water habitat of molluscs and serpulids. An overall increase in thickness of bioclastic intervals with stratigraphic depth corresponding to a higher volume of shell debris in the lower section was also noted by Parrell (2005). The thicker bioclastic horizons towards the base of the formation provide more abundant nucleation sites for cementation as well as potential calcium carbonate for up-section.

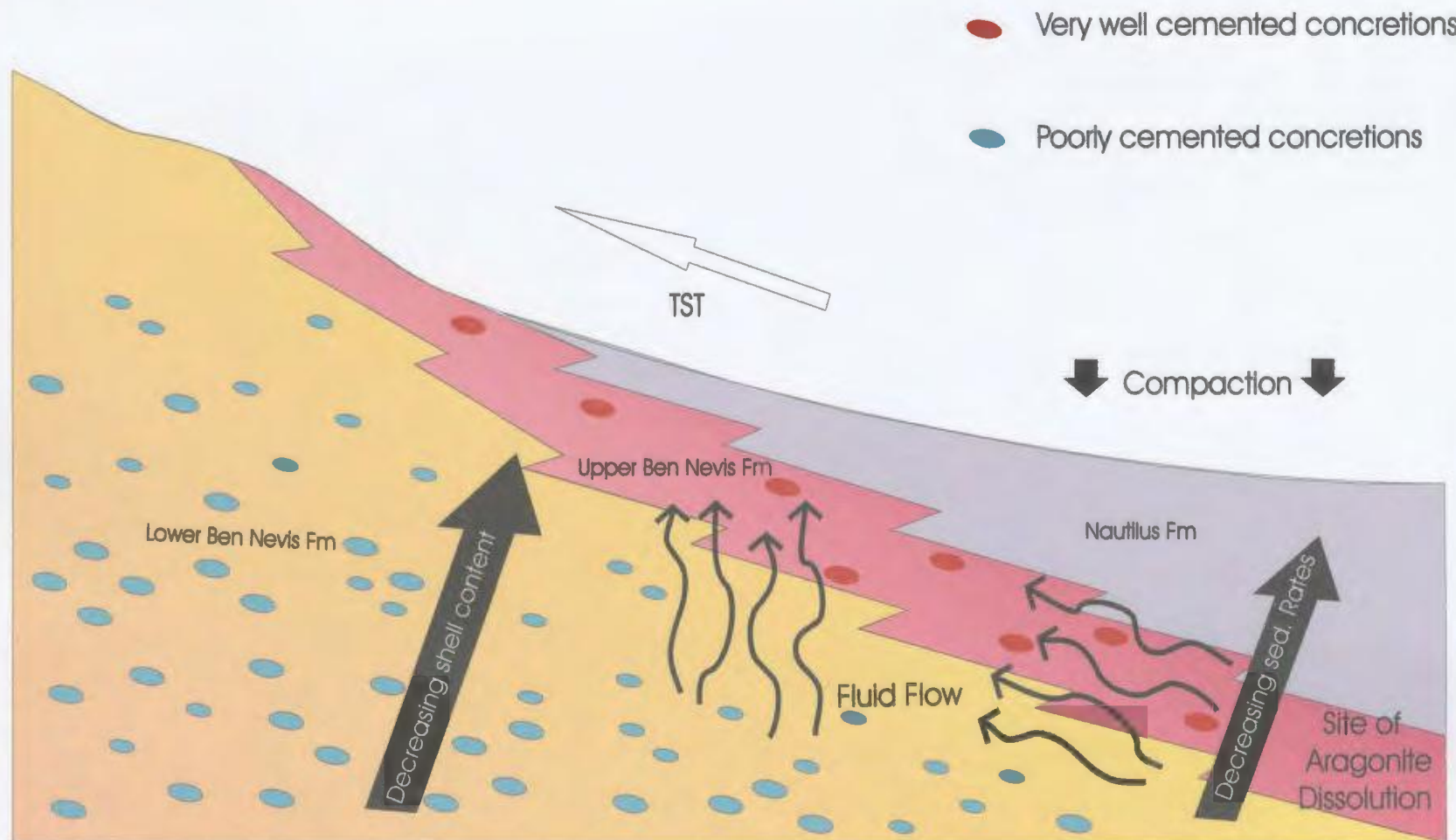


Figure 6.1: Schematic demonstrating two possible fluid flow mechanisms responsible for transfer of calcium carbonate enriched pore fluids. A) Vertical flow occurs after sufficient burial causes dissolution of shell debris in the lower Ben Nevis Fm. B) Oblique flow from site of strong aragonite dissolution within distal shoreface in the direction of the shoreline as a result of compaction of the Nautilus Shale.

6.4 Sedimentation Rate

In conjunction with the volume of calcareous debris, rate of sedimentation can also limit precipitation of authigenic calcite cement. Twenhofel (1942) believed deposition rates were the most important factor concerned with alteration of sediments after deposition. He demonstrated how micro and macro-organisms systematically feed on the nutrient matter in sediments, completely obliterating sedimentary structures. The slower the rate of deposition, the longer contact time of seawater and bottom dwelling organisms with the sea floor.

The Ben Nevis Formation represents deposition as a storm dominated lower shoreface environment characterized by rapidly deposited tempestites which were gradually transgressed by an offshore environment resulting in a decrease in sediment size, current energy and sedimentation rate. Scotchman (1991) suggested slow sedimentation rates correspond to precipitation of carbonate cement in the sulphate – reduction zone, whereas high sedimentation rates were more likely to result in carbonate cement produced in the methanogenesis and decarboxylation zones. Core description revealed the nature of concretions to vary stratigraphically. This would suggest the slow sedimentation rates and corresponding cementation in the sulphate-reduction zone at the upper part of the Ben Nevis Formation result in well to very well cemented concretions. As burial rates decrease, developing concretions have more time in the cementation zone creating more well cemented concretions in the upper Ben Nevis Formation. High sedimentation rates and cementation in the methanogenic zones produced partial to poorly cemented concretions.

Holmes and Martin (1977) estimated that storm dominated shelf sediments in the Texas Gulf Coast accumulate at a rate of 4 mm/year. For a 300m thick shelf sandstone unit such as the Ben Nevis Formation this could accumulate in as little as 75,000 years, a relatively short geological timeframe.

6.5 Early Burial Diagenesis

6.5.1 Role of Burial Rate

Sedimentation rate and creation of accommodation space are two of the most important factors affecting the rate of burial. Authigenic mineral cementation and porosity formation is determined by basin subsidence and exhumation rates, which control the residence time of certain stratigraphic horizons within important thermal windows (Reed *et al.*, 2005). Reduction in sedimentation rate modifies the burial history to allow a longer period of time in the near surface for the upper portion of the Ben Nevis Formation. This had a major impact on concretion formation as well as authigenic siderite precipitation.

Most studies of biogenic influence on concretions are based on deep, anoxic, organic rich shales, which are not applicable to early deposition of the Ben Nevis Formation but will be during subsequent burial when anoxic levels are reached. It is also important to note that in a thick, porous and permeable sandstone package such as the Ben Nevis Formation, these geochemical zones will be thick, clearly reaching greater sub-bottom depths than in impermeable shale packages. Concretionary horizons develop by localization of carbonate precipitation through anaerobic methane oxidation in

association with a decrease in the sedimentation rate or a complete hiatus in sedimentation (Raiswell, 1987).

Siderite cement is predominantly found in the upper Ben Nevis Formation with rare occurrences located in the lower Ben Nevis. This could be additional evidence in support of the role of lower burial rates and/or change in the composition of sediments. After thorough review of thin sections a relationship between siderite and the internal linings of shells was clearly established providing the association of siderite cementation with the presence of organic material. Wilkinson (1991) determined that early cementation phases control the precipitation of subsequent authigenic cements. While organic material was surely deposited in the lower Ben Nevis Formation along with the tempestites, the preservation of soft tissue within the oxic water bottom of a storm dominated shoreface would be insignificant. Isotope analyses did not isolate siderite-bearing samples; as a result, bulk analyses of siderite and calcite provide little help in isotopic distinction.

6.5.2 Pore Fluid Composition

Worden and Burley (2003) recognize pore-fluid chemistry as one of the controlling factors for diagenetic reactions. The geochemical classification of sedimentary environments based on oxygen and sulphur variables was originally introduced in 1981 by Berner. After dividing sedimentary environments into oxic and anoxic sub-environments, the anoxic environment is further subdivided into sulphidic and non-sulphidic and the final division is anoxic-nonsulfidic into post-oxic and methanic. One year later, Maynard (1982) expanded Berner's classification to include stable

isotopic composition of the carbonates and the degree of bioturbation. The degree of bioturbation is an excellent indicator of original pore chemical conditions, clearly distinguishing oxic from anoxic conditions.

The breakdown of organic matter during early diagenesis is the primary mechanism for change in pore-water chemistry (Van Der Weijden, 1988), but significant contributions to change also come from dissolution, recrystallization and neoformation of unstable mineral phases.

Hutcheon *et al.*, (1985) predicted meteoric flow through the Avalon/Ben Nevis Formations during and after the formation of the Mid Cretaceous Unconformity influencing the precipitation of authigenic cements. The Avalon Formation is nearly pinched out in the White Rose Field with the bulk of the reservoir consisting of the Ben Nevis Formation. Oxygen isotope analyses suggest that the authigenic calcite cement precipitated from marine pore waters in accordance with the range of 4 to -1 ‰ $\delta^{18}\text{O}$ reported by Wilkinson (1991). Volumetrically significant authigenic carbonate cement selectively removes $\delta^{18}\text{O}$ from pore fluids resulting in lower pore water oxygen values. Bjorlykke (1995) indicates outer shelf and turbidite depositional environments are less likely to be flushed by meteoric waters compared to fluvial and shallow marine sediments. This very logical statement suggests the Ben Nevis depositional environment may have been exposed to meteoric influence. However, the results of isotope analyses are not indicative of the influence of meteoric fluids, and this may be the result of low topographic gradients producing a weak hydrostatic head or possibly because the system is transgressive and it is constantly moving the meteoric system towards the shoreline.

Original pore fluid conditions found in the Ben Nevis Formation would be typical of Cretaceous marine waters, which shortly after burial and dissolution of aragonite shells become enriched to the point of super-saturation with calcium carbonate. Early sulphate reduction and would provide a source of iron and for both the precipitation of siderite as well as the conversion of non-ferroan calcite. At the same time bacterial degradation of organic tissue increased the pH of the fluids causing the dissolution of detrital quartz grains. Once consolidation of sediments has taken place, small fractures induced by tectonic forces or basin subsidence are filled by the calcium carbonate rich pore fluids. The final change in pore fluids determined in this study is during the late stage of diagenesis when dissolving fluids act on the ferroan calcite cement. This may be a by-product of hydrocarbon migration which may bring organic acids into the system.

6.5.3 Dissolution of aragonite shells

All three analytical methods combine to resolve an answer for the supply of calcium carbonate responsible for the precipitation of authigenic calcite cement. Petrography clearly demonstrated various stages of shell dissolution and in some cases complete dissolution of shells. Also the presence of thin, black, discontinuous residues of microcrystalline textured, curved shell fragments indicates the former presence of a substantial source of calcium carbonate.

Walderhaug and Bjorkum (1998) view an internal source as the only viable option typical of compacting sedimentary basins due to the vast fluid flux required to move considerable amounts of dissolved carbonate. The abundant amount of shells observed in

core also attest to the internal volume of calcium carbonate available for dissolution and precipitation. Aragonite dissolves more readily in settings of lower current energy (Wright, 2003), causing higher dissolution rates in what is now the upper Ben Nevis Formation. Advanced dissolution of shells combined with slower sedimentation rates resulted in well to very well cemented concretions. It is also important to note the abundance of moderately cemented horizons near the base of the Ben Nevis Formation where higher sedimentation rates may have reduced the effects of bioclast dissolution.

While core description and petrography identify the dissolution of shells as a possible source of authigenic calcite cement, it is the oxygen and in particular the carbon isotope analysis that narrows down the source. Considering the isotopic shift for Albian marine seawater (Veizer *et al.*, 1999), samples from the Ben Nevis Formation identify a relative depletion in $\delta^{13}\text{C}$ from original shell material to authigenic calcite cement that corresponds to values established by Sommer and Rye's (1978) aragonite-calcite fractionation equation. They concluded that unstable aragonite is the first to be dissolved in the burial process providing an excellent source of enriched $\delta^{13}\text{C}$ to then precipitate as authigenic calcite cement. This confirms aragonitic shells as the primary source of authigenic calcite cement in the Ben Nevis Formation.

6.6 Fluid Transport

When constructing a diagenetic history it is fundamental to consider the large scale fluid flow in the subsurface. To break it down in simplest terms, fluid flow can be sourced from above, below, laterally or through convection. Compaction, tectonic

compression, deep meteoric infiltration in areas of uplift, thermo-chemical convection, diffusion and thermal gradient variations are some of the processes responsible for pushing fluid through a sedimentary basin (Gluyas and Coleman, 1992; Aplin *et al* (1993); and Gaupp *et al.*, 1993).

Van Der Weijden (1988) defined diffusion, advection and reaction as three potential systems that transfer pore fluids. Diffusion is the random motion of ions trying to establish equilibrium, whereas advection is a unidirectional flow created by internal or external forces. A wide variety of reactions can occur in the subsurface that will consume and produce different chemicals leading to concentration changes. The Ben Nevis Formation at the White Rose Field can satisfy several different flow regimes but only one will have dominant control over the transportation of pore fluids.

Chapman (1987) uses characteristic stratigraphy and basin types to establish fluid flow patterns. A transgressive sequence will have dominant flow downwards through the mudstones to the permeable sands below. Rift basins provide much of the pore fluid from compaction of the thick unconformity-disconformity sequence overlying the rift sequence (Chapman, 1987). The Ben Nevis Formation satisfies the conditions above along with an impermeable marlstone below suggesting downwards fluid flow as a prime candidate for pushing fluid through the system.

Significant amounts of dissolved calcite can be transported by convection (Wood and hewett, 1984) generally in special settings with strongly sloping isotherms, such as adjacent to salt domes (Bjorlykke *et al.*, 1988). Bjorlykke *et al.*, (1988) suggests the requirement of a 300 m thick formation with a permeability of 1 Darcy in order for

thermal convection to take place. The Ben Nevis Formation in the White Rose Field is a rare exception of such a thick homogeneous sandstone package adjacent to salt structures with high paleo-permeabilities, which may satisfy the conditions for Rayleigh Convection Flow. This may be a major controlling factor of diagenesis and the production of calcite cemented concretions in a “closed system”, directly applicable to the White Rose Field supporting the systematic tendency for calcite cement to be concentrated near the base of the sandstone.

When considering fluid pathways it might be of interest to take a look at the migration of petroleum fluids. When petroleum enters a system it flows to the area of least resistance possibly following conduits that were previously used for cementing pore fluids. Brown *et al.*, (1989) and Hesse and Abid (1998) proposed that hydrocarbon migration occurred very late in the diagenetic sequence for the Jeanne d’Arc Basin. Williamson *et al.*, (1993) used sedimentation, compaction, seal development and thermal history to develop a model suggesting the Hibernia Field became oil charged at 40 – 60 m.y. This timeframe for oil migration could be similar for the Ben Nevis Formation at the White Rose Field or could be slightly earlier as this area had time for the build-up of an extensive gas cap.

Abid (1996) identified the presence of all Jeanne d’Arc oil and gas fields to correspond to transform faulting. Bjorlykke (1995) suggests flow can develop locally along fault planes. Transform faults may be responsible for allowing pulses of high temperature fluids into the system, precipitating authigenic calcite cement. Early emplacement of calcite cement in sandstones of rift basins may take place from hot

convected waters driven by the high geothermal gradients related to ocean opening (Giroir, *et al.*, 1989). Based on isotope results from this study calcite cements were not precipitated by high temperature fluids. Cements precipitated during shallow burial long before migration of hydrocarbons.

During early diagenesis the dominant fluid transport mechanism moving fluids through the Ben Nevis Formation is caused by burial compaction and the increasing hydrostatic head at deeper burial depths which push fluids up to areas of less resistance or laterally along permeable bedding. This obliquely upward fluid flow into nearly coeval sediments of the laterally adjacent shoreface occurs in part during transgression, placing the offshore transition setting of extensive dissolution above the shoreface section at the base of the Ben Nevis Formation. The distribution of shells and concretions, as noted previously, suggest dominant flow from the base of the Ben Nevis Formation upwards and laterally from adjacent down-dip offshore transition.

6.7 Formation of concretions

There are several schools of thought regarding the development of calcite concretions within siliciclastic sequences. Various authors ascribe to the theory that concretion development is directly related to the original distribution of biogenic carbonate (*e.g.* Hudson and Andrews, 1987; Kantorowicz *et al.*, 1987; Burns *et al.*, 1988; and Walderhaug and Bjorkum, 1998). Kantorowicz *et al.*, (1987) studied the development of laterally continuous cemented horizons in two geologically distinct depositional environments. The bioclastic-rich storm deposited Bridport Sands, have concretions

directly related to the geometry of the storm beds, while concretion formation in the Viking Group sandstones was controlled by rate of burial (Kantorowicz *et al.*, 1987). Both settings have different origins but demonstrate their distribution is related to the episodic nature of deposition in the shelf environment. It was the combination of these processes occurring “within a closed system” to produce the nodular forms found in the Ben Nevis Formation. Walderhaug and Bjorkum (1998) also note concretion formation from local diffusional redistribution of original biogenic carbonate, which is controlled by the distribution of shell debris.

Others consider sedimentation rate to be the controlling factor regarding concretion formation, Didyk *et al.*, 1978; Kantorowicz, *et al.*, 1987; Raiswell, 1987; Wilkinson 1991 and Reed *et al.*, 2005. Wilkinson (1991) associated high cement concentrations with sedimentary standstills. Sedimentation rate influences preservation of organic matter thereby controlling the formation of authigenic calcite cement (Didyk, *et al.*, 1978).

Heald and Renton (1966) conducted an experimental study of sandstone cementation suggesting the greater influx of cement into the more permeable coarse sands resulted in faster cementation rates relative to the fine grained sands but where influx volumes were the same, fine grained sandstones were cemented much more rapidly because of the greater surface area to precipitate on. On the other hand, Wilkinson (1991) concluded that grain size distributions for both concretionary and non-concretionary intervals rule out permeability as a controlling mechanism for the location of concretionary horizons. Permeability is reduced in the upper Ben Nevis Formation but

cementation is enhanced, so concretion distribution and cementation intensity in WR F-04 and WR B-07_4 appear to be consistent with Wilkinson (1991). Wilkinson (1991) also advocates the distribution of early marine cements as nucleation sites for more extensive cementation. The early non-ferroan calcite cement in the Ben Nevis Formation may act as nucleation sites for the more dominant ferroan calcite cement.

A more detailed review of the mechanisms of concretion formation was put forward by Walderhaug and Bjorkum (1998) and may be directly applicable to the concretions of the Ben Nevis Formation. Biogenic carbonate accumulations gradually dissolve, increasing the calcium carbonate ions in pore fluids until they become supersaturated and begin nucleation. The calcite cement nucleus will lower the zone of dissolved calcite within its range of influence creating a diffusion gradient towards the concretion. This process will continue until all available pore space is occluded or the biogenic source is expended.

The nodularity of the concretionary horizons in the Ben Nevis Formation is evident in core as demonstrated by the predominance of rounded contacts as well as by Formation Micro-Imaging conducted by Husky which identified more than 90 percent of the concretions seen in the core to be sub-spherical lenses in nature (www.huskyenergy.ca/whiterose/-development/downloads/Vol2_Geology.pdf). Shell horizons in the Ben Nevis Formation are highest in the lower portion of the Ben Nevis Formation and diminish slightly up-section (Parrell, 2005). Not every shell horizon is the nucleus of a concretion. This would imply that dissolution is not pervasive and some areas do not receive pore fluids super-saturated with calcium carbonate.

6.8 Paragenetic Sequence

The early stages of diagenesis were the dominate forces modifying the Ben Nevis Formation in the White Rose Field. The evolution of pore fluids within the first 390m of burial produced the groundwork for the entire diagenetic history. The paragenetic sequence identified in this study consisted of four episodes of precipitation of authigenic cement and four dissolution events of both detrital grains and authigenic cement. Petrographic methods and isotope analyses provide the most useful information regarding the timing of various cementation and dissolution phases.

6.8.1 Quartz Overgrowths

Although quartz overgrowths found on detrital quartz grains of the Ben Nevis Formation were identified as forming during a preceding depositional cycle, it is important to note in the paragenetic sequence as they can be a dominant factor in diagenesis of clastic sediments. Cathodoluminescence revealed two distinct phases of quartz overgrowths which were rounded to sub-round with truncated boundaries illustrating their recycled character.

6.8.2 Dissolution of Aragonite Shells

The earliest diagenetic event for this system was the dissolution of the chemically unstable aragonite shells. The combined effort of petrography and geochemistry facilitated the timing of aragonite shell dissolution within the Ben Nevis Formation. Petrography provided excellent examples of varying stages of shell dissolution within the

same thin-section, including complete dissolution of shells resulting in moldic porosity, as well as thin, discontinuous remnants of a micro-crystalline textured curved shell fragments. These aragonite shells are found encased in early calcite cement implying con-current phases. As aragonite shells dissolve to the point of over saturating calcium carbonate ions in the pore fluid, calcite cement will precipitate out. Then as calcite cement occludes all porosity, varying stages of shell dissolution will be captured before the process is completed.

Enrichment of carbon isotopes from original shells to authigenic calcite cement followed the aragonite enrichment equation (Sommer and Rye, 1978), suggesting that the aragonite shells may be a possible primary source for the authigenic calcite cement.

6.8.3 Dissolution of Detrital Feldspar Grains

The chemical instability of feldspar grains allows relatively easy dissolution during early stages of burial. Their absence in uncemented samples and their partially dissolved presence in cemented samples indicate a very limited exposure to dissolving pore fluids when protected by authigenic cements. This incomplete dissolution event also provides support for the early timing of calcite cementation.

6.8.4 Precipitation of Siderite Cement

Siderite cement is located primarily in the upper portion of the Ben Nevis Formation associated with the slower burial rates found in the offshore depositional environment. Petrography revealed a connection between the internal mold of shells and

siderite cement, suggesting a relationship of organic material with the precipitation of authigenic siderite cement. Core description also exposed the relationship of siderite with the organic linings of trace fossils such as *Ophiomorpha sp.*, which supports the siderite-organic affiliation. The timing of siderite cementation would be at relatively shallow burial before the organic matter would be completely exhausted by bacterial degradation.

6.8.5 Precipitation of Non-Ferroan Calcite Cement

Non-ferroan calcite cement precipitates prior to the dominant ferroan calcite cement based on petrographic observations. As discussed below the ferroan calcite cement is during very early diagenesis proclaiming the non-ferroan calcite as the earliest authigenic calcite cement. Bioclasts act as nucleation sites for the non-ferroan calcite cement which demonstrate distinct evolution into ferroan calcite cement as it precipitates into open pore space. The contact between the two calcite cements is generally irregular suggesting a hiatus in precipitation as pore fluids become enriched in iron.

6.8.6 Dissolution of Detrital Quartz Grains

Petrography clearly reveals the dissolved texture of detrital quartz grains. Free-floating grains, pitted and embayed grain boundaries, as well as the presence of small (<20 μ m) islets of quartz suggest dissolution of the detrital quartz grains. The pore fluids responsible for dissolution of quartz grains also precipitate calcite cement which completely occludes porosity preserving the corroded texture. Increase in biological activity increases pH, which will begin to dissolve quartz when pH reaches nine. The

contemporaneous dissolution of quartz and precipitation of calcite cement places this dissolution phase in the eogenesis segment of the paragenetic sequence.

6.8.7 Precipitation of Ferroan Calcite Cement

Several lines of evidence were observed through petrography to undoubtedly provide a very early timeframe for the precipitation of non-ferroan calcite cement. Determining paleo-temperatures of authigenic calcite cement through the use of oxygen isotopes also indicates very shallow burial (150 to 260 m) during the precipitation of cement.

Preservation of internal volumes of 30 to 40 % in the Ben Nevis Formation concretions represents very early cementation shortly after burial and before the commencement of compaction (Millikin, 1998). Raiswell (1987) has conclusive evidence supporting early diagenetic origin of concretions in uncompacted sediment, such as presence of uncrushed skeletal debris within the concretions and the compaction of host sediment laminae around the concretions. Very delicate spines of bivalve shells were observed in thin section within concretions of the Ben Nevis Formation. Partial dissolution of feldspar grains, suggests only a few million years burial before precipitation of calcite cement. All these factors likely suggest an early calcite cementation.

6.8.8 Calcite Veins

Calcite veins are found cross-cutting calcite cemented concretions and are generally vertical in nature. This cross-cutting relationship will place the veining slightly

after the calcite cementation in the early stages of diagenesis with similar pore fluid characteristics but with enough burial time to provide some consolidation to the sediment to allow fracturing.

6.8.9 Dissolution of Ferroan Calcite Cement

A late stage dissolution event occurred affecting the ferroan calcite cement. Rare occurrences of corrosion of small ferroan calcite crystals were observed in thin-section. These corroded crystal boundaries demonstrate a late stage of pore fluid modification, possibly related to organic acids of hydrocarbon generation and migration into the Ben Nevis Formation. This dissolution event is restricted to partially or poorly cemented intervals, enhancing the porosity and permeability of the reservoir.

6.9 Impact on Reservoir Quality

Estimated recoverable petroleum reserves for Jeanne d'Arc Basin range from 7.1 Bbbl (GSC, Proctor et al, 1984) to 12.3 Bbbl (Petroleum Directorate of NF and Lab, Sheppard and Hawkins, 1983). With only approximately 25% of suggested reserves discovered, this basin still has enormous exploration potential. A key component to understanding a maturing basin is the predictive distribution of diagenetic alteration during the existence of the reservoir.

It is clear that calcite cemented concretions are the dominant authigenic cement found in the Ben Nevis Formation at the White Rose Field and they are not a laterally continuous phenomena. Concretionary cemented intervals did not prevent burial compaction of uncemented intervals, implying that the latter are not isolated by sub-

vertical cemented columns. The spherical nature of the concretions allowed a complete oil and gas charge of the Ben Nevis Formation at the White Rose Field. While there is no compartmentalization of the Ben Nevis Formation, the volume of calcite cement will reduce the amount of recoverable oil and gas.

Future exploration should bear in mind the higher density of concretionary cemented intervals are located at the base of the formation but cementation intensity increases up-section. It is also important to note that the ideal reservoir conditions exist within the distal shoreface, farther from the source of bioclasts, but not within the overlying offshore transition, which is too fine grained, clay rich and contains the very tightly cemented concretions. The distribution of concretions will reflect size and shape of concentrations of bioclastic debris deposited during discrete storm events.

Future work on the Ben Nevis Formation in the White Rose Field requires a better understanding and location of the paleo-shoreline during the deposition of shoreface sands. This may assist in establishing a trend for the less cemented distal shoreface, as well as provide useful information on the thick bioclastic sandstone located at the base of the Ben Nevis in the WR B-07_4, WR N-30 and WR E-18 wells. While north-south wells create a good picture of the structure of the basin, additional wells to the east and west of the south pool would be invaluable to determining the basins complete evolution.

6.10 Future Research

Machel (2005) describes a six step process to investigate diagenesis, summarized below:

- 1) Facies Analysis
- 2) Petrographic Analysis
- 3) Geochemical Analysis
- 4) Burial History and Paleohydrology
- 5) Integration with existing data
- 6) Modeling

While most steps were completed in this study, a basin wide model of cementation may shed some new light on how halokinesis, petroleum migration and maturation, and tectonic activity affect this complex subject.

As with any paragenetic sequence the actual timing of events is much more important than the relative timing of events. Proper analysis of individual cements rather than bulk sampling would be beneficial to this type of study (i.e. Al-Aasm and Azmy, 1996; and Azmy *et al.*, 2001). Fluid inclusions analysis is another method that could be utilized for the relative timing of particular cements as well as for confirmation of $\delta^{18}\text{O}$ values (i.e. Azmy *et al.*, 2001). Magnetic orientation dating or zircon dating can be very important to precisely give a timing of a certain authigenic precipitant, around which the relative timing of all other events can be placed.

Laser ablation across concretions may be useful in determining the transition from non-ferroan to ferroan calcite cement, providing information on the source of iron ions. Actual tests on the destabilization of aragonite such as varying pressure, temperature and formation water composition to verify the enrichment of isotopic carbon in the aragonite to calcite transition.

When considering fluid pathways it might be of interest to take a look at the migration of petroleum fluids. When petroleum enters a system it flows to the area of least resistance possibly following conduits that were previously used for cementing pore

fluids. Abid (1996) identified the presence of all Jeanne d'Arc oil and gas fields to correspond to transform faulting. Bjorlykke (1995) suggests flow can develop locally along fault planes. Are these transform faults responsible for allowing fluid pulses into the system, precipitating authigenic calcite cement? Need to look at locations where the Ben Nevis Formation is absent of petroleum to see if it is also absent of authigenic cement.

CHAPTER 7

CONCLUSIONS

7.1 Conclusions

With forty years of exploration and development history within the Jeanne d'Arc Basin, it is moving into the mature stage and as a result it will require the application of the latest technologies and analyses to find the remaining oil and gas fields. Hopefully this thesis provides some aid in unlocking the secrets of its diagenetic evolution.

Important conclusions revealed in this study are summarized below:

- ✓ The depositional environment and sediment composition are the controlling factors influencing the formation of authigenic cements. Slow sedimentation rates and high biogenic contents significantly contribute to the precipitation of authigenic cements.
- ✓ Aragonite shells may be the primary source responsible for the precipitation of authigenic calcite cement in the Ben Nevis Formation, as defined by carbon isotope and petrographic analyses.
- ✓ Siderite precipitation was likely influenced by an organic substrate, which contributed to the reduction of permeability in the upper portion of the Ben Nevis Formation.

- ✓ Precipitation of siderite may increase with a decrease in the rate of sedimentation.
- ✓ Siderite and non-ferroan calcite cement were the earliest authigenic cements followed by ferroan calcite cement. Early diagenesis was the dominant force acting on the burial evolution of the Ben Nevis Formation. Several lines of evidence support this including preservation of delicate shell ornaments and feldspar grains, high minus cement porosity, and oxygen isotopes indicate cementation below 390m burial.
- ✓ Calcite cemented concretions are not barriers to horizontal or vertical flow.
- ✓ Quartz dissolution can occur at low temperatures when facilitated by microbial activity, which increases pH.
- ✓ Marine fluids are the primary basin fluids responsible for diagenesis in the Ben Nevis Formation. There was little or no meteoric influence during the burial history of the Ben Nevis Formation.
- ✓ Compaction driven obliquely upward fluid flow was the dominant mechanism providing fluid flow through Ben Nevis Formation at the White Rose Field.

- ✓ The lower portion of the Ben Nevis Formation contains more calcite cement and bioclastic debris but the upper section has more intensely cemented concretions.

REFERENCES

Abid, I.A.

1988: Mineral diagenesis and porosity evolution in the Hibernia oil field, Jurassic-Cretaceous Jeanne d'Arc rift graben, eastern Grand Banks of Newfoundland, Canada, Master's Thesis, McGill University, Montreal, Quebec, 280 pages.

Abid, I.A.

1996: Mixed Layer illite/smectite diagenesis in the rift and post rift sediments of the Jeanne d'Arc Basin, offshore Newfoundland, Canada, Phd Thesis, Memorial University of Newfoundland, 243 p.

Abid, I. A., Hesse, R., and Harper, J. D.

2004: Variations in mixed-layer illite/smectite diagenesis in the rift and post-rift sediments of the Jeanne d'Arc Basin, Grand Banks offshore Newfoundland, Canada, Canadian Journal of Earth Science, vol. 41, pp. 401-429.

Aigner, T.

1985: Storm Depositional Systems, Dynamic Stratigraphy in Modern and Ancient Shallow-Marine Sequences, Gerald M. Friedman, Horst J. Neugebauer and Adolf Seilacher, eds., Springer-Verlag, 174 p.

Al-Aasm, I.S., Taylor, B.E. and South, B.

1990: Stable isotope analysis of multiple carbonate samples using selective acid extraction, Chemical Geology – Isotope Geoscience Section, vol. 80, pp. 119-125.

Al-Aasm, I.S. and Azmy, F.

1996: Diagenesis and evolution of microporosity of Middle-Upper Devonian Kee Scarp reefs, Norman Wells, N.W.T., Canada: petrologic and chemical evidence. AAPG Bull., vol. 80, p. 82-100.

Amoco Canada Petroleum and Imperial Oil

1973: Regional geology of the Grand Banks: Bulletin of Canadian Petroleum Geology, vol. 21, pp. 479–503.

Anderson, T.F. and Arthur, M.A.

1983: Stable Isotopes of oxygen and carbon and their application to sedimentologic and paleoenvironmental problems in Stable Isotopes in Sedimentary Geology, SEPM Short Course No.10, Dallas, Ch. 1, pp. 1-151.

Aplin, A. C., Robinson, A. G., Warren, E. A., and Grant, S. M.

1993: Mechanisms of Quartz Cementation in North Sea Reservoir Sandstones: Constraints from Fluid Compositions in Diagenesis and Basin Development, AAPG Studies in Geology, # 36, Ch. 2.

Azmy, K., Veizer, J., Misi, A., de Oliveira, T.F., Sanches, A.L., and Dardenne, M.A.
2001: Dolomitization and isotope stratigraphy of the Vazante Formation, São Francisco Basin, Brazil, *Precambrian Research*, vol. 112, pp. 303-329.

Barker, C.A. and Kopp, O.C. (eds.)

1991: Luminescence microscopy and spectroscopy: qualitative and quantitative applications: SEPM Short Course Notes #25, 195 p.

Baron, E.J. and Washington, W.M.

1982: Cretaceous Climate: A Comparison of Atmospheric Simulations with the Geologic Record, *Palaeogeography, Palaeoclimatology, palaeoecology*, vol. 40, pp. 103-133.

Bathurst, R.G.C.

1975: Carbonate cements and their diagenesis, 2nd edition, Elsevier, Amsterdam, 658 p.

Berner, R.A.,

1980: A rate model for organic decomposition during bacterial sulphate reduction in marine sediments, *Colloques Internationaux du Centre National de la Recherche Scientifique*, no.293, pp.35-44.

Berner, R.A.,

1981: A new geochemical classification of sedimentary environments, *American Association of Petroleum Geologists Bulletin*, vol. 51, pp. 359-365.

Beard, D.C and Weyl, P.K.

1973: Influence of texture on porosity and permeability of unconsolidated sand, *The American Association of Petroleum Geologists Bulletin*, vol.57, no. 2, pp. 349-369.

Bjorkum, P.A. and Walderhaug, O.

1990: Geometrical arrangement of calcite cementation within shallow marine sandstones. *Earth Science Review*, vol. 29, pp. 145-161.

Bjorlykke, K.

1988: Sandstone Diagenesis in Relation to Preservation, Destruction and Creation of Porosity in Development, *in* Chilingarian, G. V., and Wolf, K. H., eds., *Sedimentology, Diagenesis I*, vol. 41, pp. 555-588.

Bjorlykke, K.

1995: Pore-water flow and mass transfer of solids in solution in sedimentary basins, *in* Parker, A., and Sellwood, B.W., eds., *Quantitative Diagenesis: Recent Developments and Applications to Reservoir Geology*, NATO ASI Series C: Mathematical and Physical Sciences – vol.453, pp. 189-221.

Bjorlykke, K., and Egeberg, P.K.

1993: Quartz Cementation in Sedimentary Basins, American Association of Petroleum Geologists Bulletin, vol. 77, no. 9, pp. 1538-1548.

Bjorlykke, K., Mo, A. and Palm, E.

1988: Modelling of thermal convection in sedimentary basins and its relevance to diagenetic reactions, Marine and Petroleum Geology, vol. 5, no. 4, pp. 338-351.

Bloch, J.

1990: Stable isotopic composition of authigenic carbonates from the Albian Harmon Member (Peace River Formation): evidence of early diagenetic processes: Bulletin of Canadian Petroleum Geology, vol. 38, pp. 39-52.

Bornhold, B.D. and Milliman, J.D.

1973: Generic and environmental control of carbonate mineralogy in serpulid (polychaete) tubes, Journal of Geology, vol. 81, no. 3, pp. 363-373.

Brehm, U., Gorbushina, A., and Mottershead, D.

2005: The role of microorganisms and biofilms in the breakdown and dissolution of quartz and glass, Palaeogeography, Palaeoclimatology, Palaeoecology, vol. 219, pp. 117-129.

Bruce, C.H.

1984: Smectite dehydration and its relation to structural development and hydrocarbon accumulation in Northern Gulf of Mexico Basin, American Association of Petroleum Geologists Bulletin, vol. 68, pp. 673-683.

Brown, D.M., McAlpine, K.D and Yole, R>W.

1989: Sedimentology and sandstone diagenesis of the Hibernia Formation in Hibernia oil field, Grand banks of Newfoundland, American Association of Petroleum Geologists Bulletin, vol. 73, no. 5, pp. 557-575.

Burns, S.J., Baker, P.A. and Showers, W.J.

1988: The factors controlling the formation and chemistry of dolomite in organic-rich sediments; Miocene Drakes Bay Formation, California, Special Publication – Society of Economic Palaeontologists and Mineralogists, vol. 43, pp. 41-52.

Burley, S.D., Kantorowicz, J.D. and Waugh, B.

1985: Clastic Diagenesis, Brenchley and Williams, eds., pp. 189-220.

Carpenter, S.R., Erickson, J.M., Lohmann, K.C., and Owen, M.R.

1988: Diagenesis of the fossiliferous concretions from the Upper Cretaceous Fox Hills Formation, North Dakota: Journal of Sedimentary Petrology, vol. 58, pp. 706-723.

Chapman, R.E.

1987: Fluid flow in sedimentary basins: a geologist's perspective, *in* Goff, J.C. and Williams, B.P.J., eds., 1987, Fluid Flow in Sedimentary Basins and Aquifers, Geological Society Special Publication no. 34, pp. 3-18.

Clarke, F.W.

1908: The Data of Geochemistry, U.S. Geological Survey, Bulletin 330. (The fifth edition in 1924 is U.S.G.S Bull. 770.)

Clark, I.D. and Fritz, P.

1997: Environmental Isotopes in Hydrogeology, University of Ottawa, Ottawa-Carleton Geoscience Centre, Ottawa, ON, Canada, 328 p.

Clayton, R.N., Friedman, I., Graf, D.L., Mayeda, T.K., Meents, W.F., and Shimp, N.F.

1966: The origin of saline formation waters: 1. Isotopic composition, *Journal of Geophysical Research*, vol. 71, pp. 3869-3882.

C-NLOPB Website

2004: <http://www.cnopb.nfnet.com>

2006: <http://www.cnlopb.nl.ca/>

Correia, A., Jones, F.W., and Fricker, A.

1990: Terrestrial heat flow density estimates for the Jeanne d'Arc Basin offshore eastern Canada, *Geophysics*, vol. 59, pp. 1625-1633.

Correns, C.W.

1969: The discovery of the chemical elements. The history of geochemistry. Definitions of geochemistry, *in* Wedepohl, K.H., ed., *Handbook of Geochemistry*, vol. 1, 1-11. Springer-Verlag, Berlin, 442 p.

Craig, H.

1957: Isotopic standards for carbon and oxygen and correction factors for mass-spectrometer analysis of carbon dioxide, *Geochimica et Cosmochimica Acta*, vol. 12, no. 1-2, pp. 133-149.

Craig, H.

1961: The measurements of oxygen isotope paleotemperatures, *in* Tongiorgi, E., ed., *Stable Isotopes in Oceanographic Studies and Paleotemperatures:Spoleto 1965*, CNR, Pisa, pp. 1-24.

Curtis, C.D., and Coleman, M.L.

1986: Controls on the Precipitation of Early Diagenetic Calcite, Dolomite and Siderite Concretions in Complex Depositional Sequences, Special Publication, The Society of Economic Paleontologists and Mineralogists, vol. 38, pp. 23-33.

- Deptuck, M.E., MacRae, R.A., Shimeld, J.W., Williams, G.L. and Fensome, R.A.**
 2003: Revised Upper Cretaceous and lower Paleogene lithostratigraphy and depositional history of the Jeanne d'Arc Basin, offshore Newfoundland, Canada, AAPG, vol. 87; no. 9; pp. 1459-1483.
- DeSilva, N.R.**
 1987: Structural history and hydrocarbon potential of the Cross-basin fault trend, CNOPB Report GP-CNOPB-87-2, 12 p, 4 maps.
- Dickson, J. A. D.**
 1965: A modified staining technique for carbonates in thin section, *Nature*, vol. 205, pp. 587.
- Driscoll, N. W., Hogg, J. R., Christie-Blick, N., and Karner, G.D.**
 1995: Extensional tectonics in the Jeanne d'Arc Basin, offshore Newfoundland: implications for the timing of break-up between Grand Banks and Iberia, *in* Scrutton, R.A., Stoker, M.S., Shimmield, G.B. and Tudhope, A.W., eds., *The Tectonics, Sedimentation and Palaeoceanography of the North Atlantic Region*, Geological Society Special Publication No. 90, pp. 1-28.
- Didyk, B.M., Simoneit, B.R.T., Brassel, S.C., and Eglinton, G.**
 1978: Organic geochemical indicators of palaeoenvironmental conditions of sedimentation, *Nature*, vol. 272, pp. 216-222.
- Edwards, A.**
 1990: The western margin of the Jeanne d'Arc Basin, offshore Newfoundland (eastern Canada), *in* Pinet, B., and Bois, C., eds., *The potential of deep seismic profiling for hydrocarbon exploration*: Paris, Edition Technip, pp. 161-173.
- Ellwood, B.B., Chrzanowski, T.H., Hrouda, F., Long, G.J., Buhl, M.L.**
 1988: Siderite formation in anoxic deep-sea sediments; a synergetic bacterially controlled process with important implications in paleomagnetism, *Geology (Boulder)*, vol.16, no.11, pp. 980-982.
- Enachescu, M. E.**
 1987: Tectonic and structural framework of the northeast Newfoundland continental margin, *in* C. Beaumont and A.J. Tankard, eds., *Sedimentary Basins and Basin Forming Mechanisms*: Canadian Society of Petroleum Geologist Memoir, vol. 12, pp. 117-146.
- Ervine, B.**
 1984: A synthesis of hydrocarbon maturation data for the East Newfoundland Basin, Open-File Report – Geological Survey of Canada, Report: 1178, 105 p.

Evamy, B.D.

1969: The precipitational environment and correlation of some calcite cements deduced from artificial staining: *Journal of Sedimentary Petrology*, vol. 39, pp. 787-821.

Fairchild, I., Hendry, G., Quest, M., and Tucker, M.

1988: *Chemical Analysis of Sedimentary Rocks in Techniques in Sedimentology*, Tucker, M., ed.

Falcon.tamucc.edu/.../ Montereydiagenesis.html (January, 2006)

Faure, G.

1991: *Principles and Applications for Geochemistry*, A comprehensive textbook for students, Second Edition, Prentice Hall, NJ.

Faure, G., and Mensing, T.M.

2005: *Isotopes – Principles and Applications*, 3rd Edition, John Wiley and Sons Inc., 897 p.

Ferry, M.

2005: An evaluation of the sedimentology and the influence of grain size and facies on permeability for the White Rose A-17 cored interval, White Rose Oilfield, offshore eastern Newfoundland, Master's Thesis, Earth Science Department, Memorial University of Newfoundland, 227 p.

Friedman, G.M., Ali, S.A., and Krinsley, D.H.

1976: Dissolution of quartz accompanying carbonate precipitation and cementation in reefs: Examples from the Red Sea, *Journal of Sedimentary Petrology*, vol. 46, no. 4, pp. 970-973.

Froelich, P.N., Klinkhammer, G.P., Bender, M.L., Luedtke, N., Heath, G.R., Cullen, D., Dauphin, P., Hammond, D., Hartman, B. and Maynard, V.

1979: Early oxidation of organic matter in pelagic sediments on the eastern equatorial Atlantic; suboxic diagenesis, *Geochimica et Cosmochimica Acta*, vol. 43, no. 7, pp. 1075-1090.

Galloway, W. E.

1984: *Hydrologic Regimes of Sandstone Diagenesis in Clastic Diagenesis*, McDonald, D. A., and Surdam, R. C., ed., American Association of Petroleum Geologists Memoir 37.

Gaupp, R., Matter, A., Platt, J., Ramseyer, K. and Walzebuck, J.

1993: Diagenesis and fluid flow in deeply buried Permian (Rotliegende) gas reservoirs, Northwest Germany, *Bulletin of American Association of Petroleum Geology*, vol. 77, no. 7, pp. 1111-1128.

Gautier, D.L., and Claypool, G.

1984: Interpretation of methanic diagenesis in ancient environments by analogy with processes in modern diagenetic environments, in McDonald, D.A. and Surdam, R.C., eds., *Clastic Diagenesis: American Association of Petroleum Geologists Memoir No. 37*, pp. 111-123.

Giroir, G., Merino, E. and Nahon, D.

1989: Diagenesis of Cretaceous sandstone reservoirs of the South Gabon rift basin; West Africa, mineralogy, mass transfer, and thermal evolution, *Journal of Sedimentary Petrology*, vol. 59, no. 3, pp. 482-493.

Gluyas, J. and Coleman, M.L.

1992: Material flux and porosity changes during sediment diagenesis, *Nature*, vol. 356, no. 6364, pp. 52-54.

Gluyas, J.G., Grant, S.M., and Robinson, A.G.

1993: Geochemical Evidence for a Temporal Control on Sandstone Cementation, *in Diagenesis and Basin Development, American Association of Petroleum Geologists, Studies in Geology Number 36*, ch. 3, pp. 23-33.

Grant, A. C., and McAlpine, K. D.

1990: Chapter 6, The continental margin around Newfoundland, *in Keen, M. J., and Williams, G. L., eds., Geology of the continental margin of eastern Canada: Geological Survey of Canada*, pp. 239-292.

Grossman, E.L. and Ku, T-L.

1986: Oxygen and carbon fractionation in biogenic aragonite; temperature effects, *Chemical Geology; Isotope Geoscience Section*, vol. 59, no. 1, pp. 59-74.

Handford, C.R., Loucks, R.G and Moshier, S.O.

1989: Preface, *sed geology*, vol. 63, pp. 187-198.

Harms, J.C., Southardf, J.B., and Walker, R.G.

1982: Structure and Sequences in Clastic Rocks, *Lecture Notes from Short Course #9, sponsored by Soc. Eco. Pol and Min, Ch. 8. Shallow Marine Environments – A comparison of some ancient and modern examples.*

Haworth, R.T. and Keen, C.E.

1979: The Canadian Atlantic Margin; a passive continental margin encompassing as active past, *Tectonophysics*, vol. 59, no. 1-4, pp. 83-126.

Hayden, P.R., and Graf, D.L.

1986: Studies of smectite membrane behaviour: temperature dependence, 20-180 °C, *Geochimica Cosmochimica Acta*, vol. 50, pp. 115-121.

Heald, M.T., and Renton, J.J.

1966: Experimental Study of Sandstone Cementation, *Journal of Petrology*, vol. 36, no. 4, pp. 977-991, in *Diagenesis of Sandstone: Cement-Porosity Relationships*, compiled by Earle F. McBride, Society of Economic Paleontologists and Mineralogists, Reprint Series Number 9, 1979.

Hendry, J.P., Ditchfield, P.W. and Marshall, J.D.

1995: Two stage neo-morphism of Jurassic aragonitic bivalves; implications for early diagenesis, *Journal of Sedimentary Research, Section A: Sedimentary Petrology and Processes*, vol. 65, no. 1, pp. 214-224.

Hendry, M.D.

1996: The geological legacy of small islands at the Caribbean/Atlantic boundary, *Coastal and Estuarine Studies (Washington)*, vol. 51, pp. 83-119.

Hesse, R. and Abid, I.A.

1998: Carbonate cementation-the key to reservoir properties of four sandstone levels (Cretaceous) in the Hibernia Oilfield, Jeanne d'Arc Basin, Newfoundland, Canada. *Spec. Publs int. Ass. Sediment.* 26, pp. 363-393.

Hoefs, J.

1987: *Stable Isotope Geochemistry*, Springer-Verlag, 241 p.

Holmes, C.W. and Martin, E.A.

1977: Migration of anthropologically induced trace elements (barium and lead) in a continental shelf environment, *Conference proceedings, Joint Conference on Environmental Pollutants*, vol. 4, pp. 672-676.

Horbury, A. D., and Robinson, A. G.

1993: Diagenesis, Basin Development, and Porosity Prediction in Exploration – An Introduction, in Horbury, A.D., and Robinson, A.G., eds., *Diagenesis and Basin Development*.

Hubbard, R.J., Pape, J. and Roberts, D.G

1985: Depositional sequence mapping as a technique to establish tectonic and stratigraphic framework and evaluate hydrocarbon potential on a passive continental margin, *American Association of Petroleum Geology, Memoir*, vol. 39, pp. 79-91.

Hudson, J.D.

1978: Concretions, isotopes, and the diagenetic history of the Oxford Clay (Jurassic) of central England: *Sedimentology*, vol. 5, pp. 339-370.

Hudson, J.D. and Andrews, J.E.

1987: The Diagenesis of the Great Estuarine Group, Middle Jurassic, Inner Hebrides, Scotland, *Geological Society Special Publications*, vol.36, pp., 259-276.

Husky web site

2004: <http://www.huskywhiterose.com>, White Rose DA Volume 2 {Development Plan}, 2001

Hutcheon, I., Nahnybida, C., and Krouse, H.R.

1985: The Geochemistry of Carbonate Cements in the Avalon Sand, Grand Banks of Newfoundland, *Mineralogical Magazine*, vol. 49, pp.457-467.

Irwin, H., Curtis, C., and Coleman, M.

1977: Isotopic evidence for source of diagenetic carbonates formed during burial of organic-rich sediments, *Nature*, vol. 269, pp. 209-213.

Jackson, J. (ed.)

1997: Glossary of geology, Fourth Edition, American Geological Institute Alexandria, Virginia.

James, N.P., and Choquette, P.W.

1990: Limestones - the meteoric diagenetic environment, *in* McIlreath, I.A., Morrow, D.W., eds., *Diagenesis*. Geosci. Can. Repr. Ser., vol. 4, pp. 35-73.

Jansa, L. F., and Wade, J. A.

1975a: Geology of the continental margin off Nova Scotia and Newfoundland, *in* van der Linden, W. J. M. and Wade, J. A., eds., *Offshore geology of eastern Canada: Geological Survey of Canada Paper 74-30*, pp. 51-105.

Jansa, L. F., and Wade, J. A.

1975b: Paleogeography and sedimentation in the Mesozoic and Cenozoic, southeastern Canada, *in* Yorath, C. J., Parker, E. R. and Glass, D. J., eds., *Canada's continental margins and offshore petroleum exploration: Canadian Society of Petroleum Geologists Memoir 4*, pp. 79-102.

Kantorowicz, J.D., Bryant, I.D., and Dawans, J.M.

1987: Controls on the geometry and distribution of carbonate cements in Jurassic sandstones: Bridport Sands, southern England and Viking Group, Troll Field, Norway, *in* *Diagenesis of Sedimentary Sequences*, Geological Society Special Publication No 36 edited by J.D. Marshall, vol.36, pp. 103-118.

Keen, C. E., Boutilier, R., de Voogd, B., Mudford, B. S. and Enachescu, M. E.

1987: Crustal geometry and models of the evolution of the rift basins on the Grand Banks of eastern Canada: Constraints from deep seismic data, *in* Beaumont, C. and Tankard, A.J., eds., *Sedimentary basins and basin-forming mechanisms: Canadian Society of Petroleum Geologists Memoir 12*, pp. 101-115.

Keen, C. E., Loncarevic, B. D., Reid, I., Woodside, J., Haworth, R. T. and Williams, H.

1990: Chapter 2: Tectonic and geophysical overview, *in* Keen, M. J. and Williams, G. L., eds., *Geology of the continental margin off eastern Canada: Geological Survey of Canada*, pp. 31-85.

Keith, M. L., Anderson, G. M., and Eichler, R.

1963: Carbon and oxygen isotopic composition of mollusc shells from marine and fresh-water environments, *Geochimica et Cosmochimica Acta*, vol. 28, pp. 1757-1786.

Keith, M.L. and Weber, J.N.

1964: Carbon and Oxygen isotopic composition of selected limestones and fossils, *Geochimica et Cosmochimica Acta*, vol. 28, no. 11, pp. 1787-1816.

Knauth, L.P., and Beeunas, M.A.

1986: Isotope geochemistry of fluid inclusions in the Permian halite with implications for the isotopic history of ocean water and the origin of saline formation waters, *Geochimica Cosmochimica Acta*, vol. 50, pp.419-433.

Knauth, L.P., Kumar, M.B., and Martinez, J.D.

1980: Isotope geochemistry of water in the Gulf Coast salt domes, *Journal of Geophysical Research*, vol. 85, pp. 4863-4871.

Koepnick, R.B.

1976: Luminescent zonation of carbonate cements in Upper Cambrian Straight Canyon and Fera Formations of the Dugway Range, Utah: *Nuclide Spectra*, vol. 9, pp 1.

Kroopnick, P.M.

1985: The distribution of ^{13}C of CO_2 in the 2 world oceans. *Deep Sea Research* 3, pp. 57-84.

Land, L.S.

1983: The Application of Stable Isotopes to Studies of the Origin of Dolomite and to Problems of Diagenesis of Clastic Sediments, *in* Arthur, M.A., Anderson, T.F., Kaplan, I.R., Veizer, J., and Land, L.S. (Eds.), *Stable Isotopes in Sedimentary Geology*, SEPM Short Course No. 10, Dallas 1983.

Larson, G., and Chilingar, G.V. (eds.)

1967: *Diagenesis in Sediments*. Amsterdam: Elsevier. 551p. (developments in sedimentology, 8)

Lee, J.

1987: Sedimentology and diagenesis of the Avalon member of the Missisauga Formation, Hibernia field, Grand Banks of Newfoundland, Master's Thesis, University of Calgary, 135 p.

Lide, D.R., and Frederikse, H.P.R.

1995: Handbook of Chemistry and Physics, 76th ed., CRC Press, Boca Raton, Florida.

Longstaffe, F.J.

1987: Stable isotope studies of diagenetic processes, Short Course Handbook, vol. 13, pp. 187-257.

Longstaffe, F.J., and Ayalon, A.

1987: Oxygen-isotope studies of clastic diagenesis in the Lower Cretaceous Viking Formation, Alberta: implications for the role of meteoric water, *in* Diagenesis of Sedimentary Sequences, Geological Society Special Publication No 36, Marshall, J.D., ed., pp. 277-296.

Louden, K.E., and Chian, D.

1999: The deep structure of non-volcanic rifted continental margins, Philosophical Transactions – Royal Society. Mathematical, Physical and Engineering Sciences, vol. 357, no. 1753, pp. 767-804.

Lowenstam, H.A.

1954: Factors affecting the aragonite-calcite ratios in carbonate-secreting marine organisms, Journal of Geology, vol. 62(3), pp. 284-322.

Lowenstam, H.A., and Weiner, S.

1989: On Biomineralization, Oxford University Press, 324 p.

MaCauley, C.I., Haszeldine, R.S., and Fallick, A.E.

1993: Distribution, Chemistry, Isotopic Composition and Origin of Diagenetic Carbonates: Magnus Sandstone, North Sea, Journal of Sedimentary Petrology, vol. 63, pp. 33-43.

MaCauley, C.I., Fallick, A.E., McLaughlin, O.M., Haszeldine, R.S. and Pearson, M.J.

1998: The significance of $\delta^{13}\text{C}$ of carbonate cements in reservoir sandstones: a regional perspective from the Jurassic of the northern North Sea, Special Publication Number 26 of the International Association of Sedimentologists, Carbonate Cementation in Sandstones, edited by Sadoon Morad, pp. 395-408.

Machel, H.G., and Burton, E.A.

1991: Factors governing cathodoluminescence in calcite and dolomite and their implications for studies of carbonate diagenesis, *in* Luminescence microscopy and spectroscopy; qualitative and quantitative applications SEPM Short Course Notes, vol. 25, pp. 37-57.

Machel, H.G.

2005: Investigations of burial diagenesis in carbonate hydrocarbon reservoirs, Geoscience Canada, Journal of the Geological Society of Canada, vol. 32, no. 3, pp. 103-128.

Machemer, S.D., and Hutcheon, I.

1988: Geochemistry of the early carbonate cements in the Cardium Formation, Central Alberta: Journal of Sedimentary Petrology, vol.58, pp. 136-147.

Majewske, O. P.

1969: Recognition of invertebrate fossil fragments in rocks and thin section, International Sedimentary Petrographical Series, Volume XIII, 101 p.

Manheim, F.T., and Sayles, F.L.

1974: Composition and origin of interstitial waters of marine sediments, based on deep sea drill cores, *in* Goldberg, E.D., ed., The Sea, Marine Chemistry: New York, Wiley, vol. 5, pp. 527-568.

Maynard, J.B.

1982: Extension of Berner's "New Geochemical Classification of Sedimentary Environments" to Ancient Sediments. American Association of Petroleum Geologists Bulletin, vol. 57, pp. 1270-1273.

McAlpine, K.D.

1990: Mesozoic Stratigraphy, Sedimentary Evolution, and Petroleum Potential of the Jeanne d'Arc Basin, Grand Banks of Newfoundland, Paper - Geological Survey of Canada, vol. 89-17, 50 pp. 1990.

McConnaughey, T.A., and Whelan, J.

1997: Calcification generates protons for nutrient and bicarbonate uptake. Earth Science Review, vol. 42, pp. 95-117.

McCrea, J.M.

1950: On the isotopic chemistry of carbonates and a paleotemperature scale: Journal of Chemistry and physics, vol. 18, pp. 849-857.

McKay, J.L., Longstaffe, F.J., and Plint, A.G.

1995: Early diagenesis and its relationship to depositional environment and relative sea-level fluctuations (Upper Cretaceous Marshybank Formation, Alberta and British Columbia), *in* Sandstone Diagenesis: Recent and Ancient, reprinted from Sedimentology, vol. 42, pp. 161-190.

McMillan, N.J.

1982: Canada's east coast; the new super petroleum province, Journal of Canadian Petroleum Technology, vo. 21, no. 2, pp. 95-109.

Meyers, W.J.

1974: Carbonate cement stratigraphy of the Lake Valley Formation (Mississippian), Sacramento Mountains, New Mexico: *Journal of Sedimentary Petrology*, vol. 44, pp. 837-861.

Meyers, W.J.

1978: Carbonate Cements: their regional distribution and interpretation in Mississippian limestones of southwestern New Mexico: *Sedimentology*, vol. 25, pp. 371-399.

Milliken, K.L.

1998: Carbonate diagenesis in non-marine foreland sandstones at the western edge of Alleghanian overthrust belt, Southern Appalachians, Special Publication of the International Association of Sedimentologists, vol. 26, pp.87-105.

Mook, W.G., and Tan, F.C.

1991: Stable Isotopes in Rivers and Estuaries, Chapter 11 *in* Degens, E.T., Kempe, S., and Richey, J.E., eds., *Biochemistry of Major World Rivers*, vol.42, pp.245-264.

Morad, S.

1998: Carbonate cementation in sandstones: distribution patterns and geochemical evolution, *in* Carbonate cementation in sandstones, Morad, S., ed., Special Publication #26, IAS, pp. 1-26.

Morse, J.W. and Mackenzie, F.T.

1990: Geochemistry of sedimentary carbonates, *Developments in Sedimentology*, vol. 48, 707 p.

Mozley, P. S., and Burns, S. J.

1993: Oxygen and Carbon Isotopic composition of marine carbonate concretions, *Journal of Sedimentary Petrology*, vol. 63, pp. 73-83.

Nagihara, S., Brooks, J. M., Bernard, B. B., Cole, G., Summer, N., and Lewis, T.

2002: Application of marine heat flow data important in oil and gas exploration, *Oil and Gas Journal*, July, 2002, http://www.tdi-bi.com/our_publications/ogj-hf-july02/marine-heatflow.htm

Neff, J.M.

1969: Mineral regeneration by serpulid polychaetes worms, *Biological Bulletin* vol. 136, p. 76-90.

Odin, G. S. and Fullagar, P. D.

1988: Geological significance of the glaucony facies, *in* Odin, G. S., ed., *Green Marine Clays*: Amsterdam, Elsevier, pp. 295-232.

Paces, T.

1983: Rate constants of dissolution from the measurement of mass-balance in hydrological catchments. *Geochim. Cosmochim. Acta*, 47, vol.47, no. 11, pp. 1855-1863.

Palmer, T.J. and Wilson, M.A.

2004: Calcite precipitation and dissolution of biogenic aragonite in shallow Ordovician calcite seas. *Lethaia*, vol. 37, pp. 417-427, Oslo. ISSN 0024-1164.

Parnell, J.

1994: Hydrocarbons and other fluids: paragenesis, interactions and exploration potential inferred from petrographic studies, *in* Parnell, J., ed., 1994, *Geofluids: Origin, Migration and Evolution of Fluids in Sedimentary Basins*, Geological Society Special Publication No. 78, pp. 275-291.

Parnell, J., Middleton, D., Honghan, C., and Hall, D.

2001: The use of integrated fluid inclusion studies in constraining oil charge history and reservoir compartmentation: examples from the Jeanne d'Arc Basin, offshore Newfoundland, *Marine and Petroleum Geology*, vol.18, pp. 535-549.

Parrell, A.L.

2005: Stratigraphic and Depositional Significance of Bioclastic Horizons within the Ben Nevis Formation (Lower Cretaceous), White Rose Field, Jeanne d'Arc Basin, Honours Thesis, Department of Earth Sciences, Memorial University of Newfoundland, 52 p.

Pemberton, S. G., Spila, M. V., Pulham, A. J., Saunders, T., MacEachern, J. A., Robbins, D. and Sinclair, I.

2001: Ichnology and sedimentology of shallow and marginal marine systems: Ben Nevis and Avalon reservoirs, Jeanne d'Arc Basin: Geological Association of Canada Short Course Notes 15, 353 p.

Plint, A.G.

1999: Husky et al White Rose N-30 Preliminary Core Description and Revised Stratigraphy for the White Rose area. Husky Oil consultant report, 54 p.

Powell, T.G.

1984: Hydrocarbon-source relationships, Jeanne d'Arc and Avalon basins, offshore Newfoundland, Open-File Report – Geological Survey of Canada, Report; 1094, 31 p.

Powers, M.C.

1967: Fluid release mechanisms in compacting marine mudrocks and their importance in oil exploration, *American Association of Petroleum Geologists*, vol. 51, pp. 1240-1254.

Proctor, R.M., Taylor, G.C., and Wade, J.A.

1984: Oil and natural gas resources of Canada – 1983; Geological Survey of Canada, Paper 83-31, 59 p.

pubs.usgs.gov/.../USGS_3D/ssx_txt/diagenes.htm (February 2006)

Raiswell, R.

1987: Non-steady state microbiological diagenesis and the origin of concretions and nodular limestones, *in* Marshall, J.D., ed., *Diagenesis of Sedimentary Sequences*, Geological Society Special Publication No 36, pp. 41-54.

Reed, J.S., Eriksson, K.A., and Kowalewski, M.

2005: Climatic, depositional and burial controls on diagenesis of Appalachian Carboniferous sandstones: qualitative and quantitative methods, *Sedimentary Geology*, vol. 176, pp. 225-246.

Rimstidt, J.D.

1997: Quartz Solubility at low temperatures, *Geochimica et Cosmochimica Acta*, vol. 61, N0.13, pp. 2553-2558.

Rubinson, M., and Clayton, R.N.

1969: Carbon-13 fractionation between aragonite and calcite: *Geochemica et Cosmochimica Acta*, vol. 33, pp. 997-1002.

Roh, Y., Zhang, C.L., Vali, H., Lauf, R. J., Zhou, J. and Phelps, T. J.

2003: Biogeochemical and environmental factors in Fe Biomineralization: magnetite and siderite formation, *Clays and Clay Minerals*; vol. 51; no. 1; pp. 83-95.

Sass, E., and Kolodny, T.

1972: Stable isotopes, chemistry and petrology of carbonate concretions (Mishhash Formation, Isreal): *Chemical Geology*, vol. 10, pp. 261-286.

Scholle, P. A.

1979: A Color Illustrated Guide to Constituents, Textures, Cements and Porosities of Sandstones and Associated Rocks, Memoir 28, U.S. Geological Survey, published by The American Association of Petroleum Geologists, no. 28, 201 pp.

Schidlowski, M.

1988: A 3,800-million-year isotopic record of life from carbonin sedimentary rocks, *Nature*, vol. 333, no. 6171, pp. 313-318.

Scotchman, I.C.

1991: The geochemistry of concretions from the Kimmeridge Clay Formation of southern and eastern England, *Sedimentology*, vol. 38, pp. 79-106.

Shackleton, N.J., and Kennet, J.P.

1975: Paleotemperature history of the Cenozoic and the initiation of the Antarctic glaciation: oxygen and carbon isotope analyses in the DSDP sites 277, 279 and 281, *in* Initial reports of the Deep Sea Drilling Project, Kennet, J.P., and Hontz, R.E. vol. 29, pp. 743-755, US Government Printing Office, Washington.

Shepard, M.G. and Hawkins, D.

1983: Petroleum resource potential of offshore Newfoundland and Labrador; Resource Assessment Division, Petroleum Directorate of Newfoundland and Labrador, Special Report PD 83-1, 14 p.

Sinclair, I.K.

1988: Evolution of Mesozoic-Cenozoic sedimentary basins in the Grand Banks area of Newfoundland and comparison with Falvey's (1974) Rift Model, *Bulletin of Canadian Petroleum Geology*, vol. 36, no. 3, pp. 255-273.

Sinclair, I. K., McAlpine, K. D., Sherwin, D. F., McMillan, N. J., Taylor, G. C., Best, M. E., Campbell, G. R., Hea, J. P., Henao, D., Procter, R. M.

1992: Petroleum resources of the Jeanne d'Arc Basin and environs, Grand Banks, Newfoundland--Resources petrolieres du bassin de Jeanne d'Arc et des environs, Grand Bancs, Terre-Neuve Paper - Geological Survey of Canada, Report: 92-08, pp.100.

Sinclair, I.K.

1993: Tectonism: the dominant factor in mid-Cretaceous deposition in the Jeanne d'Arc Basin, Grand Banks, *Marine and Petroleum Geology*, vol. 10, pp. 530-549.

Sinclair, I. K.

1995: Sequence stratigraphic response to Aptian-Albian rifting in conjugate margin basins: A comparison of the Jeanne d'Arc Basin, offshore Newfoundland, and the Porcupine Basin, offshore Ireland, *in* Scrutton, R. A., Stoker, M. S. Shimmield, G. B. and Tudhope, A. W., eds., *The tectonics, sedimentation and palaeoceanography of the North Atlantic region*: Geological Society (London) Special Publication 90, pp. 29-49.

Sippel, R.F.

1968: Sandstone Petrology, evidence from luminescence petrography, *Journal of Sedimentary Petrology*, vol. 38, pp. 530-554.

Sommer, M.A., and Rye, D.

1978: Oxygen and Carbon Isotope Internal Thermometry Using Benthic Calcite and Aragonite Foraminifera Pairs, U.S. Geological Survey, Open File Report 78-701, pp. 408-410, U.S. Geological Survey, Washington, D.C.

Soliman, O.M.

1995: Depositional facies and calcite cementation in the Avalon Formation, Hibernia Oil Field, Jeanne d'Arc Basin, Grand Banks of Newfoundland, Phd. Thesis, Memorial University of Newfoundland, 284 p.

Swift, J.H. and Williams, J.A.

1980: Petroleum source rocks, Grand Banks area; *in* Maill, A.D., ed., Facts and Principles of World Petroleum Occurrences, Canadian Society of Petroleum Geologists, Memoir 6, pp. 567-588.

Tankard, A. J. and Welsink, H. J.

1987: Extensional tectonics and stratigraphy of the Hibernia oil field, Grand Banks, Newfoundland: American Association of Petroleum Geologists Bulletin, vol. 71, pp. 1210-1232.

Tankard, A. J. and Welsink, H. J.

1988: Extensional tectonics, structural styles and stratigraphy of the Mesozoic Grand banks of Newfoundland, Developments in Geotectonics, vol. 22, no. Parts A and B, pp. 129-165.

Tankard, A. J. and Welsink, H. J.

1989: Mesozoic extension and styles of basin formation in Atlantic Canada, American Association of Petroleum Geologists Memoir, vol. 46, pp. 175-195.

Tankard, A. J., Welsink, H. J. and Jenkins, W. A. M.

1989: Structural styles and stratigraphy of the Jeanne d'Arc Basin, Grand Banks of Newfoundland, *in* Tankard, A. J. and Balkwill, H. R., (eds.), Extensional tectonics and stratigraphy of the North Atlantic margins: AAPG Memoir 46, pp. 266-282.

ten Hove, H.A., and van den Hurk, P.

1993: review of Recent fossil serpulid 'reefs'; actuopalaeontology and the 'Upper Malm' serpulid limestones in NW Germany, Geologie en Mijnbouw, vol. 72, pp. 23-67.

Thompson, S.L. and Baron, E.J.

1981: Comparision of Cretaceous and present Earth albedos; implications for causes of paleo-climates, Journal of Geology, vol. 89, no. 2, pp. 143-167.

Thyne, G.D., and Boles, J.R.

1989: Isotopic evidence for origin of the Moeraki septarian concretions, New Zealand: Journal of Sedimentary Petrology, vol. 59, pp. 272-279.

Twenhofel, W.H.

1939: Principles of Sedimentology, 1st ed. New York: McGraw-Hill. 610 p.

Twenhofel, W.H.

- 1942: The rate of deposition of sediments: A major factor connected with alteration of sediments after deposition, *Journal of Sedimentary petrology*, vol. 12, no. 3, pp. 99-110, in *Sedimentary Processes: Diagenesis*, Society of Economic paleontologists and Mineralogists, Reprint Series Number 1, 1976.

Van Der Weijden, C.H.

- 1988: Early Diagenesis and Marine Pore Water, In *Developments in Sedimentology*, 47, edited by Wolf and Chilingarian, ch. 2, pp.13-134.

Veizer, J.

- 1983: Chemical diagenesis of carbonate rocks: Theory and application of trace element technique. in Arthur, M.A., and Anderson, T.F., eds., *Stable Isotopes in Sedimentary Geology* Society of Economic Paleontologists and Mineralogists. Short Course, No 10: 3.1-3.100.

Veizer, J., Ala, D., Azmy, K., Bruckschen, P., Buhl, D., Bruhn, F., Carden, G. A.F., Diener, A, Ebneith, S., Godderis, Y., Jasper, T., Korte, C., Pawellek, F., Podlaha, O., and Strauss, H.

- 1999: $^{87}\text{Sr}/^{86}\text{Sr}$, $\delta^{13}\text{C}$ and $\delta^{18}\text{O}$ evolution of Phanerozoic seawater, *Chemical Geology*, vol. 161, pp. 59-88.

Veizer, J.

- 2003: Isotopic evolution of seawater on geological time scales: sedimentological perspective, in Lentz, D.R., ed., *Geochemistry of Sediments and Sedimentary Rocks: Evolutionary Considerations to Mineral Deposit-Forming Environments*: Geological Association of Canada, *GeoText* 4, pp. 53-68.

Voigt, S., and Wiese, F.

- 2000: Evidence for Late Cretaceous (Late Turonian) climate cooling from oxygen-isotope variations and paleobiogeographic changes in Western and Central Europe, *Journal of the Geological Society of London*, vol. 157, pp. 737-743.

Walderhaug, O.

- 1994: Temperatures of quartz cementation in Jurassic sandstones from the Norwegian continental shelf – evidence from fluid inclusions. *Journal of Sedimentary Research*, A64, no.2, pp. 311-323.

Walderhaug, O., and Bjokum, P.A.

- 1998: Calcite cement in shallow marine sandstones: growth mechanism and geometry, in Morad, S., ed., *Carbonate Cementation in Sandstones*, Special Publication of the International Association of Sedimentologists, pp.179-192.

Wanless, H.R.

- 1969: Sediments of Biscayne Bay - distribution and depositinal history, *Inst. Mar. Atmos. Sci. Univ. of Miami, Tech. Report*, 62-6, 260 pp.

Wilkinson, M.

1991: The Concretions of the Bearreraig Sandstone Formation: geometry and geochemistry, *Sedimentology*, vol. 38, pp. 899-912.

Wilkinson, M., Hasveldine, R. S., Fallick, A. E., and Osborne, M. J.

2000: Siderite zonation within the Brent Group: microbial influence or aquifer flow?, *Clay Minerals*, vol. 35, pp. 107-117.

Williamson, M.A., DesRoches, K., and King, S.

1993: Overpressures and hydrocarbon migration in the Hibernia-Nautilus area of the Jeanne d'Arc Basin, offshore Newfoundland, *Bulletin of Canadian Petroleum geology*, vol. 41, pp. 389-406.

Wood and Hewett,

1984: *in* *Clastic Diagenesis*, Memoir, American Association of Petroleum Geologists, vol. 37, pp. 99-110.

Worden, R.H., and Burley, S.D., 2003.

2003: Sandstone Diagenesis: the evolution of sand to stone *in* Burley and Worden, eds., *Sandstone Diagenesis: Recent and Ancient*, Blackwell Publishing.

Wright, P., Cherns, L., and Hodges, P.

2003: Missing Molluscs: Field testing taphonomic loss in the Mesozoic through early large-scale aragonite dissolution, *Geology*, vol. 31, pp. 211-214.

APPENDIX A

ANALYSIS OF CALCITE CEMENTED CONCRETIONS

White Rose B-07_4 Measured apparent thickness will be slightly greater than true vertical thickness due to well deviation.

#	Type	Core / Box	TVD	Thickness cm	Lower Contact	Upper Contact	Nucleation Site	Beds Below	Beds Above	Degree of cementation and General Comments
1	B2	3: 12&11	2960.21-2960.54	33	Sharp and wavy: Erosional	Sharp and convex: Cross cuts lithology	None	Marlstone	Light/dark alternating partially cemented zone	Well
2	D1	3: 11&10	2959.84-2960.21	37	Sharp and convex: Bounded by underlying concretion	Gradual: becoming less cemented as oil stain becomes more prominent	None, more worm tubes at the base	Concretion	Reservoir SS	Partially cemented
3	A2	3: 8&7	2957.57-2958.35	78	Sharp and slightly concave:	Sharp and Linear: Cross cuts lithology	12 cm accumulation of shells (Up to 8 cm wide) near top	Trough cross-bedded reservoir ss	Partially cemented zone	Very well cemented
4	D2	3: 7&6	2957.39-2957.57	18	Sharp and linear: Bounded by underlying concretion	Gradually becoming uncemented with a sharp and linear final upper boundary	None, shell frags increasing towards the base	Concretion	Reservoir SS	Partially cemented
5	D3	3 5	2956.32-2956.63	31	Sharp and slightly concave:	Sharp and irregular: defined by 2 cm thick calcite vein	Possibly calcite veins	Reservoir SS	Reservoir SS	Veins have well developed zonation, forming perpendicular to bedding and eventually squeezing along bedding boundaries. Lateral extension of concretion is captured in core.
6	D4	3 3	2955.47-2955.63	16	Gradual	Gradual	Calcite Veins?	Reservoir SS	Reservoir SS	Zoned calcite veining perpendicular to bedding and limited by bedding planes.
7	C5	3 2	2954.85-2954.99	14	Sharp and slightly concave:	Gradual and irregular	Calcite Veins?	Parallel laminated SS	Crypto-bioturbated SS	

White Rose B-07_4 Measured apparent thickness will be slightly greater than true vertical thickness due to well deviation.

#	Type	Core / Box	TVD	Thickness cm	Lower Contact	Upper Contact	Nucleation Site	Beds Below	Beds Above	Degree of cementation and General Comments
8	C6	3 1 & 2 27	2954.08- 2954.18	10	Gradual	Unknown, missing core	3 cm long oyster shell	Parallel laminated SS	Missing core, between core runs	Moderately cemented, excellent cross-beds, becoming structureless at the top.
9	C7	2: 27&26	2953.03- 2953.78	75	Unknown, missing core	Gradual	Calcite Veins?	Missing Core	Parallel laminated SS	Moderately cemented, cross-bedding, calcite veins at the top.
10	C4	2 25	2952.34- 2952.62	28	Gradual	Sharp and irregular: defined by an erosional surface	None	Parallel laminated SS	Bioclastic build-up	Moderately cemented, cross-bedding, neptunian dykes. Bioclastic buildup resulting from wash-over lobes of a localized reef system. Multiple episodes creating a fairly thick sequence, sometimes becoming colonized by living organisms (as demonstrated by in situ directions) being preserved by another dump of bioclastic debris. Has mass debris flows, possible slumping and soft sedimentary features throughout. General normal grading of bioclastic beds, becoming interbedded with fine grained parallel laminated reservoir ss beds (fining upwards sequence) which increase from 5 to 50 cm throughout the entire unit. Parallel laminated f gm ss seem to cap the bioclastic sequences.
11	E	2 25 to 2 14	2945.99- 2952.34	635	Sharp and irregular	Gradual?	Bioclastic debris	Moderately cemented SS		
12	D5	2 11	2944.60- 2944.74	14	Sharp and wavy	Gradual	Bioclastic debris, worm tubes	Parallel laminated SS	Parallel laminated SS	May be the very top of the bioclastic debris flows, wavy scoured base with normal grading but more clastic input.
13	A3	2 10& 9	2943.66- 2944.18	52	Sharp and concave; cross cutting lithology	Sharp and irregular, slightly convex	Calcite Veins?	Parallel laminated SS	Parallel laminated SS	Calcite veins in the upper central vey well (white) cemented portion of concretion. Captures concave lower and convex upper boundaries.
14	C3	2 8	2942.58- 2942.65	7	Sharp and irregular	Sharp and irregular	Worm tubes and shell fragments	Structureless ss Ss	Parallel laminated SS	Catches lateral extension of a thin 10 cm moderately cemented concretion. Slight hint of crossbedding within the concretion.

White Rose B-07_4 Measured apparent thickness will be slightly greater than true vertical thickness due to well deviation.

#	Type	Core / Box	TVD	Thickness cm	Lower Contact	Upper Contact	Nucleation Site	Beds Below	Beds Above	Degree of cementation and General Comments
15	A1	2 6	2941.71-2941.99	28	Sharp and concave; cross cutting lithology	Sharp and convex: Cross cuts lithology	None	Parallel laminated SS	Moderately cemented bioclastic concretion	Very well cemented
16	A4	2 6&5	2941.25-2941.71	46	Sharp and convex; cross cutting lithology	Sharp and convex: Cross cuts lithology	Bioclastics decreasing from base to top	Well defined concretion	Moderately cemented bioclastic concretion	Partially cemented
17	C10	2 5&4	2940.87-2941.25	38	Sharp and convex; cross cutting lithology	Gradually becoming uncemented with a wavy boundary	Bioclastic debris fining upwards	Well cemented SS	Parallel laminated SS	Fining upwards moderately cemented bioclastic unit capped by a 5 cm thick laminated ss.
18	C2	2 4	2940.77-2940.84	7	Sharp and linear	Gradually becoming uncemented	Bioclastic debris fining upwards	Parallel laminated SS	Parallel laminated SS	Thin fining upwards moderately cemented bioclastic concretion.
19	D6	2 1	2938.75-2938.99	24	Gradual with wavy boundary	Missing; top of core	Bioclastic debris	Parallel laminated SS	Top of core	Well cemented
20	A2	1 84	2935.61-2935.82	21	Sharp and concave; bottom of core	Sharp and Linear: Cross cuts lithology (Seems like there is missing core!)	None	Bottom of core 1	Parallel laminated SS	Very well cemented
21	D7	1 84 to 80	2933.58-2935.61	203	Sharp and linear, cross cutting lithology	Gradual increase in oil stain	None	Well defined concretion	Parallel and cross laminated reservoir ss	Moderately cemented (Not a concretion)
22	D2	1 79 to 74	2930.34-2932.75	241	Sharp and linear	Sharp and linear	None	Parallel to cross laminated ss	Structureless reservoir ss	Very slightly cemented interval, no apparent lithology changes
23	A2	1 71 & 70	2928.00-2928.66	66	Sharp and slightly concave:	Sharp and linear	Shell lag in center of concretion	Planar to cross laminated reservoir ss	Planar to cross laminated reservoir ss	Very well cemented

White Rose B-07_4 Measured apparent thickness will be slightly greater than true vertical thickness due to well deviation.

#	Type	Core / Box	TVD	Thickness cm	Lower Contact	Upper Contact	Nucleation Site	Beds Below	Beds Above	Degree of cementation and General Comments
24	D7	1 70 to 68	2927.09-2928.00	91	Sharp and linear	Gradual	5 cm thick weak shell lag	Well defined concretion	Planar to cross laminated reservoir ss	Partially cemented
25	C9	1 66-63	2924.23-2925.76	153	Sharp and wavy	Gradual	5 cm thick black wispy shell layer	Planar to cross laminated reservoir ss	Structureless reservoir ss	Moderate Cementation
26	C10	1 62-59	2921.99-2923.81	182	Sharp and linear	Sharp and linear	Abundant shell fragments and worm tubes in center of concretion	Structureless Ss	Planar to cross laminated reservoir ss	Moderate Cementation
27	A5	1 55	2919.51-2919.72	21	Sharp and linear, cross cutting lithology	Sharp and linear, cross cutting lithology	None	Planar to cross laminated reservoir ss	Concretion above	Very well cemented. (Looks like boxes 55 and 54 may have misplaced core...contacts don't match)
28	B5	1 55-54	2919.20-2919.51	31	Sharp and linear, conformable	Gradational	None	Concretion	Planar to cross laminated reservoir ss	Well cemented
29	B3	1 54	2918.81-2919.02	21	Sharp and linear, cross cutting lithology	Sharp and slightly convex	None	Planar to cross laminated reservoir ss Planar to cross laminated reservoir ss	Structureless reservoir ss	Well cemented
30	C8	1 39-38	2909.94-2910.47	53	Sharp and concave; cross cutting lithology	Sharp and linear; cross cutting lithology	Worm tubes at base	cross laminated reservoir ss	Concretion above	Moderately cemented
31	A1	1 38-35	2908.51-2909.94	143	Sharp and concave; cross cutting lithology	Sharp and convex; cross-cutting lithology	Excellent 15 cm thick shell lag in center of concretion	Moderately cemented SS	Almost connecting with overlying concretion	Very well cemented.
32	B4	1 35	2908.19-2908.51	32	Sharp and concave; cross cutting lithology	Sharp and linear, conformable	5 cm thick worm tube lag	Almost connecting with underlying	Faintly parallel laminated reservoir SS	Well cemented

White Rose B-07_4 Measured apparent thickness will be slightly greater than true vertical thickness due to well deviation.

#	Type	Core / Box	TVD	Thickness cm	Lower Contact	Upper Contact	Nucleation Site	Beds Below	Beds Above	Degree of cementation and General Comments
33	B6	1 29-28	2904.52-2904.87	35	Sharp and linear; conformable	Sharp and irregular; slightly wavy, conformable	10 cm thick slumped shell lag with soft sed features	Planar to cross laminated reservoir ss	Planar to cross laminated reservoir ss	Well cemented in the center and moderately cemented above and below.
34	A6	1 27-26	2903.33-2903.79	46	Sharp and irregular	Sharp and irregular	None	Planar to cross laminated reservoir ss	Planar to cross laminated reservoir ss	Very well cemented
35	A1	1 21	2900.53-2900.85	32	Sharp and concave; cross cutting lithology	Sharp, irregular and convex; cross cutting lithology	None	Planar to cross laminated reservoir ss	Planar to cross laminated reservoir ss	Well cemented lateral edge of concretion
36	C2	1 18	2898.75-2898.93	18	Sharp and linear; conformable	Gradational	Worm tubes throughout	Structureless ss Ss	Planar to cross laminated reservoir ss	Moderately cemented
37	A7	1 16-15	2897.28-2898.09	81	Sharp, concave, irregular; cross cutting lithology	Sharp, concave; cross-cutting	10 cm thick well developed shell lag	Planar to cross laminated reservoir ss	Planar to cross laminated reservoir ss	Very well cemented
38	B7	3 3	2890.20-2890.27	7	Sharp, irregular, wavy; conformable	Sharp, irregular, slightly concave	Worm tubes throughout	Planar to cross laminated reservoir ss	Structureless reservoir ss	Moderately to well cemented, dark grey cement. Top of B-07_4

White Rose F-04

#	Type	Core:Box	Depth	Thickness	Lower Contact	Upper Contact	Nucleation Site	Beds Below	Beds Above	Degree of cementation and General Comments
39	A1	2 65	2870.80-2870.60	20 cm	Sharp and concave; cross cutting lithology	Sharp and convex; cross cutting lithology	None	Faint planar to wavy parallel bedding, slightly bioturbated	Faint planar to wavy parallel bedding, slightly bioturbated	Very well cemented
40	B8	2 59	2864.65-2864.60	5 cm	Sharp and irregular	Sharp and irregular	Large mollusc and gastropod shells	Bioturbated bioclastic ss	Structureless reservoir ss	Well cemented
41	D8	2 52	2859.02-2859.00	2 cm	Sharp and irregular	Sharp and irregular	Abundant worm tubes	Faintly laminated bioclastic reservoir ss	Faintly laminated bioclastic reservoir ss	Early stage of concretion formation
42	A1	2 47-44	2855.05-2853.09	196 cm	Sharp and slightly concave	Sharp and convex; cross cutting lithology	Six, 1 to 18 cm thick worm tube/shelly lags	Cryptobioturbated reservoir ss	Cryptobioturbated reservoir ss	Very well cemented, possibly the coalescence of 3 separate cemented intervals.
43	A1	2 33-29	2843.74-2840.58	316 cm	Sharp and slightly concave; cross cutting lithology	Sharp and convex; cross cutting lithology	Six, 3 to 18 cm thick slightly porous worm tube lags	Cryptobioturbated reservoir ss	Faintly laminated bioclastic reservoir ss	Very well cemented, possible amalgamation of several concretions.
44	D8	2 28	2839.80-2839.78	2 cm	Sharp and irregular	Sharp and irregular	Abundant worm tubes and shells	Faintly laminated bioclastic reservoir ss	Faintly laminated bioclastic reservoir ss	Early stage of concretion formation, only partially cemented
45	B8	2 10	2826.35-2825.90	45 cm	Sharp and irregular; cross cutting lithology	Sharp and irregular; cross cutting lithology	Abundant worm tubes and shells throughout	Shelly worm tube lag	Faintly laminated black, wispy, dissolved shells	Well cemented

White Rose F-04

#	Type	Core:Box	Depth	Thickness	Lower Contact	Upper Contact	Nucleation Site	Beds Below	Beds Above	Degree of cementation and General Comments
48	A6	1 57-56	2811.00-2810.15	85 cm	Sharp and irregular; cross cutting lithology	Sharp, irregular, slightly convex, cross cutting lithology	Shell lags at top and base of concretion	Faintly laminated reservoir ss	Planar to cross bedded reservoir ss	Very well cemented
49	B8	1 49	2804.25-2804.11	14 cm	Sharp and irregular	Sharp and irregular	Abundant shells and calcite veins	Structureless ss slightly burrowed reservoir ss	Faintly laminated, cryptobioturbated reservoir ss	Well cemented
50	B2	1 48-47	2803.25-2802.80	45 cm	Sharp and irregular, slightly concave	Sharp, irregular, slightly convex, cross cutting lithology	Major shell lag at the base and calcite veins at the top	Muddy siltstone	Parallel laminated reservoir ss	Well cemented
51	A6	1 46	2801.90-2801.30	60 cm	Sharp and wavy; cross cutting lithology	Sharp and irregular, cross cutting lithology	Shells, worm tubes and septarium calcite veins	Structureless ss slightly burrowed reservoir ss	Planar laminated reservoir ss	Very well cemented with an interesting uncemented oval shape within the concretion
52	B1	1 44	2800.35-2800.20	15 cm	Sharp concave, cross cutting lithology	Sharp and convex; cross cutting lithology	Minor shells	Slightly bioturbated reservoir ss	Faintly bedded reservoir ss	Well cemented concretion seems to disrupt upper and lower bedding planes
53	B7	1 43	2799.45-2798.80	65 cm	Sharp and irregular; cross cutting lithology	Sharp, irregular, slightly concave, cross cutting lithology	Worm tube lag at base and center of concretion	Silty bioturbated ss	Parallel laminated reservoir ss	Moderately to well cemented
54	B2	1 41	2797.85-2797.40	45 cm	Sharp and irregular, slightly concave	Sharp, irregular, slightly convex, cross cutting lithology	Worm tubes throughout	Planar laminated reservoir ss	Parallel laminated reservoir ss	Well cemented

55	D8	1	39-38	2796.85-2796.70	15 cm	Sharp and irregular	Sharp and irregular	Worm tubes throughout	Bioturbated reservoir ss	Structureless reservoir ss	Partiallt cemented, soft sediment features, mass slumping
----	----	---	-------	-----------------	-------	---------------------	---------------------	-----------------------	--------------------------	----------------------------	---

White Rose F-04

#	Type	Core:Box	Depth	Thickness	Lower Contact	Upper Contact	Nucleation Site	Beds Below	Beds Above	Degree of cementation and General Comments
56	D8	1 38	2795.40-2795.35	5 cm	Sharp and irregular	Sharp and irregular	Worm tubes throughout	Bioturbated reservoir ss	Bioturbated reservoir ss	Chaotic layer of cemented clasts, partial cementation
57	D8	1 38	2795.15-2795.10	5 cm	Sharp and irregular	Sharp and irregular, convex	Worm tubes throughout	Bioturbated reservoir ss	Bioturbated reservoir ss	Partially cemented
58	A1	1 37-36	2794.95-2793.95	100 cm	Sharp and slightly concave	Sharp and convex; cross cutting lithology	Abundant shells, worm tubes and calcite veins in top section	Structureless reservoir ss	Bioturbated muddy siltstone	Very well cemented, possibly two concretions joining together.
59	B1	1 35	2793.10-2792.65	45 cm	Sharp and slightly concave	Sharp, slightly convex	Large shells and calcite veins	Bioturbated reservoir ss	Unknown: Scale 4	Moderately to well cemented
60	B2	1 31	2789.55-2789.15	40 cm	Sharp and irregular	Sharp and irregular slightly convex	Worm Tubes towards the top	Muddy siltstone	Muddy siltstone	Well cemented
61	F	1 28	2786.95-2786.60	35 cm	Sharp, irregular, slightly concave	Sharp and irregular	Worm tubes throughout	Bioturbated reservoir ss	Structureless reservoir ss	Siderite concretion

Thin Section Modal Analysis

APPENDIX B

Depth Adjusted

	Thin Section	Porosity	Quartz	Ferroan Calcite Cement	Non- ferroan calcite cement	Shells	Detrital Carb.	Siderite	Opaque s	Clay	Ass.
WR F-04	160	20	40	12	3	30	0	24	0	0	1 glauc & rr wood
WR F-04	161	5	55	1	0	0	0	40	1	0	1 wood
WR F-04	162	25	45	2	2	0	0	25	1	0	tr wood & glauc
WR F-04	163	10	49	10	2	0	0	29	0	0	0
WR F-04	164 UC	20	56	2	20	25	0	2	0	0	0
WR F-04	164 C	1	58	15	1	0	0	25	0	0	0
WR F-04	165	15	50	10	0	25	0	0	0	0	0
WR F-04	166 UC	28	70	1	1	0	0	0	0	0	0
WR F-04	166 C	0	59	35	5	1	0	0	0	0	0
WR F-04	167	1	50	25	5	20	1	0	0	0	rr wood
WR F-04	168	2	53	30	5	10	0	0	0	0	0
WR F-04	169 UC	0	50	40	0	10	0	0	0	0	0
WR F-04	169 C	30	63	2	0	5	0	0	0	0	tr wood
WR F-04	170	0	50	35	0	15	0	0	0	0	0
WR F-04	171	0	50	49	0	1	0	0	0	0	0
WR F-04	172 UC	20	70	5	0	5	0	0	0	0	0
WR F-04	172 C	1	45	35	0	19	0	0	0	0	0
WR F-04	172 mudst	1	70	0	0	0	0	0	0	30	rr wood
WR F-04	173	0	60	0	30	5	5	0	0	0	0
WR F-04	174	35	50	2	0	5	5	2	1	0	0
WR F-04	175	35	60	1	0	2	2	0	0	0	0
WR F-04	176	1	40	20	0	39	0	0	0	0	0
WR F-04	177	0	45	45	0	5	5	0	0	0	0
WR F-04	178	5	25	40	0	30	5	0	0	0	0
WR F-04	179	5	10	50	0	35	0	0	0	0	0

	Thin Section	Porosity	Quartz	Ferroan Calcite Cement	Non- ferroan calcite cement	Shells	Detrital Carb.	Siderite	Opaque s	Clay	Ass.
WR F-04	180 UC	18	80	1	0	1	5	0	0	0	0
WR F-04	180 mud	2	60	1	0	5	1	0	0	31	0
WR F-04	181	10	55	1	0	28	1	0	0	5	0
WR F-04	182 UC	10	55	0	0	25	5	0	0	5	0
WR F-04	182 C	5	50	10	0	30	5	0	0	0	0
WR F-04	183	0	35	30	0	30	2	0	2	0	0
WR F-04	184 UC	15	80	5	0	0	0	0	0	0	0
WR F-04	184 C	0	60	35	0	4	1	0	0	0	0
WR F-04	185	20	55	0	0	20	0	3	0	2	0
WR F-04	186	15	50	0	1	15	1	13	0	0	0
WR F-04	187 UC	10	80	1	0	1	1	0	0	5	0
WR F-04	187 C	0	55	43	0	1	1	0	0	0	0
WR F-04	188	0	55	35	0	9	1	0	0	0	0
WR F-04	189	2	55	35	0	7	1	0	0	0	0
WR F-04	190	15	52	5	0	22	1	5	0	0	0
WR F-04	191	15	55	3	0	13	2	12	0	0	0
WR F-04	192	15	60	1	0	15	1	8	0	0	0
WR F-04	193 UC	10	78	0	0	5	2	0	0	5	0
WR F-04	193 C	5	55	15	5	20	0	0	0	0	0
WR F-04	194 UC	5	85	0	0	5	1	0	4	0	0
WR F-04	194 C	5	70	15	0	9	1	0	0	0	0
WR F-04	195	2	60	22	0	15	1	0	0	0	0
WR F-04	196	0	55	29	0	15	1	0	0	0	0
WR F-04	197 UC	20	78	0	0	1	1	0	0	0	0
WR F-04	197 C	0	55	44	0	0	1	0	0	0	0
WR F-04	198	20	77	0	0	0	1	0	2	0	0
WR F-04	199	0	60	38	0	1	1	0	0	0	0
WR F-04	200	0	37	40	0	20	1	0	2	0	0
WR F-04	201	0	45	43	0	10	0	0	2	0	0
WR F-04	202 UC	20	78	0	0	0	1	0	1	0	0
WR F-04	202 C	0	55	43	0	0	1	0	1	0	0

	Thin Section	Porosity	Quartz	Ferroan Calcite Cement	Non- ferroan calcite cement	Shells	Detrital Carb.	Siderite	Opaque s	Clay	Ass.
WR F-04	203 UC	15	56	0	0	25	2	0	2	0	0
WR F-04	203 C	0	43	30	0	25	1	0	1	0	0
WR F-04	204 UC	30	68	0	0	0	1	0	1	0	0
WR F-04	204 C	5	39	17	22	15	1	0	1	0	0
WR F-04	205 UC	20	78	0	0	0	1	0	1	0	0
WR F-04	205 FC	2	55	41	0	0	1	0	1	0	0
WR F-04	205 NFC	0	50	0	47	0	1	0	2	0	0
WR B-07_4	159 UC	38	55	0	0	5	1	0	1	0	0
WR B-07_4	159 C	1	50	30	12	5	1	0	1	0	0
WR B-07_4	158	20	60	0	0	10	1	8	1	0	0
WR B-07_4	157	23	67	0	0	10	0	0	1	0	0
WR B-07_4	156	17	80	0	0	1	1	0	1	0	0
WR B-07_4	155 UC	20	66	1	0	10	2	0	1	0	0
WR B-07_4	155 C	5	39	40	0	15	0	0	1	0	0
WR B-07_4	154 UC	12.5	86.5	0	0	0	1	0	1	0	0
WR B-07_4	154 C	0	50	47	0	1	1	0	1	0	0
WR B-07_4	153	1	48	46	0	2	2	0	1	0	0
WR B-07_4	152	25	71	0	0	1	2	0	1	0	0
WR B-07_4	151 UC	25	69	0	0	2	2	0	2	0	0
WR B-07_4	151 C	5	50	40	0	5	0	0	0	0	0
WR B-07_4	150	27.5	69.5	0	0	1	1	0	1	0	0
WR B-07_4	149 UC	20	64	0	0	10	3	2	1	0	
WR B-07_4	149C	10	80	1	1	2	5	0	1	0	
WR B-07_4	148	0	55	42	0	1	1	0	1	0	
WR B-07_4	147	20	70	1	1	3	5	0	1	0	
WR B-07_4	146	2	29	30	0	35	2	1	0	0	
WR B-07_4	145	10	71	3	0	1	8	4	3	0	
WR B-07_4	144	20	77	0	0	0	2	0	1	0	tr fldsp & orgai
WR B-07_4	143	15	83	0	0	0	1	1	1	0	tr fldsp
WR B-07_4	142	18	80	0	0	0	1	0	1	0	tr fldsp
WR B-07_4	141	20	77	0	0	1	1	0	1	0	

	Thin Section	Porosity	Quartz	Ferroan Calcite Cement	Non- ferroan calcite cement	Shells	Detrital Carb.	Siderite	Opaque s	Clay	Ass.
WR B-07_4	140	15	76	4	0	2	3	0	0	0	
WR B-07_4	139	20	74	0	0	1	4	0	1	0	tr fldsp
WR B-07_4	138	20	71	1	0	2	5	0	1	0	
WR B-07_4	137	15	79	1	0	1	3	1	0	0	
WR B-07_4	136	12	81	0	0	1	3	0	1	0	2 fldsp
WR B-07_4	135	0	50	40	4	3	2	0	1	0	
WR B-07_4	134	12	78	3	0	3	4	0	0	0	
WR B-07_4	133	15	78	2	0	1	2	0	2	0	
WR B-07_4	132	15	76	2	0	2	3	0	2	0	tr fldsp
WR B-07_4	131	12	75	9	1	1	2	0	0	0	
WR B-07_4	130	15	71	8	1	3	2	0	0	0	tr
WR B-07_4	129	20	76	0	0	0	2	0	1	0	1 fldsp
WR B-07_4	128	10	25	39	0	20	5	0	1	0	
WR B-07_4	127	10	27	1	30	25	5	0	2	0	tr fldsp
WR B-07_4	126	5	33	5	1	35	2	15	2	0	
WR B-07_4	125	1	45	48	0	3	2	0	1	0	
WR B-07_4	124	1	48	30	15	3	2	0	1	0	
WR B-07_4	123	15	65	10	0	5	5	0	0	0	
WR B-07_4	122	20	64	0	0	5	5	1	2	3	tr fldsp
WR B-07_4	121	12	64	8	0	5	10	0	1	0	
WR B-07_4	120	12	81	1	0	2	2	0	1	1	
WR B-07_4	119	6	55	11	15	5	1	0	2	5	
WR B-07_4	118	25	61	0	0	10	1	0	1	0	
WR B-07_4	117	15	38	0	35	10	1	0	1	0	
WR B-07_4	115 UC	30	50	0	0	11	0	0	9	0	
WR B-07_4	115 C	5	40	0	44	8	0	0	3	0	
WR B-07_4	114	15	60	20	0	1	2	0	2	0	
WR B-07_4	113	30	56	7	0	1	5	0	1	0	
WR B-07_4	112	27	60	4	0	1	6	0	2	0	
WR B-07_4	111UC	15	74	5	0	2	3	0	1	0	
WR B-07_4	111 C	10	65	5	15	2	2	0	1	0	

	Thin Section	Porosity	Quartz	Ferroan Calcite Cement	Non- ferroan calcite cement	Shells	Detrital Carb.	Siderite	Opaque s	Clay	Ass.
WR B-07_4	110	30	55	10	0	1	3	0	1	0	
WR B-07_4	109	0	50	45	0	1	3	0	1	0	
WR B-07_4	108	5	30	20	10	30	3	0	2	0	
WR B-07_4	107	0	50	46	0	0	3	0	1	0	
WR B-07_4	106	40	56	1	0	1	1	0	1	0	
WR B-07_4	105	18	55	6	4	10	2	0	5	0	
WR B-07_4	104	0	50	45	0	1	2	0	2	0	
WR B-07_4	103	30	50	10	0	3	4	0	3	0	
WR B-07_4	102	0	45	20	20	5	2	0	8	0	
Average	101	11.685	58.472	14.1575	2.8189	8.0787	1.84252	1.7402	0.92913	0.72441	
Sum		1495.69	7484.5	1812.16	360.82	1034.1	235.843	222.74	118.929	92.7244	
Count		127	127	127	127	127	127	127	127	127	
Max		40	86.5	50	47	39	10	40	9	31	
Min		0	10	0	0	0	0	0	0	0	

APPENDIX C

Carbon and Oxygen Isotopes

Sample #	$\delta^{13}\text{C}$	$\delta^{18}\text{O}$	TVD
301 B-07_4	1.430	-6.126	2977.26
302 B-07_4	0.454	-4.819	2975.07
303 B-07_4	1.028	-4.729	2973.31
304 B-07_4	1.146	-5.495	2971.57
305 B-07_4	1.814	-2.914	2969.82
306 B-07_4			2968.26
307 B-07_4	1.864	-5.068	2967.35
308 B-07_4			2966.10
309 B-07_4	-0.169	-8.894	2964.00
310 B-07_4	2.578	-5.319	2961.73
311 B-07_4	5.831	-2.634	2960.32
312 B-07_4	1.647	-4.315	2947.79
313 B-07_4	2.012	-2.992	2947.57
314 B-07_4	1.723	-4.299	2947.42
315 B-07_4	2.069	-3.102	2947.28
316 B-07_4	1.874	-3.194	2947.21
317 B-07_4	-0.512	-5.805	2909.95
318 B-07_4	-2.618	-6.195	2909.52
319 B-07_4	1.096	-5.216	2909.28
320 B-07_4	0.068	-5.502	2909.11
321 B-07_4	1.092	-4.616	2908.97
322 B-07_4	3.021	-3.861	2908.80
323 B-07_4	3.771	-3.514	2908.55
324 B-07_4	2.711	-5.347	2908.35
325 B-07_4	5.076	-5.574	2908.10
326 B-07_4	4.832	-5.834	2907.86
327 B-07_4	0.108	-2.319	2907.65
328 B-07_4	1.658	-8.076	2907.61
329 B-07_4	1.046	-1.864	2907.30
330 B-07_4	-0.640	-5.7	2907.16
331 B-07_4	-0.100	-5.417	2907.02
332 B-07_4	3.888	-3.604	2897.26
333 B-07_4	3.917	-3.744	2897.25
334 B-07_4	5.923	-4.656	2896.98
335 B-07_4	1.544	-4.056	2896.88
336 B-07_4	6.755	-4.989	2896.62
337 B-07_4	4.106	-3.85	2896.50
338 F-04	-0.411	-5.319	2764.24
339 F-04	2.442	-3.514	2765.97
340 F-04	1.179	-6.507	2767.42
341 F-04	2.806	-5.28	2769.13
342 F-04	-1.672	-6.101	2769.89
343 F-04	1.756	-6.135	2770.50
344 F-04	1.506	-6.278	2772.08
345 F-04	10.990	0.842	2773.35

Sample #	δ13C	δ18O	TVD
347 F-04	1.292	-6.119	2781.28
348 F-04	1.524	-6.681	2784.26
349 F-04	0.989	-6.43	2786.70
350 F-04	2.420	-3.748	2786.98
351 F-04	0.902	-9.247	2789.16
352 F-04	6.651	-3.866	2789.84
353 F-04	3.882	-3.389	2793.32
354 F-04	4.659	-3.426	2794.33
355 F-04	1.888	-5.297	2795.02
356 F-04	0.800	-1.511	2795.76
357 F-04	2.845	-3.995	2801.53
358 F-04	1.021	-4.625	2801.55
359 F-04	4.459	-3.254	2801.81
360 F-04	3.042	-6.942	2810.06
361 F-04	2.668	-8.286	2810.46
362 F-04	3.624	-3.715	2810.88
363 F-04	3.303	-2.59	2811.32
364 F-04	3.973	-3.568	2811.37
365 F-04	8.775	-4.009	2811.71
366 F-04	3.320	-2.513	2811.86
367 F-04	2.527	-4.905	2812.09
368 F-04	2.402	-5.079	2812.09
369 F-04	2.811	-2.739	2819.41
370 F-04	0.461	-4.032	2821.75
371 F-04	2.302	-3.322	2823.49
372 F-04	4.072	-4.77	2826.08
373 F-04	4.661	-3.994	2826.29
374 F-04	2.668	-3.128	2826.35
375 F-04	1.810	-3.321	2828.49
376 F-04	2.063	-3.667	2830.02
377 F-04	-0.677	-5.088	2832.37
378 F-04	1.716	-3.695	2835.23
379 F-04	2.300	-4.825	2837.06
380 F-04	-6.608	-4.991	2839.80
381 F-04	2.960	-3.252	2840.58
382 F-04	5.032	-3.554	2841.40
383 F-04	10.417	-3.709	2842.82
384 F-04	3.801	-2.996	2843.71
385 F-04			2848.25
386 F-04	1.421	-2.674	2852.82
387 F-04	7.601	-3.139	2853.07
388 F-04	3.641	-3.262	2854.59
389 F-04	3.199	-3.55	2854.98
390 F-04	0.434	-4.181	2859.00
391 F-04	-9.089	-4.036	2864.60
392 F-04	-13.908	-3.597	2870.00
393 B-07_4	3.359	-4.976	2940.79
394 B-07_4	2.427	-3.454	2940.79

Sample #	δ13C	δ18O	TVD
396 B-07_4	1.278	-1.526	2955.39
397 B-07_4	2.631	-2.18	2949.85
398 B-07_4	2.645	-5.643	
399 B-07_4	1.398	-4.796	
400 B-07_4	2.847	-2.708	
M-36 2340 (05-03-30)	-0.663	-1.997	2340.00
M-36 2440 (05-03-30)	1.266	-1.899	2440.00
M-36 2460 (05-03-30)	2.396	-0.923	2460.00
M-36 2480 (05-03-30)	2.550	-0.5	2480.00
M-36 2580	-2.836	-2.968	2580.00
M-36 2680 (05-03-30)	-0.799	-2.882	2680.00
M-36 2780 (05-03-30)	1.118	-1.847	2780.00
M-36 2860	1.534	-1.97	2860.00
M-36 2920 (05-03-30)	1.606	-2.136	2920.00
M-36 2980 (05-04-22)	1.647	-2.449	2980.00
M-36 3040	2.671	-1.808	3040.00
M-36 3100	2.115	-1.737	3100.00
M-36 3140	1.111	-2.065	3140.00
K-19 3800 (05-04-22)	-1.148	-0.664	3800.00
K-19 3830 (05-04-22)	-2.404	-3.495	3830.00
K-19 3860 (05-04-22)			3860.00
K-19 3890	-1.321	-4.025	3890.00
K-19 3920 (05-04-22)	0.620	-2.481	3920.00

